

University of Bath



PHD

The structural performance of glass-adhesive T-beams

Pye, Andrew John

Award date:
1998

Awarding institution:
University of Bath

[Link to publication](#)

General rights

Copyright and moral rights for the publications made accessible in the public portal are retained by the authors and/or other copyright owners and it is a condition of accessing publications that users recognise and abide by the legal requirements associated with these rights.

- Users may download and print one copy of any publication from the public portal for the purpose of private study or research.
- You may not further distribute the material or use it for any profit-making activity or commercial gain
- You may freely distribute the URL identifying the publication in the public portal ?

Take down policy

If you believe that this document breaches copyright please contact us providing details, and we will remove access to the work immediately and investigate your claim.

Download date: 13. May. 2019

**THE STRUCTURAL PERFORMANCE OF GLASS-ADHESIVE
T-BEAMS**

submitted by Andrew John Pye
for the degree of PhD
of the University of Bath
1998

This thesis may be made available for consultation within
the University Library and may be photocopied or lent to other libraries
for the purposes of consultation.

A handwritten signature in black ink, reading "Andrew J. Pye". The signature is written in a cursive style with a horizontal line underneath the name.

UMI Number: U169114

All rights reserved

INFORMATION TO ALL USERS

The quality of this reproduction is dependent upon the quality of the copy submitted.

In the unlikely event that the author did not send a complete manuscript and there are missing pages, these will be noted. Also, if material had to be removed, a note will indicate the deletion.



UMI U169114

Published by ProQuest LLC 2014. Copyright in the Dissertation held by the Author.
Microform Edition © ProQuest LLC.

All rights reserved. This work is protected against
unauthorized copying under Title 17, United States Code.



ProQuest LLC
789 East Eisenhower Parkway
P.O. Box 1346
Ann Arbor, MI 48106-1346

LIBRARY OF CONGRESS
SERIALS ACQUISITION
85 - 0 DEC 2193
PhD

Acknowledgements

The author wishes to express his thanks to all those who have assisted with this work. To Dr. Stephen Ledbetter for his supervision and constant enthusiasm. To the University of Bath for funding this work. To Pilkington United Kingdom Limited for the information and materials that they have provided. Particular thanks are due to John Colvin, John Evason and Howard McKenzie. To 3M United Kingdom Plc. for the information and materials that they have provided. Particular thanks are due to Dr. Keith Fisher and Dr. Bernard Sikkel. To Professor Robert Adams of Bristol University and Dr. Alan Hutchinson of Oxford Brookes University for their help in understanding the issues of adhesive selection, testing and stress analysis. To Dr. Stephen Ring and David Skinner for their guidance and enthusiasm in all aspects of the laboratory test work. To final year undergraduate students David Wells (1996) and Martin Feakes (1997) for their contributions to the work presented in section 4.

Last, but not least, special thanks are due to my parents who have supported and encouraged me and without whom this work would not have been possible.

The Structural Performance Of Glass-Adhesive T-beams

Index

Acknowledgements.....	2
Index	3
Index of figures.....	7
Index of tables	13
Notation	15
Synopsis	18
1 INTRODUCTION.....	20
2 LITERATURE REVIEW	26
2.1 Glass.....	26
2.1.1 Fracture mechanics.....	26
2.1.2 Glass types	29
2.1.3 Choice of glass type.....	36
2.2 Adhesives.....	37
2.2.1 Terminology.....	37
2.2.2 Precedent for the structural use of adhesives.....	39
2.2.3 Classification of structural adhesives.....	39
2.2.4 Stress analysis	44
2.2.5 Stress analysis and factors of safety in real design	48
2.2.6 Testing of adhesives to determine mechanical properties.....	49
3 TESTING OF MATERIALS	54
3.1 Achieving a simple support condition for a flat glass plate	54
3.2 Evaluating critical shear stresses in glass.....	58
3.3 The choice of an adhesive for the construction of a glass-adhesive T-beam	65
3.3.1 Evaluation of stress-strain behaviour of 2216 and DP 190.....	69
3.3.2 Results	72
3.3.3 Discussion.....	75
3.3.4 Creep resistance of DP190 and 2216	77
3.3.5 Adhesion to glass and cyclic performance	78

The Structural Performance Of Glass-Adhesive T-beams

4 THEORETICAL CONSIDERATIONS	79
4.1 Introduction	79
4.1.1 Sign conventions	79
4.2 Composite bending.....	79
4.2.1 Solution of the governing differential equation.....	82
4.2.2 Glass and adhesive strains.....	83
4.2.3 Shear deflection.....	84
4.2.4 Special case of a beam supported at distances α and β from each end ...	85
4.3 Shear lag.....	86
4.3.1 Derivation of adhesive shear stresses and web bending stresses.....	91
4.3.2 Stress ratio and effective width.....	92
4.4 Buckling	94
4.4.1 Overall buckling	94
4.4.2 Introduction of web stiffeners.....	102
4.4.3 The need for finite element modelling and physical testing and large factors of safety	102
4.4.4 Limitations of this thesis with regard to buckling analysis.....	104
4.4.5 Finite element buckling analysis	104
5 NUMERICAL IMPLEMENTATION OF COMPOSITE BENDING EQUATION AND FINITE ELEMENT ANALYSIS.....	108
5.1 Numerical implementation of composite bending equation.....	108
5.1.1 How many Fourier terms to use?	108
5.1.2 Variation of joint thickness and adhesive shear modulus.....	110
5.1.3 The concept of the composite constant.....	111
5.1.4 Effect of span	112
5.1.5 Position of the neutral axis.....	112
5.1.6 Adhesive shear distribution and the effect of overhangs	114
5.1.7 Multiple spans	115
5.1.8 Design charts.....	116
5.2 Finite element modelling.....	119
5.2.1 Finite element modelling to validate the algebraic model	119

The Structural Performance Of Glass-Adhesive T-beams

5.2.2 Three dimensional distribution of stresses within the adhesive joint	120
6 NUMERICAL IMPLEMENTATION OF SHEAR LAG EQUATION AND FINITE ELEMENT ANALYSIS	125
6.1 Numerical implementation of shear lag equation	125
6.1.1 How many Fourier terms to use?	125
6.1.2 The effect of load distribution	126
6.1.3 Modifying the joint stiffness	128
6.1.4 Effects of modifying span	130
6.1.5 Effects of modifying the depth of the web	131
6.1.6 Effects of modifying the width off the flange	131
6.1.7 Effects of modifying the depth of the flange	132
6.1.8 Simplified calculation of stresses ratio	132
6.2 Finite element validation of algebraic model	133
6.2.1 Uniformly distributed load cases	134
6.2.2 The three point bending cases	135
7 NUMERICAL IMPLEMENTATION OF BUCKLING EQUATIONS AND FINITE ELEMENT ANALYSIS	138
7.1 Algebraic models	138
7.2 Eigen value finite element problem	140
7.2.1 The case of three half waves	144
7.2.2 The cases of four and five half waves	144
7.2.3 Non-linear geometry finite element problem	144
7.2.4 Discussion of the various buckling models	146
8 EXPERIMENTAL WORK	147
8.1 Introduction	147
8.1.1 Basic beam types	148
8.1.2 Support arrangements	149
8.1.3 Loading arrangements	150
8.1.4 Instrumentation	153
8.1.5 Sequence of events for beam fabrication process	155
8.1.6 Safety issues	158

The Structural Performance Of Glass-Adhesive T-beams

8.2 Short term static testing	159
8.2.1 Basic three point and six point bending tests	159
8.2.2 Shear lag tests	159
8.3 Cyclic testing	160
8.4 Buckling	163
9 RESULTS AND DISCUSSION	165
9.1 Composite bending.....	166
9.1.1 Type 1 beams	166
9.1.2 Type two beams	168
9.2 Shear lag effects.....	171
9.3 Cyclic testing	176
9.4 Buckling	183
10 CONCLUSIONS	186
11 FURTHER WORK.....	189
12 REFERENCES.....	191
13 APPENDIX A	201
13.1 Testing of aluminium-polyamide composite cladding sections	201
13.1.1 Results	202
13.1.2 Conclusion	202
14 APPENDIX B	203
14.1 Derivation of Equation 4-14.....	203

Index of figures

Figure 1.1 An early stained glass window formed from very small cast glass plates and held together with lead strips.....20

Figure 1.2 The Crystal Palace.20

Figure 1.3 The glass walls of the Sydney Opera House.....22

Figure 1.4 The glass plates in the Serres at La Villette carry loads in plane as well as wind loads perpendicular to the plate.....22

Figure 1.5 Glass entrance canopy to the Tokyo underground23

Figure 1.6 A cantilevered glass staircase at the Pilkington research and development headquarters in Lathom.....23

Figure 1.7 Proposed Millennium sculpture at the entrance to the NEC23

Figure 1.8 Pedestrian bridge at the Science Museum23

Figure 1.9 Root of an adhesive laminated helicopter blade25

Figure 1.10 Modern cars use adhesives for making many important structural joints.....25

Figure 2.1 Stress strain plots to failure for steel, glass and timber26

Figure 2.2 Surface damage on a plate of glass26

Figure 2.3 Stress trajectories at the tip of a flaw27

Figure 2.4 Typical fracture pattern of annealed glass29

Figure 2.5 Summary of principal stress distributions in a plate of toughened glass30

Figure 2.6 Typical fracture pattern of toughened glass.31

Figure 2.7 Toughening may impart a wave profile to the glass.....32

Figure 2.8 Typical stress distribution across a plate of chemically toughened glass35

Figure 2.9 Five layer model of an adhesive joint38

Figure 2.10 Classification of failure modes for adhesive joints38

Figure 2.11 Seven layer model of an adhesive joint38

Figure 2.12 Adhesive joints may be required to resist a variety of stresses.45

Figure 2.13 F18 wing to fuselage attachment.45

Figure 2.14 Distribution of principal stresses in a simple lap joint subject to shear45

Figure 2.15 Stress distribution in a simple butt joint subject to tension.....45

The Structural Performance Of Glass-Adhesive T-beams

Figure 2.16 The behaviour of a simple lap joint in shear	46
Figure 2.17 Modelling small scale geometry tends to reduce artificial stress concentrations in finite element modelling	46
Figure 2.18 The SH&G building, Detroit	48
Figure 2.19 The napkin ring test.....	53
Figure 2.20 The thick adherend shear test	53
Figure 2.21 Assembly of samples for the thick adherend shear test	53
Figure 3.1 Typical support systems for glass plates	54
Figure 3.2 Arrangement of four point bending tests on toughened glass	55
Figure 3.3 Three support conditions evaluated in the four point bending tests	56
Figure 3.4 Graphical summary of results for four point bending tests.....	57
Figure 3.5 Glass shear failures.....	58
Figure 3.6 Mohr circle approach to shear failure	58
Figure 3.7 Resultant tensile stress approach to shear failure.....	60
Figure 3.8 Punching shear tests on square glass plates.....	60
Figure 3.9 Distribution of failure loads	62
Figure 3.10 Typical failure patterns	62
Figure 3.11 Finite element mesh with boundary conditions for model of punching shear tests.	63
Figure 3.12 Principal stresses obtained from the axisymmetric FE model.....	64
Figure 3.13 Construction of a pressure sensitive adhesive / structural bonding tape.	67
Figure 3.14 EPX mixer applicator nozzle used for DP 190.....	67
Figure 3.15 Measurement of adhesive slip using the Wallace light extensometer.....	71
Figure 3.16 Measurement of adhesive slip using displacement transducers.....	72
Figure 3.17 Typical failure of DP 190 and 2216 shear specimens.....	73
Figure 3.18 Stress-strain plots for DP 190 and 2216, method one	74
Figure 3.19 Stress-strain plots for DP 190, method two	74
Figure 3.20 Stress-strain plots for 2216, method two	75
Figure 4.1 Sign conventions.....	79
Figure 4.2 Principles of composite action	80
Figure 4.3 Stresses, moments and forces in an idealised composite section	81

The Structural Performance Of Glass-Adhesive T-beams

Figure 4.4 Shear deflection in a small beam element	84
Figure 4.5 A simply supported beam with cantilevered ends	85
Figure 4.6 Typical distribution of bending stresses across a wide flanged beam.....	86
Figure 4.7 The Sainsbury Centre.....	86
Figure 4.8 Origin and orientation of axis used in the solution of the shear lag problem..	88
Figure 4.9 Adhesive shear in the web of the composite T-section	90
Figure 4.10 Overall buckling and local buckling of a channel section	94
Figure 4.11 Various buckling modes for a T-beam	95
Figure 4.12 Simplified models for web buckling	97
Figure 4.13 Calculation of m for complex bending moment distributions	97
Figure 4.14 Effect of imperfections on buckling loads	99
Figure 4.15 Solution of simplified model for the simply supported top edge condition	100
Figure 4.16 Solution of simplified model for elastically supported top edge condition.	100
Figure 4.17 Solution of simplified model for fixed top edge condition	100
Figure 4.18 Eigen value and non-linear geometry FE analyses	103
Figure 4.19 Tangent stiffness K_T	106
Figure 4.20 Incremental drift.....	106
Figure 4.21 Newton Raphson convergence	107
Figure 4.22 Modified Newton Raphson convergence	107
Figure 5.1 Standard beam sections.....	109
Figure 5.2 Standard UDL and three point bending arrangements	109
Figure 5.3 The effect of the composite constant on the degree of composite action	112
Figure 5.4 The effect of the span on the degree of composite action.....	113
Figure 5.5 Standard section with a 30 mm wide joint	113
Figure 5.6 Adhesive shear stress distribution	114
Figure 5.7 Maximum glass stresses	116
Figure 5.8 Adhesive stress distribution.....	116
Figure 5.9 Design chart for a simply supported beam carrying a UDL	118
Figure 5.10 Design charts for a simply supported beam carrying a UDL.....	118
Figure 5.11 Finite element mesh with boundary conditions for a standard beam carrying a 2.5 kN/m UDL over a 5 m span with two 100 mm overhangs.....	119

The Structural Performance Of Glass-Adhesive T-beams

Figure 5.12 Distribution of adhesive shear stresses	120
Figure 5.13 The three models used to evaluate the stress distribution within the adhesive joint.....	122
Figure 5.14 A refined version of the model two mesh.....	123
Figure 5.15 Shear stress plots at the location of peak average stress.....	124
Figure 6.1 Comparison of the distribution of stress in the flange under uniformly distributed loading and three point bending.....	127
Figure 6.2 Comparison of the stress ratios for uniformly distributed loading and three point bending.	127
Figure 6.3 The effect of span upon shear lag	129
Figure 6.4 Comparison of three shear lag theories	129
Figure 6.5 The effect of span upon shear lag	130
Figure 6.6 The effect of web depth upon shear lag	132
Figure 6.7 The effect of flange depth upon shear lag	132
Figure 6.8 Mesh and boundary conditions for standard beam.....	134
Figure 6.9 Mesh and boundary conditions for wide standard beam.	134
Figure 6.10 Distribution of bending stresses in the standard beam section subject to a uniformly distributed load according Song, modified Song and finite element analysis	135
Figure 6.11 Distribution of bending stresses in the wide standard beam section subject to a uniformly distributed load according Song, modified Song and finite element analysis	135
Figure 6.12 Distribution of bending stresses in the standard beam section subject to three point bending according Song, modified Song and finite element analysis	136
Figure 6.13 Distribution of bending stresses in the wide standard beam section subject to three point bending according Song, modified Song and finite element analysis ..	136
Figure 7.1 Beam and loading arrangement for buckling work.....	138
Figure 7.2 Finite elements models with boundary conditions for eigen value analyses .	141
Figure 7.3 Mode shapes for the first three buckled modes of model 1.....	141
Figure 7.4 Mode shapes for the first three buckled modes of model 2.....	142
Figure 7.5 Mode shapes for the first three buckled modes of model 3.....	142

The Structural Performance Of Glass-Adhesive T-beams

Figure 7.6 Typical shell mesh, half model.....	143
Figure 7.7 First eigen buckling mode for shell model.....	143
Figure 7.8 Convergence path for non-linear finite element solution with 0.2% destabilising load.....	145
Figure 7.9 Time deflection plot for non-linear finite element solution with 0.2% destabilising load.....	145
Figure 7.10 Plan view of buckled web, non-linear finite element analysis.	146
Figure 7.11 Elevation of buckled web, non-linear finite element analysis.....	146
Figure 8.1 Beam types and loading arrangements for test work	148
Figure 8.2 Potential application of type 1 beams.....	149
Figure 8.3 Cross section detail of web patch plates.....	150
Figure 8.4 Web patch plates.....	150
Figure 8.5 The influence of usage on load distribution.....	151
Figure 8.6 Load arrangement 1	152
Figure 8.7 Load arrangement 2	152
Figure 8.9 Load arrangement 3	153
Figure 8.10 Original beam fabrication setup	158
Figure 9.1 Load deflection plot for beams 1 to 3	166
Figure 9.2 Failure origin test 1	167
Figure 9.3 Region of poorly mixed/cured adhesive, beam 2	167
Figure 9.4 Illustration of the inherent flaw in the support arrangements for beams 1, 2 and 3.....	167
Figure 9.5 Beam 2, as the fracture front moved into the region of properly cured adhesive the failure mode became one of glass plucking.	167
Figure 9.6 Load deflection plot for beams 4, 5 and 8.....	168
Figure 9.7 Midspan stress distribution in the webs of tested beams	169
Figure 9.8 Position of neutral axis test 2 to 8	170
Figure 9.9 Load deflection plot for beams 5 to 8	171
Figure 9.10 Shear lag in laboratory beam tests according to algebraic theory.....	172
Figure 9.11 Stress ratio for laboratory beam tests according to algebraic theory	172
Figure 9.12 Finite element mesh for laboratory beam models.....	173

The Structural Performance Of Glass-Adhesive T-beams

Figure 9.13 Longitudinal stress distribution in the flange	174
Figure 9.14 Explanation of the rocking behaviour observed in test15	174
Figure 9.15 Summary of results for longitudinal stress distribution in flange of laboratory beams	175
Figure 9.16 Load displacement plot for test 10.....	178
Figure 9.17 Load stress plot for test 10.....	178
Figure 9.18 Load displacement plot for test 15.....	179
Figure 9.19 Load stress plot for test 15.....	179
Figure 9.20 Load displacement plot for test 19.....	180
Figure 9.21 Load stress plot for test 19.....	180
Figure 9.22 Top of flange after de-bond of tension plate.	181
Figure 9.23 Top of flange after de-bond of tension plate (adhesive removed).	181
Figure 9.24 Load displacement plot for test 7.....	182
Figure 9.25 Load stress plot for test 7.....	182
Figure 9.26 Unusual fracture mechanism in highly stressed web glass.....	184
Figure 11.1 Potential redundancy mechansim in laminated T-beams	190
Figure 11.2 Potential rotation of the adhesive joint in T-beams subject to non-symmetric loading.....	190
Figure 13.1 Briggs Amasco aluminium-polyamide composite cladding section	201
Figure 13.2 Heuck aluminium-polyamide composite cladding section.....	201

Index of tables

Table 2.1 Extract from ASTM C 1048..... 33

Table 2.2 Flatness of Pilkington Architectural toughened glass plates..... 33

Table 2.3 Structural applications of adhesives 42

Table 2.4 Summary of different adhesive types..... 43

Table 2.5 Predictions of joint strength..... 47

Table 2.6 Summary of codified test procedures for adhesives and adhesive bonded joints
..... 51

Table 3.1 Summary of loading rates and average failure loads for punching tests on thin
glass plates..... 61

Table 3.2 Summary of predicted failure loads for glass plates in punching shear 63

Table 3.3 Published shear strengths of DP 190, 2216 and 9245 67

Table 3.4 Overlap shear strengths for 2216 after environmental ageing..... 68

Table 3.5 Summary of failure loads for thick adherend lap specimens tested in shear. ... 73

Table 3.6 Summary of long term tests on DP 190 and 2216. 78

Table 5.1 Number of Fourier terms needed converge solutions to composite bending
problems..... 109

Table 5.2 Variation in percentage composite action with varying t and G_a 110

Table 5.3 Summary of maximum stresses in three beam sections used over a 5 m simply
supported span to carry a 2.5 kN/m UDL..... 113

Table 5.4 Summary of maximum stress values and locations from Figure 5.6 115

Table 5.5 Summary of midspan deflections and stresses for the problem shown in Figure
5.11. 120

Table 5.6 Summary of material constants used in the finite element analysis of the
adhesive joint..... 121

Table 5.7 Summary of the results for the models shown in Figure 5.13..... 122

Table 6.1 Number of Fourier terms required to converge solutions to composite shear
lag equation 125

Table 7.1 Summary of buckling loads and modes for the all-glass T-beam. 143

The Structural Performance Of Glass-Adhesive T-beams

Table 8.1 Summary of test programme.....	154
Table 9.1 Summary of the basic test results.....	165
Table 9.2 Summary of peak stresses for different loading arrangements and different loading arrangements	177
Table 13.1 Section properties of composite cladding sections.....	202

The Structural Performance Of Glass-Adhesive T-beams

Notation

Co-ordinates

- x span
- y perpendicular to span in plane of flange
- z perpendicular to span in plane of web

Dimensions

- i indicates a subscript, see Page 17
- A area
- b breadth
- d overall depth of T-section
- e eccentricity = $\frac{d - h_f}{2}$
- h height
- hb_f flange outstand (half breadth of flange) = $\frac{b_f - b_w}{2}$
- I second moment of area
- L span
- t_a thickness of adhesive
- w_a width of adhesive

Material properties

- E elastic modulus
- G shear modulus
- ν Poisson ratio

The Structural Performance Of Glass-Adhesive T-beams

Constants

$$\alpha = \frac{n\pi}{L}$$

A_n Fourier term used in the solution of the shear lag equations

B_n Fourier term used to describe load distribution

$$c = \frac{\cosh \alpha y}{\cosh \alpha h_b}$$

c_1, c_2, \dots general unknown constants

C composite constant

$$D \text{ plate constant} = \frac{Eh^3}{12(1-\nu^2)}$$

f_n Fourier term used in stress function

J torsional constant

K buckling factor

m equivalent uniform moment factor

n number of half waves (buckling) or index to Fourier series (composite bending and shear lag)

r torsional rigidity of support condition

S bending stiffness = EI

$$t = \tanh \alpha h_b$$

ξ length of overhang at left hand end of beam

ζ length of overhang at right hand end of beam

Forces, stresses and strains

ϵ direct strain

F direct force

ϕ stress function

γ shear strain

M moment

The Structural Performance Of Glass-Adhesive T-beams

M_{cr}	buckling moment
q	shear flow
T	shear force
s	adhesive slip
SR	stress ratio
σ	direct stress
τ	shear stress

Subscripts

a	adhesive
b	bottom section
bb	bottom of the bottom section
bt	top of the bottom section
C	according to composite theory
f	flange
g	glass
l	equivalent layered section
m	equivalent monolithic section
n	index to Fourier series
SL	according to shear lag theory
t	top section
tb	bottom of the top section
tt	top of the top section
w	web

Synopsis

It is proposed that flat architectural glass plates may be joined using a structural adhesive to form a beam with a T-shaped cross-section. In contrast to existing forms of glass construction such beams have the potential to carry high loads over long spans with minimal deflection.

It is shown that toughened glass is appropriate for the construction of glass T-beams. The selection of an adhesive for this work is shown to be principally dependent upon shear modulus and not shear strength. Three adhesives are initially selected and are evaluated by physical testing. One is chosen for use in the construction of full-scale glass-adhesive T-beams.

An equation based upon linear elastic bending theory is developed to describe the behaviour of the glass-adhesive-glass composite. This equation forms the basis for a scoping study to investigate the effects of joint geometry and adhesive shear modulus. Adhesive stresses are determined using this theory and from three-dimensional finite element models.

The shear lag in the flange of composite T-beams is described by a modified form of the Song shear lag equation, Song (1984). The results from this are compared with those obtained from a three-dimensional finite element model.

Overall buckling of the web is investigated. It is proposed that the buckling load may be evaluated by using the plate stability equation and by treating the web as an isolated plate with suitable boundary conditions. These results are compared with those obtained using a three-dimensional finite element eigen-value buckling analysis and a three-dimensional non-linear finite element buckling analysis.

The Structural Performance Of Glass-Adhesive T-beams

Ten glass-adhesive beams have been constructed and tested. The results are shown to correlate well with the theories that are presented to describe composite bending, shear lag and buckling. The behaviour of the beams under long term loading has been established by tests on the adhesive. Finally, it is shown that the glass-adhesive beams are able to sustain repeated loading without suffering cyclic fatigue.

1 INTRODUCTION

Structural engineers would have little interest in glass if it were not transparent. Despite having a high theoretical tensile strength the glass products used in the building industry are both weak and brittle. However, its ability to transmit light and heat has made it an important part of the building fabric.

The earliest window glass was formed from small cast glass plates that were held together with lead strips, Figure 1.1. The Crown glass process which was introduced circa 1330 allowed the production of rectangular plate up to 0.75 m by 0.5 m. By the 1830's Bicheroux and the Pittsburgh Plate Glass Company had independently developed methods of continuously casting glass. It was this development in mass production that enabled the construction of the Crystal Palace, London, in 1851. The race was on to build bigger and better. Glass was good and the aesthetic results were beyond comparison, Figure 1.2.



Figure 1.1 (Left) An early stained glass window formed from very small cast glass plates and held together with lead strips

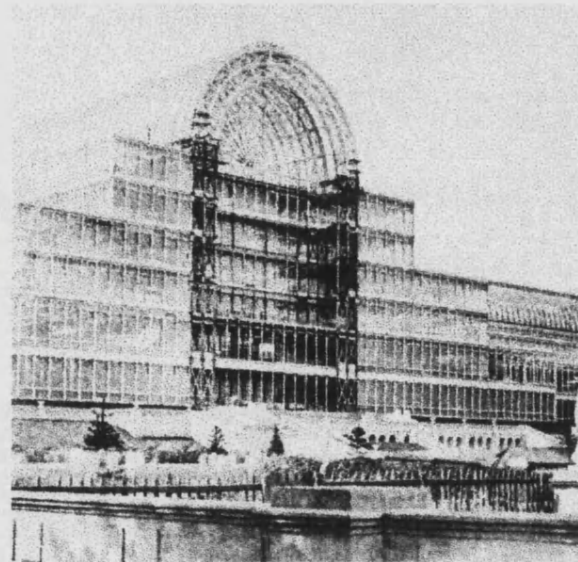


Figure 1.2 The Crystal Palace, 1851.

In 1959 Pilkington Brothers Ltd. presented the float glass process that revolutionised glass production. It produces perfectly flat glass of constant thickness, combining the quality of polished glass with the manufacturing speed and economy of continuously cast plate. In the first part of the process a continuous ribbon of glass is cast. It is then passed across a bed of molten tin during which both surfaces are fire polished. This gives the surface its perfectly flat, parallel, polished finish. Glass was now an affordable material, which could be used in all buildings. Its ability to sustain wind loading in large glazed openings was primarily determined by experiment and experience. This information was made available by the glass manufacturers and its design was the realm of the architect.

The super-glazed openings that were pioneered in the 1970's brought the design of glass to the field of the structural engineer. The glass walls of the Sydney Opera House were constructed between 1970 and 1972 and used glass plates up to 4 m by 2.1 m, Figure 1.3. By the time the Sainsbury Centre was built in 1978 glass plates of 10 m were being used and had to be stabilised by glass fins perpendicular to the facade, (see Figure 4.7, Section 4.3.) It was now necessary to consider the potential buckling of the glass web. Glass had definitely become the concern of the structural engineer.

The glass Serres at La Villette, 1984, were landmark structures, Figure 1.4. The glass was no longer supported along its edges but was carried by a system of articulated bolts. Furthermore the glass facade not only carried the wind load but also carried load in the plane of the glass. Each plate of glass was supported by the plate immediately above it. Redundancy in the structure was critical. The consequence of breakage in each plate was considered and ultimately the whole system was tested in a series of full-scale tests, Dutton and Rice (1995).

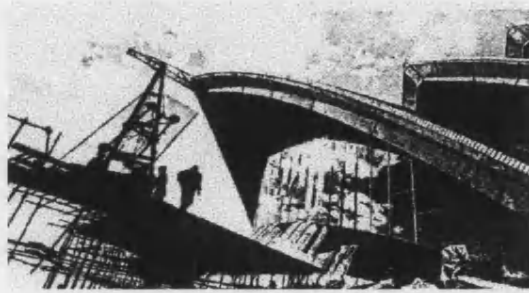
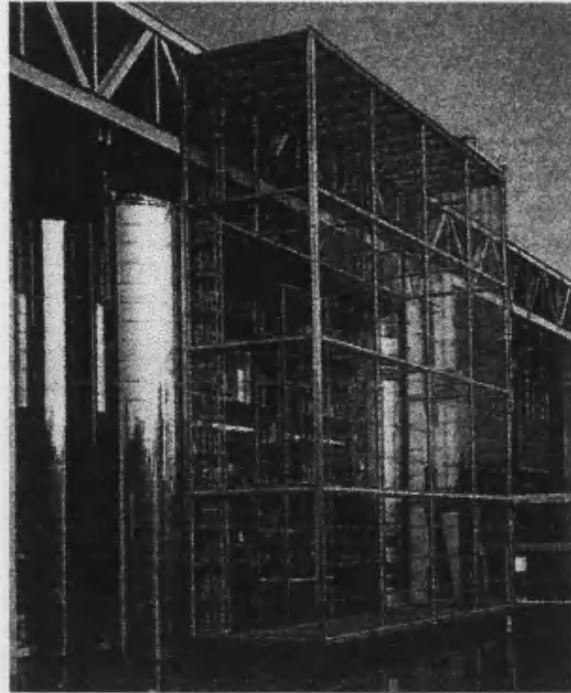


Figure 1.3 (Above) The glass walls of the Sydney Opera house were one of the largest glazed openings when completed in 1972.

Figure 1.4 (Right) The glass plates in the Serres at La Villette carry loads in plane as well as wind loads perpendicular to the plate.



In the latter half of the 1980's and throughout the 1990's glass has been used as structure in places other than the facade. In the United Kingdom much of this work has been pioneered by Tim Macfarlane of Dewhurst Macfarlane (engineers), whilst in mainland Europe much work has been done by Mick Eekhout. Glass canopies, bridges, staircases and sculptures have now become a common part of showcase architecture, Figures 1.5 to 1.8.

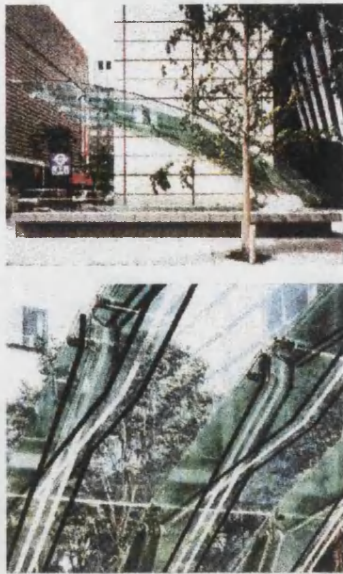


Figure 1.5 (Top) Glass entrance canopy to the Tokyo underground, Tim Macfarlane, Dewhurst Macfarlane, 1997. (Above) Detail.



Figure 1.6 A cantilevered glass staircase at the Pilkington research and development headquarters in Lathom, John Colvin, Pilkington Architectural, 1996.

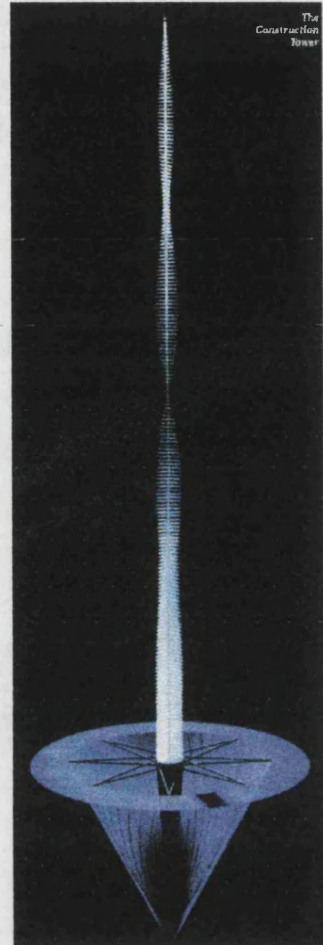


Figure 1.7 (Above) Proposed Millennium sculpture at the entrance to the NEC, Birmingham, Tim Macfarlane, Dewhurst Macfarlane, 1997.

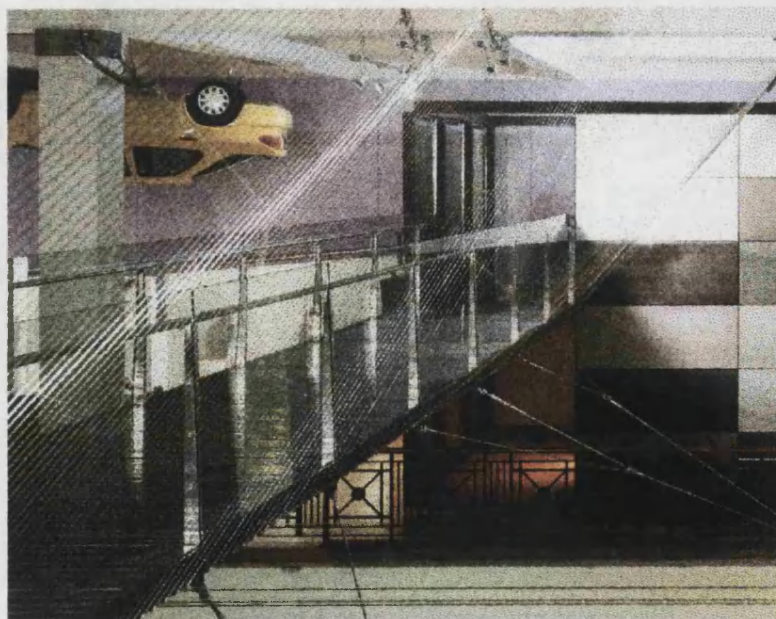


Figure 1.8 (Left) Pedestrian bridge at the Science Museum, London, Bryn Bird, Whitby and Bird 1997.

At present the design of glass structures is limited by two concerns. Firstly, stress concentrations around mechanical connections often result in the use of excessively thick glass or very large connections. Secondly, the majority of glass used in these structures is thin plate glass that is inherently flexible. In order to minimise deflections, spans must be short and loads must be small. Whilst thicker glass may be used, glass thicker than 15 mm tends to become uneconomical in cost and weight. Furthermore, small spans increase the number of mechanical connections. Not only does this dramatically increase the cost of the structure but it often detracts from the aesthetic being pursued by the architect.

It is a primary aim of this work to demonstrate that it is possible to construct stiff beam sections out of plate glass. Potential beam sections include T, I, Π and box sections although only T-beams will be considered in this work. This is because the T-section involves only a single joint between two plates. This simplifies both fabrication and analysis.

There are three potential methods of making a glass T-beam. These are; extruding the complete section, sintering (glass welding) the two plates or using a structural adhesive. For reasons of increased strength and ensuring that the glass breaks in a safe manner, structural glass is often toughened. This involves setting up beneficial residual stresses within the glass, see Section 2.1.2. However, only flat glass can be successfully toughened and toughening an extruded T-beam is not an option. Sintering toughened glass is not likely to be successful either because in heating the glass to the high temperature needed for sintering, the residual stresses set-up during the toughening process are redistributed. Therefore, the only option left is to bond the two plates using a structural adhesive.

The first use of structural adhesives began with the construction of timber fabric aircraft. To those early pioneers today's adhesives would be unrecognisable. However, it is still the aeronautical industry that leads the way in this field. The bonding of wings onto the

fuselage and the bonded construction of helicopter rotor blades are established methods of construction, Figure 1.9. In the automotive industry bonding of body panels is already established whilst the bonding of more major structural components such as suspension systems and roof columns are becoming accepted, Figure 1.10. It is the confidence which has been developed in these industries that has led the author to believe that it may be possible to realise the glass-adhesive T-beam.

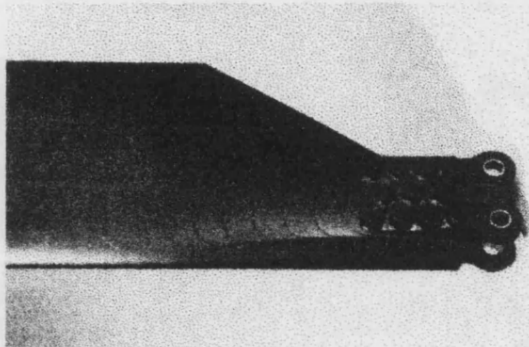


Figure 1.9 The root of this laminated helicopter blade can only be made by using adhesives to achieve the contoured profile from the main part of the blade to the bolt head.

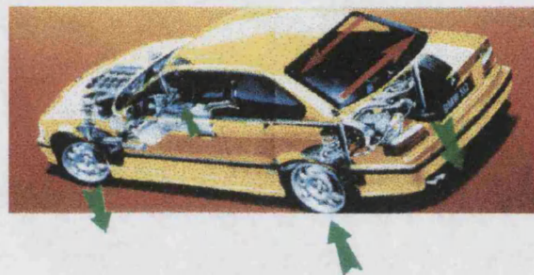


Figure 1.10 Modern cars use adhesives for making many important structural joints.

What unites both glass and adhesive is the general reluctance with which both are accepted as engineering materials by structural engineers. It is hoped that this work may go some way to redress this issue.

2 LITERATURE REVIEW

2.1 Glass

2.1.1 Fracture mechanics

Glass is a perfectly linear elastic material which displays no plastic deformation at failure, Figure 2.1. Therefore it should be possible to determine its strength from the strength of the interatomic bonding forces, Broek (1978). Estimates put this between $11 \times 10^3 \text{ N/mm}^2$ and $40 \times 10^3 \text{ N/mm}^2$, Gordon (1976) and Swedish Council for Building Research (1993). However, the strength of commercial plate glass is more likely to be between 20 N/mm^2 and 100 N/mm^2 , Sedlacek et al (1995). The cause of this discrepancy is small flaws which cover the surface of the glass Figure 2.2. These accumulate during production and subsequent handling and are called Griffith flaws after the man who first proposed their existence, Griffith (1921). In contrast the core of the glass is likely to be flaw free.

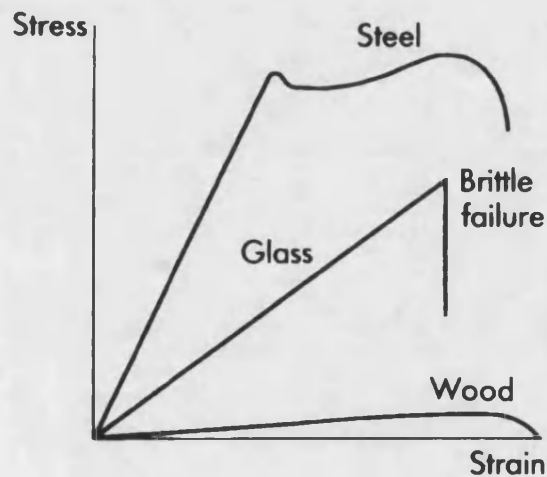


Figure 2.1 (Above) Stress strain plots to failure. Button and Pye (1993)

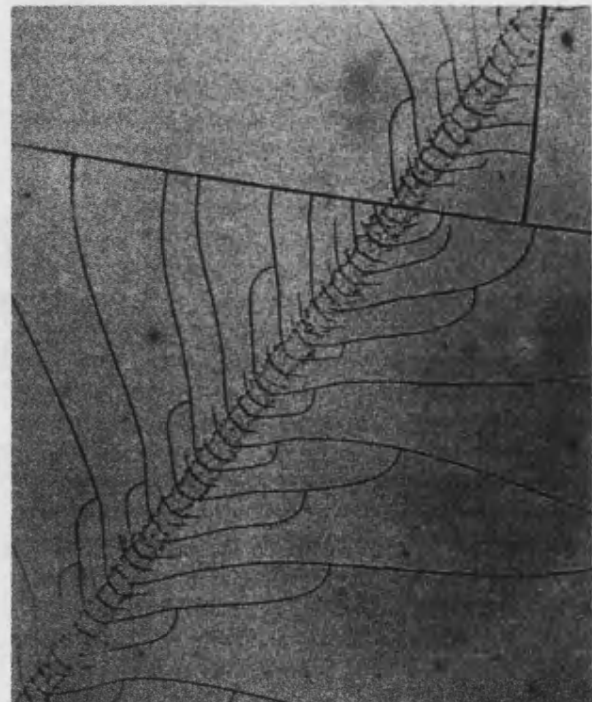


Figure 2.2 (Right) Surface damage on a plate of glass. Gordon (1976).

It is because glass has no ability to yield that stress concentrations are so critical, Figure 2.3. An elliptical crack of length l with a crack tip radius R will magnify the applied stress by a factor K ;

$$K = 2\sqrt{\frac{l}{R}}$$

In practice R is likely to have a value comparable to atomic dimensions; say one Ångström unit (10^{-10} m). Therefore a crack length of one micron will result in a stress magnification of;

$$K = 2\sqrt{\frac{10^{-6}}{10^{-10}}} = 200$$

If the strength of the glass is 20×10^3 N/mm² then an applied stress of 100 N/mm² would cause failure.

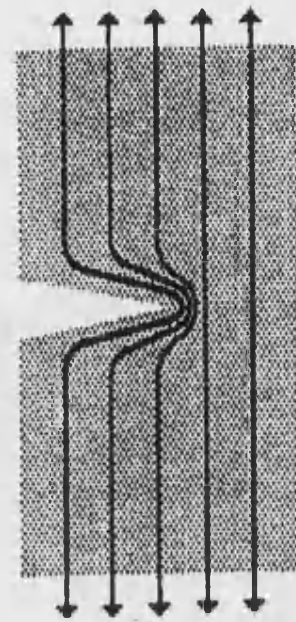


Figure 2.3 Stress trajectories at the tip of a flaw. Gordon (1976).

The random size and distribution of the Griffith flaws causes a wide variation in the observed strength of glass. When a large number of nominally identical samples are broken the results are often fitted to either a normal distribution curve or a Weibull distribution curve, Behr et al (1991) and Weibull (1939). Therefore, whilst we may be 90 percent sure that 95 percent of the samples will not fail below x N/mm² it is never possible to be 100 percent sure that 100 percent of the samples will not fail.

As surface damage accumulates during the life of the glass its strength will decrease. Even after installation damage continues to accumulate because of cleaning and exposure to the environment. Fortunately, this decrease in strength reaches a virtually stable condition, Button and Pye (1993). However, it is important that this is borne in mind if laboratory results obtained using fresh glass are to be used as a basis for design guidance.

The occurrence of a major flaw is not in itself enough to cause failure; a critical combination of stress and flaw must exist, Griffith (1921). Equally failure will rarely originate at the point of highest tensile stress, Sedlacek et al (1995). Therefore glass

strength is also a function of stress distribution and glass area. That is, the larger the plate the greater the probability that it will contain a particularly severe flaw and if the plate is uniformly stressed the greater the chance that the flaw will be critically stressed.

The strength of glass decreases in the presence of water. Baker and Preston (1946a) found that glass was 20 percent stronger when dry than wet. Charles (1958a) investigated how water vapour corrosion of soda-lime glass affected the time dependence of the rupture strength. He concluded that surface flaws could grow by corrosive mechanisms brought about by a reaction of water vapour in the atmosphere with the glass. Wiederhorn (1967) found that crack velocities were also affected by the concentration of water vapour in the atmosphere.

Whilst strength is likely to be affected by extremes of temperature the author is not aware of any work which addresses the variation in strength brought about within the normal operating temperatures of architectural glass.

The duration of loading is known to affect the strength of glass. Baker and Preston (1946b) showed a three fold decrease in strength between glass rods loaded for 0.01 seconds and those loaded for 24 hours. It was noted that the time dependence was a function of the medium in which the glass was tested and that in the case of a vacuum there was no time dependency. They concluded that the time dependency was related to the presence of water vapour which was able to attack the glass's structure at the crack tip. This has become known as static fatigue and design codes impose a major reduction in strength to account for it. The draft Eurocode, "The design of glass panes," CEN (1996a), reduces the long term strength of glass to 37.5 per cent of its short term strength. The Swedish Council for Building Research (1993) recommend that stresses should be maintained below 8 to 9 N/mm² for medium and long term loading.

2.1.2 Glass types

Nearly all building glass is the soda lime silicate type. It is transparent, durable and cheap. Its basic constitution varies very little between different manufactures, McCann (1982), Button and Pye (1993), Swedish Council for Building Research (1993), but there are many ways in which the basic product may be processed to give enhanced properties.

In considering the choice of glass for the construction of a structural glass beam the basic choice is between annealed and toughened glass. Annealed glass tends to be produced by the float process and as part of that process it is heat treated to reduce any residual stresses, Shand (1958). It is mass produced and is cheap although it is relatively weak and will break in a dangerous manner Figure 2.4.



Figure 2.4 Annealed glass breaks into large dagger-like fragments

Toughened glass is annealed glass which has been through a second thermal process during which beneficial residual stresses are set up, Gardon (1980). The glass is uniformly heated to a temperature above its glass transition temperature. In its semi-molten state any stresses which were locked into the glass are released. The glass is then air quenched. As the glass cools the outer layers solidify first and as the molten core continues to cool and contract the glass in the outer surfaces is pulled into compression. The resulting stress distributions at various locations across the plate are indicated in Figure 2.5, Laufs (1998).

The tensile stresses in the core of the toughened glass plate do not cause failure as this region is free of Griffith flaws. In order to break the plate it will generally be necessary to propagate one of the surface flaws. However, the residual stresses have effectively increased the strength of the glass by an amount equal to the surface compression. Only

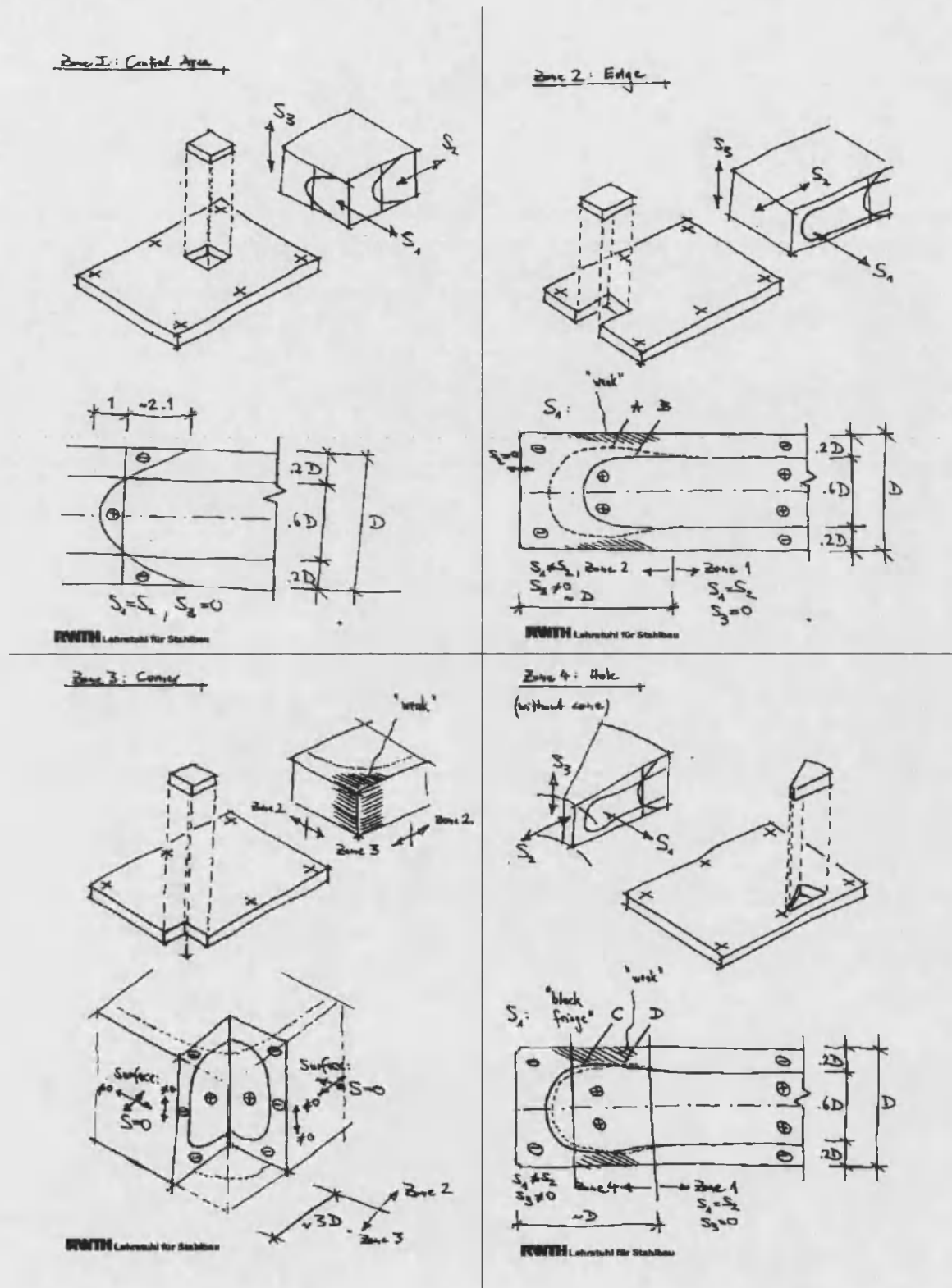


Figure 2.5 Summary of principal stress distributions in different locations of a toughened glass plate.

once a flaw is critically stressed will it extend into the tensile zone, in the core of the plate. The stored energy which is then released propagates the crack front and causes it to bifurcate at some critical velocity. This process continues resulting in the fracture pattern shown in Figure 2.6. The glass dice which are formed in this process are small and tend to have blunt edges and for this reason toughened glass is often used as a safety glass, BS (1991) and Reid (1985.) One consequence of this fracture mechanism is that glass cannot be cut or drilled after it has been toughened.

An important quality of toughened glass is that the residual stresses do not decrease with time, Sedlacek (1995).

Therefore, if the natural strength of the glass is ignored and only the component resulting from the surface compression is taken into account we have a very dependable engineering material. This may be considered as similar to the way in which we design reinforced concrete. Toughened glass is still brittle and will fail without warning if over stressed. However, unlike annealed glass it is not necessary to adopt a stochastic approach. Another benefit is that whilst the surface is in compression static fatigue cannot occur. Therefore, structures manufactured from toughened glass are able to carry high, long-term loads.

Relying on the surface compressive stress of toughened glass means that it is necessary to measure and specify this. In America minimum levels of surface compression are specified in ASTM C 1048-92 at 67 N/mm^2 , ASTM (1992). The equivalent British code

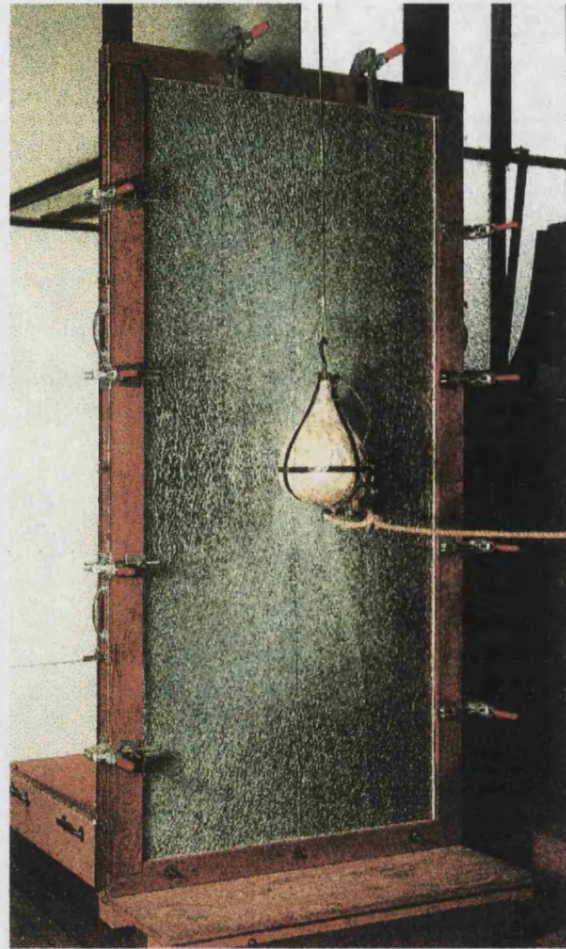


Figure 2.6 Typical fracture pattern of toughened glass.

is BS 6206 but this does not specify any minimum level, BS (1992). However, the proposed Euronorm prescribes a level of 100 N/mm^2 , CEN (1996b). Several methods are available for measuring the surface stresses. They rely on either the change in refractive index of the glass or the ability of the glass to bifurcate polarised light. Pilkington Glass achieve surface compressive stresses above 100 N/mm^2 , although they will not guarantee this, Pye (1996a). Saint Gobain will guarantee a minimum surface stress of 120 N/mm^2 for their toughened glass products, Pye (1998). Eekhout (1990) claims that surface stresses of up to 200 N/mm^2 may be achieved although Gardon (1980) suggests that this is unlikely unless liquids are used to quench the glass. However, it is likely that compressive stresses of up to 140 N/mm^2 are commonly achieved by many glass manufactures and tougheners.

One difficulty in toughening glass is that it can be particularly difficult to keep the glass plate flat. Although glass was originally hung during the toughening process it is now customary to support it on rollers, Flat Glass Marketing Association (1990). During the semi-molten state the glass starts to deflect under its own weight. This imparts a wave profile to the glass, Figure 2.7. Furthermore, if both faces of the glass are not cooled at identical rates the plate may develop an overall bow. ASTM C 1048-92 is the only international standard that addresses the flatness of toughened glass plates, Table 2.1. However, many glass tougheners achieve far higher tolerances. Table 2.2 shows the values that are published for Pilkington Architectural toughened glass plates, Pilkington (1995).

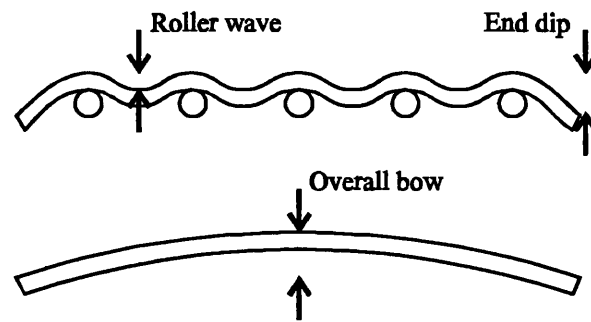


Figure 2.7 Toughening may impart a wave profile to the glass. Thin plates are particularly susceptible.

Flatness - Due to the nature of the process used in manufacturing tempered and heat-strengthened glasses, these glasses are not as flat as annealed glass. The deviation for flatness depends on thickness, width, length and other factors. Usually greater thicknesses yield flatter products.

Localised Warp - Localised warp for rectangular glass shall not exceed 1.6 mm over any 300 mm span. Localised warp for strips shall not exceed 2.4 mm over any 300 mm span.

Tong Kink - Any localised kink centred at any tong location shall not exceed 1.6 mm in a 50 mm span.

Overall Bow and warpage Tolerances - Overall bow and warpage tolerances shall not exceed the deviations shown below.

Glass Thickness mm	Warp Tolerance for Glass Dimension mm											
	0-460 mm	460- 910 mm	910- 1220 mm	1220- 1520 mm	1520- 1830 mm	1830- 2130 mm	2130- 2440 mm	2440- 2740 mm	2740- 3050 mm	3050- 3350 mm	3350- 3660 mm	3660- 3960 mm
3	3.2	4.8	7.1	9.5	12.7	15.9	19.0	22.2	25.4
4	3.2	4.8	7.1	9.5	12.7	15.9	19.0	22.2	25.4
5	3.2	4.8	7.1	9.5	12.7	15.9	19.0	22.2	25.4
6	1.6	3.2	4.8	7.1	9.5	12.7	15.9	19.0	22.2	25.4	28.6	31.8
8	1.6	2.4	4.0	5.6	7.1	8.7	11.1	14.3	17.5	20.6	23.8	27.0
10	1.6	2.4	3.2	4.8	6.4	7.9	9.5	12.7	15.9	19.0	22.2	25.4
12												
to 22	1.6	1.6	2.4	3.2	4.8	6.4	7.1	9.5	12.7	15.9	19.0	22.2

Table 2.1 Tolerance limits on flat glass plate according to ASTM C 1048-92.

Maximum roller wave depth	0.05 mm in 300 mm
Maximum edge dip	0.25 mm
Maximum bow	1.00 mm/m

Table 2.2 Published data from Pilkington Architectural concerning the flatness of their toughened glass plates.

Toughened glass has received much bad press because of nickel sulphide inclusions. This is a chemical inclusion which expands as it changes from its alpha phase to its beta phase. The localised stress concentration is often sufficient to cause spontaneous fracture and this has caused problems in many buildings across the whole world. Careful monitoring of the raw materials helps to minimise this problem, Pye (1995). In addition glass may be heat soaked. This involves heating the glass to a temperature of 290°C for approximately eight hours and this works because the alpha to beta conversion is accelerated in the presence of heat, Sedlacek (1995). Some success has also been obtained in using photographic methods to find the nickel sulphide inclusions, Ford (1997). In fact modern production methods have reduced the problem considerably and many suspected cases of nickel sulphide inclusion are often attributed to other causes after further investigation. In window glass a small chance of failure may be deemed acceptable but in structural applications measures must be taken to limit the effect of any failure. However, as failure may also arise from accidental impact or vandalism the designer should have already provided sufficient redundancy to cater for such breakage. Therefore the small potential of a nickel sulphide inclusion should not present a major problem.

Other alternative types of glass include heat strengthened glass. This has properties intermediate between annealed and toughened glass, CEN (1996c). The glass goes through the same toughening process as the toughened glass but the surface compression is limited to about 45 N/mm². When fractured the glass breaks into a number of moderately sized fragments which may have sharp dagger like edges. The only advantages of heat strengthened glass over toughened glass are that it is less prone to breakage from nickel sulphide inclusions, Sedlacek (1995) and that localised damage, such as a chipped edge, will not necessarily cause the spontaneous fracture of the whole plate. It should be noted that toughened glass and heat strengthened glass are referred to as fully tempered and partially tempered in America and Canada.

Glass may also be chemically toughened. In this process residual stresses are set up by a process of ion exchange, Bartholomew and Garfinkel (1980). However, the distribution

of residual stresses in chemically toughened glass are not appropriate for use in building structures as the compressive layer is too thin, Figure 2.8.

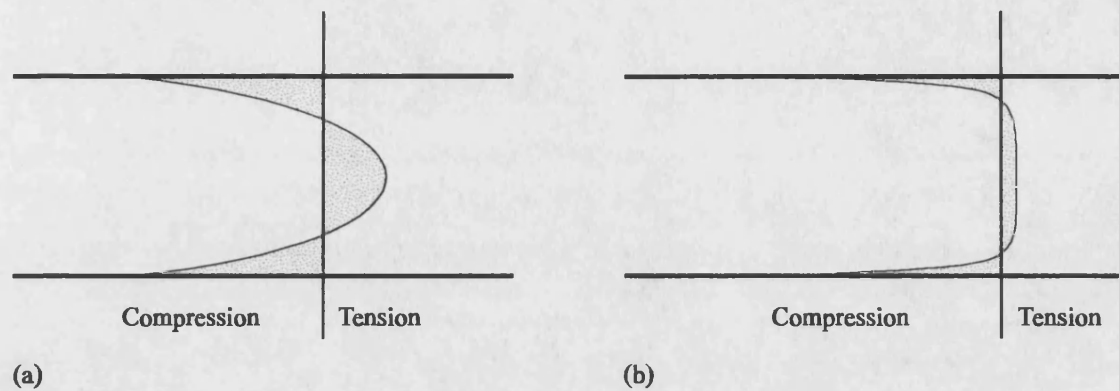


Figure 2.8 Typical stress distribution across a plate of (a) Thermally toughened glass, (b) Chemically toughened glass.

One remaining option is laminated glass. In fact this is not a different type of glass but is simply two or more plates of glass which have been bonded together using a thin adhesive interlayer. Therefore the properties of the laminate are dependent upon the glass plates that are laminated and the adhesive chosen to laminate them, CEN (1996d). The adhesive will either be an adhesive film, such as polyvinylbutyral (PVB), or a liquid resin. Under short term loading laminated glass behaves in a monolithic manner, Hooper (1972), Minor and Reznik (1990) and Behr et al (1993) and in the case where one or more plies of glass are broken the laminate will hold the broken fragments in place. In this sense laminating offers redundancy and reduces the risk of injury, Pantelides (1992) and Reid (1985). In practical structural applications laminating plays an important role, Friedland (1992), Dawson (1996) and Dawson (1997). However, laminating introduces analytical complications; particularly when medium and long term loads are applied. This is because laminated glass which has been loaded for a long period of time starts to behave in a layered manner as the adhesive interlayer begins to creep, Behr et al (1985). In order to simplify the analytical work in this thesis laminated glass has not been used. However, in practice it may be considered appropriate to manufacture glass-adhesive T-beams from laminated glass.

2.1.3 Choice of glass type

Toughened glass was chosen for this work for a variety of reasons. Its break-safe nature makes for safe laboratory practice and its strength allows the beam to be loaded to a higher load than would have been possible had other glass types been used. If the composite beam develops the full strength of the toughened glass the results obtained at lower loads can still be applied to glass beams manufactured from heat strengthened or annealed glass. In addition, whilst the imposed stresses remain below the level of the residual surface compression it is not necessary to adopt a fracture mechanics approach to the strength of the glass and the analytical work is thus simplified. Toughened glass is also more durable against impact loads and so is more likely to survive any knocks it receives whilst being stored and moved in the laboratory. In addition toughened glass can sustain higher bearing stresses and therefore the potential of failure at the support and loading conditions is reduced.

The main obstacle to the use of toughened glass is its lack of flatness and this has consequences upon the dimension of the adhesive joint. It is necessary to minimise the variation in thickness of the adhesive joint in order to limit stress concentrations within the adhesive. For a plate of given flatness the relative variation in thickness of the adhesive joint may only be decreased by increasing the overall thickness of the joint. However, there is a limited choice of gap filling adhesives, see next section, and it tends to be that the thicker a joint the weaker the bond, Harris and Fay (1992). Therefore if an adhesive can be found that will work in this scenario it should also be possible to use the same adhesive with annealed glass where it may also be possible to utilise a thinner joint.

2.2 Adhesives

Vinceti (1990) argues that science is concerned with understanding whilst engineering is concerned with knowledge. It would be possible to discuss both the science of adhesion and the engineering of adhesive joints. However, the science of adhesion is still in its infancy. Whilst there are several theories which explain how glue is able to form a strong bond between two dissimilar materials they are subject to frequent revision and qualification, Packham (1995). Despite this, engineers have developed the knowledge which has allowed them to bond wings onto aeroplanes and to stick cladding glass onto skyscrapers, Krieger (1986) and O'Connor (1988). It may be that future research will allow us to better understand the mechanics of adhesive bonds but at the moment the available theories do little to help the practising engineer. Therefore the work presented here concentrates upon the engineers' approach to the design of adhesive joints.

2.2.1 Terminology

Figure 2.9 shows a simple five layer model of an adhesive joint. The components being joined together are referred to as the adherends and the bonded surfaces are termed substrates. The adhesive, or glue, has three distinct layers. The cohesive layer is the largest part of the joint and comprises the bulk adhesive. The adhesion interface is of atomic thickness and it is here that the bond between adhesive and substrate is made.

When an adhesive joint fails it is usual to describe the failure as either cohesive or adhesive, Figure 2.10. However, it is held in some quarters that adhesive failures are simply cohesive failures which have occurred very close to the surface of the substrate leaving only a thin film of adhesive behind, Packham (1995).

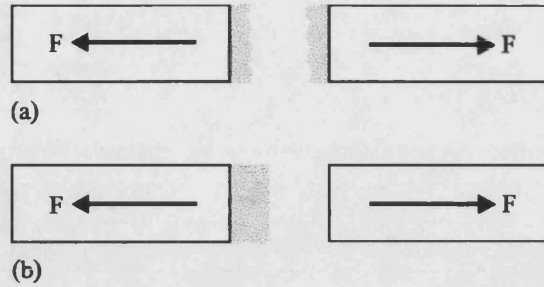
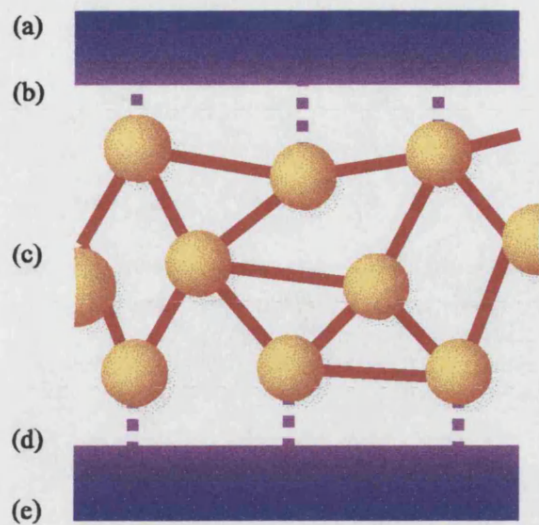


Figure 2.9 (Top right) Five layer model of an adhesive joint. (a) Substrate 1, (b) Adhesion interface 1, (c) Cohesion, (d) Adhesion interface 2, (e) Substrate 2

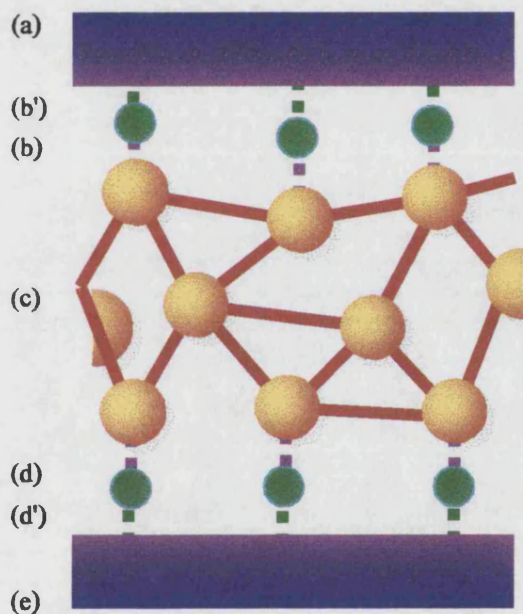


Figure 2.10 (Above) Classification of failure modes. (a) Cohesive failure (b) Adhesive failure

Figure 2.11 (Left) Seven layer model of an adhesive joint. (a) Substrate 1, (b') Coupling agent 1, (b) Adhesion interface 1, (c) Cohesion, (d) Adhesion interface 2, (d') Coupling agent 2, (e) Substrate 2

Failure at the adhesion interface will occur if the substrate has not been properly prepared. Preparation may involve cleaning, priming and the use of a coupling agent. Cleaning is important to remove dirt, oil or protective coatings which might otherwise prohibit the formation of a good bond between the substrate and the adhesive. However, some adhesives will not bond to some materials because of the incompatible polarities of the two materials. In such cases the substrates must be primed. The primer will modify the surface of the substrate, making it compatible with the adhesive. A coupling agent is different to a primer in that it exists as a definite atomic layer between the substrate and

the adhesive. Coupling agents not only enable the formation of a good bond but may give other benefits such as enhanced durability, Pye (1996a). Where coupling agents are used we can consider a seven layer model for the adhesive joint, Figure 2.11. Silanes are the most common coupling agents and often used with steel substrates and glass substrates, Plueddemann (1982). The formulation of silane coupling agents is still a black art, Brockmann (1986). Unfortunately a coupling agent which improves the bond between one substrate and adhesive may be detrimental if used on a different substrate. Therefore the specification of coupling agents is based upon precedent rather than chemistry.

2.2.2 Precedent for the structural use of adhesives

Table 2.3 illustrates the use of adhesives in different industries. It may be concluded that structural adhesives have an established history spanning more than 30 years. Adhesives are used across a broad range of environmental regimes and in situations where long term durability is required. It may also be seen that there is a trend in recent years to use adhesives at higher stresses and in more safety critical applications. It should be noted that without exception the applications utilise the shear capacity of the adhesives; shear strengths range from less than 1 N/mm^2 to nearly 25 N/mm^2 . Therefore it is suggested that it should be possible to realise a glass-adhesive T-beam provided that the adhesive is primarily stressed in shear and provided that the shear stresses can be kept to a sufficiently low level.

2.2.3 Classification of structural adhesives

The adhesives listed in Table 2.4 represent the more common adhesive types that have been used in structural applications. The table's primary listing is based upon the chemical nature of the adhesive although in some cases adhesives may be classified by other means.

Application	First date	Adhesive type	Adhesive requirements	References to published papers and codes
Construction applications				
Glu-lam construction	1930's	Urea-formaldehyde and resonol-formaldehyde	τ 3.5 N/mm ² , T 50+ °C	BS 1204 (1979), BS 4619 (1998)
Structural silicone glazing	1960's	Silicone	τ 0.15 N/mm ² , t 5-10 mm, LS 20+ yrs	Tanno (1997)
Steel/concrete composite bridge deck construction	1965	1 or 2 part epoxies	LS 7.5 m cycles, LS 120 yrs	Kreigh and Richard (1966), Mays and Vardy (1982), Vardy and Hutchinson (1986)
Strengthening of bridge decks <ul style="list-style-type: none"> with steel plates with CFRP 	1970	2 part epoxies	τ 1 N/mm ² , T -25 °C to 20 °C, t 3±2 mm	Hutchinson (1996)
	1991	2 part epoxies	τ 1 N/mm ² , T -25 °C to 20 °C, t 3±2 mm	Meier (1997)
Earthquake retrofitting of structures with FRP <ul style="list-style-type: none"> concrete structures masonry structures 	1990	Epoxies		Roberts (1997), Seible (1997), Xiao (1997)
	1994	Epoxies		Schwegler (1997)
Steel girder repair with CRFP	1995	Epoxies		Gillespie et al (1997)
Anchorage systems for CFRP stay cables	1996	Epoxies		Meier and Meier (1997)
Glass timber composites	1997	?	T -30°C to 70°C, RH 80%	Natterer and Hamm (1997)

Table 2.3 Cont.

Application	First date	Adhesive type	Adhesive requirements	References to published papers and codes
-------------	------------	---------------	-----------------------	--

Automotive applications				
Clinching of hems on body panels to increase torsional rigidity	1970's	PVC plastisols Epoxies	τ 7 N/mm ²	Chang et al (1985)
Stiffening ribs on body panels	1976	Hot melt acrylic, hot melt epoxy	t 0.15-2 mm, T -40°C to 90°C, impact resistance, oily surfaces	Kemp (1986), Harris and Fay (1992), Satoh et al (1996)
Suspension and main body joints (in conjunction with welding)	1984	Epoxies		Harrison (1986)
Structural bonding of windcreens to stiffen monocoque	1985	Polyurethanes	t 2 mm	Fay (1994)
Composite bonding of complete monocoques	1990	Polyurethanes Epoxies		Fay (1994)

Aeronautical applications				
Timber/fabric bonded aircraft	1903	Animal proteins Milk based casein		Browne (1993)
Stiffening ribs in wings	1940's	Epoxies		Kuno (1979), Wake (1986)
Missiles	1950's	Epoxy phenolic BMI's, PI's	T up to 10,000°F, LS mins/hrs	Kuno (1979), Leone-Bay (1994)
Honeycomb panels	1952	Epoxies		Browne (1993), Wake (1986)
Helicopter rotor blades	1959	Nylon epoxy Modified epoxy	τ 7±2.1 N/mm ² , LS 1000 hrs	Kuno (1979), Wake (1986)

Table 2.3 Cont.

Application	First date	Adhesive type	Adhesive requirements	References to published papers and codes
Repairs to fuselage and wings	1970's	Epoxies	LS 1 to 5 yrs / 1000 to 20,000 hrs	Armstrong (1986)
Bonding of wings to fuselage	1985	Modified epoxy	LS 24,000 hrs	Krieger (1986)
Fully composite fuselage	1990	Epoxy		Cressy (1990)
Naval applications				
Repair of aluminium fatigue cracks	1983	Modified epoxy	t 0.1 mm; good fatigue	Allan et al (1986)

Table 2.3 Structural applications of adhesives. τ - maximum design shear stress, t - thickness of adhesive joint, LS - life span, T - operating temperatures, RH - relative humidity.

Category/Chemistry	Applications	Strength	Cure mechanism	Gap filling	Durability	Notes
--------------------	--------------	----------	----------------	-------------	------------	-------

Phenolic						
neoprene phenolic	Metal to metal	M	HP	s	L	
phenolic nitrile	Metal to metal	M	HP	s	L	difficult to process
calendared rubber phen.	Metal to metal	M	H	s	H	expensive
phenol-formaldehyde	Metal to metal	M	HP	s	M	
Polyaromatic	Missiles	M	HP	X	M	difficult to process
Epoxies						
Epoxy phenolic	Missiles	H	H+P	✓	H	
Nylon epoxy	Helicopter blades	VH	H+P	✓	H	expensive
Modified epoxy	see Table 1.1	U	RT	✓	H	
Rubber epoxy	Helicopter blades	VH	RT	✓	H	
Epoxy	no longer used	H	RT	✓	M	brittle
Toughened acrylics	vehicle construction	VH	RT	s	H	volatile monomers
Polyurethanes	car windscreens	M	RT	s	M	resilient
Protein based adhesives	wood/fabric aircraft	L	RT	X	L	poor perf. in moist.
Bismaleimides (BMI's)	aircraft engines	H	H	X	H	durable up to 500°F
Urea formaldehyde	timber structures	M	P	s	M	
Resorcinol formaldehyde	timber structures	M	P	s	M	
Structural silicone	structural glazing	M	RT	✓	M	
Cyanoacrylates	super-glue	H	RT	X	M	very fast cure
Polyamides (PI's)	engines/missiles	H	H	X	H	durable up to 700°F

Adhesives not classified by chemistry						
Pressure sensitive adhesives (PSA's)	Vehicle trim	L	P(+H)	s	M	display high creep
Structural bonding tape (SBT's)	Signs, glazing?	M	H+P	s	M	display high creep
Anaerobics	thread locking	H	EoA	X		fast cure

Table 2.4 Summary of different adhesive types. Based upon, Hubbard (1951), Wilson (1986), Lees (1986), Cope (1995) and Loctite (1996). L - low, M - Medium, H - high, VH - very high, U - ultimate, P - pressure, H - heat, RT - room temperature, EoA exclusion of air, s - semi

It is important to realise that the primary groupings listed in Table 2.4 include adhesives which may have very different characteristics, Lees (1986). For example, whilst a particular adhesive group may not generally be resistant to high temperatures a few formulations may be able to operate at moderately high higher temperatures.

One quick method of delimiting the choice of adhesives is to specify a gap filling adhesive. There is no general rule about what constitutes a gap filling adhesive, although the boundary between gap filling and non-gap filling adhesives is often taken as the ability to fill gaps in excess of 0.1 to 0.25 mm, Pye (1996a). Although some nominally non-gap filling adhesives may be tailored by modifying the hardening agents the choice in the case of structural adhesives is normally limited to either modified epoxies or acrylics. In fact epoxies form the basis of most of the structural adhesives used within the aeronautical industry, Leone-Bay (1994). They also form the basis of many of the adhesives used in the automotive and construction industries, Table 2.4

2.2.4 Stress analysis

Adhesive joints may be used in a variety of configurations and will be required to resist a variety of stresses, Figure 2.12. The configuration of many real-life joints is complex and it is not immediately obvious how these should be analysed, Figure 2.13. Even apparently simple adhesive joints prove to be analytically complex when compared to the beam and plate structures that structural engineers are accustomed to, Figure 2.14 and Figure 2.15.

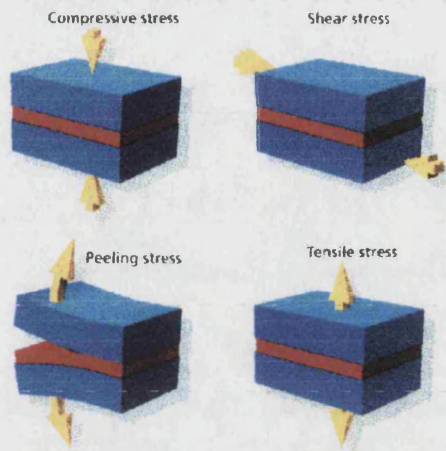


Figure 2.12 Adhesive joints may be required to resist a variety of stresses.

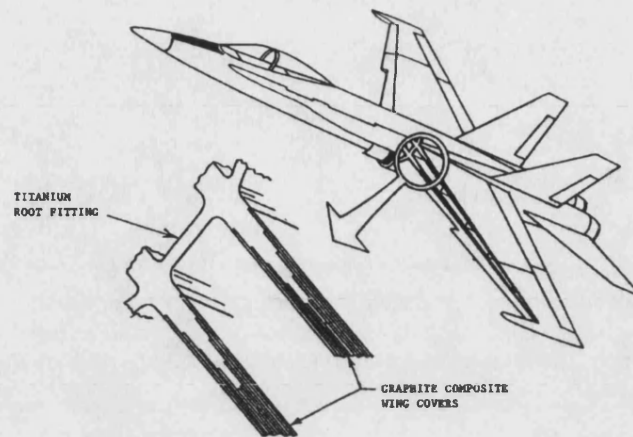


Figure 2.13 F18 wing to fuselage attachment, Krieger (1986).

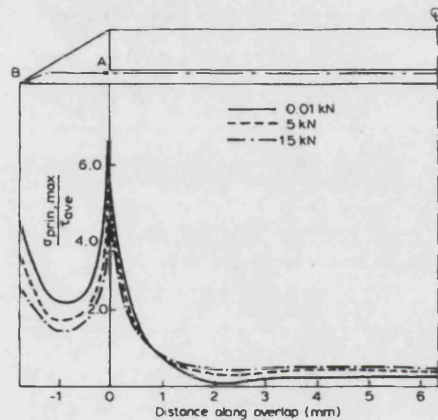


Figure 2.14 Distribution of principal stresses in a simple lap joint subject to shear, Harris and Adams (1984). B - tip of adhesive fillet, A - corner of upper adherend, CL - centre-line of joint.

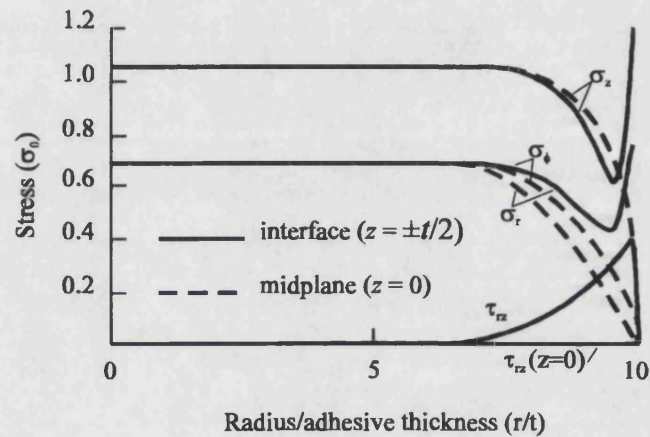


Figure 2.15 Stress distribution in a simple butt joint subject to tension, Adams (1978). σ_0 - average tensile stress, σ_z - normal stress across joint, σ_ϕ - normal circumferential stress, σ_r - normal radial stress, τ_{rz} - shear stress in plane of joint.

The lap joint is the most used and most studied adhesive joint. It is discussed here in order to highlight the difficulties that are likely to be encountered in the analysis of any adhesive joint. The most basic approach would be to assume that the shearing force, F , causes the adhesive to be uniformly strained along its length. The first realistic model was proposed by Volkersen (1938) who presented an algebraic approach which is based upon plane stress and takes into account the differential straining of the adherends, Figure 2.16a. Demarkles (1955) refined this model by including the effect of shearing of

the adherends, Figure 2.16b. Goland and Reisner (1944) took into account the bending of the adherends, Figure 2.16c. This led to Goland and Reisner proposing a peak stress concentration factor which was twice that proposed by Volkersen. Wooley and Carver (1971) produced the first finite element model. Cooper and Sawyer (1979) produced a non-linear finite element model in which the adhesive was modelled as five layers and were the first to show the significant variation of shear stress across the depth of the adhesive joint. Adams and Peppiatt (1974) investigated the effect of spew fillets using finite element techniques and concluded that the provision of a fillet could increase the strength of the joint by up to 25 percent. Crocombe and Adams (1981) showed that significant stresses existed across the joint.

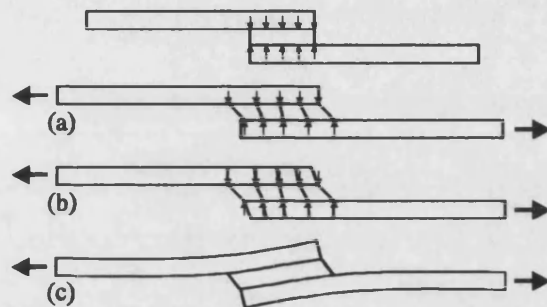


Figure 2.16 The behaviour of a simple lap joint in shear. (a) Differential straining of the adherends (b) Shear straining of the adherends (c) Rotation of the adherends.

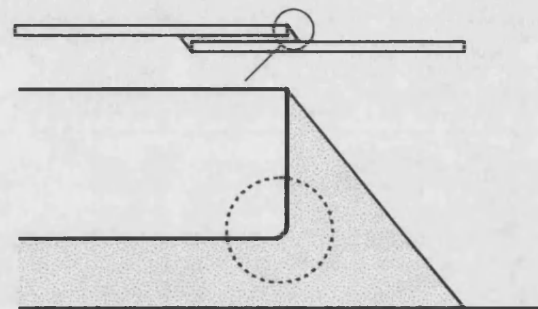


Figure 2.17 Modelling small scale geometry tends to reduce artificial stress concentrations.

Hart-Smith (1981) was the first to consider the effects of material non-linearity. His basic approach was similar to that of Volkersen and was therefore only applicable to joints where bending and stretching of the adherend is negligible. Harris and Adams (1984) were the first to produce a finite element model which modelled both the adhesive and adherend material non-linearities. They considered stress and strain failure criterion and observed that the strain failure criterion was most appropriate in the case of toughened adhesives and that the stress failure criterion was more appropriate in the case of untoughened adhesives, Table 2.5. Adams and Harris (1987) investigated the effects of small-scale geometry and concluded that unrealistic modelling of the substrates could increase stresses by up to 25%, Figure 2.17. The effects of varying the macro geometry

of the lap joint have also been studied. Hart-Smith (1973) investigated the effect of tapered adherends and step joints. Wah (1976) and Webber (1981) investigated the effect of scarf joints and Tham (1976) investigated the effect of scarf and bevel joints as he recognised that the adherend is never fully tapered.

Adhesive	Predicted strength (kN)		Experimental mean strength (kN)
	Stress criterion	Strain criterion	
MY750 ¹	5.05	7.2	4.8
AY103 ¹	5.5	9.95	5.9
ESP105 ²	6.0	8.85	9.9
CTBN ²	4.3	14.7	15.9

Table 2.5 Predictions of joint strength, Harris and Adams (1984). ¹Untoughened adhesives, ²Toughened adhesives.

Half a century has been spent trying to understand the stress distribution within the lap joint. Many of the lessons that have been learnt are being used in the analysis of other joint configurations. The general availability of finite element modelling now allows the analysis of more complex geometries. However, even though it may be possible to determine the stress distribution it is not necessarily possible to predict failure. Adams has proposed various failure criteria based upon strain, stress and strain energy although he now concedes that none of these offers a totally reliable failure criterion, Pye (1997a). In an interview with the author Adams stated that finite element techniques should be used to optimise the joint geometry in order to create as uniform a stress field as possible. Ultimately adhesive joints can only be proven by physical testing.

2.2.5 *Stress analysis and factors of safety in real design*

The analysis of the adhesive lap joint is very well documented in open literature. The analysis of other generic joint types also receives some attention. However, the analysis of joints used in real projects is rarely published. This may be because this information is commercially sensitive or else it maybe that the use of analytical techniques is secondary to testing. Either way it makes it difficult for engineers considering the use of adhesives. In particular there is virtually no guidance on acceptable factors of safety. The consequence of this is that engineers are forced to rely upon the adhesive manufacturers. However, manufacturers may not be able to offer simple solutions. As the adhesive is likely to represent only a small part of the cost of the overall product they are unlikely to invest in research and development work without some guarantee of capital return. Therefore whilst structural adhesives have found a foothold in mass production they are little used in one-off projects.

One exception to the rule that adhesives are not used in bespoke projects is the field of structural silicone glazing. Structural silicone has been used to fix glass to buildings since the 1960's. The first major application of a structural silicone glazed facade was the Smith, Hincham and Grylis (SH&G) building in Detroit, 1971, Figure 2.18. Although mechanical fixings were also used in this early application, the adhesive jointing technology has now been

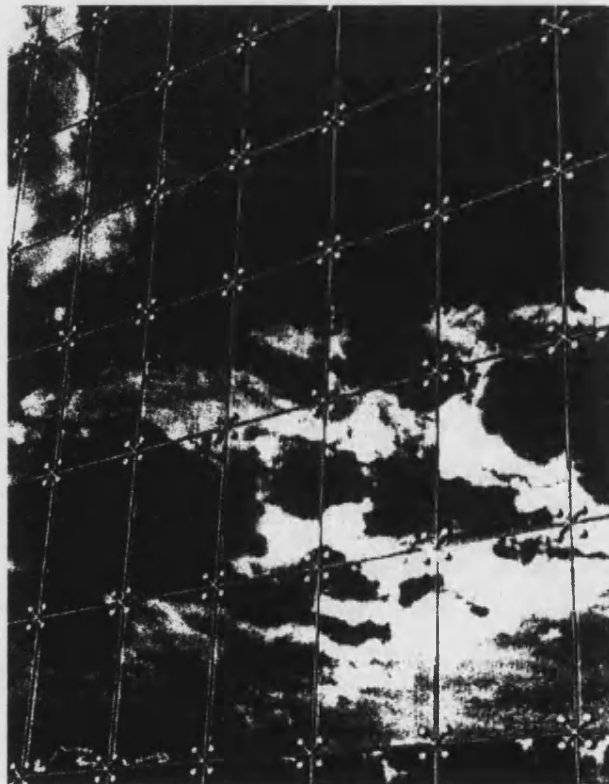


Figure 2.18 The SH&G building, Detroit, 1971, is one of the first examples of four-sided structural silicone glazing.

proved and modern applications rely solely upon the structural silicone sealant. In the case of the SH&G building the minimum factor of safety was 9:1, although nowadays this has been reduced to 5:1, O'Connor (1988). For engineers wishing to evaluate the performance of structural silicone sealant joints there is a wealth of information available in open literature. Haugsby (1988) provides a comprehensive treatise on calculating the strength of structural silicone joints. Schmidt et al (1988) address the issues of using different elastic modulus sealants and joint geometries. Information regarding the testing of structural silicone adhesives is available, Sandberg (1988) and Schmidt et al. (1988) and general information on principles and issues of compatibility is also available, O'Connor (1988). Standards such as BS 6262 even codify the use of structural silicone sealant for special applications, BS (1997). Therefore the design engineer will already have a carefully developed proposal at the time the adhesive manufacturer is approached. The result is a cost-effective solution that may be used on relatively small projects and although the adhesive manufacturers are dealing with a large number of small projects they have developed a multi-million dollar business.

An approach where the structural engineer has sufficient information available to evaluate the potential of a particular adhesive application appears to be the key to the structural use of adhesives in an industry where each application is likely to be a one-off. This is seen in timber glulam construction and the retro-strengthening of bridge and floor structures with bonded plates; as well as in the field of structural silicone glazing. If the use of glass-adhesive beam structures is to be similarly successful it will be necessary to follow a similar approach.

2.2.6 Testing of adhesives to determine mechanical properties

Adhesives are commonly tested for one of the following reasons, Todd (1995).

1. To check the quality of an adhesive.
2. To determine the effectiveness of the pre-treatment.
3. To gather information for the prediction of joint behaviour.

4. To select an adhesive from a group.
5. To evaluate the effects of ageing.

In this work adhesives have been tested for reasons 3 and 4. Whilst evaluating the effect of ageing would have been a valuable exercise, neither the time nor the equipment was available to do this.

A variety of tests are commonly performed to determine the mechanical performance of adhesive and these are summarised in Table 2.6. Whilst most manufacturers publish strength data, the availability of stress strain data is much more limited. This may be due to the difficulty in obtaining this data and the further difficulties in using it.

Test type	Illustration	References
Determination of cleavage strength of adhesive bonds		BS 5350: Part C1, BS (1991b)
Determination of the tensile bond strength of butt joints		BS EN 26922, BS (1993a)
Determination of impact resistance of adhesive bonds		BS EN 29653, BS (1994a)
Determination of bond strength in longitudinal shear		BS 5350: Part C5, BS (1990a)
Determination of creep resistance to sustained application of force		BS 5350: Part C7, BS (1990b)

Table 2.6 cont.

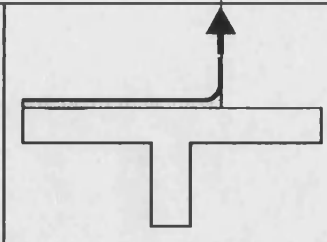
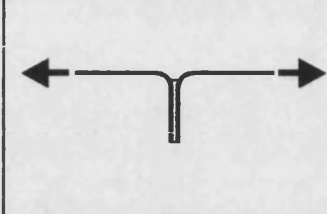
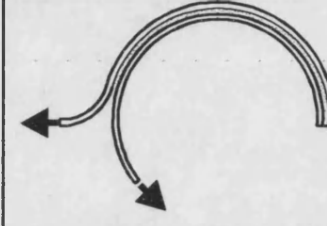
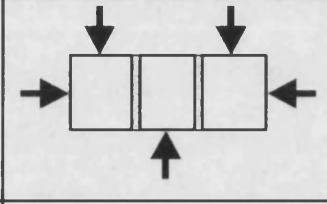
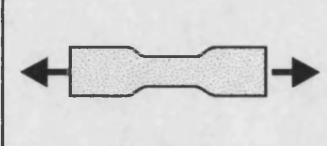
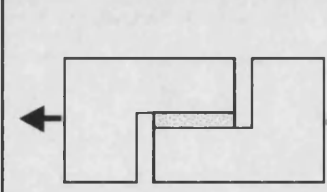
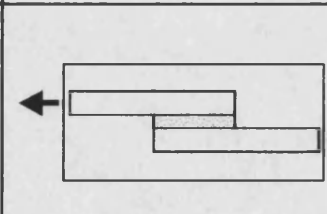
Determination of peel strength for flexible to rigid bonded assemblies		BS EN 28510, BS (1993b).
Determination of peel strength for flexible to flexible bonded assemblies		BS 5350: Part C12, BS (1994b)
Determination of peel strength for rigid to rigid bonded assemblies		BS 5350: Part C14, BS (1991c)
Determination of bond strength in compressive shear		BS 5350: Part C15, BS (1990c)
Determination of tensile properties of cast bulk adhesives		ASTM D 638M, ASTM (1993a)
Determination of shear modulus of non-rigid adhesives		ASTM D 3983, ASTM (1993b)
Determination of the durability of adhesive joints exposed to humidity and temperature		ISO 14615, ISO (1997)

Table 2.6 Summary of principal codified test procedures for adhesives and adhesive bonded joints.

As most adhesives are primarily used to carry shear, stress-strain data usually reflects the shear-stress shear-strain behaviour. The problem in obtaining this data is that none of the

standard test methods shown in Table 2.6 uniformly stress the adhesive. Test methods such as the napkin ring, Figure 2.19 and a derivative of this which is called the butterfly wing, are reported to more uniformly stress the adhesive, Pye (1997a). However only Bristol University and the National Physics Laboratory are able to perform these tests at present. Whilst both methods are elegant and theoretically accurate, in practice it is difficult to obtain pure shear without secondary bending, Krieger (1985). In addition these tests are expensive to perform and the collection of sufficient data for statistical analysis is usually prohibitively expensive.

The most common method used to determine stress strain behaviour is the thick adherend shear sample, ASTM D 3983, ASTM (1993), Figure 2.20. The adherends are thick to ensure that they undergo no plastic deformation. However the problems of differential straining and sample rotation still exist. The test method is based upon the Goland and Reisner theory and makes use of the fact that the adhesive strains tend to be uniform over the middle 60 per cent of the joint. The test sample is manipulated to optimise this stress uniformity and the strain over the middle 60 per cent of the joint is measured using a dual transducer slip gauge, Figure 2.20. Such transducer slip gauges are normally manufactured in-house. The cost would typically be in the order of £5,000, Pye (1997b).

There is some dispute concerning the manufacture of the thick adherend samples. ASTM D 3983 stipulates the use of two flat adherends that are carefully jigged during assembly. Two inclined tension grips, Figure 2.21, are then used to hold the sample and it is pulled apart in a laboratory testing machine. However Krieger (1986) prescribes the manufacture of a continuous sample into which two cuts are made, Figure 2.20. This method ensures better alignment of the two adherends but Adams argues that damage to the adhesive at the cut locations leads to the premature failure of the sample. However, the whole test method is also brought into question by the observation of Chalkley and Chiu (1993) that at a fixed cross-head speed the adhesive will not be strained at a constant rate. It is commonly known that the adhesive stiffness is time-dependent and

therefore without a feedback loop such as that proposed by Chalkley and Chiu it is not possible to determine accurate stress-strain data. Unfortunately this type of instrumented test is beyond all but a few specialist test houses.

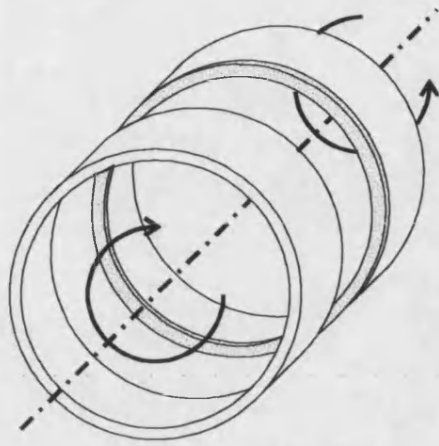


Figure 2.19 The napkin ring tests allows the adhesive to be uniformly stressed and is sometimes used to collect stress-strain data.

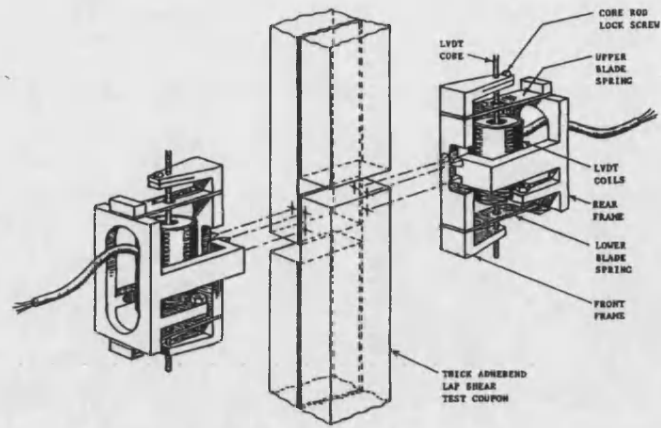


Figure 2.20 The thick adherend shear sample is often used to collect adhesive stress-strain data. The sample is instrumented with a dual transducer slip gauge to measure the strain over the middle portion of the joint.

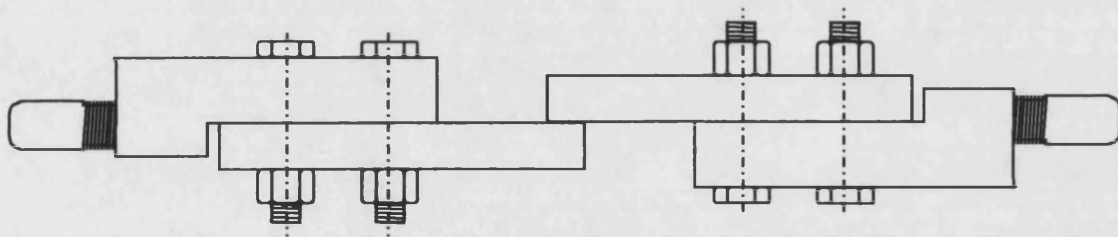


Figure 2.21 Assembly of samples for the thick adherend shear test according to ASTM D 3983.

It may appear to some that the selection, testing and analysis of adhesives for the fabrication of structural adhesive joints is more of an art than a science. It is true that there are many gaps in our understanding and engineers accustomed to operating within the codified world of steel and concrete may feel unsure about the use of these new materials. In 1963 adhesives accounted for only 20 per cent of the world fasteners market (adhesives, nuts, bolts, nails, welding materials). By 1977 it had grown to 30 per cent, Kuno (1979). Their use has continued to grow throughout the 1980's and the 1990's and the construction industry is unlikely to escape the growth of this new technology.

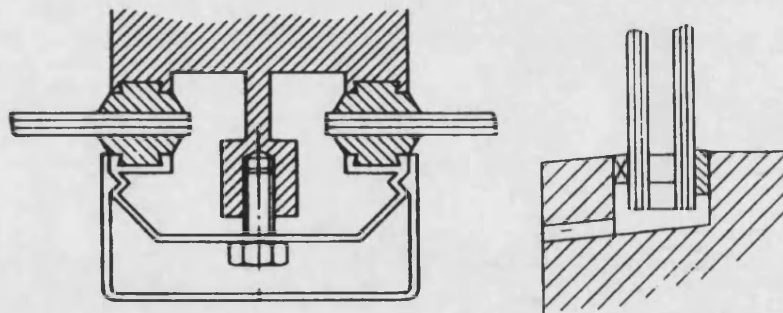
3 TESTING OF MATERIALS

This section is concerned with the testing of materials that were selected for use in the construction of the glass-adhesive T-beam. Tests have been undertaken to gain qualitative understanding of material behaviour, to rank material performance and to obtain quantitative data needed for analysis. However, this has only been undertaken on occasions where information was not available in open literature or through industrial partners. As a result the test methods often fall outside recognised codes and therefore form a major part of this work.

3.1 Achieving a simple support condition for a flat glass plate

Analytically it is easiest to consider a support condition which is either simply supported or else fully clamped. However, in practice support systems for glass tend to fall between these two extremes, Figure 3.1. Furthermore, it is generally acknowledged that glass should never be supported in contact with a hard material because of the stress concentrations that are likely to arise in the glass, BS (1982) and Flat Glass Marketing Association (1990).

Figure 3.1 Typical support systems for glass plate structures are neither simple supports nor fully fixed supports.



The object of these tests was to achieve a support condition that approximated the engineers' simply supported condition without inducing failure of the glass at the supports. The tests took the form of four point bending tests performed on plates of toughened glass measuring 900 mm by 250 mm by 6 mm, Figure 3.2. The 250 mm and 6 mm dimensions were chosen as the smallest dimensions that could be supplied by the

local glass merchant. The 900 mm dimension was chosen as one that could be easily handled within the laboratory.

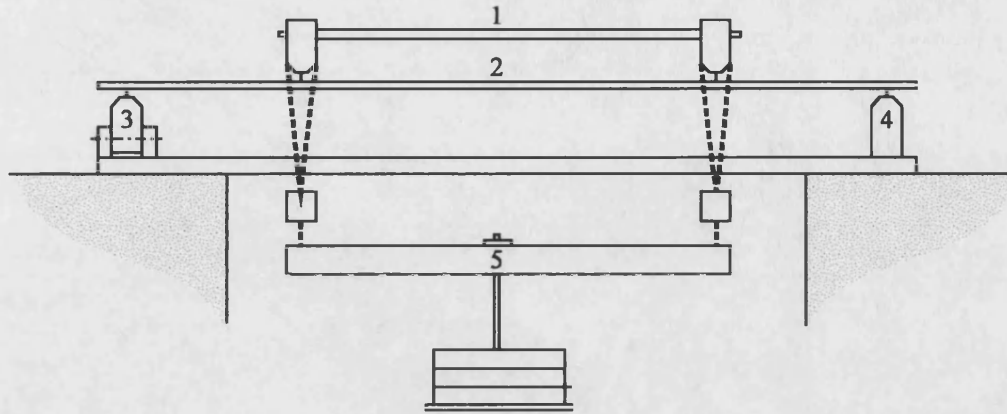


Figure 3.2 Arrangement of four point bending tests on toughened glass plates with knife edge supports. 1-Loading beams and spacing bar, 2-Glass plate, 3-Articulated support, 4-Fixed support, 5-Wiffel tree and hanging weights

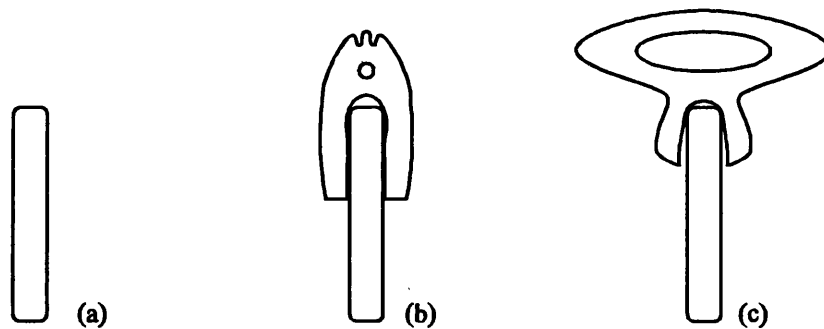
Three support conditions were evaluated, Figure 3.3. For the bare aluminium knife edge the weight was incremented from 0 N to 800 N and back in steps of 100 N. For the gasket clad knife edges this loading pattern was repeated in order to allow the glass to bed on the gaskets. At the beginning of each test the thickness of the glass was measured at several points across the plate and the average value was recorded. Dial gauges and strain gauges were used to record the deflection and strain of the plate. The strain gauges were 120 ohm with a 2.05 gauge factor. They were fixed using Loctite 454 Prism cyanoacrylate gel and were wired back in a quarter bridge arrangement to a Mowlem Microsystems 700 series ADU. Load-deflection and load-strain plots are shown in Figure 3.4. The calculated deflections and strains are based upon small deflection theory assuming that $E = 70 \times 10^3 \text{ N/mm}^2$, Sedlacek et al (1995).

During the tests no plates failed. The load was not increased above 800 N because of the potential of failing the glass in bending which would have been difficult to tell apart from a bearing failure. Figure 3.4 a to c shows that the mid-span deflection closely correlates with the theory in each of the support arrangements. No account has been taken of the compression of the gaskets. The load-strain plot in the case of the bare aluminium support again shows a close correlation with the theory, Figure 3.4.

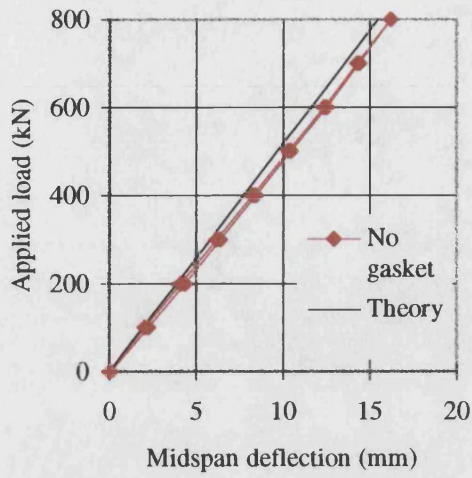
However, where gaskets were used the plots are erratic; particularly in the case of the large gasket, Figure 3.3c. Considerable sliding of the glass plate over the supports was noted during the tests with the bare aluminium edge. This amounted to an overall lengthening of the beam of 5 mm at the maximum deflection. In the presence of the gaskets it is assumed that the increased friction between the support and the glass prevented this sliding from occurring. However, in doing this the gaskets had to maintain a membrane force in the plate and when this force became too high the frictional bond would be broken and the plate would jump. This was corroborated by the observation that at the end of the test the plate would not necessarily be in the same horizontal position as it was at the beginning.

Figure 3.3 The three support conditions evaluated in the four point bending tests.

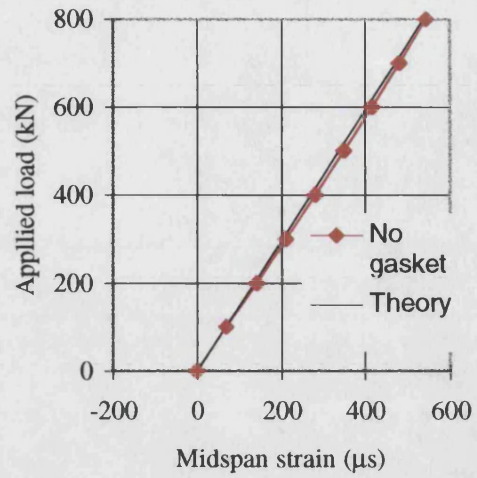
(a) Bare aluminium knife edge, (b) Small gasket, (c) Large gasket.



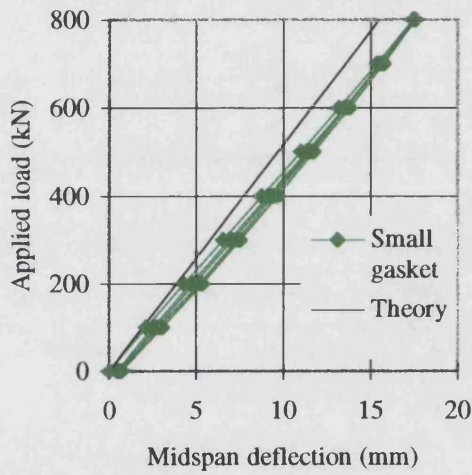
Whilst the bearing load was only 1.6 N/mm the initial success in the use of bare aluminium edge supports has led to its use in later work, see Section 8. Steel has also been used as a bearing material and bearing loads in excess of 250 N/mm have been successfully carried, see Section 3.2. However, it should be noted that these bearing surfaces had been carefully machined to a smooth surface and that good alignment between the glass and the bearing surface has always been maintained. In these two respects the laboratory conditions differ greatly from those achievable on site and it is not suggested that this arrangement be used for anything other than test work. In one case it was not possible to ensure good alignment between the support and the glass and it became necessary to use a gasket. This modified the support system in a similar manner to that seen above.



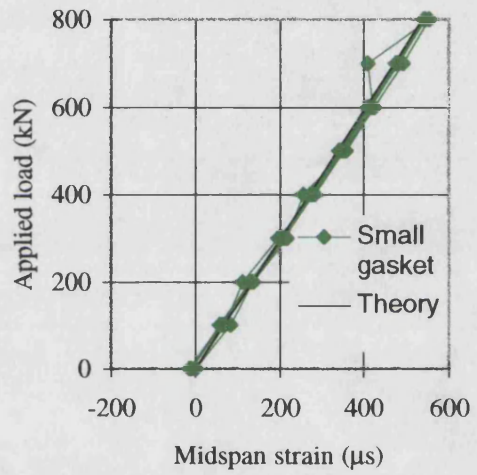
a



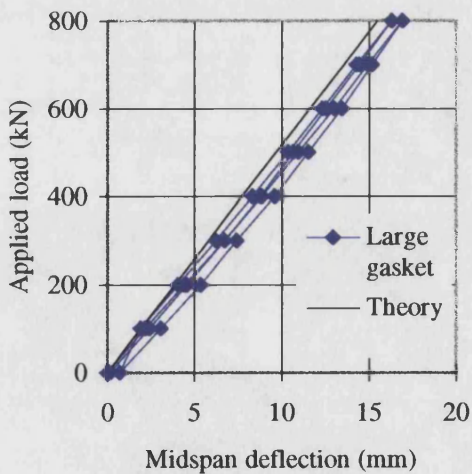
d



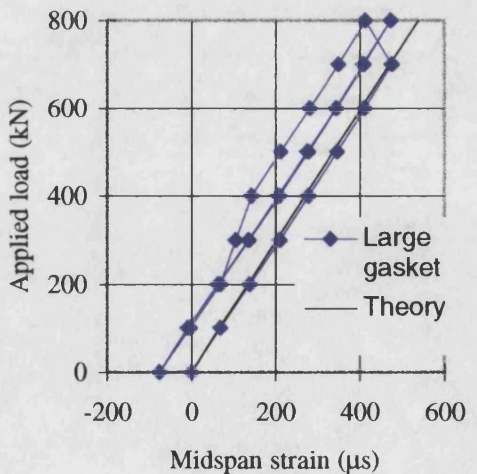
b



e



c



f

Figure 3.4 Graphical summary of results for four point bending tests

3.2 Evaluating critical shear stresses in glass

Information regarding design stresses for glass is very limited and in the case of evaluating critical shear stresses there is no information available in open literature. The new draft Euronorm, "Design of glass panes. Part 1: General basis of design," CEN(1996c), does not even consider the potential of shear failure. However, Figure 3.5 shows two scenarios in which shear type failures may occur.

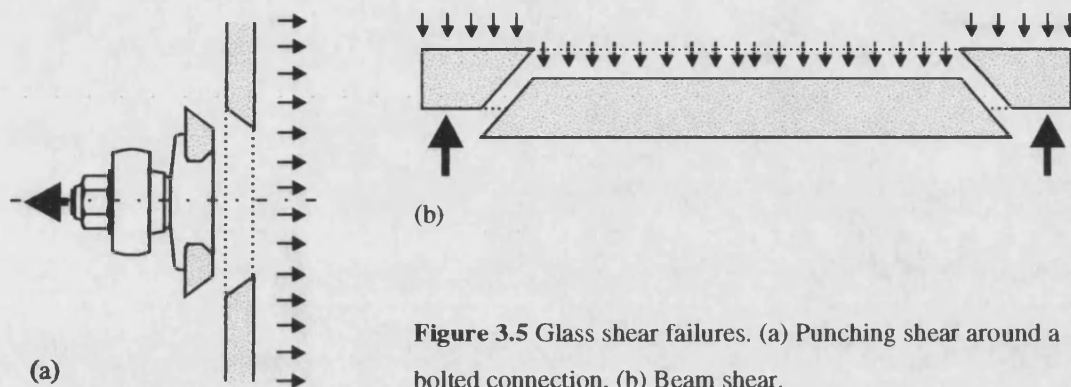


Figure 3.5 Glass shear failures. (a) Punching shear around a bolted connection, (b) Beam shear.

Bolted connections such as that shown in Figure 3.5a have been used without major problem for more than ten years. A 2 metre square, 10 mm thick glass panel will typically be supported by four bolts, Ryan et al. (1998). Such a panel may be subjected to a wind load of 2 kPa such that each bolt notionally carries 2 kN. Therefore if a cylindrical failure surface of 50 mm is proposed the average shear stress may be determined as 1.3 N/mm^2 . In practice it may be assumed that the shear strength is higher than this as no account has been taken of the bending stresses which will be present within the plate. Nor has any account been taken of the non-uniform distribution of the shear forces.

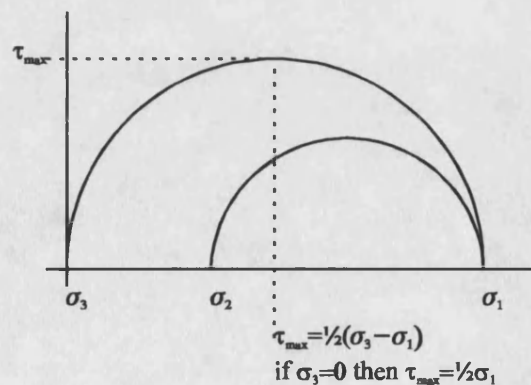


Figure 3.6 Mohr circle approach to shear failure

Another approach is shown in Figure 3.6. taking a maximum principal stress of 45 N/mm², CEN (1996a) and constructing the Mohr circle it may be proposed that the failure stress is $\frac{1}{2}\sigma_{\max}$; that is $\tau_{\max} = 22.5 \text{ N/mm}^2$. However, this Mohr circle construction is based upon the assumption that the glass is a perfect isotropic material. In practice the accumulated surface damage is such that it is possible to consider a plate of glass as a layered composite with a very strong core bound by much weaker layers. Within the core tensile stresses of up to 5000 N/mm², Gordon (1976), may be permitted but at the surface stresses in the region of 45 N/mm² are likely to cause failure.

Figure 3.7 indicates how the distribution of shear stresses will lead to the set up of direct tensile stresses within the glass. It can be seen that the distribution of the resultant tensile stresses across the depth of the plate will be similar to the distribution of shear stresses. It may therefore be shown that the direct tensile stress set up as a result of a shear force F may be expressed as, Case et al (1993);

$$\sigma_T = \sqrt{2}\tau = \sqrt{2} \frac{12F}{bd^3} \left(\frac{d^2}{8} - \frac{y^2}{2} \right) \quad \text{Equation 3-1}$$

where

d is the overall depth of the section

b is the breadth of the section

y is the distance from the neutral axis of the section to the point under consideration

That is, the tensile stresses are greatest in the core where the glass is strongest and fall to zero at the surface where the glass is weakest. Consider a 6 mm thick plate with a Griffith flaw of length 1 micron which is orientated at 45° to the surface of the plate. Assuming a characteristic tensile strength of 45 N/mm² the average shear stress necessary to critically stress this flaw would be 170 N/mm².

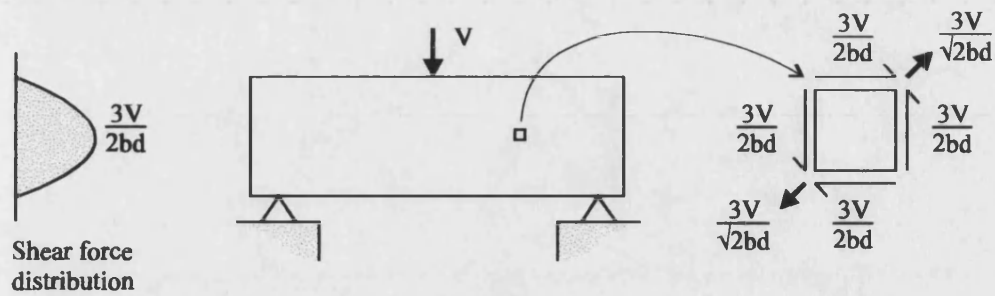


Figure 3.7 Resultant tensile stress

In the light of the previous argument it becomes apparent that initiating a shear failure in glass will be difficult. However, in order to prove this theory it was decided to perform a series of punching shear tests, Figure 3.8a. This is a modified version of the standard co-axial bending test pr EN 1288-5, CEN (1996e).

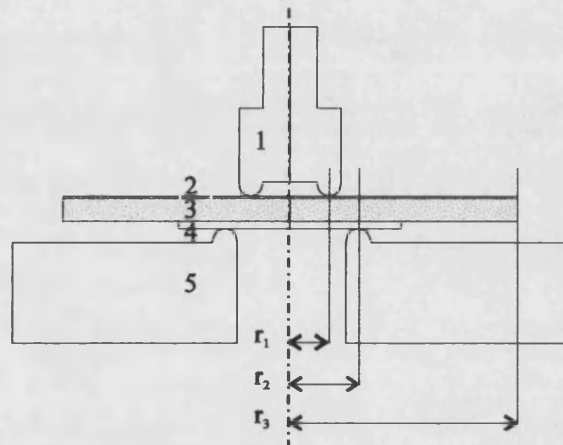
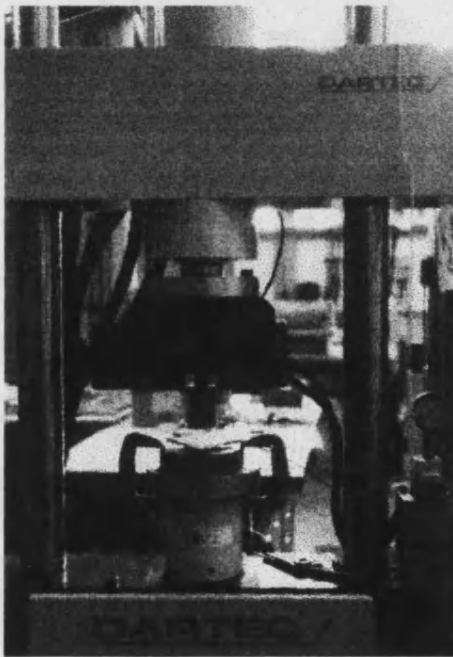


Figure 3.8 Punching shear tests on square glass plates.
1-Steel punch, 2-Adhesive film, 3-100 mm square 6 mm thick annealed glass plate, 4-Gasket, 5-Steel support

In the case of a circular disc the inner part of the plate is bent to a spherical shell and the principal tensile stress may be derived from Equation 3-2, Timoshenko and Winowsky-Kreiger (1959). Pr EN 1288-5 allows a square plate to be substituted for the circular disc. In this case the equivalent radius should be taken as 0.6 times the length of the square plate. If the glass plate has a tensile strength of 45 N/mm^2 and bending failure is presumed then the failure load, F , may be calculated as 10.6 kN.

$$\sigma_{\max} = \frac{3(1+\nu)}{2\pi} \left[\ln \frac{r_2}{r_1} + \left(\frac{1-\nu}{1+\nu} \right) \frac{r_2^2 - r_1^2}{2r_3^2} \right] \frac{F}{d^2} \quad \text{Equation 3-2}$$

where;

ν Poisson ratio = 0.22

r_1 loading ring diameter = 45 mm

r_2 support ring diameter = 57 mm

r_3 Overall plate diameter = 0.6L for a square plate = 60 mm

In total 29 plates were tested to failure. The test details and results are summarised in Table 3.1 and Figure 3.9. The distribution of failure loads was shown to fit a normal distribution, Feakes (1997). Near the centre of each plate was a single point from which all of the fracture lines radiate, Figure 3.10. These were assumed to be the points from which bending failure had originated. When the fracture point was well within the loading ring it is possible to be sure that the failure was due to bending, Figure 3.10a. However, when the fracture point is near to the line of the loading ring it is not possible to differentiate between bending failure and potential shear failure, Figure 3.10b. Whilst the theory presented earlier may lead the reader to conclude that the failure was most probably due to bending it is not possible to prove this.

No of samples	Load rate (mm/s)	Average failure load (kN)
17	0.0126	27.1
6	0.1008	28.0
6	0.8064	29.9

Table 3.1 Summary of loading rates and average failure loads for punching tests on thin glass plates

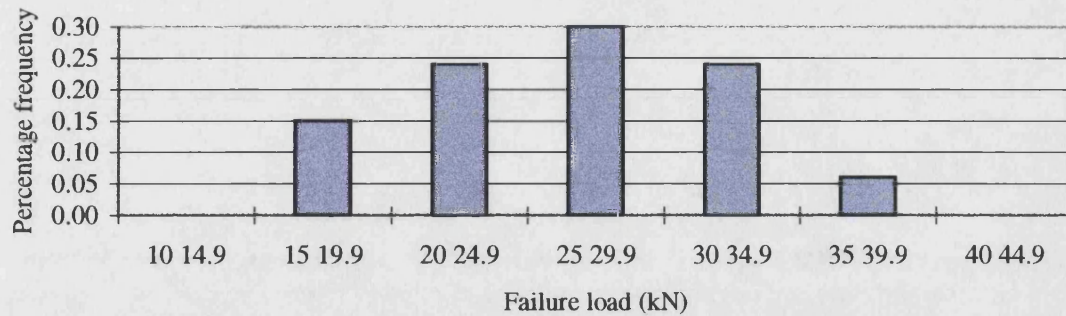


Figure 3.9 Distribution of failure loads for the 17 samples loaded at 0.0126 mm/s

The difference between the predicted failure load of 10.5 kN and the average failure load of 27.1 kN was a cause for concern. Back substituting the failure load into Equation 3-2 would lead to the conclusion that the average tensile strength of the glass approached 120 N/mm^2 . This seemed highly unlikely and so Equation 3-2 was checked against two finite element models, Figure 3.11. Both models used isoparametric elements with midside nodes and linear theory was assumed in both cases. The results are summarised in Table 3.1.

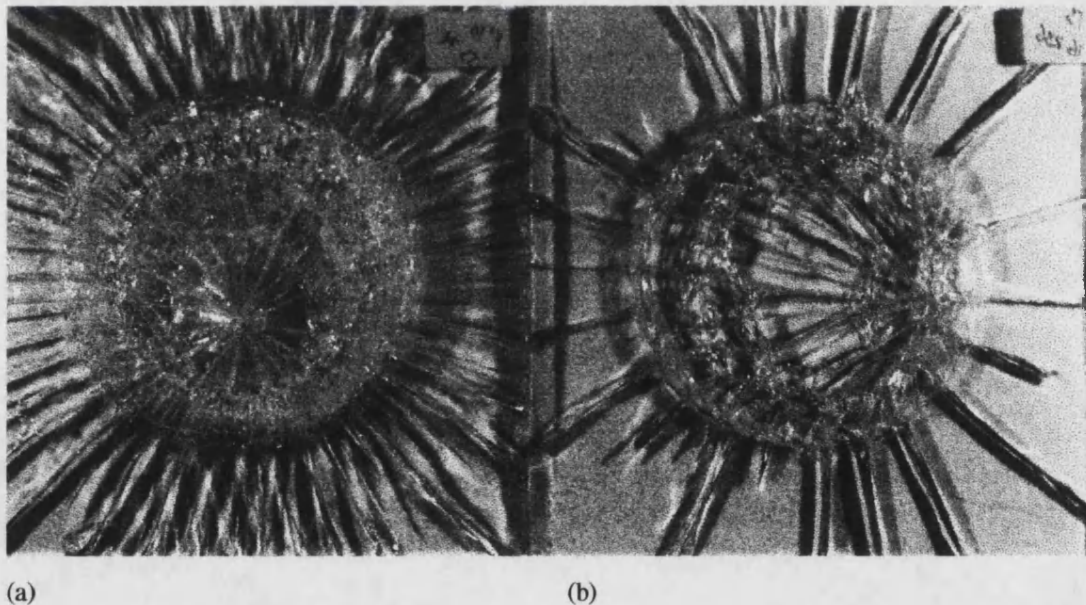


Figure 3.10 Typical failure patterns. (a) Fracture origin within loading ring, definite bending failure. (b) Fracture origin near loading ring, potential shear failure?

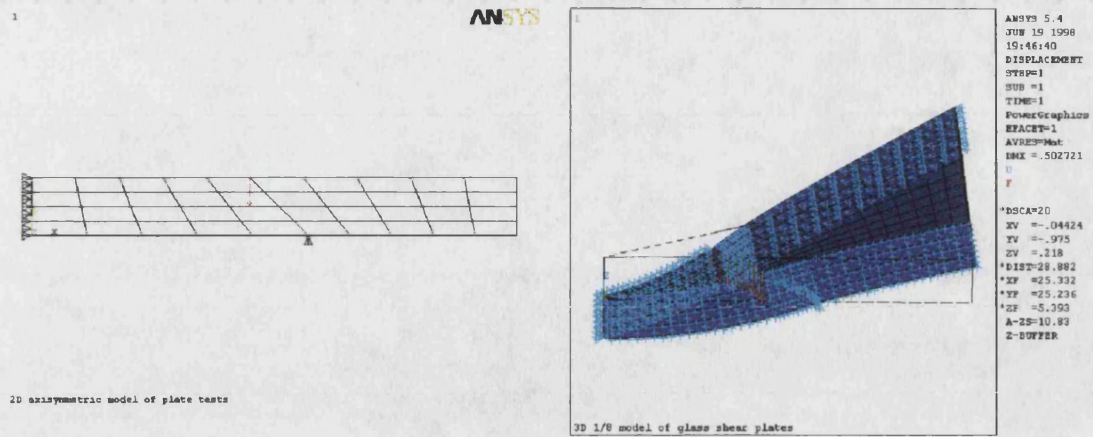


Figure 3.11 FE model meshes with boundary conditions. Left, 2D axisymmetric model. Right, 3D model using one eighth symmetry.

Model	Predicted failure load, assuming bending failure (assumes characteristic bending stress of 45 N/mm ²)
Classical	10.6 kN
FE - 2D axisymmetric	10.0 kN
FE - 3D with eighth symmetry	10.3 kN

Table 3.2 Summary of predicted failure loads for glass plates in punching shear

As the finite element models validated the classical approach it was decided to strain gauge and test two remaining plates. A small strip of gasket material was removed in order that the strain gauge cable could be taken to the ADU but in all other respects the tests were identical to the original tests.

It became apparent that the gasket material was preventing the lateral displacement of the plates and thereby imposing a compressive membrane stress. This mechanism was confirmed by introducing an arbitrary constraint in the finite element model, Figure 3.12. A similar problem in using gasket materials has already been highlighted in Section 2.1

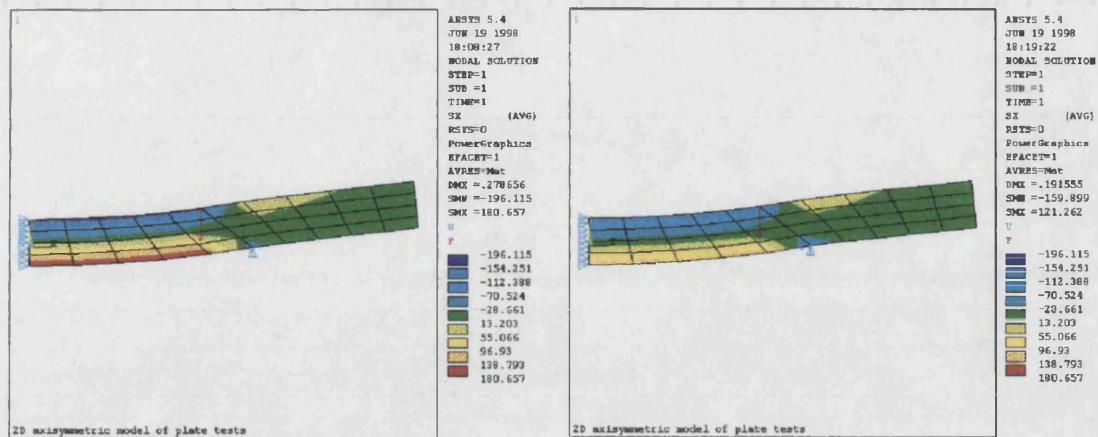


Figure 3.12 Principal stresses obtained from the axisymmetric FE model with a punching shear load of 39 kN. Left, no horizontal restraint at support, peak stress 181 N/mm^2 . Right, partial horizontal restraint at support, peak stress 121 N/mm^2 .

The results from the modified finite element analyses were used to calculate the correct tensile stresses for the different load cases. As a result it was shown that the average tensile strength of the glass was approximately 75 N/mm^2 . Whilst this is higher than the characteristic strength it should be noted that these samples were new, small and loaded rapidly.

Based upon the theoretical discussions it may be concluded that it is not realistically possible to fail glass in shear. Proving this in practice has been difficult because the loads necessary to generate high shear stresses generated even higher bending stresses. Furthermore it was not possible to differentiate between glass which had been fractured in bending and glass which may have been fractured in shear. However, it is possible to propose a safe shear stress based upon the failure load of the weakest sample. This is 16.7 N/mm^2 and this is high enough to cause little concern in practice.

3.3 The choice of an adhesive for the construction of a glass-adhesive T-beam

The following points were identified as key issues that would affect the choice of adhesive, Pye and Ledbetter (1997).

Mechanical properties.

1. The adhesive should have a shear modulus greater than 25 N/mm^2 . See Section 5.1.1.
2. The adhesive should have a shear strength of at least 10 N/mm^2 . See Section 5.1.6.
3. The adhesive must be capable of being used in a 1 mm wide joint. See Section 2.1.2.

Application and curing properties.

1. In order to apply and tool the large volume of adhesive necessary to form a joint which may be several metres long the adhesive should have a work time of at least 15 minutes.
2. As the joint is visible the adhesive should be capable of being neatly applied and tooled. Preferably the adhesive would be clear.
3. The adhesive should be sufficiently thixotropic that it does not flow out of the joint during cure.
4. Any heat required to cure the adhesive must be applied in a reasonably uniform manner to avoid the possibility of thermal fracture of the glass. Considering the potential size of the beams, a solution not requiring heat cure would be preferable.

Bonding mechanisms and durability.

1. The surface of toughened glass cannot be etched or otherwise roughened in order to improve the adhesion of the adhesive to the substrate.
2. The adhesive should be capable of operating in high-temperature, high-humidity environments such as Hong Kong (glass temperature 40°C , relative humidity 95%.)
3. The adhesive should be capable of operating in low temperature environments (glass temperature -10°C .)

4. The design life of the assembly would ideally be in the order of 30 years. Both structural and visual durability would be expected over this period.
5. The adhesive should be able to cope with high levels of ultraviolet radiation.

In order to select a suitable adhesive the author approached Dr Bernard Sikkel and Dr Keith Fisher at 3M United Kingdom Plc. It was considered that only a modified epoxy adhesive was likely to be able to offer the strength, stiffness, gap filling ability and room temperature cure that would be required for this application, Pye (1996b). However, it was also decided to evaluate a structural bonding tape (SBT). SBT's are new adhesive products that are a development from pressure sensitive adhesives (PSA's). They consist of a carrier and two thin layers of adhesive, Figure 3.13. PSA's cure under pressure and the carrier is sufficiently flexible to allow a slight mismatch between the two substrates being bonded, Fitzgerald (1986) and Edmonds (1992). The SBT's differ only in that they are heat cured and develop a higher shear strength. Being new products little is known about their performance, although work is being undertaken by Brockmann at the University of Kaiserslautern and Adams at the University of Bristol.

Three adhesives were selected. These were; 3M Scotch-Weld 2216 B/A Grey Epoxy Adhesive, 3M Scotch-Weld EPX Adhesive DP190 and 3M Structural Bonding Tape 9245. In each case it was recommended that 3M Scotch-Weld 3901 Silane Primer be used to ensure the formation of a strong durable bond between the glass substrate and the adhesive.

2216 is a modified epoxy resin. It is grey in colour and has been in use for over 30 years. It is a two-part adhesive which may be cured at room temperature. Each part is stored in a separate drum and the two parts must be measured and mixed in the correct ratio immediately prior to application. DP 190 is also a modified epoxy resin. It is grey in colour and may be cured at room temperature. It is a two-part adhesive which is dispensed from pre-measured cartridges. It is dispensed directly from the cartridge and mixed using an EPX applicator nozzle, Figure 3.14. 9245 is a 0.5 mm thick grey

coloured tape which must be heat cured. The minimum cure temperature is 120°C. The shear strengths of the three adhesives are summarised in Table 3.3. Overlap shear strengths for 2216 after environmental ageing are shown in Table 3.4.



Figure 3.13 Construction of a pressure sensitive adhesive / structural bonding tape.

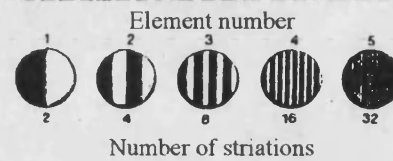


Figure 3.14 EPX mixer applicator nozzle used for DP 190.

Adhesive	2216	DP 190	9245
Test method	ASTM D 1002 64	Unknown	ISO 4587
Test temperature (°C)	Shear strength (N/mm ²)	Shear strength (N/mm ²)	Shear strength (N/mm ²)
-55	13.8	X	X
25	17.2	17.6	11.4
82	2.8	X	X

Table 3.3 Shear strength of selected adhesives

Environment	Time	Test results at 25°C (N/mm ²)
100% Relative humidity at 49°C	14 days	20.3
	30 days	13.7
	90 days	10.4
Salt spray at 35°C	14 days	15.9
	30 days	3.4
	60 days	2.1
Tap water at 25°C	14 days	21.5
	30 days	20.3
	90 days	14.3

Table 3.4 Overlap shear strengths for 2216 after environmental ageing.

Despite the ease of applying the 9245 tape this adhesive was rejected because of the potential problems in curing the adhesive. Methods of curing the adhesive include heating the whole beam in a large oven (such as those used for heat soaking glass), heating the whole beam under a collection of heat lamps, locally heating the glass at the adhesive joint using heating tapes, Raychem (1995) and locally heating the adhesive by burying a copper wire in the joint, Chang et al. (1985). Whilst it was felt that these methods could be realised it was also felt that pioneering these methods would absorb the time allocated to the analysis and testing of the T-beam.

The only information provided by 3M on the stress-strain behaviour of the adhesives was that 2216 has a shear modulus of 127 N/mm² and an elastic modulus of 352 N/mm². The author approached Dr Alan Hutchinson at the Joining Technology Research Centre at Oxford Brookes University and Professor Bob Adams at Bristol University in an attempt to obtain existing stress-strain data for the adhesives. No information was found.

3.3.1 Evaluation of stress-strain behaviour of 2216 and DP 190.

The primary aim in testing the two epoxy adhesives was to determine their stress-strain behaviour. This data was then to be used for the purposes of analysing the structural performance of the composite T-beam and selecting one adhesive for use in full scale laboratory tests. Bath University does not have the equipment necessary to perform the napkin ring or butterfly wing tests, nor were sufficient funds available to pay another laboratory to perform the tests on our behalf. Therefore, it was decided by default that the thick adherend test would have to be the primary method of collecting this data. The test method followed was a modified form of that detailed in ASTM D 3983-93. This involves preparing a minimum of five thick adherend samples that are pulled apart in a tension test machine whilst the strain is measured over the middle 60 per cent of the joint. The tests are conducted at $23\pm 2^\circ\text{C}$ and 50 ± 5 per cent relative humidity. Steel adherends to the dimensions specified in the code were prepared. The substrates were cleaned by sanding with grit paper. They were then wiped with a proprietary degreasing wipe before being primed with 3M 3901 silane primer. The primer was applied in a wipe-on wipe-off manner and allowed to dry in a clean environment for 24 hours. The joint was assembled in a jig similar to that illustrated in the code and the adhesives were applied and cured according to the manufacturer's guidelines.

The only deviation from the test procedure laid down in ASTM D 3983-93 was the manner in which the adhesive strain was measured. Bath University does not possess a dual transducer slip gauge of the type shown in Figure 2.20, Section 2.2.6. The lack of long term work in this field and the high cost involved in building the gauge meant that an alternative method of measuring the strains had to be sought. Two methods were evaluated.

3.3.1.1 Method one

The School of Material Science owns a Wallace light extensometer which provides a maximum displacement resolution of 0.05 mm/cm of chart paper. ASTM D 3983-93

states that the displacement transducers should provide several ranges of displacement resolution - between 0.0005 and 0.5 mm/cm of chart paper. Therefore the Wallace light extensometer falls within the upper range of the limits specified by the code. The light extensometer works by using two collimated beams of light which follow the movement of two lines that have been marked on the test sample, Figure 3.15a. The potential problems of this method included;

1. The two lines must be a minimum of 25 mm apart. Therefore the joint must be a minimum of 42 mm long in order that the two lines mark the middle 60 per cent of the joint; the portion over which the strain is most uniform. Although this falls within the code's limits for the joint length, because the adhesive is strong it means that the force required to fail the sample sometimes exceeded the code's 10 kN force limit. Presumably the force limit is imposed to ensure that the adherends are not plastically deformed. However, the use of steel adherends ensured that this did not occur.
2. As the strain is only measured on one side of the adhesive joint it was not possible to account for any rotational displacement in the plane of the joint, Figure 3.15b.
3. As the light extensometer follows only vertical movement of the lines it was not possible to account for any rotational displacement in the plane perpendicular to the adhesive joint, Figure 3.15c.

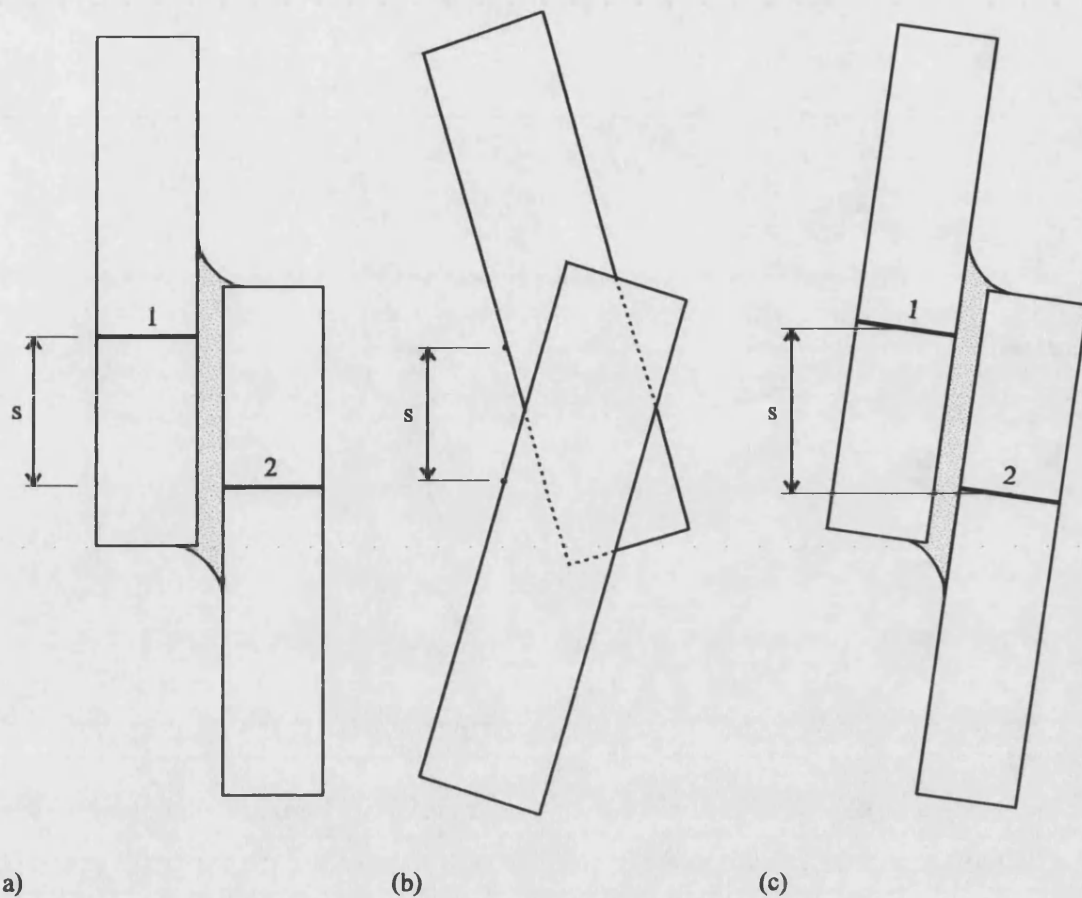


Figure 3.15 Measurement of adhesive slip using the Wallace light extensometer. (a) Marked lines 1 and 2, (b) This method is unable to take into account rotational displacement in the plane of the joint, (c) This method is unable to take into account rotational displacement in the plane perpendicular to the joint.

3.3.1.2 Method two

In this method strain gauge displacement transducers were used to measure the deflection of two aluminium cantilevers which were attached to the samples at the top and bottom of the middle 60 per cent of the joint. Two variations of this test were performed and these are shown in Figure 3.16. Both methods are able to account for rotation in the plane of the joint and perpendicular to the plane of the joint. However, variation one assumes that the outer faces of the adherends remain parallel whilst variation two is able to take into account any variation in the rotation.

The strain gauge displacement transducers had a full range of 25 mm and were connected to a Mowlem Microsystems 700 series ADU. However, the gain for the transducers was set high which reduced their range to approximately 3.5 mm and gave a maximum resolution of 0.002 mm. The potential problems of this method included;

1. The displacement transducers were being used in a somewhat unconventional manner. Whilst the available 2048 bits resolved to give a resolution of 0.0017 mm/bit the output tended to flutter which suggested that the actual resolution was somewhat coarser than this.
2. There is a large potential for accumulated errors when using three or four displacement transducers to calculate a single quantity.

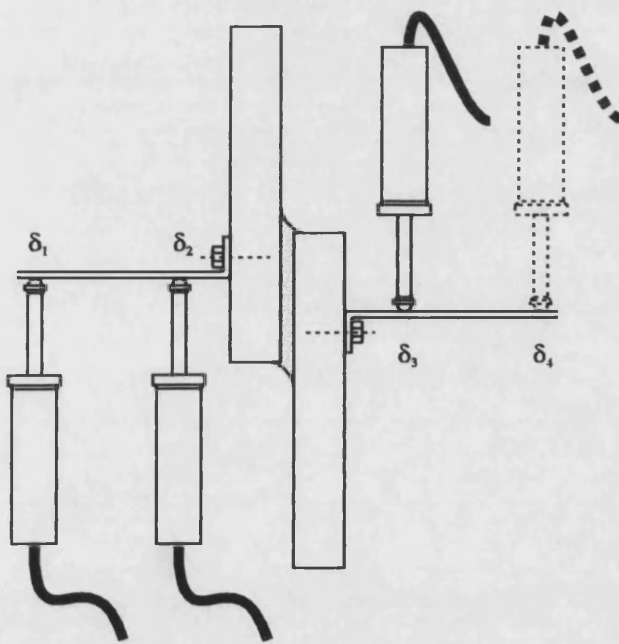


Figure 3.16 Measurement of adhesive slip, method two. Variation one uses δ_1 , δ_2 and δ_3 , see Equation 3-3.

Variation two uses δ_1 , δ_2 , δ_3 and δ_4 , see Equation 3-4

$$s \approx (\delta_2 + \delta_3) - \frac{a}{b}(\delta_1 - \delta_2)$$

Equation 3-3

$$s \approx (\delta_3 + \delta_2) - \frac{a}{b}(\delta_1 - \delta_2 - \delta_3 + \delta_4)$$

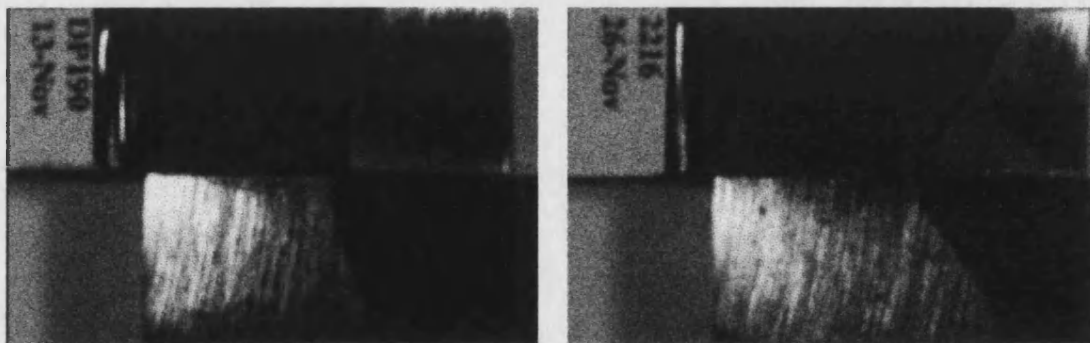
Equation 3-4

3.3.2 Results

The failure loads are summarised in Table 3.5. All of the failures appeared to occur at the interface between the adhesive and the substrate, Figure 3.17. Stress-strain plots are shown in Figure 3.18, Figure 3.19 and Figure 3.20.

DP 190			2216		
Sample	Failure load	Equivalent uniform stress	Sample	Failure load	Equivalent uniform stress
	(kN)	(N/mm ²)		(kN)	(N/mm ²)
Method 1					
1	8.2	10.3	1	9.0	11.3
2	7.6	9.5	2	11.6	14.5
3	9.0	11.3	3	9.2	11.5
4	8.5	10.7	4	8.2	10.3
5	8.1	10.2	5	x	x
Average		10.4 N/mm ²	Average		11.9 N/mm ²
Method 2					
6	12.9	16.2	6	7.2	9.0
7	11.	13.8	7	8.6	10.8
8	11.7	14.7	8	9.3	11.7
9	11.9	14.9	9	8.4	10.5
10	11.0	13.8	10	8.9	11.2
11	9.7	12.2	11	9.5	11.9
12	9.3	11.7	12	9.7	12.2
13	8.5	10.7	13	9.7	12.2
14	9.4	11.8	14	10.0	12.5
15	9.0	11.3	15	x	x
Average		13.1	Average		11.3

Table 3.5 Summary of failure loads for thick adherend lap specimens tested in shear.



(a)

(b)

Figure 3.17 Typical failure of shear specimens. (a) DP 190. (b) 2216.

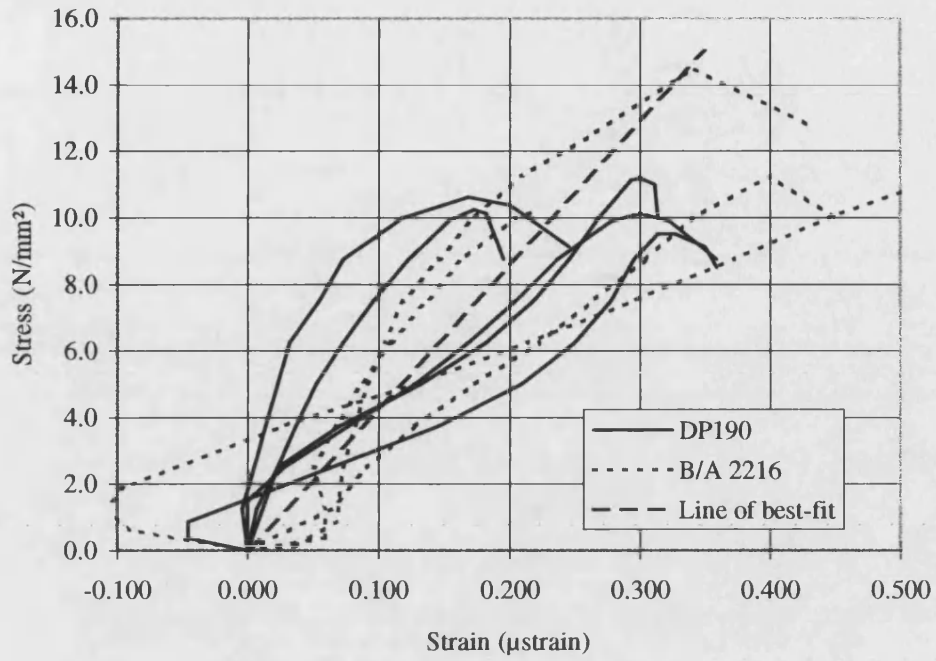


Figure 3.18 Stress-strain plots for DP 190 and 2216, method one. Data points omitted for clarity.

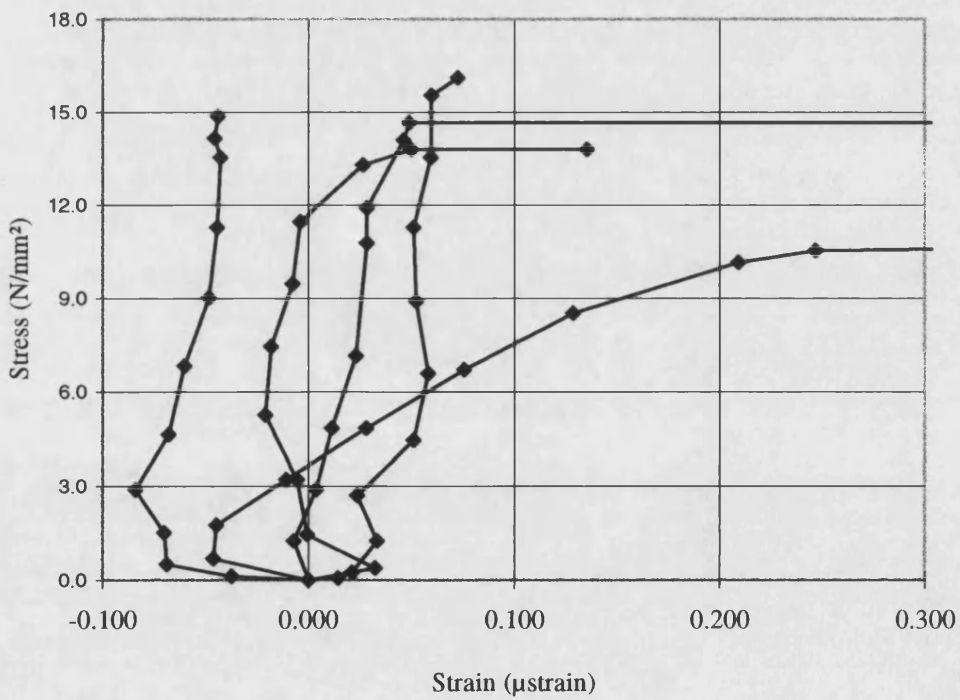


Figure 3.19 Stress-strain plots for DP 190, method two.

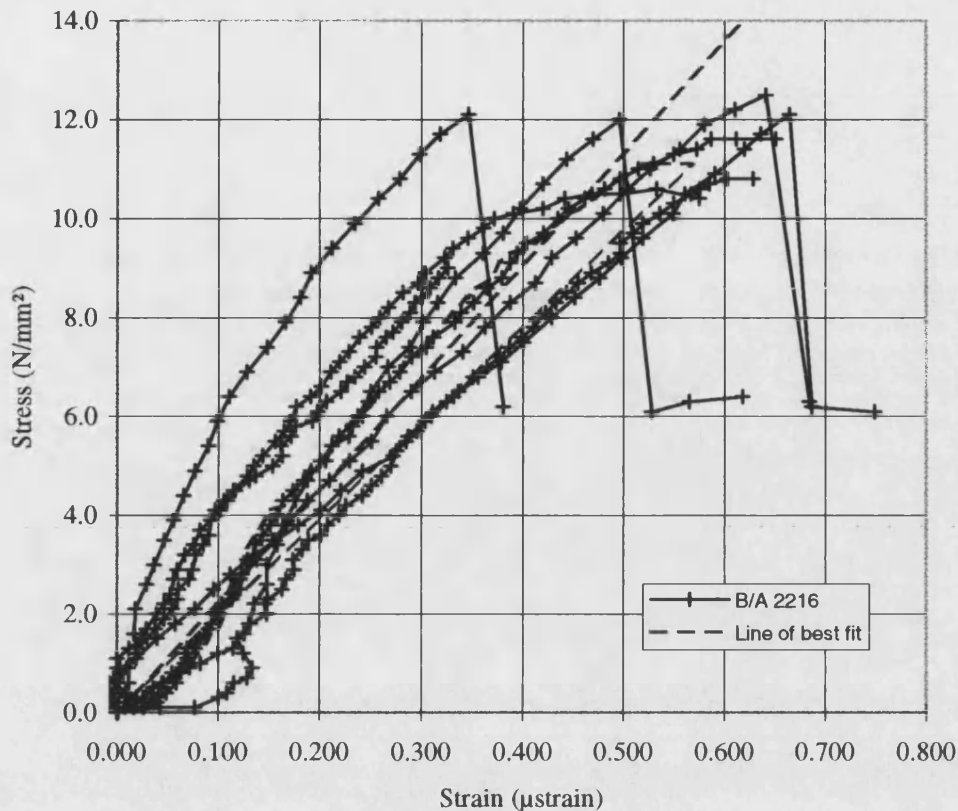


Figure 3.20 Stress-strain plots for 2216, method two.

3.3.3 Discussion

3.3.3.1 Failure stresses

The failure stresses observed during the method one tests were lower than expected. The average DP 190 failure stress was only 59 per cent of its published shear strength and the average 2216 failure stress was 69 per cent of its published shear strength. 3M suggested that the poor results may have been because of inadequate degreasing of the substrate prior to bonding. Therefore for the method two tests the adherends were degreased using dichloromethylethane instead of the proprietary degreasing wipe. All other aspects of the preparation, assembly and cure remained unchanged. The result was that the average DP 190 failure stress rose to 74 percent of its published shear strength.

However, the 2216 failure stress fell by 3 per cent, to 66 per cent of its published shear strength. The failures again appeared to occur at the interface between the adhesive and the substrate which seems to suggest that the issue of surface preparation had still not been resolved.

3.3.3.2 *Stress strain data*

The stress-strain plots from test method one do not show a consistent stress-strain relationship for either adhesive, Figure 3.18. The straight line shown on the plot is an attempt to determine a linear relationship from these results. No attempt has been made to differentiate between the two adhesives. Based upon this line the shear modulus may be calculated as 47 N/mm^2 . This is clearly very different from the value of 127 N/mm^2 published for the 2216 adhesive.

The stress-strain plots from test method two for DP 190 make little sense, Figure 3.19. Apparently this arrangement of three displacement transducers was an inappropriate method of determining the adhesive strains. This may have been because the transducers were not sensitive enough or it may have been that the mechanical resistance of the transducer needle caused the aluminium cantilevers to bend. Alternatively it may have been that the two outer faces of the adherend did not remain parallel which would have rendered Equation 3-3 incorrect. Therefore the tests on the 2216 samples utilised four displacement transducers.

The stress-strain plots for 2216, Figure 3.20, are consistent and look more realistic than those for DP 190. However, the shear modulus which is calculated from the best fit line is only 23 N/mm^2 . Clearly this is very different from the 127 N/mm^2 value quoted by 3M and the 47 N/mm^2 value calculated from the method one tests.

It seems likely that neither method one nor method two are appropriate ways of measuring the adhesive slip. It is shown in Section 5.1.2 that the difference between using an adhesive with a shear modulus of 25 N/mm^2 and one of 100 N/mm^2 is actually

quite small. Therefore the disparities between the measured and published shear moduli are not a cause for major concern. Unfortunately, this set-back does mean that it has not been possible to obtain stress-strain relationships for use in non-linear finite element modelling of the adhesive joint.

In the absence of accurate stress-strain data the choice of adhesive was made on other grounds. 2216 became the obvious choice for several reasons. It was the only adhesive for which 3M were able to specify the shear modulus. It has a proven track record and it is easy to mix and apply in large quantities. In contrast DP 190 is a relatively new adhesive and its cartridge applicator is not ideally suited to applying the large volume of adhesive required in the construction of a full-scale glass T-beam.

3.3.4 Creep resistance of DP190 and 2216

After the difficulties experienced in determining the stress-strain relationship for the two adhesives the tests to determine the creep resistance of the two adhesives was kept as simple as possible. 3M informed the author that both adhesives exhibited very little creep under sustained loading at low loads and therefore the creep resistance was not considered to be a major issue, Pye (1996b).

Both DP 190 and 2216 were tested under sustained loading. The samples took the same form as those used in the thick adherend tests. In each case five samples were loaded to 5.4 kN for a minimum period of one week. If the sample had not failed after one week the load was increased to 10.8 kN and a week later to 16.2 kN. Three samples from each batch were tested at room temperature whilst the two remaining samples were tested at a higher temperature. These two samples were heated by placing them close to an infra-red heat lamp. During each test the temperature of the sample was monitored using a thermocouple. The results are summarised in Table 3.6.

DP190				2216			
Sample	Load/ stress (kN)/ (N/mm ²)	Av. Temp. (°C)	Duration (Days)	Sample	Load/ stress (kN)/ (N/mm ²)	Av. Temp. (°C)	Duration (Days)
1	5.4/6.8	18	7	1	5.4/6.8	18	7
	10.8/13.5	18	7		10.8/13.5	18	7
	16.2/20.3	18	0		16.2/20.3	18	0
2	5.4/6.8	18	7	2	5.4/6.8	19	7
	10.8/13.5	19	7		10.8/13.5	18	7
	16.2/20.3	18	0		16.2/20.3	18	0
3	5.4/6.8	18	7	3	5.4/6.8	17	7
	10.8/13.5	18	7		10.8/13.5	17	7
	16.2/20.3	18	0		16.2/20.3	17	0
4	5.4/6.8	33	7	4	5.4/6.8	35	7
	10.8/13.5	33	0		10.8/13.5	36	0
5	5.4/6.8	34	7	5	5.4/6.8	35	7
	10.8/13.5	34	0		10.8/13.5	35	0

Table 3.6 Summary of long term tests on DP 190 and 2216.

3.3.5 Adhesion to glass and cyclic performance

Although 2216 was chosen as the preferred adhesive for manufacturing the primary adhesive joint, DP 190 was used to bond steel tension plates to the glass flange, see Section 9. The ability of both adhesives to form a strong bond to a glass substrate and the ability of both adhesives to withstand cyclic fatigue was demonstrated during full scale testing of the glass-adhesive T-beams. See sections 9 and 10.

4 THEORETICAL CONSIDERATIONS

4.1 Introduction

This chapter is concerned with the theory that describes the structural behaviour of the glass-adhesive T-beam. Specifically it develops a two dimensional plane stress composite theory, a two dimensional plate theory approach to shear lag in the flange and a two dimensional plate buckling approach to the localised buckling of the web. These theories are not wholly new. They are generally based upon existing theory although they are subject to minor modifications to suit their application to this new problem.

4.1.1 Sign conventions

Throughout this thesis a left handed co-ordinate system is assumed, such that clockwise shear forces and sagging bending moments are considered positive, Figure 4.1.



Figure 4.1 Sign conventions

4.2 Composite bending

It is necessary to describe the stress distribution in the glass-adhesive sandwich construction. In the case where the adhesive has no structural properties the two glass plates will behave in a layered manner, Figure 4.2a. At the other extreme the two plates will behave in a monolithic manner, Figure 4.2b. In general the behaviour will lie between these two extremes, Figure 4.2c. It will be useful to describe the degree of composite action and this may be expressed as a relationship between the behaviour of the composite section and its equivalent layered and monolithic sections. As a primary

objective of this work is to reduce deflection
this relationship is expressed in terms of
midspan deflection, Equation 4-1.

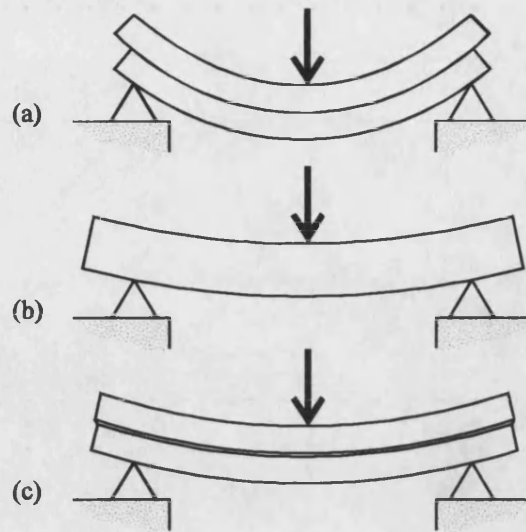


Figure 4.2 Principles of composite action

- (a) Layered, 0% composite action,
(b) Monolithic, 100% composite action,
(c) Composite, 0-100% composite action.

$$\text{Percentage composite action} = \frac{\delta_l - \delta_c}{\delta_l - \delta_m} \times 100\%$$

Equation 4-1

- δ_l midspan deflection of equivalent layered section
 δ_c midspan deflection of composite section
 δ_m midspan deflection of equivalent monolithic section

In deriving the governing equation of bending for the composite section the following assumptions are made;

1. A condition of plane stress exists in the beam.
2. All materials behave linearly and elastically.
3. Plane sections remain plane in the two outer layers
4. The outer layers are much stiffer than the adhesive. Consequently the contribution of the adhesive to the total bending moment and axial force at any cross section is sufficiently small that it can be ignored.
5. There is no slip at the glass-adhesive interface.

6. The thickness of the adhesive joint remains constant.
7. The deflection of the beam is sufficiently small that the curvature can be approximated

to $\frac{d^2z}{dx^2}$.

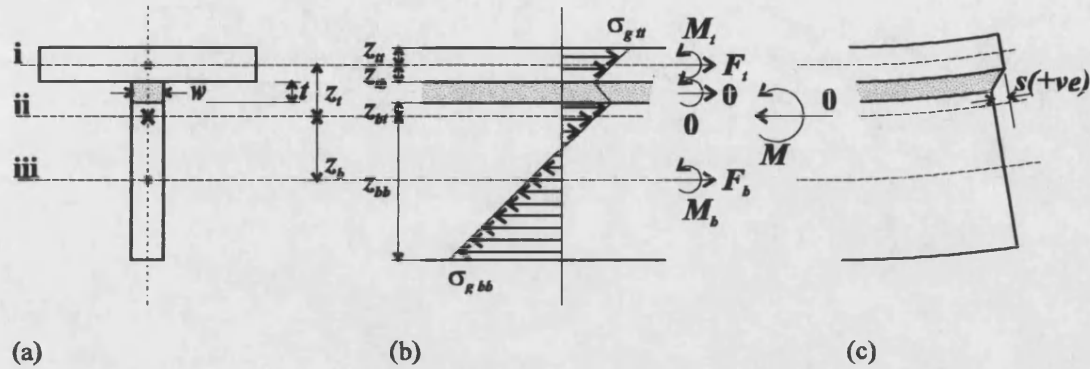


Figure 4.3 Stresses, moments and forces in an idealised composite section. (a) Cross section perpendicular to span, (b) Distribution of stresses, moments and forces, (c) Sign convention for slip. (i) Neutral axis of flange, (ii) Neutral axis of equivalent monolithic section, (iii) Neutral axis of web

Figure 4.3 shows a generalised composite beam. Considering equilibrium;

$$F = -F_t + F_b \tag{Equation 4-2}$$

$$M = M_t + M_b + F_b z_b - F_t z_t \tag{Equation 4-3}$$

$$A_t z_t = A_b z_b \tag{Equation 4-4}$$

$$F_t' = -F_b' = q \tag{Equation 4-5}$$

From conditions 3 and 7 the following compatibility equations may be written;

$$M_t = E_g I_t z'' \tag{Equation 4-6}$$

$$M_b = E_g I_b z'' \tag{Equation 4-7}$$

$$\epsilon_{tb} = \epsilon_t + z_{tb} z'' \tag{Equation 4-8}$$

$$\epsilon_{bt} = \epsilon_b - z_{bt} z'' \tag{Equation 4-9}$$

$$\varepsilon_{tb} - \varepsilon_{bt} = s' - z''t \quad \text{Equation 4-10}$$

Finally the constitutive relationships may be written;

$$q_a = G_a \gamma_a w \quad \text{Equation 4-11}$$

$$F_t = \varepsilon_t E_g A_t \quad \text{Equation 4-12}$$

$$F_b = \varepsilon_b E_g A_b \quad \text{Equation 4-13}$$

By re-arranging equations 2 to 13 (see Appendix B) it may be shown that;

$$E_g I_t \frac{d^4 z}{dx^4} - C E_g I_m \frac{d^2 z}{dx^2} = \frac{d^2 M}{dx^2} - CM \quad \text{Equation 4-14}$$

Where C is the composite constant,

$$C = \frac{G_a w (z_b + z_t)}{t E_g A_t z_t} \quad \text{Equation 4-15}$$

In the case where $C \rightarrow \infty$ Equation 4-14 reduces to the Bernoulli bending equation for a beam of stiffness $E_g I_m$. Similarly if $C \rightarrow 0$ Equation 4-14 reduces to the Bernoulli bending equation for a beam of stiffness $E_g I_t$. Therefore it can be seen that the governing equation satisfies both extremes of composite action. However, we are normally interested in the non-trivial cases of $0 < C < \infty$.

4.2.1 Solution of the governing differential equation

The general solution may be taken in the form;

$$z = c_1 + c_2 x + c_3 \cosh \lambda x + c_4 \sinh \lambda x + PI \quad \text{Equation 4-16}$$

where c_1 to c_4 are constants to be determined. For the case of a simply supported beam the boundary conditions are;

$$z(0) = z''(0) = 0$$

$$z(L) = z''(L) = 0$$

and if the particular integral is chosen such that it satisfies the above boundary conditions it may be shown that;

$$c_1 = c_2 = c_3 = c_4 = 0$$

If the beam is subject to a load distribution;

$$p(x) = -\sum_{n=1}^{\infty} B_n \sin(\alpha x) \quad \text{Equation 4-17}$$

then the moment will be;

$$M(x) = \sum_{n=1}^{\infty} \frac{B_n \sin(\alpha x)}{\alpha^2} \quad \text{Equation 4-18}$$

If the solution to the particular integral is then proposed as being;

$$z = \sum_{n=1}^{\infty} c_5 \sin(\alpha x)$$

the constant c_5 is shown to equal;

$$c_5 = B_n \frac{\alpha^2 + C}{S_1 \alpha^6 + CS_m \alpha^4}$$

Therefore the displacement is shown to be;

$$z = \sum B_n \frac{\alpha^2 + C}{S_1 \alpha^6 + CS_m \alpha^4} \sin(\alpha x) \quad \text{Equation 4-19}$$

4.2.2 Glass and adhesive strains

The derivation of other quantities is now achieved by back substitution into Equations 4.2 to 4.13. In this manner it is shown that the longitudinal strain at any point in the upper glass plate is;

$$\epsilon_t(x, z) = \frac{S_1 z'' - M}{E_g A_t (z_t + z_b)} - z z'' \quad \text{Equation 4-20}$$

Similarly the strain at any point in the lower plate is;

$$\epsilon_b(x, z) = \frac{-S_1 z'' + M}{E_g A_b (z_t + z_b)} - z z'' \quad \text{Equation 4-21}$$

The shear strain in the adhesive is shown to be;

$$\gamma_a = \frac{1}{G_a w(z_b + z_t)} [M' - S_1 z'''] \quad \text{Equation 4-22}$$

4.2.3 Shear deflection

It was stated in the assumptions that for the outer layers plane sections remain plane. Whilst this is a reasonable approximation for beams which are very long in comparison to their depth, toughened glass plates are often limited to an aspect ratio of 10. In such cases the shearing deflection becomes significant and can account for 20 percent of the total deflection. Figure 4.4 indicates the shear deflection at the

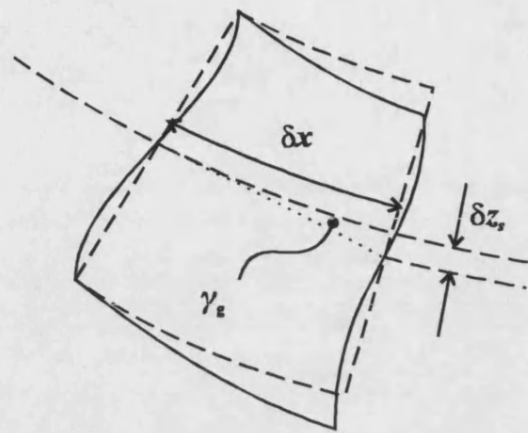


Figure 4.4 Shear deflection in a small beam element

neutral axis of a short beam section of length δ_x . Accepting that the shearing deflection is a secondary effect to beam bending and therefore ignoring warping effects it may be written that, Case et al. (1993);

$$\delta z_s = \gamma \delta x$$

In the case of the monolithic beam the shear deflection at any point then becomes;

$$z_{sm}(x) = \frac{A_b(z_b - z_{bb})}{2wI_m} M'(x) \quad \text{Equation 4-23}$$

In the case of the layered beam only the shear deflection in the web need be considered as the aspect ratio of the flange is likely to be so high as to make shear deflections insignificant. In this case the shear deflection is simply;

$$z_{sl}(x) = \frac{3M'(x)}{2A_b G_s} \quad \text{Equation 4-24}$$

It would be possible to calculate the shear deflection of the composite section.

However, this would be a lengthy calculation and it will generally be adequate to base the shear deflection upon the deflection of the equivalent monolithic section.

4.2.4 Special case of a beam supported at distances α and β from each end

In practical construction beams are supported at a distance in from each end of the beam, Figure 4.5. In this case the boundary conditions become;

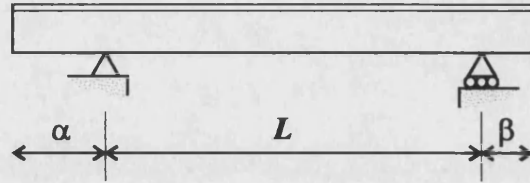


Figure 4.5 A simply supported beam with cantilevered ends

$$z(\alpha) = 0 \quad z(\alpha + L) = 0$$

$$z''(0) = z''(\alpha + L + \beta) = 0$$

Applying the last two boundary conditions the equation for z reduces to;

$$z = c_1 + c_2x + \sum B_n \frac{\alpha^2 + C}{S_1\alpha^6 + CS_m\alpha^4} \sin(\alpha x)$$

That is that c_1 and c_2 represent a rigid body translation and rotation. As the direct strains and shear strains are based upon the second and third differentials it is seen that strain Equation 4-20 to Equation 4-22 are still valid.

The case of multiple spans is more complex and is dealt with in an iterative manner in Section 5.1.7. The case of fixed end supports is not dealt with as this is not a condition met in practice.

4.3 Shear lag

In wide flanged beams the stress distribution predicted using conventional bending theory may differ significantly from those stresses encountered in practice. This is because the plane stress approximation which conventional bending theory is based upon is no longer valid as the section becomes wider. Away from the web the longitudinal stresses in the flange will fall below those values predicted using conventional bending theory.

However, at the intersection of the web and flange the stress will peak above those values predicted by conventional theory, Figure 4.6. This effect is known as shear lag and has been studied in the cases of concrete and steel beam sections for many years. Much of the work has been codified. For example, in the case of concrete design to BS 8110, BS (1985), the effective width of the flange is limited to one fifth of the span in order to control the effects of shear lag.

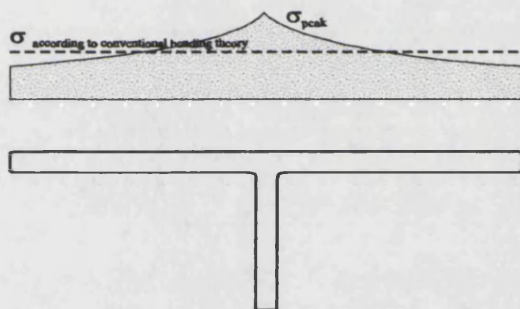


Figure 4.6 Typical distribution of bending stresses across a wide flanged beam

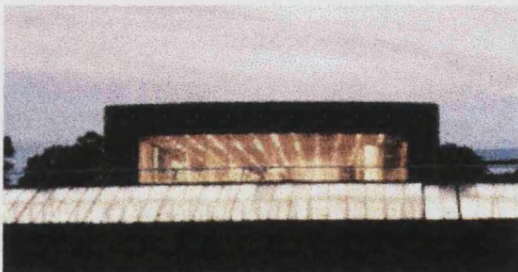


Figure 4.7 The Sainsbury Centre, Norfolk. A tall glazed facade stabilised with fins which support wide glass window plates

There are two reasons why shear lag is a particular concern in the construction of glass adhesive beam sections. Firstly, the inability of glass to yield and thereby re-distribute stress means that it is important to be able to determine the value of any stress peaks.

Otherwise a generally low stressed glass structure may be locally over stressed causing a catastrophic failure of that element. In the case of the T-beams investigated here, this concern is somewhat reduced. When the flange is in tension the web will obviously be in compression and generally the compressive stresses at the base of the web will be much

higher than the tensile stresses in the flange. Therefore buckling of the web is likely to occur before local over stressing of the flange. As glass can sustain high compressive stresses the reverse action is not of major consequence.

The scenario of locally over stressing the flange becomes far more realistic in the case of I-beams and box beams. Whilst these sections will not be discussed as a part of this thesis the mechanism of shear-lag in glass adhesive beams may be established with the T-beam. In this manner it may be possible to apply this work to the case of these other sections at a later date.

The second reason why shear lag is an important concern is that glass is often used in long wide beam sections, Figure 4.7. This is particularly the case where glass is used as a cladding material. The geometry that these applications impose makes shear lag a very real issue. Whereas BS 8110 limits flange effective widths to one fifth of the span it is common to find glass panels that have a width which approaches their span.

The work presented here is based upon the original work of Song (1984). Song subsequently published several papers in which he and Scordelis demonstrated the validity of this approach by comparison with known problems, Song and Scordelis (1990a). They also have shown how the analytical approach may be simplified for use in hand calculations, Song and Scordelis (1990b). The accessibility of Song's mathematics and the demonstration of its validity are the main reasons that this work was chosen as the basis for investigating the shear lag in the glass adhesive T-beam.

The work of Song is based upon the stress function; sometimes known as the Airy stress function, see Timoshenko and Woinowsky-Kreiger (1959). This function describes the behaviour of a thin plate loaded in its own plane. It is assumed that all the materials are perfectly linear-elastic and that a condition of plane stress exists across the depth of the plate. Song assumes that the flange is infinitely flexible out of its own plane and that the stresses in the web can be determined by elementary beam theory. The first of these assumptions amounts to a condition of plane stress across the depth of the flange.

Effectively, this means that flange must be reasonably thin in comparison to the depth of the web. However, the second Song assumption needs to be modified because the web stresses can no longer be determined by elementary bending theory.

It is first necessary to summarise the work of Song. The stress in the flange may be described using the stress function;

$$\frac{\partial^4 \phi}{\partial x^4} + 2 \frac{\partial^4 \phi}{\partial x^2 \partial y^2} + \frac{\partial^4 \phi}{\partial y^4} = 0$$

$$\phi = \sum_n f_n(y) \sin(\alpha x)$$

Equation 4-25

The following boundary conditions are applied. See Figure 4.8.

At the free edge, $y = 0$;

$$\sigma_y = 0$$

$$\tau_{xy} = 0$$

At the junction of the web, $y = b$;

displacement $v = 0$

$$(\epsilon_x)_{flange} = (\epsilon_x)_{web}$$

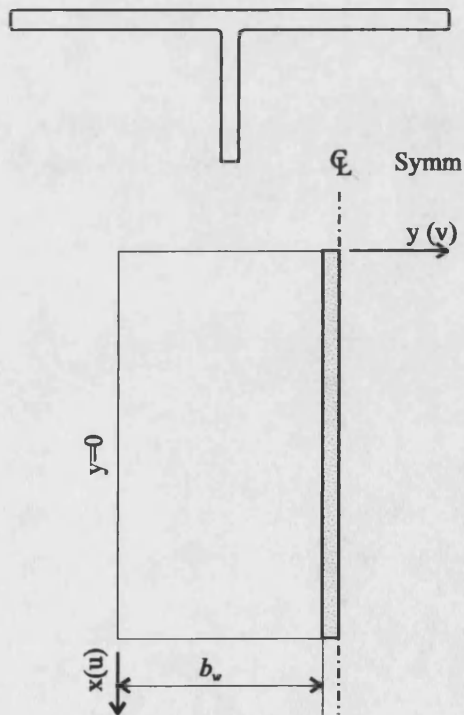


Figure 4.8 Origin and orientation of axis used in the solution of the shear lag problem

Accordingly it may be written that;

$$\sigma_y = -\sum_{n=1}^{\infty} A_n c(y) [\alpha y \tanh \alpha y + \gamma (\alpha y - \tanh \alpha y)] \sin \alpha x$$

$$\sigma_x = -\sigma_y + 2 \sum_{n=1}^{\infty} A_n c(y) (1 + \gamma \tanh \alpha y) \sin \alpha x$$

$$\tau_{xy} = -\sum_{n=1}^{\infty} A_n c(y) [\tanh \alpha y + \alpha y (1 + \gamma \tanh \alpha y)] \cos \alpha x$$

As in the case of the composite bending equation the moment at any section may be expressed as;

$$M(x) = \sum_{n=1}^{\infty} \frac{B_n \sin(\alpha x)}{\alpha^2} \quad \text{Equation 4-18}$$

For the flange;

$$(E\varepsilon_x)_{y=b} = \sum_{n=1}^{\infty} A_n \{2 + (1 + \nu)\alpha b t + \gamma[(1 - \nu)t + (1 + \nu)\alpha b]\} \sin \alpha x \quad \text{Equation 4-26}$$

And in addition the total shear transfer from the flange may be written;

$$T = 2 \int_0^x \left(\tau_{xy} \right)_{y=b} h dx \quad \text{Equation 4-27}$$

It is in determining the bending strain in the web that we deviate from the original theory. Figure 4.9 shows the web with the adhesive joint. As with the composite theory it is assumed that there is no slippage at the glass-adhesive interface and it is also assumed that the thickness of the adhesive joint remains constant. Furthermore it is now assumed that the thickness of the adhesive joint is very small. In this case the bending stiffness of the web is based upon the full height of the web; that is it includes the thickness of the adhesive. The effect of shear in the adhesive is then accounted for by subtracting the necessary stress component from the web stress. This is shown in Figure 4.9 and Equation 4-28 and Equation 4-29.

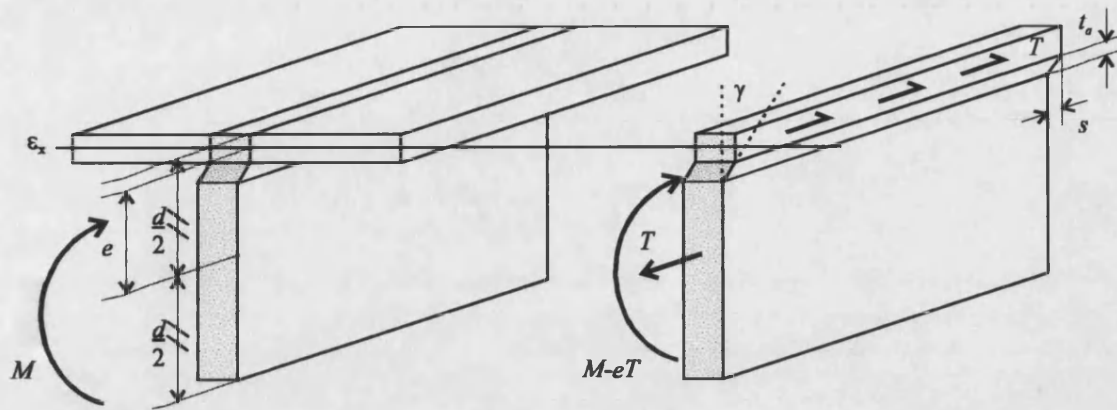


Figure 4.9 Adhesive shear in the web of the composite T-section

$$E_g \epsilon_x = \left(\frac{1}{A} + \frac{e^2}{I_w} \right) T - \frac{eM}{I_w} - E_g \frac{ds}{dx} \quad \text{Equation 4-28}$$

Where;

$$I_w = \frac{b_w d^3}{12} \quad \text{Equation 4-29}$$

As in the case of the composite theory it may be written;

$$\frac{dT}{dx} = q = s \left(\frac{Gw}{t} \right)_a \quad \text{Equation 4-30}$$

Therefore;

$$E_g \epsilon_x = \left(\frac{1}{A} + \frac{e^2}{I_w} \right) T - \frac{eM}{I_w} - E_g \left(\frac{t}{Gw} \right)_a \frac{d^2 T}{dx^2} \quad \text{Equation 4-31}$$

$\frac{d^2 T}{dx^2}$ is determined from Equation 4-27. Therefore by substituting Equation 4-27 into

Equation 4-31 and equating with Equation 4-26 it is possible to determine the unknown constant A_n . After some re-arrangement it can be shown that A_n equals;

$$A_n = \frac{\frac{e}{I_w} \frac{B_n}{\alpha^2}}{\left(2 + (1 + \nu) \alpha b_w + \beta [(1 - \nu) t \alpha b_w] + \left(\frac{1}{A} + \frac{e^2}{I_w} + E_g \alpha^2 \left(\frac{t}{Gw} \right)_a \right) 2 b_w h_w \left(1 + \beta t + \frac{t}{\alpha b} \right) \right)}$$

Equation 4-32

This is not the same A_n term as Song uses because it incorporates the effect of shear in the adhesive joint. However, this new A_n term may be used in Song equations to give the correct stress distribution within the flange of the composite beam. It transpires that the only difference in the two A_n terms is the inclusion of the $E_s \alpha^2 \left(\frac{t}{Gw} \right)_a$ term in the denominator of the composite shear lag formula. The physical significance of this is easily determined by considering the extremes of G tending to infinity and G equals zero. As G tends to infinity the new term tends to zero and A_n reverts to the original Song equation. That is, when the composite behaves in a way which approaches the monolithic state, such that the web stresses can be determined by elementary bending theory, the composite shear lag may be described using the Song equations. In the second extreme where G equals zero the A_n term equals zero and the flange is in an unstressed state. In this case the web carries all of the applied load. In practice the flange will carry a small portion of the load according to its bending stiffness relative to that of the web. The fact that the flange is considered unstressed is a function of the assumption that it has no bending stiffness. Whilst we will not generally be interested in the case of G equals zero the effect of the flange having no bending stiffness may become apparent in other scenarios. We should expect the web stresses predicted using the composite shear lag formula to be slightly higher than we would observe in practice because of neglecting this bending stiffness in the flange. This will be particularly apparent in the case of deep flanges with shallow webs.

4.3.1 Derivation of adhesive shear stresses and web bending stresses

From the previous theory it is also possible to determine information regarding the stresses in the adhesive and the web. The approach to determining the stresses differs considerably from that taken in the derivation of the composite bending theory. Accordingly the stresses will differ from those calculated using the composite bending theory. There will generally be two reasons for this; firstly the inclusion of the shear lag effects in wide span beams and secondly the assumption that the flange has no bending stiffness. It will be important to differentiate between these two causes. In the case of

thin flange beams the second difference will be minimal. Where the flange possesses a significant bending stiffness this difference will need to be accounted for to determine the true effect of the shear lag. The simplest way of doing this will be to remove the I_f term for the flange in the composite theory. This will reduce the bending stiffness of the equivalent layered section to;

$$I_t = I_b$$

$$I_m = I_b + A_t z_t^2 + A_b z_b^2$$

In this manner it will be possible to assess the true contribution of the shear lag effect to the stress distribution of the whole beam.

The adhesive shear stress, according to the composite shear lag theory, may be determined by differentiating Equation 4-27 and substituting into Equation 4-30.

$$\gamma_a = -\frac{2b_f h_f}{G_a w_a} \sum_{n=1}^{\infty} A_n \alpha \left(1 + \beta t + \frac{t}{\alpha b_w} \right) \cos \alpha x \quad \text{Equation 4-33}$$

The glass stresses in the web are determined in exactly the same manner as in Equation 4-31 only this time we lose the $\frac{d^2 T}{dx^2}$ term. Therefore the stress at the base of the web may be written;

$$\sigma_x = \left(\frac{1}{A_w} - \frac{ed}{2I_w} \right) T + \frac{d}{2I_w} M$$

Which when expanded becomes;

$$\sigma_x = \sum_{n=1}^{\infty} \left(\left(\frac{ed}{2I_w} - \frac{1}{A_w} \right) 2b_w h_w A_n \left(1 + \beta t + \frac{t}{\alpha b_w} \right) - B_n \frac{d}{2\alpha^2 I_w} \right) \sin \alpha x \quad \text{Equation 4-34}$$

4.3.2 Stress ratio and effective width

Two useful concepts in the discussion of the shear lag phenomena are the stress ratio and the effective width. The stress ratio is the ratio of the stress calculated assuming shear lag to that calculated using conventional bending theory. In this case conventional bending theory will be the composite bending theory derived in Section 4.2. The concept is useful as the stress ratio may be used to predict the peak stress in a beam from the

conventional bending theory. Of course, this does mean that it is first necessary to determine the stress ratio for the particular load, span and beam section being considered. The stress ratio may be written;

$$SR = \frac{\sigma_{SL}}{\sigma_C} \quad \text{Equation 4-35}$$

An alternative approach is to consider the effective width of the flange. The effective width is simply the width of the equivalent beam, i.e. all other dimensions remain unaltered, that when analysed using conventional bending theory would give a peak stress equal to that calculated assuming shear lag. The effective width is therefore defined as;

$$\sigma_{SL}(b_f) = \sigma_C(b_{ef}) \quad \text{Equation 4-36}$$

This means that the equivalent layered and monolithic second moments of area must now be written as a function of a b_{ef} . They therefore become;

$$I_t = \frac{b_f h_f^3 + b_w h_w^3}{12} \quad \text{and} \quad I_m = I_t + A_t z_t^2 + A_b z_b^2$$

where

$$z_t = \frac{A_t \frac{h_f}{2} + A_b \left(h_f + \frac{h_w}{2} \right)}{A_t + A_b} - \frac{h_f}{2} \quad \text{and} \quad z_b = \frac{A_t \left(h_w + \frac{h_f}{2} \right) + A_b \frac{h_w}{2}}{A_t + A_b} - \frac{h_w}{2}$$

It is not easily possible to re-arrange the stress equations for the composite bending theory as a function of b_{ef} and therefore the solution should be found using either a graphical or numerical method. Whilst this may seem inconvenient, it should be appreciated that the software needed to handle the large number of Fourier terms in the composite and shear lag theories is also capable of solving this numerical problem.

4.4 Buckling

Buckling is an instability phenomenon. It occurs at some critical load at which, or just before which, the deflection of the structure is no longer directly proportional to the applied load. The deflection of the structure may increase to such a point that the structure collapses or else it may regain stability as in the case of snap through buckling. Generally the buckling of the glass adhesive T-beams can be expected to display no post buckle stability as there are no obvious mechanisms by which the buckled beam could regain stability. Therefore an eigen value approach to the problem (first order stability analysis) will yield the relevant information to determine the buckling loads and mode shapes.

Buckling may be an overall buckling effect or localised buckling effect, Figure 4.10. Within this thesis only overall buckling of the web is considered.

4.4.1 Overall buckling

Potential forms of overall buckling include lateral torsional buckling, overall buckling of the web and overall buckling of the flange, Figure 4.11. In the case of the T-beams that are discussed and tested as a part of this thesis lateral torsional buckling cannot occur because the beam is bent about its minor axis. If the equation for lateral torsional buckling is derived taking into account the deflections in the plane of the applied load, the critical bending moment at which buckling will occur can be written, Kirby and Nethercot (1979);

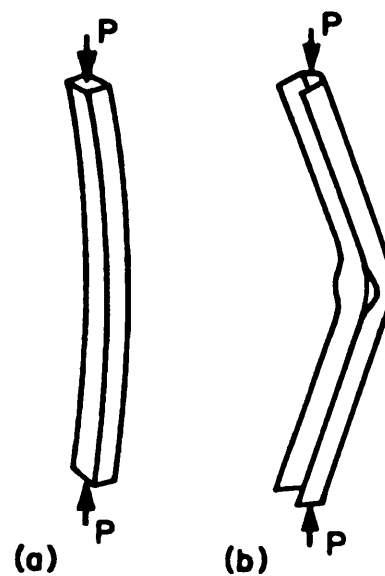


Figure 4.10 (a) Overall buckling and (b) local buckling of a channel section

$$M_{cr} = \frac{\pi}{L} \frac{\sqrt{EI_z GJ}}{\sqrt{(I_y - I_z)/I_y}} \sqrt{\left(1 + \frac{\pi^2 EI_w}{L^2 GJ}\right)}$$

Equation 4-37

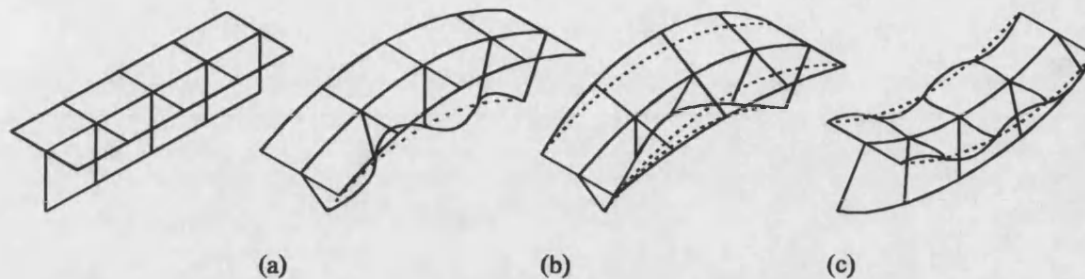


Figure 4.11 Various ways in which a T-beam may buckle. (a) Overall buckling of web, (b) Lateral torsional buckling, (c) Overall buckling of flange.

It can be seen that as the value of I_z approaches I_y a singularity develops in the denominator of the expression. As I_z is typically greater than I_y for the glass-adhesive beam structures discussed here it is apparent that this mode of buckling cannot occur.

The section geometry of most practical glass-adhesive T-beams is such that the horizontal neutral axis tends to be located close to the flange. As a result the flange stresses tend to be far less than the peak web stresses. Whilst this does not preclude the possibility of flange buckling, particularly in the case of wide thin flanges, it does mean that over-stressing of the web is likely to be the most common cause of failure. During the laboratory tests of wide thin-flanged T-beams no flange buckling was witnessed, see Section 10. As a result of this no work has been conducted concerning the issues of flange buckling. Whilst this may be deemed acceptable in the case of T-beams it will clearly not be so in the case of other sections, such as I beams. In such cases the flanges may be subjected to very high compressive forces and flange buckling is likely to be a serious issue. In the case of I-beams bent about their major axis it will also be necessary to investigate the interaction of lateral torsional buckling and flange buckling. This is because this interaction may lead to a buckling load lower than that predicted by considering the two effects separately, Murray (1984). In these scenarios it may also be necessary to take into account the fact that the flange stresses will reduce towards the free edges. This has already been discussed in the previous section on shear lag.

Whilst the section geometry of T-beams is such that flange stresses tend to be small the converse is true for the stresses at the bottom of the web. It is possible to generate high compressive stresses at this location and the nature of the free edge makes buckling a real possibility. The only buckling witnessed in the laboratory tests was in the web.

In most practical T-beams the stress distribution in the web will be approximately triangular with the highest stresses occurring at the free edge. As the free edge is the most unstable part of the plate and also the most highly stressed part, it will govern the buckling behaviour of the plate. It is therefore suggested that the buckling of the web may be approximated to the buckling of a uniformly loaded plate with suitable boundary conditions. Various boundary conditions are shown in Figure 4.12. Clearly the application of the compressive load in the upper part of the plate is unrealistic but it is permitted because the behaviour of this part of the plate is less critical in controlling buckling. A further assumption that has been made is that the compressive stresses are uniform along the full length of the web. In practice the very high stresses will only tend to occur at the midspan (dependent upon the load distribution) and they will fall away towards the supports. This is a problem often encountered when considering lateral torsional buckling. It is usual to determine the buckling load assuming a uniform moment, when in practice the moment will often vary along the span. One approach to this problem is the use of an equivalent uniform moment factor, m .

$$m = \frac{M_{critical \text{ (constant moment)}}}{M_{critical \text{ (actual moment distribution)}}} \qquad \text{Equation 4-38}$$

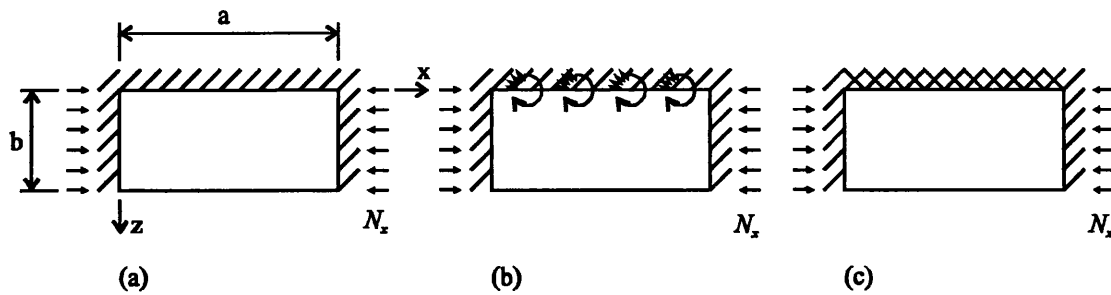


Figure 4.12 Simplified models for web buckling. Free lower edge, two opposite edges simply supported and subject to compressive force N_x , various conditions along top edge. (a) Simply supported top edge, (b) Elastically supported edge, (c) Fixed top edge.

For the case of a uniformly distributed load the value of m is 0.88; i.e. the critical value of M in the case of the uniformly distributed load is 14 per cent higher than in the case of constant moment. With the uniformly distributed load the peak compressive stress occurs at the midspan and the bending stresses fall to zero at the support conditions. In the case of a four point bending distribution m is 0.96, although in the three point bending distribution m falls to 0.76. It can be seen that the important aspects are the magnitude of the midspan stress and how quickly this falls to zero. This is illustrated in Figure 4.13. The equivalent uniform moment factor is determined according to the moment in the beam under consideration. However, what is really addressed in the distribution of compressive stress and in the prismatic beam the shape of the plot of the compressive stresses would be identical to the bending moment plot. There therefore

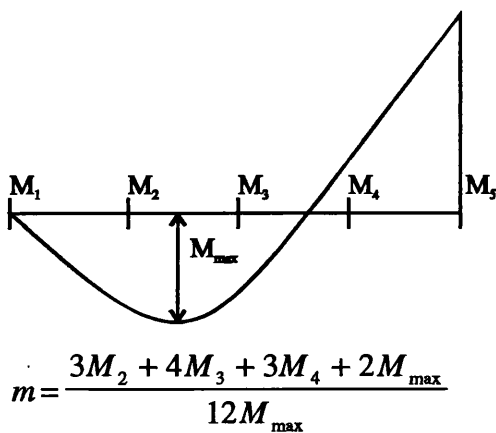


Figure 4.13 Calculation of m for complex bending moment distributions

seems some sense in considering the use of uniform equivalent moment factors as being applicable to the plate buckling of the web.

The above discussion highlights that there is only a small difference between the buckling loads for a beam with a constant moment and one with a uniformly distributed load. It can therefore be expected that there will be only a small difference between the buckling load

predicted using the models in Figure 4.11 and those which take into account the variation of compressive stress along the span.

The consideration of the fixity condition along the top edge is affected by two factors. Firstly the rotation of the flange as the web buckles will be such that the web cannot be considered fixed along its top edge. Secondly the rotation permitted by the adhesive at the web-flange interface will mean that the web no longer remains perpendicular to the flange. Clearly a fixed scenario may be unrealistic although the simply supported scenario may be pessimistic, whilst safe. The question exists: how much rotational restraint are the flange and the adhesive able to provide?

The issue of web rotation restraint due to the adhesive is temporarily put to one side. All the remaining problems shown in Figure 4.11 are treated in the "Theory of elastic stability", Timoshenko and Gere (1961). The solutions are all derived from the linear stability equation, Equation 4-39. That is, they are first order stability analyses and yield information about buckling load and mode shapes but not about deformations. In addition they are based upon the assumption that the plate is perfectly flat. However, it has already been seen, Section 2, that glass plates may be far from flat. In the case of toughened glass overall bow and end dip may lead to a significant $P-\delta$ effect which will drastically reduce the buckling load of the web, Figure 4.14. Furthermore it is assumed that the loads are put into the plate in a perfectly true manner such that there is no eccentricity.

$$\frac{\partial^4 w}{\partial x^4} + 2 \frac{\partial^4 w}{\partial x^2 \partial y^2} + \frac{\partial^4 w}{\partial y^4} = - \frac{N_x}{D} \frac{\partial^2 w}{\partial x^2} \quad \text{Equation 4-39}$$

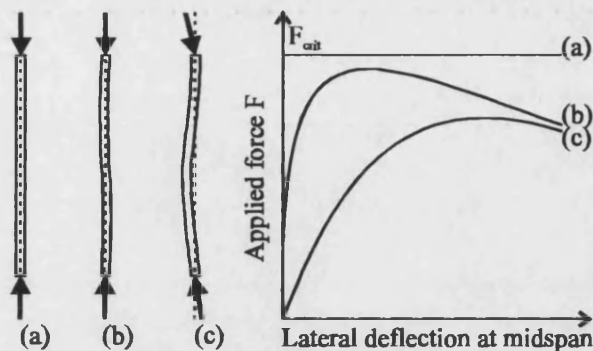


Figure 4.14 Effect of imperfections on buckling loads. (a) Theoretical behaviour for a perfect beam, (b) Physical test on a beam with negligible imperfections, (c) Test on a beam with a realistic level of imperfection.

The solutions to the linear instability equation for the three sets of boundary conditions shown in Figure 4.11 may be represented by the equation:

$$\sigma_x = \frac{N_x}{h} = K \frac{\pi^2 D}{b^2 h} \quad \text{Equation 4-40}$$

K is a dimensionless constant to be determined. Values of K for each of the boundary conditions are shown in Figure 4.15, Figure 4.16 and Figure 4.17. In each case it is assumed that the depth of the plate buckles into one half sine wave. For the case of the simply supported and fixed edge conditions the solution is solely dependent upon the aspect ratio of the plate, $a:b$. The number of half sine waves, n , that the plate buckles into along its edge is determined by the lowest value of K .

In the case of a simply supported top edge the lowest value of K is always given by the value of $n=1$. In the case of the fixed edge the plate will try to buckle into squares of aspect ratio 8:5. In this case n may be easily determined by plotting K against the aspect ratio for various values of n . The value of n is then determined by selecting the aspect ratio for the plate being considered and drawing a vertical line upwards. The first curve which this line intersects indicates the number of half waves into which the plate will buckle.

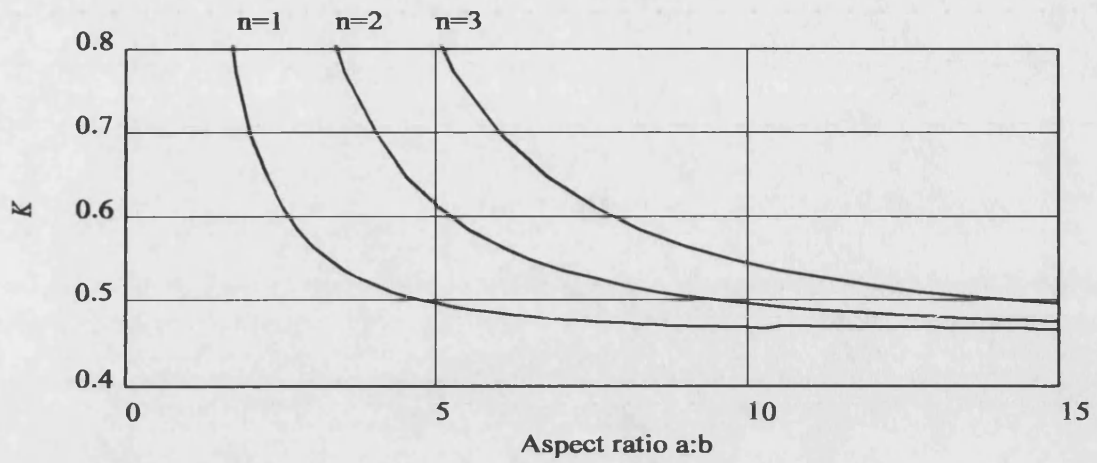


Figure 4.15 Solution for simply supported top edge

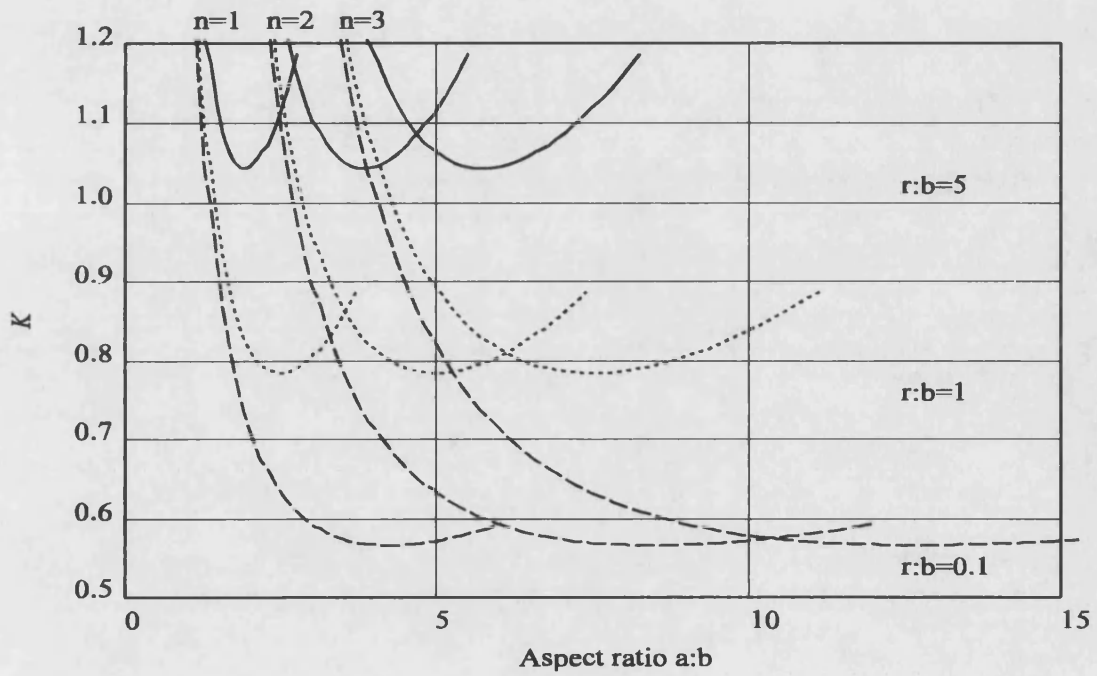


Figure 4.16 Solution for elastically supported top edge

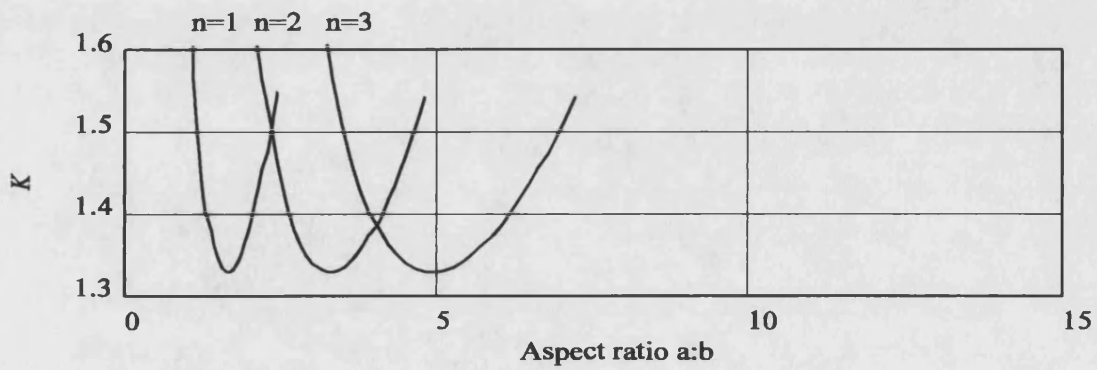


Figure 4.17 Solution for fixed top edge

In the case of the simply supported edge K tends to a value of 0.46 whereas for the fixed case K will tend to a value of 1.33. This represents a difference in buckling load of three. Clearly it is important to determine which of these cases the buckling of the glass web will be closest to.

When considering the top edge as being elastically built-in it is necessary to determine the torsional rigidity of the flange. For a thin rectangular flange this may be approximated to:

$$C = \frac{1}{3} Gbt^3$$

Now the solution for K is based not only upon the aspect ratio and the number of half waves but also the torsional rigidity. Timoshenko and Gere express this as the ratio $r:b$ where r is defined as the equal to;

$$r = \frac{C \pi^2}{D a^2} \quad \text{Equation 4-41}$$

It is found that as the ratio $r:b$ approaches infinity, the solution to the linear stability equation is the same as that for the condition of the fixed top edge. At the other extreme, as $r:b$ approaches zero, the solution is the same as that for the condition of the simply supported top edge. This is shown in Figure 4.16. The other difference is that of the number of half waves that the plate buckles into. This is also a function of the ratio $r:b$.

In considering the fixity at the top edge of the web no account has yet been taken of the rotation in the adhesive joint. However, finite element modelling by the author, Section 7, has indicated that very little rotation of the web relative to the flange occurs at the adhesive joint. On this basis it is proposed that the effect of rotation at the adhesive joint may be neglected and that the buckling load be calculated using the elastically built-in edge model. As an alternative the simply supported edge may be taken as a conservative approach to assessment of the buckling load.

4.4.2 Introduction of web stiffeners

The thinking behind the introduction of web stiffeners must be to increase the number of half waves that the plate buckles into. In this way the buckling load may be increased. It is therefore important that the web stiffeners are placed at locations where they will force this change in mode shape. For example, if it is assumed that the simply supported edge is the most realistic buckling model a web stiffener placed at the midspan will prevent the formation of a single half wave and result in the formation of two half waves, Figure 4.15. If, however, it is assumed that the fixed edge is the most realistic model and the plate has an aspect ratio of 3.3:1 then a web stiffener at the midspan would have no effect. This is because at an aspect ratio of 3.3:1 the plate already buckles into two half waves. However the introduction of two web stiffeners at the third points would cause the plate to buckle into three half waves and the buckling load would be greatly increased.

4.4.3 The need for finite element modelling and physical testing and large factors of safety

The preceding discussion has outlined the buckling mechanism for a perfect beam which has been loaded in the plane of the web. It has been necessary to make a large number of approximations in order to develop a set of solvable equations. In practice these assumptions may prove too crude. In particular the conditions that the beam is perfectly flat and the loads are only applied in the plane of the web are unrealistic. As a result, if these methods of calculation are used in practice it will be necessary to apply a large factors of safety to account for these assumptions. However, in the absence of test data and more accurate models it is impossible to determine what these factors should be. Therefore it is necessary to perform physical testing and finite element modelling to gain a better understanding of the real behaviour of these structures.

The use of a finite element eigen value solution can go a long way to improve the model. In this way it will be possible to determine the effects of idealising the web as an isolated plate subject to a uniform compressive stress. This method will account for the action of

the adhesive and it will be possible to investigate the effect of various load distributions. However, the eigen value approach is based on theory that does not take account of the geometric non-linear behaviour of the structure. The eigen value approach will predict the bifurcation point for the structure and this may differ from the limit load determined from a non-linear analysis, Figure 4.18.

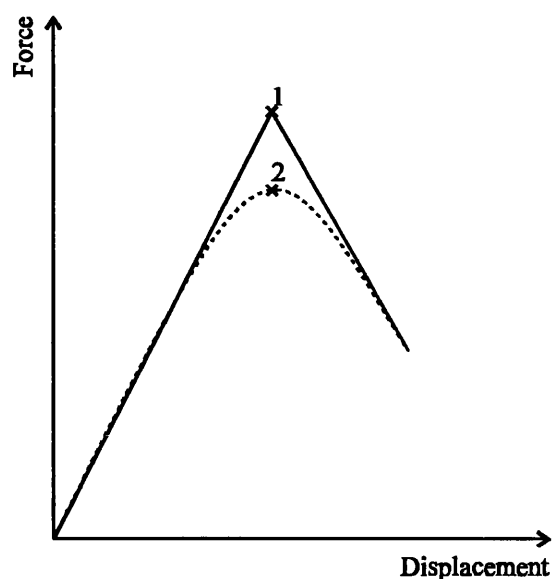


Figure 4.18 Eigen value and non-linear geometry FE analyses. 1-Bifurcation point, eigen value approach. 2-Limit load, non-linear geometry approach.

In the case of a non-linear finite element analysis it will be necessary to apply a small de-stabilising force to initiate buckling. The limit load will be sensitive to the magnitude and location of this de-stabilising load. The choice of load will be important because it represents an imperfection in the previously assumed perfect loading. The sensitivity of the limit load to this de-stabilising load may be taken as a measure of the sensitivity of the beam to imperfections in both loading and flatness. However, the only true way to investigate the effect of imperfections is to test real beams which have been manufactured, installed and loaded in an identical manner to those which will be used in practice. Even so a large number of tests would have to be conducted because notionally identical tests are likely to give quite different results. Only at this stage will it be possible to comment upon the suitability of the simple methods discussed at the beginning of the section. It may even be concluded that the simple methods of predicting buckling loads are so distant from the results obtained in practice that an empirical approach is best.

4.4.4 Limitations of this thesis with regard to buckling analysis

Various methods have been outlined which may provide a suitable approach to the problem of determining buckling loads in the case of glass adhesive T-beams. However, it is not an aim of this thesis to provide absolute guidance on this point. Much work on this topic, both theoretical and empirical, has already been undertaken for other materials and beam sections.

The approach taken here has been to examine the buckling of one section using an algebraic approach, a finite element eigen value approach, a finite element approach with non-linear geometry and a limited number of tests on real beams. It is not intended that this should be seen as a general solution to the buckling of glass adhesive beam sections. Rather, it should be seen as an example of how the subject could be approached in future work.

4.4.5 Finite element buckling analysis

This section is a brief summary of the theory used in the finite element buckling analysis of structures. It is presented as background information for those who may be unfamiliar with these methods of analysis. The most part of what follows is based upon NAFEMS (1987) and ANSYS (1997).

The basis of finite element methods is that a set of loads, \mathbf{R} , maybe related to a set of displacements, \mathbf{r} , by a stiffness matrix \mathbf{K} ;

$$\mathbf{R} = \mathbf{K}\mathbf{r}$$

In reaching this relationship three linear relationships are assumed. Firstly that load is linearly proportional to stress. Secondly that stress is linearly proportional to strain and thirdly that strain is linearly proportional to displacement. In the case of non-linear geometry it is the third condition that is violated. The key to solving this problem is to consider small incremental displacements $\delta\mathbf{r}$ due to small increments in load $\delta\mathbf{R}$. The problem is linear in $\delta\mathbf{r}$ and $\delta\mathbf{R}$ but the total displacements \mathbf{r} and the current stresses must

be summed over all the previous results. The relationship between the $\delta\mathbf{r}$ and $\delta\mathbf{R}$ is called the tangent stiffness, \mathbf{K}_T , Figure 4.19. This may be expressed as;

$$\delta\mathbf{R} = \mathbf{K}_T \delta\mathbf{r} \quad \text{Equation 4-42}$$

\mathbf{K}_T has two components. The first is the elastic stiffness \mathbf{K}_E which takes account of the changed geometry of the structure. The second term represents the resistance to load caused by a re-aligning of the internal stresses when displacements occur. This is called the geometric stiffness, \mathbf{K}_G and is evaluated in terms of the current stresses. Thus in the case of a compressed bar which is acted upon by some force P the tangent stiffness matrix is given by;

$$\mathbf{K}_T = \mathbf{K}_E + P\mathbf{K}_G$$

In the case of more general structures this must be assembled into the global tangent stiffness matrix. This may be done in one of several ways dependent upon the assumptions that have been made regarding the magnitude of the deflections. In the case where P is a compressive force it may be written that;

$$\mathbf{K}_T = \mathbf{K}_E - P\mathbf{K}_G$$

There will be some value of P for which the modulus of \mathbf{K}_T is zero and this is the bifurcation point of the structure. At $|\mathbf{K}_T| = 0$ the structure has lost all stiffness. The same principle is applied to the global tangent stiffness matrix. The first solution for which the modulus of the global tangent stiffness matrix equals zero is the first eigen solution. The second solution for which $|\mathbf{K}_T| = 0$ is the second eigen solution and so on. It is usual to determine the eigen values using an iterative process. This method will deliver eigen values and eigen modes but it does not provide information on deflections or stresses. For this an incremental solution is needed.

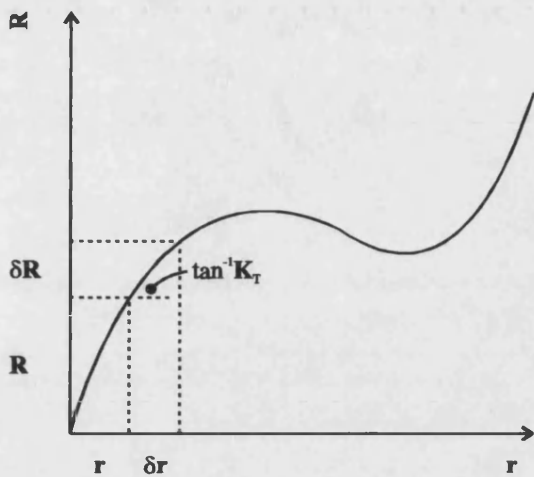
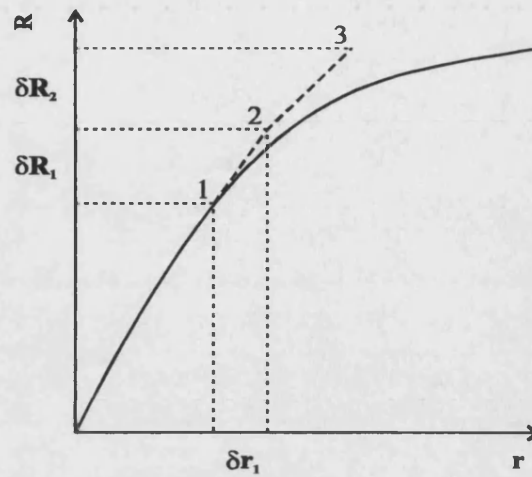
Figure 4.19 Tangent stiffness K_T 

Figure 4.20 Incremental drift

In the incremental solution a non-linear history is built up using Equation 4-42. The case of the pure incremental solution is discussed using Figure 4.20. Assuming that at point 1 we know the current displacement r and local stress field σ_x , it is possible to determine K_T . Considering small increments in load δR it is now possible to determine δr according to Equation 4-42. Therefore the solution can now be projected to point 2. The problem is that the value of K_T actually changed over the small distance δr , and now point 2 no longer lies on the path of the true solution. As the process is repeated and the solution is projected to point 3 this incremental drift becomes larger.

One commonly applied solution to this problem is to calculate the out of balance nodal forces $\delta R'$, Figure 4.21. In this manner the solution may be returned to the correct path. It is now necessary to re-calculate the tangent stiffness matrix before proceeding to the next point where again the out of balance forces will be evaluated and the solution corrected. This is called the Newton Raphson method. However, having to re-evaluate the tangent stiffness matrix at each step is a lengthy process and sometimes the decision is taken to not re-evaluate, Figure 4.22. This means that more iterations will generally be needed to converge that step of the solution but each iteration becomes far faster. This process is known as the modified Newton Raphson method.

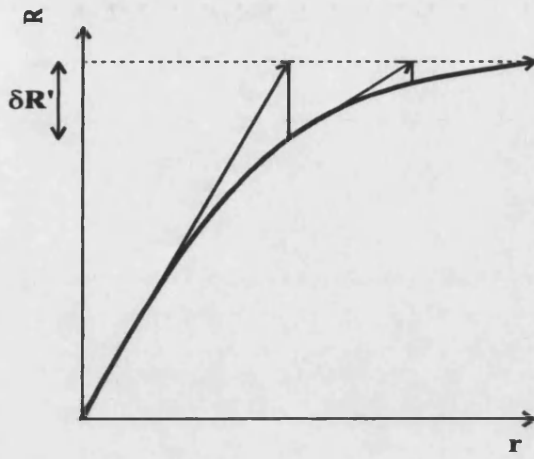


Figure 4.21 Newton Raphson convergence

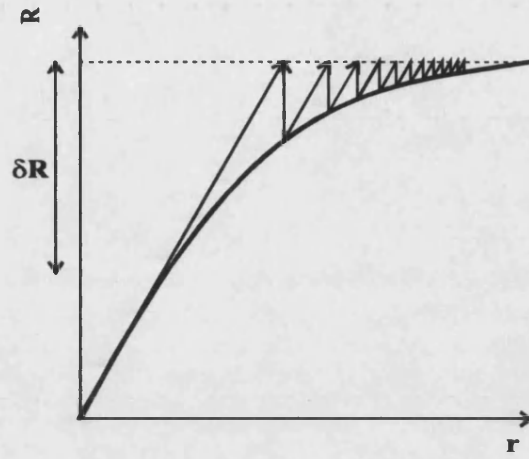


Figure 4.22 Modified Newton Raphson convergence

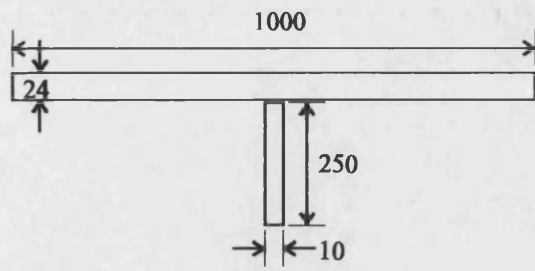
5 NUMERICAL IMPLEMENTATION OF COMPOSITE BENDING EQUATION AND FINITE ELEMENT ANALYSIS

In this section the physical meaning of the theory derived in the previous chapter is explored by putting it into practice to solve real problems. In this manner practical adhesive properties, joint dimensions and section properties are determined. The theory is partially validated by comparing these results with those generated using finite element methods. Finite element methods are also used to investigate the three dimensional stress distribution in the adhesive joint.

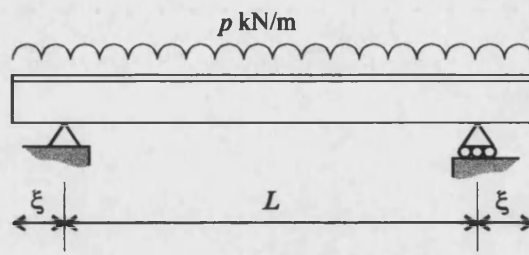
5.1 Numerical implementation of composite bending equation

5.1.1 How many Fourier terms to use?

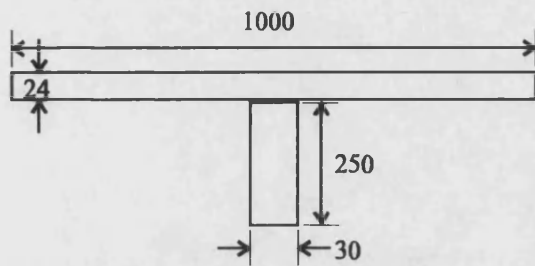
The section shown in Figure 5.1a was evaluated in the two loading conditions shown in Figure 5.2. In each case the use of a number of Fourier terms was evaluated. The results are summarised in Table 5.1. Convergence in the case of the uniformly distributed load (UDL) is very quick and sufficient accuracy is obtained in the first two terms to contemplate evaluating the solution by hand. However, the point load in the second case causes problems. Whilst the deflections converge quickly a minimum of ten Fourier terms are needed to converge the stresses. The solution of these problems will generally need to be performed using a computer, unless the methods outlined in sections 5.1.3 or 5.1.8 are used. Throughout this work all solutions are based on 100 Fourier terms.



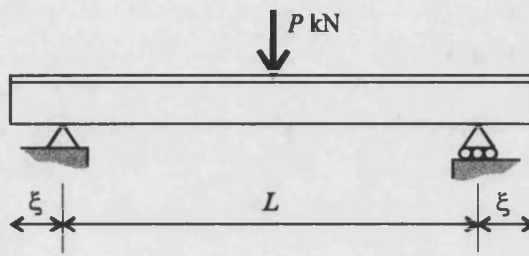
(a)



(a)



(b)



(b)

Figure 5.1 Two beam cross sections

Figure 5.2 Two load span conditions

No terms	UDL (Figure 5.2a)			3 point bending (Figure 5.2b)		
	Midspan deflection (mm)	Max glass stress (N/mm ²)	Max adhes. stress (N/mm ²)	Midspan deflection (mm)	Max glass stress (N/mm ²)	Max adhes. Stress (N/mm ²)
1	-5.30	35.9	2.74	-8.39	56.3	4.30
2	-5.31	34.7	3.10	-8.52	63.2	3.00
10	-5.31	34.7	3.17	-8.55	70.9	3.40
100			3.18	-8.55	73.3	3.42
1000					73.6	3.42
10000					73.6	

Table 5.1 Number of Fourier terms needed converge solutions to composite bending problems

5.1.2 Variation of joint thickness and adhesive shear modulus

Throughout this chapter the section in Figure 5.1a will be referred to as the standard cross section as it is the one on which most of the discussions will be based. Table 5.2 shows the standard section evaluated for different values of t and G_a . This table indicates the percentage composite action (Equation 4-1) which is achieved when the beam section has been used in a 5 m simply supported span with a UDL.

			G (N/mm ²)	
		0.25	25	2500
t (mm)		—————→		Stiffer
0.1	↑	62	99	100
0.5		24	97	100
1.0		14	94	100
5.0	Stiffer	3	76	100

Table 5.2 Variation in percentage composite action with varying t and G_a . Based upon the standard section (Figure 5.1a) in a 5 m simply supported span with a UDL.

$G_a = 0.25 \text{ N/mm}^2$ is representative of a typical structural silicone sealant whilst $G_a = 2500 \text{ N/mm}^2$ is a stiff epoxy. Clearly an adhesive shear modulus above 25 N/mm^2 used in a joint of 1 mm thickness, or less, would perform well in an application such as this. The degree of composite performance cannot be significantly bettered and so decisions regarding t and G_a within the broad limits set above are best made on grounds other than the degree of composite action. For example a lower modulus adhesive will better distribute stress concentrations and absorb shock, Harris and Fay (1992). As discussed in Section 2.1 the minimum thickness of the adhesive joint is fixed by flatness of the glass. It is likely to be in the order of 1 mm.

5.1.3 The concept of the composite constant

Figure 5.3 shows the effect of varying the composite constant in various spans subject to a UDL. The absolute properties of the section are not specified as the composite constant establishes the relationship between the equivalent layered and monolithic sections. The curves are therefore valid for any cross-section.

The calculation of the composite constant is a simple hand calculation. Knowing this, the degree of composite action can be established by selecting the appropriate curve or by interpolating between curves. If the degree of composite action is high then design calculations may be based upon the equivalent monolithic section. It should be appreciated that this will yield low glass stresses and beam deflections and high adhesive stresses. The curves shown in Figure 5.3 are only valid for UDL's. Other curves may be produced for different loading conditions.

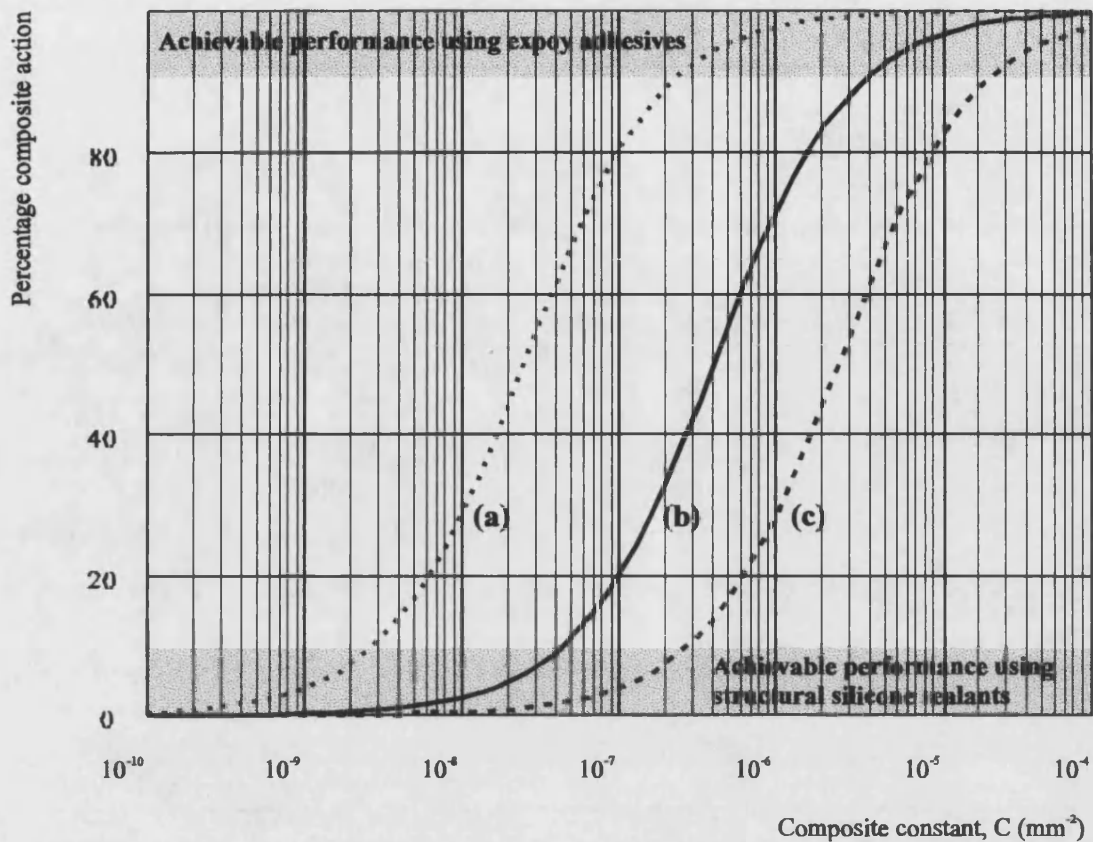


Figure 5.3 The effect of the composite constant on the degree of composite action for three simply supported beams with a UDL (a) 10 m span, (b) 5 m span, (c) 1 m span

5.1.4 Effect of span

Figure 5.4 shows the variation in the percentage composite action for the standard section subject to a UDL as the span is increased. It shows the increasing dominance of shear effects in short deep beam sections. If several curves for different values of C had been plotted this graph could be used in a similar way to Figure 5.3.

5.1.5 Position of the neutral axis

In the case of the standard beam the adhesive joint occurs at the position of the monolithic neutral axis. In the case of the monolithic beam this would be the position of highest shear stress and may be deemed a poor location for the adhesive joint. Clearly

the joint must occur at the web flange interface although by modifying the relative proportions of the web and flange it is possible to move the neutral axis away from this joint. This is what has been done in the case of the beam shown in Figure 5.1b (modified standard section). Here the monolithic neutral axis is located 20 mm below the adhesive joint. The peak stresses for these beams used over a 5 m simply supported span to carry a 2.5 kN/m UDL are shown in Table 5.3. Also shown is the case where the thickness of the web is locally increased at the junction to the flange, Figure 5.1.

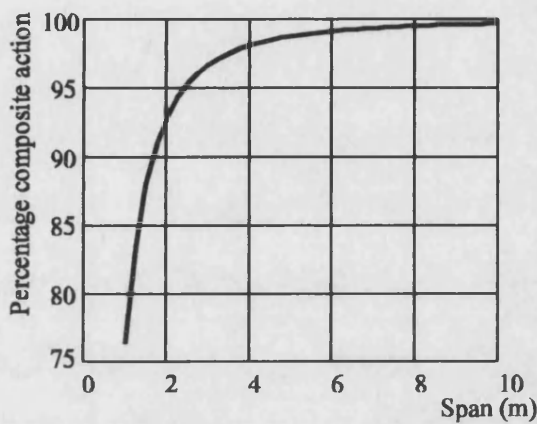


Figure 5.4 The effect of the span on the degree of composite action for the standard section subject to a UDL

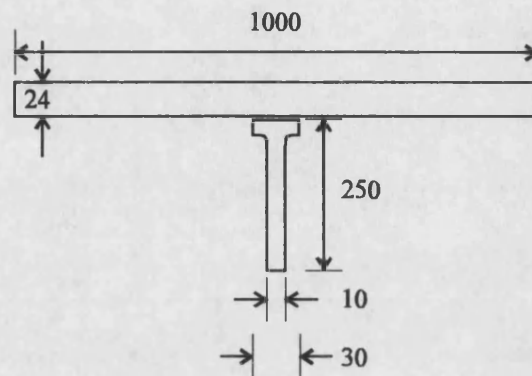


Figure 5.5 Standard section with a 30 mm wide joint

Beam	Max glass stress (N/mm ²)	Max adhesive stress (N/mm ²)
Standard section (Figure 5.1a)*	34.7	3.17
Standard section with a 30 mm wide joint (Fig 5.5)*	34.5	1.09
Modified standard section (Figure 5.1b)*	12.8	0.98

* $t = 1.0 \text{ mm}$ and $G = 125 \text{ N/mm}^2$

Table 5.3 Summary of maximum stresses in three beam sections used over a 5 m simply supported span to carry a 2.5 kN/m UDL

The reduction in adhesive stress caused by using the 30 mm wide web is significant. In the case where the web locally increased in thickness there is a similar dramatic decrease

in maximum adhesive stress. Therefore it can be seen that most of the reduction in adhesive stress is attributable to increasing the width of the joint. The movement of the neutral axis has only contributed a further three percent decrease in stress. In most practical situations it will not be easy to move the position of the neutral axis by any appreciable amount and a better solution to reducing adhesive stress will be to provide a wider joint.

5.1.6 Adhesive shear distribution and the effect of overhangs

Figure 5.6 shows the adhesive shear stress distribution in the standard section used over a 5 m simply supported span to carry a 2.5 kN/m UDL. $t = 1.0$ mm and $G = 125$ N/mm². The case of no overhang does not differ significantly from the stress distribution that would be expected in a monolithic beam. However, the introduction of an overhang has two important effects. Firstly the stress peak is reduced. Secondly the location of the stress peak moves towards the centre of the beam as the overhang is increased, Table 5.4. This observation is important as in most practical scenarios the beam will be supported in a distance from both ends. This is to allow room for a fixing through the glass. Taking this into account will reduce the adhesive design stress.

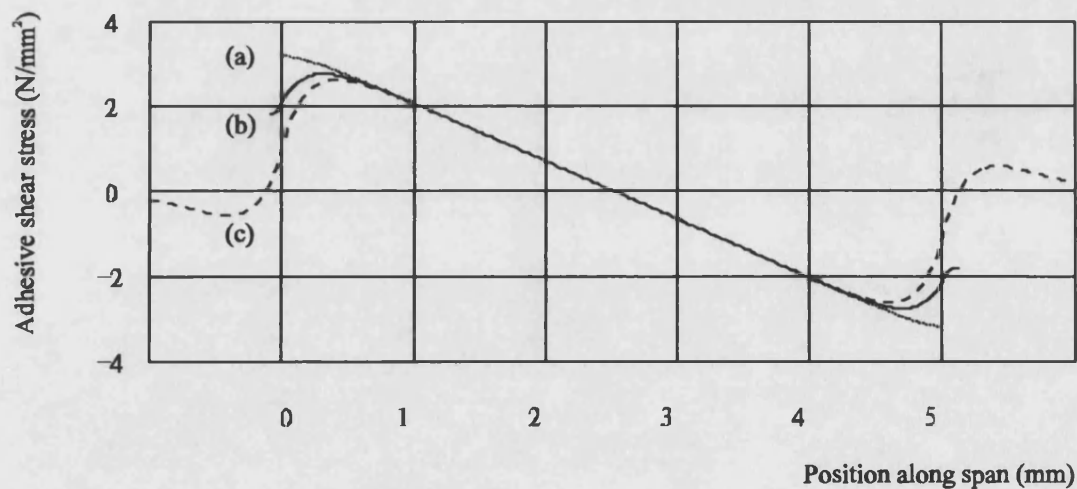


Figure 5.6 Adhesive shear stress distribution in standard section used over a 5 m simply supported span to carry a 2.5 kN/m UDL. $t = 1.0$ mm and $G = 125$ N/mm². (a) No overhang, (b) 100 mm overhang, (c) 1 m overhang.

Overhang (mm)	Maximum adhesive stress (N/mm ²)	Position of maximum stress
0	3.17 (100%)	Support
100	2.76 (87%)	300 mm from support
1000	2.70 (85%)	400 mm from support

Table 5.4 Summary of maximum stress values and locations from Figure 5.6

5.1.7 Multiple spans

The advent of stiffer beam sections makes longer glass beams a reality. However, there may be situations where engineers wish to consider multiple spans with a continuous beam. In these cases the solution to the composite bending problem may still be achieved using the solutions derived in Section 5.2 provided that the moment along the beam can be described. The reactions for a symmetric double span subject to a UDL would normally be calculated as $0.375wL$, $1.25wL$ and $0.375wL$. From this the moments along the beam can be calculated. In the cases where $C \rightarrow 0$ and $C \rightarrow \infty$ this is true. However, in the more general case of composite action the use of these reactions in calculating the moment will not yield zero deflection at the centre support. In the case of the standard section it is found that $R_1 = R_3 = 0.3762wL$ and $R_2 = 1.248wL$. These values have been determined iteratively. If these corrections are not applied the error in the stresses is unlikely to be great. The use of the $0.375wL$ and $1.25wL$ reactions resulted in a non zero deflection at the central support which was equal to seven percent of the midspan deflections.

Figures 5.8 and Figure 5.9 show the maximum glass stresses and the adhesive stresses for the standard section used across a double 5 m span with two 100 mm overhangs to carry a UDL. The maximum glass stress occurs at the middle support and the maximum adhesive stresses occur either side of the support.

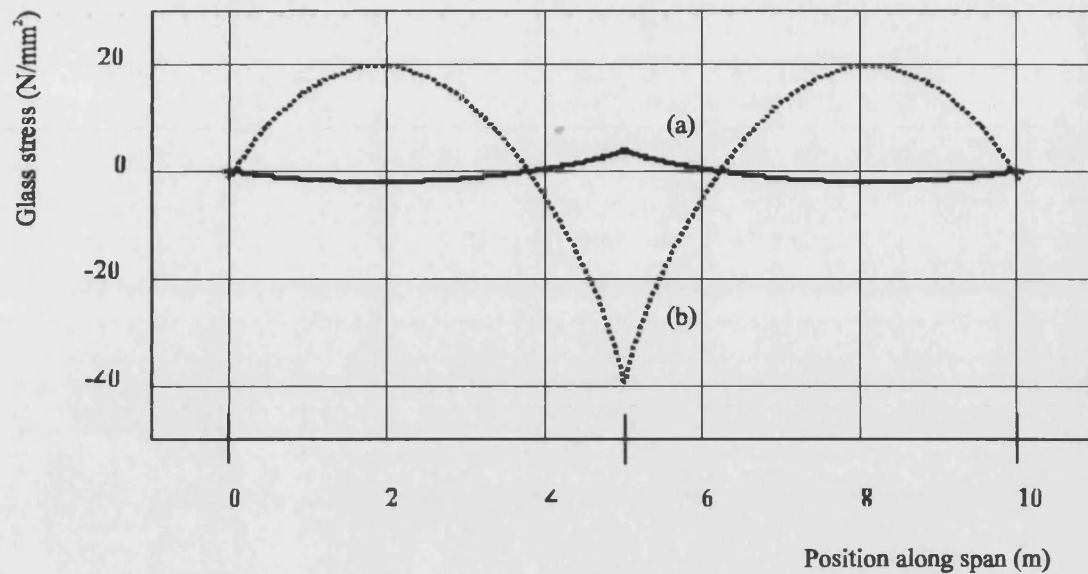


Figure 5.7 Maximum glass stresses in the standard beam section used in a continuous double 5 m span with a 2.5 kN/m UDL. (a) Glass stresses at the top of the flange, (b) Glass stresses at the bottom of the web.

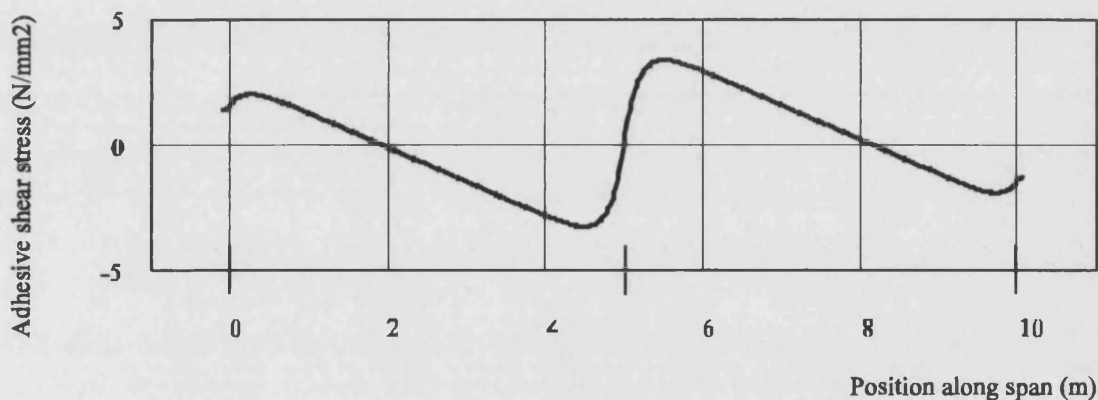


Figure 5.8 Adhesive stress distribution along a standard beam section used in a continuous double 5 m span with a 2.5 kN/m UDL

5.1.8 Design charts

The fastest and most accurate way of solving the governing equation is to use a computer and a suitable mathematics application. In this way it is easy to use a large number of Fourier terms and it possible to visualise the results using the software package's built in graph functions. However, if this is not possible and the degree of

composite action is not close enough to 100 percent to warrant treating the beam as its monolithic equivalent then it is possible to use a design chart. Re-calling that the midspan deflection of the beam is given as;

$$z = \sum B_n \frac{C + \alpha^2}{S_l \alpha^6 + C S_m \alpha^4} \sin \frac{n\pi}{2}$$

Then re-arranging and assuming that B_n is a function of some load p , it may be shown that;

$$\frac{z S_m}{p L^4} = \sum \frac{B_n}{p} \frac{\frac{C L^2}{n^2 \pi^2} + 1}{\frac{S_l}{S_m} + \frac{C L^2}{n^2 \pi^2}} \frac{1}{n^4 \pi^4} \sin \frac{n\pi}{2} \quad \text{Equation 5-1}$$

There are now three variable groups and these may be plotted as shown in Figure 5.9.

The chart will apply for the support conditions and load distribution described by the

Fourier term $\frac{B_n}{p}$. However, the absolute span and the magnitude of the load are

independent of the curves plotted in this chart. In this case the curves apply to a single simply supported span of length L with no overhangs and a UDL of p kN/m. Similar charts can be constructed for z'' and z''' , Figure 5.10. It would be usual to evaluate z and z'' at the locations of maximum deflection and maximum stress. z''' should be evaluated at the location of maximum shear stress. In this manner simple problems may be accurately and simply evaluated by hand.

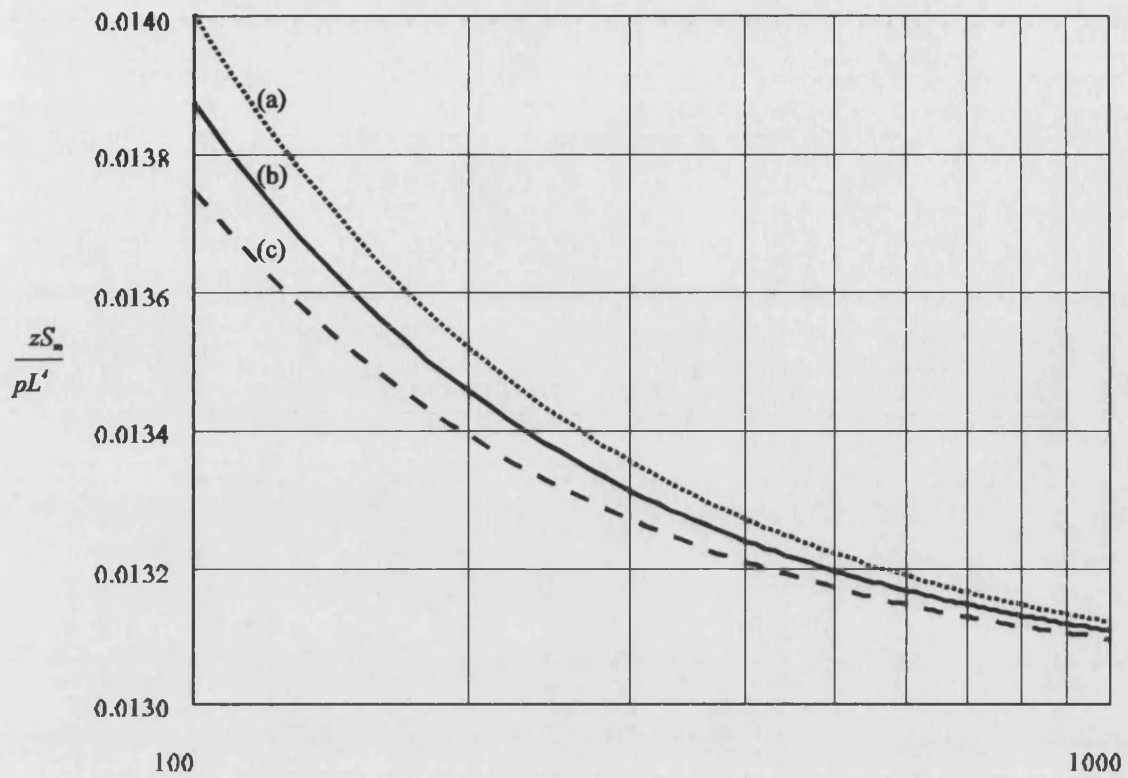


Figure 5.9 Design chart for a simply supported beam carrying a UDL (evaluation of z). (a) $s_t:s_m$ 0.2, (b) $s_t:s_m$ 0.3, (c) $s_t:s_m$ 0.4.

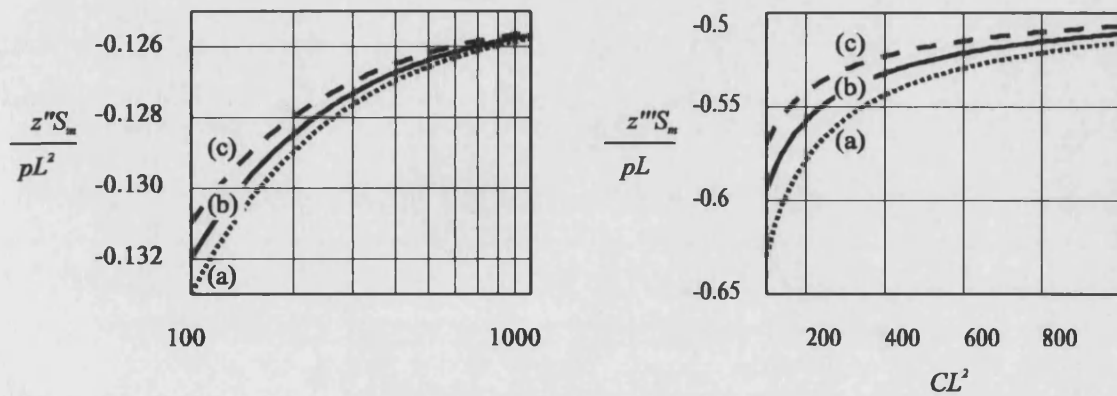


Figure 5.10 Design charts for a simply supported beam carrying a UDL (evaluation of z'' and z'''). (a) $s_t:s_m$ 0.2, (b) $s_t:s_m$ 0.3, (c) $s_t:s_m$ 0.4.

5.2 Finite element modelling

Finite element modelling was undertaken in order to validate the algebraic model and to investigate the three dimensional distribution of stresses in the adhesive joint.

5.2.1 Finite element modelling to validate the algebraic model

The structural behaviour of a standard beam carrying a 2.5 kN/m UDL over a 5 m span with two 100 mm overhangs has been evaluated using both the algebraic model and a finite element model. The finite element model is constructed from 8 node, isoparametric quadrilateral elements with plane stress and thickness. The element mesh with boundary conditions is shown in Figure 5.11. The high mesh density is as a result of the dimension of the adhesive joint. The joint is modelled with a single layer of elements having an aspect ratio of 10:1. This results in there being 260 elements along the half length of the beam. Therefore in this simple two dimensional analysis there are a total of 2340 elements.

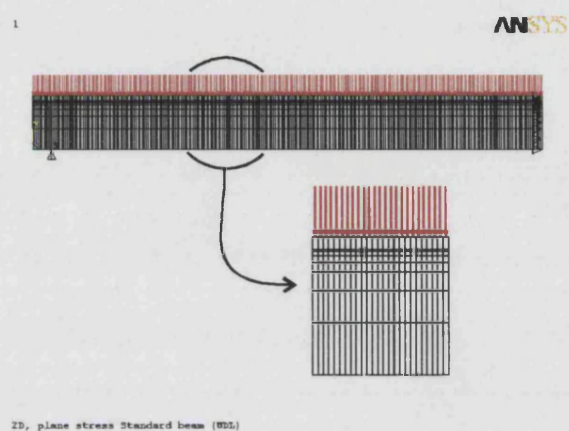


Figure 5.11 Finite element mesh with boundary conditions for a standard beam carrying a 2.5 kN/m UDL over a 5 m span with two 100 mm overhangs.

The midspan deflection and midspan stresses are summarised in Table 5.5 and the shear stresses along the length of the half beam are plotted in Figure 5.12. It can be seen that the correlation between the two models is very good and it may be concluded that the finite element model validates the algebraic model.

	Algebraic model	Finite element model
Midspan deflection	-5.3 mm	-5.4 mm
Stress at top of flange	3.5 N/mm ²	3.5 N/mm ²
Stress at bottom of web	34.7 N/mm ²	34.5 N/mm ²

Table 5.5 Summary of midspan deflections and stresses for the problem shown in Figure 5.11.

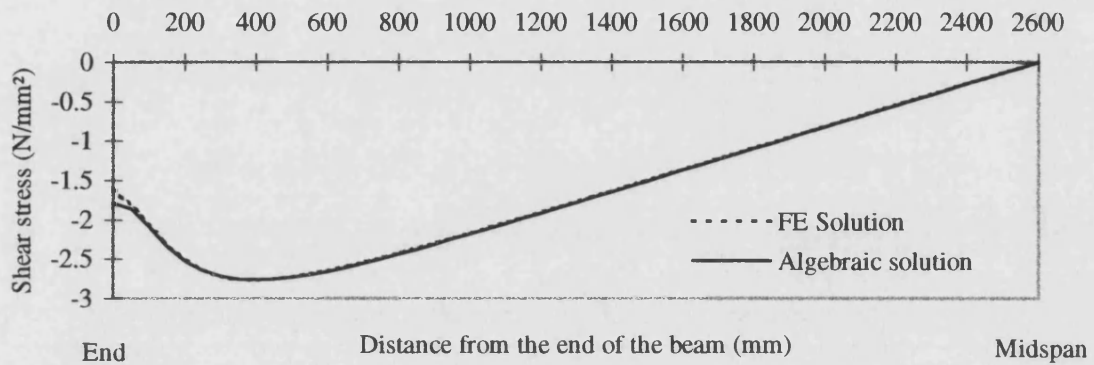


Figure 5.12 Distribution of adhesive shear stresses for the problem shown in Figure 5.11.

5.2.2 Three dimensional distribution of stresses within the adhesive joint

Whilst the algebraic model yields the average adhesive stress distribution, it gives no insight to the variation in stress across the width and depth of the joint. It was shown in Section 3.2 that the stress distribution within a lap shear joint is complex. The stresses not only vary along the length of the joint but also across the depth of the joint. It was also shown that the provision of adhesive fillets may do much to alleviate stress concentrations within the joint.

It was feared that there may be severe stress concentrations within the adhesive joint of the glass-adhesive T-beam. It was also felt that the provision of an adhesive fillet may go some way to reducing any stress concentrations. Therefore it was decided to construct a three-dimensional model of the adhesive joint in order to determine the true stress distribution and to investigate the effects of providing an adhesive fillet.

The relative dimensions of the adhesive joint and the T-beam meant that it was necessary to model the joint in isolation. In this manner it was possible to include sufficient elements within the adhesive joint to determine the variation in stress distribution. The analysis reported here relates to the standard laboratory test beam loaded to 40 kN in three point bending, Section 8.2.1. 40 kN was the highest load that the laboratory test beam was taken to in the three point bending tests. It was assumed that the behaviour of the glass and the adhesive was linear and elastic. The assumed material constants are given in Table 5.6. Whilst this level of load may have resulted in the adhesive being plastically strained the lack of accurate stress-strain data for the adhesive meant that non-linear modelling was not possible.

	Glass	Adhesive
Elastic modulus	$70 \times 10^3 \text{ N/mm}^2$	352 N/mm^2
Poisson ratio	0.22	0.39

Table 5.6 Summary of material constants used in the finite element analysis of the adhesive joint

The starting point for the analysis was a three-dimensional model of the whole beam. This was constructed from eight node isoparametric shell elements. Quarter symmetry was used to reduce the size of the model. Following this a series of the three-dimensional models of the most highly stressed part of the joint were constructed. These were built using 20 node isoparametric brick elements and displacement boundary conditions were applied along the cut edges of the models. The boundary conditions were derived from the three-dimensional shell model.

According to St Venant (1855) a part of a stressed body may be cut from the whole to which it belongs and provided that the forces which are applied along its boundary are in equilibrium with and are distributed in a similar manner to the whole from which it was cut the distribution of stresses a short distance from the boundary will be the same as when the part was attached to the whole. It is this principle which has been used to justify the approach outlined above. The only concern was how much of the beam had

to be modelled to ensure that the approximated boundary conditions did not affect the stress distribution at the location being studied. Therefore three models were initially considered and these are shown in Figure 5.13. In each case the stress distribution was studied at the centre of the model. This corresponded with the highest shear stress location determined from the three-dimensional shell model. The maximum and minimum stress values for each case are recorded in Table 5.7.

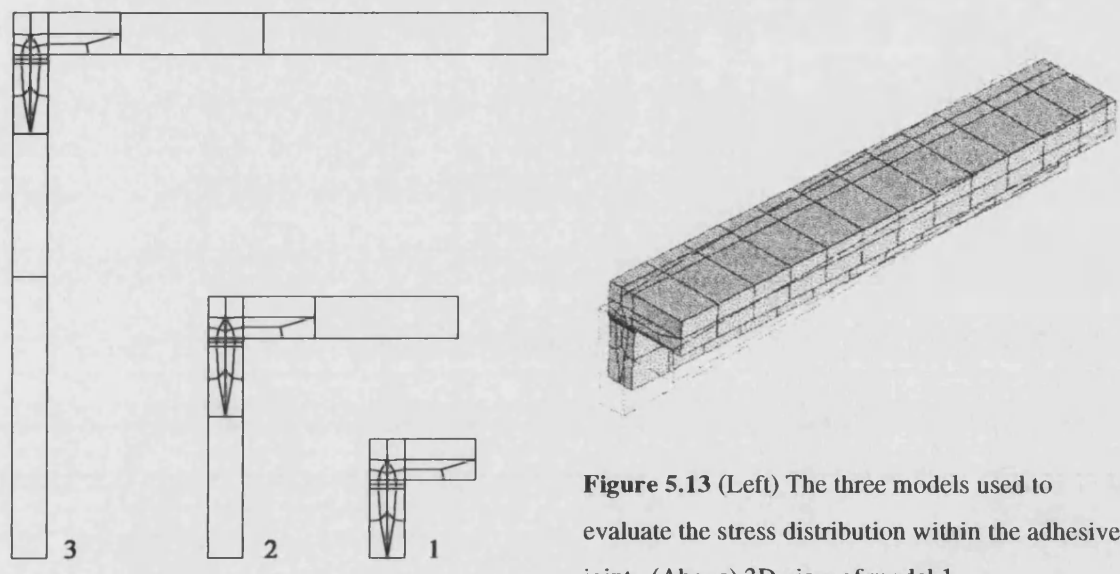


Figure 5.13 (Left) The three models used to evaluate the stress distribution within the adhesive joint. (Above) 3D view of model 1

	Model 1	Model 2	Model 3
Maximum shear stress (N/mm ²)	11.9	12.3	12.3
Minimum shear stress (N/mm ²)	11.7	12.1	12.1

Table 5.7 Summary of the results for the models shown in Figure 5.13

The peak stress according to the algebraic theory is 12.8 N/mm² which is not substantially different from the stresses indicated in Table 5.7. There is clearly little difference amongst the three models although it may be concluded that the slightly lower stresses observed in the case of model one indicate that the approximated boundary condition is too close to the area being studied. Therefore model two was chosen as the basis for further modelling. As the model is much longer than it is wide the approximated boundary conditions at the two ends were assumed to have no effect upon

the area being studied. It was considered possible that the mesh may have been overly coarse and therefore the mesh was refined as shown in Figure 5.14. This had the effect of reducing the maximum and minimum stresses to 12.0 N/mm^2 and 11.8 N/mm^2 respectively. It was therefore concluded that the original mesh was adequate.

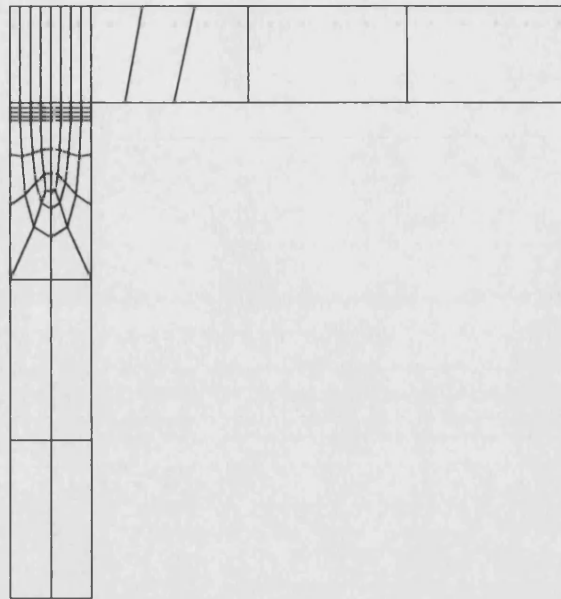


Figure 5.14 A refined version of the model two mesh

It was necessary to consider two small scale geometries. Firstly toughened glass is arressed in order to protect the edges of the glass. This normally takes the form of a 1 mm arris on each edge. Secondly it was considered prudent to include an adhesive fillet to increase the perimeter of the bonded area and so to hopefully reduce the adhesive stress. These were modelled and shown in Figure 5.15b and Figure 5.15c.

Stress plots for the plain joint, the plain joint with arressed glass and the filleted joint are shown in Figure 5.15. In the case of the plain joint there is a virtually uniform stress distribution. The introduction of the arris makes no difference to the stress distribution at the centre of the joint although the stresses at the free edge are relaxed. However, this also introduces a stress concentration at the step between the arris and the flat of the glass. This is most probably brought about by the limitations in the modelling of the joint. In practice this step would be radiused and had it been possible to model this then the stress concentration may not have been present. Adams and Harris (1987) addressed this issue and showed that inaccuracies in the modelling of micro geometry could increase model stresses by up to 25 percent.

The introduction of the adhesive fillet causes the stresses at the free edge to fall to virtually zero. However, the fillet has had little effect in reducing the stresses at the centre of the joint.

Using similar techniques the three-dimensional stress distribution at the ends of the beam were studied. No significant stress concentrations were found.

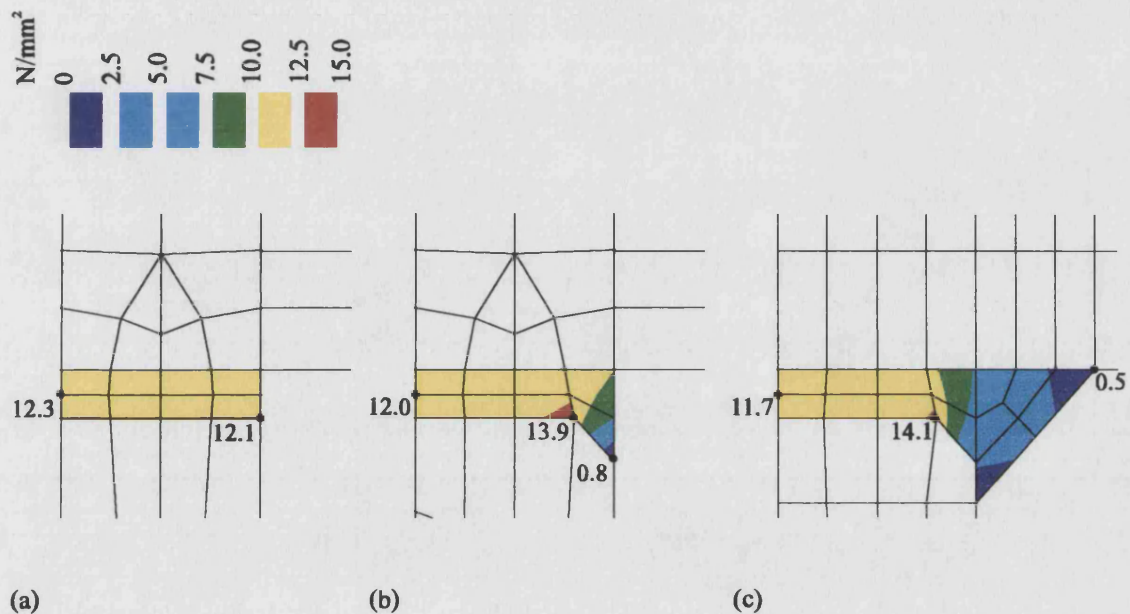


Figure 5.15 Shear stress plots at the location of peak average stress. (a) Plain joint, (b) Plain joint with arressed glass, (c) Filleted joint with arressed glass.

In conclusion it appears that the concerns about severe stress concentrations within the adhesive joint were unfounded. It also appears, that the provision of an adhesive fillet is unlikely to have any significant effect in reducing the peak adhesive stresses. However, the fillet may still be important if bending of the web in the plane of the T-section were to occur. Although the joint is not designed to be loaded in this manner it may be done inadvertently during handling or because of practical eccentricities in the support conditions. Therefore the use of adhesive fillets may still perform a valuable function.

6 NUMERICAL IMPLEMENTATION OF SHEAR LAG EQUATION AND FINITE ELEMENT ANALYSIS

The standard section is used as a basis for examining the shear lag equation derived in Section 4.3. The effect of modifying the number of Fourier terms, load distribution, span, depth of web and width of flanges are investigated and some general conclusions are drawn. In the second part of this section the results derived from the shear lag equation are compared with the results derived from finite element models. Conclusions are drawn regarding the relative merits of the two solution types.

6.1 Numerical implementation of shear lag equation

6.1.1 How many Fourier terms to use?

The standard section was evaluated in a 5 m simply supported span carrying a UDL and a point load, Table 6.1. As with the composite bending theory the case of the UDL is seen to converge faster than the case of the point load. However, both problems have

No terms	UDL (Figure 5.2a)		3 point bending (Figure 5.2b)	
	Max flange stress at free edge (N/mm ²)	Max web stress (N/mm ²)	Max flange stress at free edge (N/mm ²)	Max web stress (N/mm ²)
1	-1.9	35.6	-3.0	55.9
2	-1.9	35.4	-3.6	64.4
10		35.3	-4.0	71.9
100			-4.1	74.1
1000				74.3
10000				74.3

Table 6.1 Number of solutions required to converge solutions to composite shear lag problems

converged after 100 terms. Therefore throughout this work a hundred Fourier terms will be used in the solution of the algebraic shear lag problems. It is appreciated that this convergence test does not cover all scenarios and that for different load distributions it may be necessary to include more terms. For example, this could be the case where the loading arrangement is not symmetric. In such cases it will be necessary to re-evaluate the number of terms needed to converge the solution.

It is worth noting that much of the work undertaken by Song was concerned with the convergence of the solution. In particular he addressed ways in which the convergence could be improved in difficult cases, such as the un-symmetric application of point loads. Whilst these issues were important at the time of his work the author feels that modern computing power renders this approach unnecessary. The use of a modern desktop computer running general mathematics software is able to solve these equations in fractions of a second. The solutions presented here, were evaluated using a Pentium 233 MHz desktop computer running MathCad 6.0. With this set-up the evaluation of a million Fourier terms takes only a few seconds. It is due to the advent of software such as MathCad that the author has not written problem specific computer code. Song implemented his mathematics using purpose-written computer code. This code is now unavailable but there are several good mathematics packages that may be used to solve the original equations.

6.1.2 The effect of load distribution

One effect of the different load distributions has been seen in the number of Fourier terms needed to converge the solution. Another effect is shown in Figure 6.1. Here the flange stresses have been plotted for the midspan condition. In the case of the uniformly distributed load the stresses at the free edge are very similar to those at the web junction. In fact the peak stress is only 10 per cent higher than the minimum stress. The case of the three point bending arrangement is somewhat different. The peak stress is 40 per cent higher than the stress at the free edge. This demonstrates that the shear lag phenomenon is more prevalent in the case of point loads than the case of uniformly

distributed loads. We should therefore pay particular attention to the effects of shear lag in these scenarios.

The plots in Figure 6.2 show the stress ratio along the length of the two beams. In the UDL case the stress ratio is generally about 1.1. However in the case of the point load there is a visible peak where the stress ratio reaches 1.25. This means that the peak stress will be 25 per cent greater than that calculated using the conventional composite bending theory. Put another way; had the load carrying capacity of the beam been based upon the conventional bending theory the beam would have failed at 80 per cent of its predicted failure load.

Figure 6.1 (Right) Comparison of flange stress distribution for UDL and 3 point bending loading. (a) UDL, (b) 3 point bending.

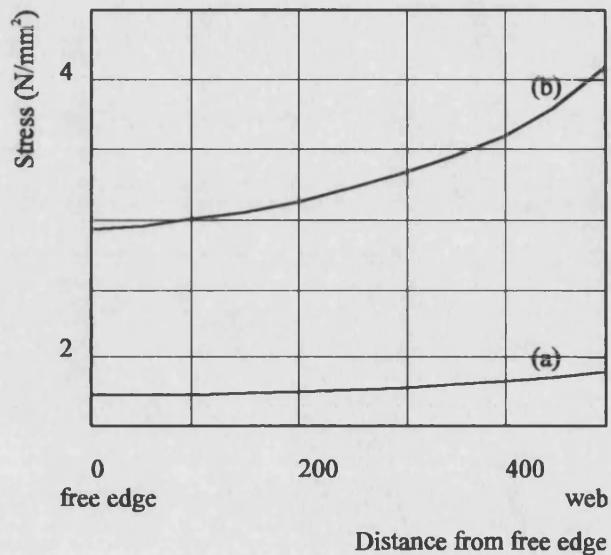
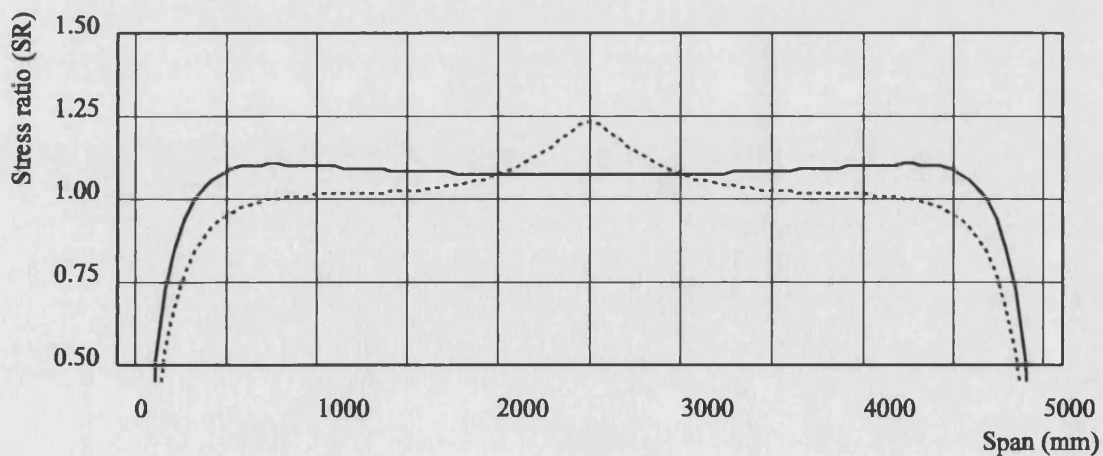


Figure 6.2 (Below) Comparison of the stress ratios for UDL and 3 point bending load cases. Solid - stress ratio for UDL case, Dashed - stress ratio for three point bending case.



In the remainder of the section point loads will not form the focus of the discussion. This is for the simple reason that point loads are rarely encountered in practice with glass.

6.1.3 Modifying the joint stiffness

The joint stiffness is a function of the adhesive shear modulus and the joint geometry. We can identify the joint stiffness as $S_a = G_a w_a / t_a$ and thereby simultaneously consider the effect of varying all three variables. Figure 6.3 shows the effect of $S_a=0$, $S_a=1250$ N/mm², and $S_a=\infty$. This example is based upon the standard section carrying a 2.5 kN/m UDL over a 5 m span with two 100 mm overhangs. The case of $S_a=1250$ N/mm² may be taken as a 125 N/mm² shear modulus adhesive in a 10 mm wide 1 mm thick adhesive joint. This is the same as the adhesive and joint dimensions used for the laboratory beams and it is representative of the likely joint stiffness that may be achieved in practice.

Figure 6.3a indicates that at $S_a=0$ no load is transferred into the flanges. Figure 6.3b and Figure 6.3c show that there is little difference between the cases of $S_a=1250$ N/mm² and $S_a=\infty$. In the case of $S_a=\infty$ the peak stress is only by 1.3 per cent higher than the case of $S_a=1250$ N/mm². This difference is insignificant.

This observation is important. It means that composite beams with a high degree of composite action may be analysed using the conventional shear lag theory. In such cases it is permissible to use the simplified methods proposed by Song and Scordelis. These methods apply to the analysis of T-beams, I-beams and box beams and they may be evaluated by hand.

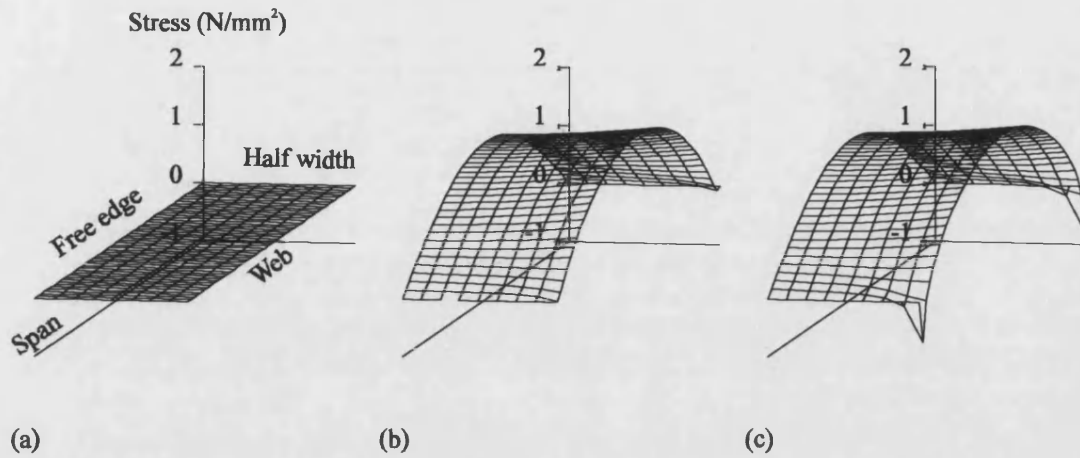


Figure 6.3 Standard section used across a 5 m span to carry a 2.5 kN/m UDL. (a) $S_a=0 \text{ N/mm}^2$, (b) $S_a=1250 \text{ N/mm}^2$, (c) $S_a=\infty$.

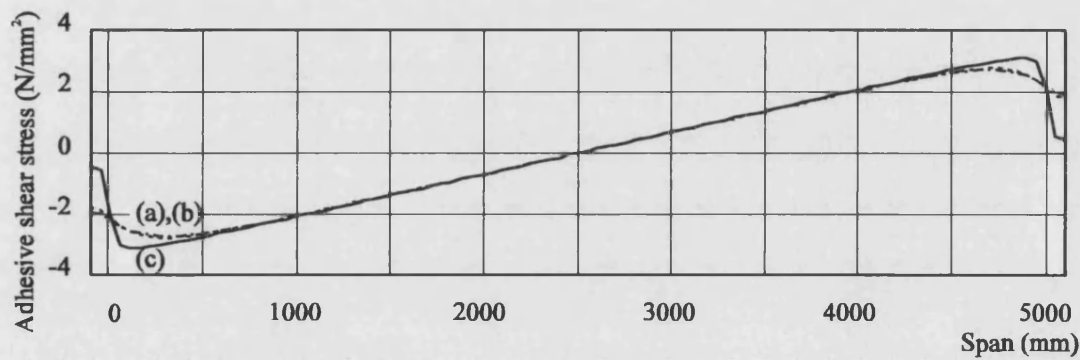


Figure 6.4 Adhesive shear stress distribution in the standard section used across a 5 m span to carry a 2.5 kN/m UDL, $S_a=1250 \text{ N/mm}^2$. (a) Shear stress distribution according to composite theory, (b) Shear stress distribution according to shear lag theory, (c) Shear stress distribution according to Song (1984)

The composite shear lag theory and the original Song theory predict different adhesive shear stress distributions. Figure 6.4 shows the stress distribution for these two solutions. It illustrates that the shear stress distribution calculated according to the composite theory coincides with that calculated using the composite shear lag theory. In this case it appears acceptable to determine the shear stress according to the conventional composite theory. However, in the case of Song’s solution the magnitude of the peak shear stress is higher than the composite theories. The peak stress in this case is 7.5 per cent higher and occurs nearer to the support.

6.1.4 Effects of modifying span

In this example the standard section has been used in 1m, 5m and 10m spans. In each case a UDL was applied and the stress results have been normalised so that it is the relative stress distribution which is compared. Figure 6.5 shows the surface stress plots for the three scenarios. In the 10 m span the flange is in a state of plane stress. In the 5 m span a small decrease in stress is seen at the free edge. However, this is insignificant when compared to the case of the 1 m span. In this case the midspan stress ratio reaches a value of 2.1.

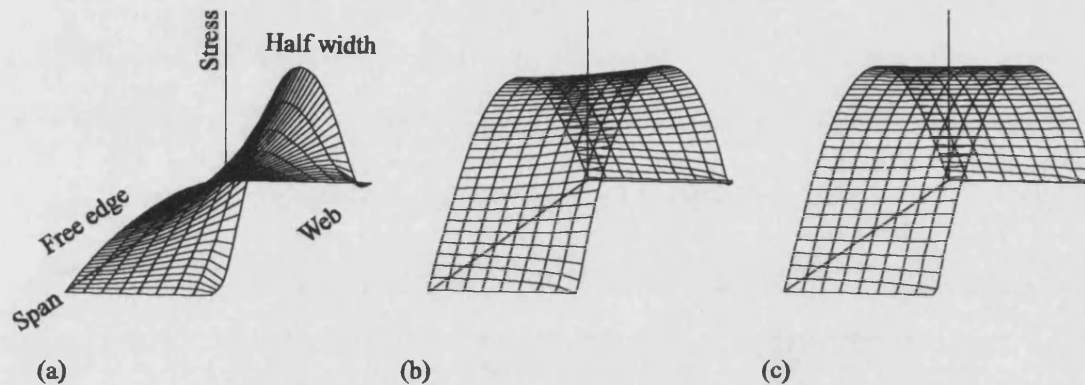


Figure 6.5 The effect of span upon shear lag. Stresses and span dimensions have been normalised. All plots based upon the standard section carrying a UDL, $S_a=1250 \text{ N/mm}^2$. (a) 1 m span, (b) 5 m span, (c) 10 m span

Clearly the shear lag phenomenon is affected by span. In order to determine an appropriate limit for the width:span ratio it is first necessary to decide upon a limiting stress ratio. In the 5 m span the 110 per cent stress ratio is probably acceptable although the 210 per cent stress ratio in the case of the 1 m span is unacceptable. In the cases considered here the 5 m span marks the threshold between acceptable and unacceptable. In this case the width:span ratio is 1:5. This is the same limiting ratio used in clause 3.4.1.5 of BS 8110.

6.1.5 Effects of modifying the depth of the web

The depth of the web was modified to see if this had any effect upon stress distribution. On this occasion modified standard sections with 10 mm, 250 mm and 1,000 mm deep webs were studied. All other dimensions remained unchanged and the beams were used to carry a UDL. The stresses have again been normalised so that it is the relative stress distribution which is compared in each case. The normalised midspan stresses are shown in Figure 6.6. All three curves coincide and it would appear that altering the depth of the web has no effect on the nature of the stress distribution within the flange. As the depth and breadth are both contained in the I_w term and are indistinguishable, it may also be reasoned that the width of the web will also have no effect. The only potential exception to this would be if the width of the web was of a similar order of magnitude to the width of the flange.

6.1.6 Effects of modifying the width of the flange

Modifying the width of the flange whilst keeping the span constant is similar to Section 6.1.3 where the flange width was kept constant and the span was modified. In this example flange widths of 0.5 m, 1 m and 5 m are evaluated in a 5 m span. These represent width:span ratios of 1:10, 1:5 and 1:1. Whilst the absolute stresses may be different the stress distribution and the stress ratios are identical to the examples considered in Section 6.1.3, Figure 6.5. The 0.5 m flange in this example corresponds to the 10 m span in the previous example (flange:span ratio 1:10). Similarly the 1 m flange corresponds to the 5 m span (flange:span ratio 1: 5) and the 5 m flange corresponds to the 1 m span (flange:span ratio 1: 1). The width:span ratio is obviously a key variable in determining the severity of the stress concentrations brought about by the shear lag phenomenon.

6.1.7 Effects of modifying the depth of the flange

The only effect that has not been examined is the depth of the flange. In this exercise the standard section carrying a UDL over a 5 m span was modified to have 4 mm, 24 mm and 100 mm deep flanges. As before the flange stresses were normalised. They are shown in Figure 6.7. Whilst the flange depth did have an effect on the absolute magnitude of the stresses the relative stress distributions coincide.

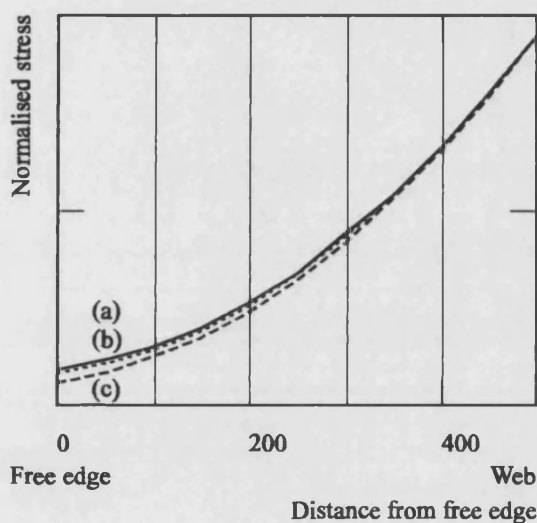


Figure 6.6 The effect of web depth upon shear lag. All plots based upon the standard section carrying a UDL, $S_a=1250 \text{ N/mm}^2$. (a) $d_w=10 \text{ mm}$, (b) $d_w=250 \text{ mm}$, (c) $d_w=1000 \text{ mm}$.

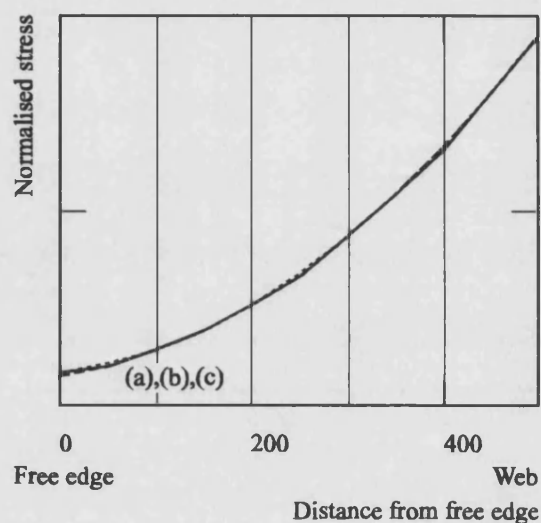


Figure 6.7 The effect of flange depth upon shear lag. All plots based upon the standard section carrying a UDL, $S_a=1250 \text{ N/mm}^2$. (a) $d_f=4 \text{ mm}$, (b) $d_f=25 \text{ mm}$, (c) $d_f=100 \text{ mm}$.

6.1.8 Simplified calculation of stresses ratio

It may be concluded that the only significant factors affecting stress distribution within the flange are the nature of the load distribution and the width:span ratio. It is therefore apparent why codes, such as BS 8110, stipulate the width:span ratio and it appears appropriate to take a similar approach in the design of glass-adhesive beams. Limiting the width:span ratio to 1:5 limited peak stress ratio to 110 per cent in the UDL case and 125 per cent in the three point bending case. It is up to individuals to determine an

acceptable limit for the stress ratio but the author feels that the 1:5 width:span ratio would be a good starting point.

6.2 Finite element validation of algebraic model

Finite element analysis has been undertaken to validate the algebraic solution. Two load distributions for two beam sections have been considered. The first beam section is the standard beam, **Figure 5.1**, which has been used in a 5 m span with a 100 mm overhang at each end. In the first case the application of the uniformly distributed load is considered. In the second case a point load is applied at the midspan. These two load span scenarios were then repeated using a modified standard section with a 5 m wide flange. The finite element results are therefore directly comparable with the analytical solutions presented in sections 7.1.1 and 7.1.5.

The mesh pattern for the standard beam section is shown in **Figure 6.8**. It also shows the boundary conditions in the uniformly distributed load case. Quarter symmetry has been used to reduce the size of the model and the mesh is built from 8 node isoparametric brick elements. The flange and web are built from a single thickness layer of these elements and the maximum permitted aspect ratio for the elements is 20:1. This generated 2,080 elements and approximately 50,000 degrees of freedom. As with the two-dimensional models the need for this high mesh density is dictated by the dimension of the adhesive joint. This high mesh density meant that it was not possible to use 20 node isoparametric brick elements. Models built from shell elements were not used because of problems that were encountered whilst performing eigen value buckling analyses, see **Section 7.1.2**.

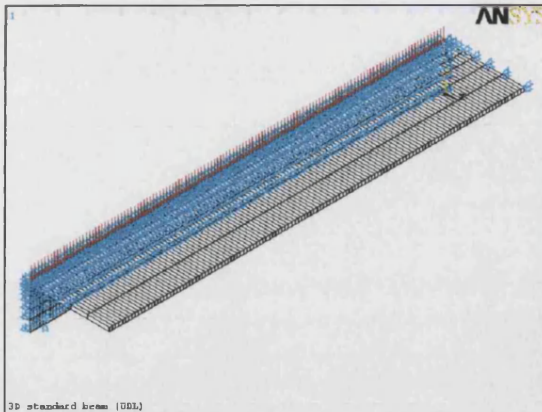


Figure 6.8 Mesh and boundary conditions for standard beam.

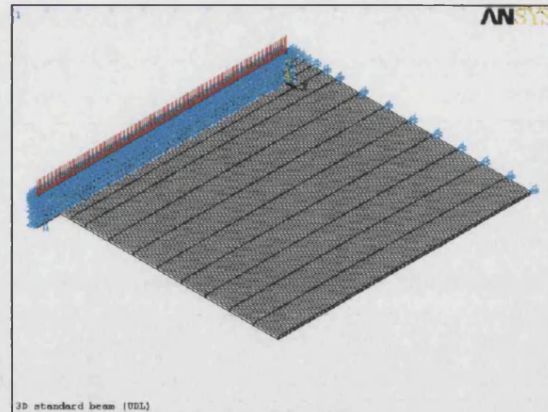


Figure 6.9 Mesh and boundary conditions for wide standard beam.

6.2.1 Uniformly distributed load cases

The results for the finite element and algebraic shear lag analyses are shown in Figure 6.10 and Figure 6.11. The results in the case of the finite element solution indicate the stresses at the top and bottom of the flange. The plots also show the solution obtained using the composite bending theory. The algebraic shear lag solution lies midway between the values predicted using the finite element method. If the finite element solutions are averaged and compared with the algebraic solutions the mean error is two per cent. The correlation between the two models is good. The difference between the midplane stresses calculated using the algebraic solution and the outer surface stresses calculated using the finite element method may be accounted for by the bending of the flange. These bending stresses may be calculated using the composite bending theory.

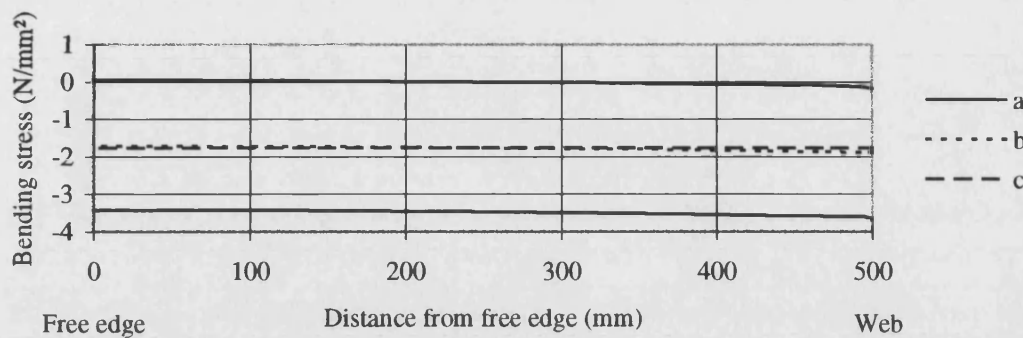


Figure 6.10 Finite element and algebraic analyses for bending stress distribution in the flange of a standard beam, spanning 5 m, carrying a UDL of 2.5 kN/m, $S_a=1250 \text{ N/mm}^2$. (a) Finite element solutions, top and bottom of flange, (b) Shear lag theory, (c) Ordinary composite theory.

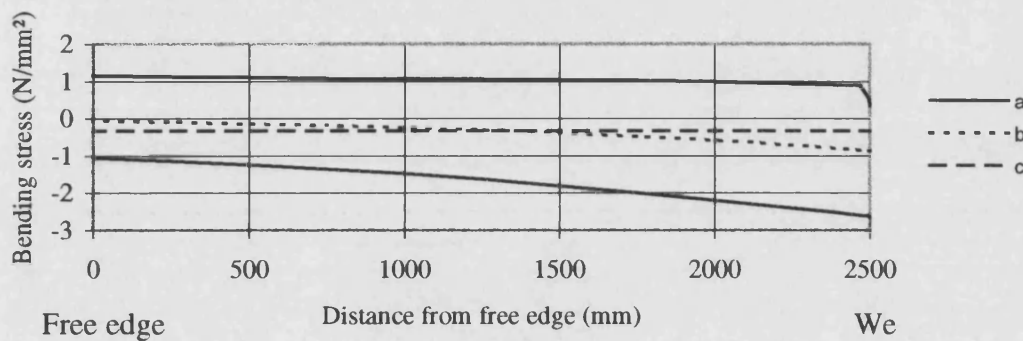


Figure 6.11 Finite element and algebraic analyses for bending stress distribution in the flange of a wide standard beam, spanning 5 m, carrying a UDL of 2.5 kN/m, $S_a=1250 \text{ N/mm}^2$. (a) Finite element solutions, top and bottom of flange, (b) Shear lag theory, (c) Ordinary composite theory.

6.2.2 The three point bending cases

In the case of the standard section the point load was applied at the point of quarter symmetry. The solutions are shown in Figure 6.12 and Figure 6.13. There are two causes for concern. The first is that the peak stress indicated by the finite element solution is an order of magnitude higher than that calculated using the algebraic solution. If the finite element solution is correct then failure of the beam can be expected at a much lower load than that predicted using the algebraic solution. The second cause for

concern is that the algebraic solution no longer lies midway between the calculated finite element solutions. In fact the finite element solution for the top face and the algebraic solution for the midplane are asymptotic. If the finite element solutions are averaged and compared with the algebraic solution the average error is 100 per cent.

For the case of the modified standard section the point load was applied as a pressure. The load was applied over an equivalent area of 2600 mm^2 (650 mm^2 considering the quarter symmetry). The solutions in this case are shown in Figure 6.13. Applying the

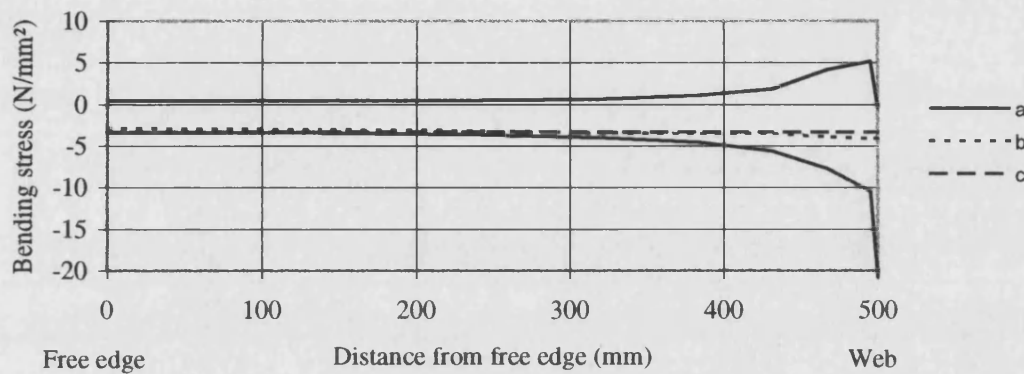


Figure 6.12 Finite element and algebraic analyses for bending stress distribution in the flange of a standard beam, spanning 5 m, 3 point bending, $P=12500 \text{ kN}$, $S_a=1250 \text{ N/mm}^2$. (a) Finite element solutions, top and bottom of flange, (b) Shear lag theory, (c) Ordinary composite theory.

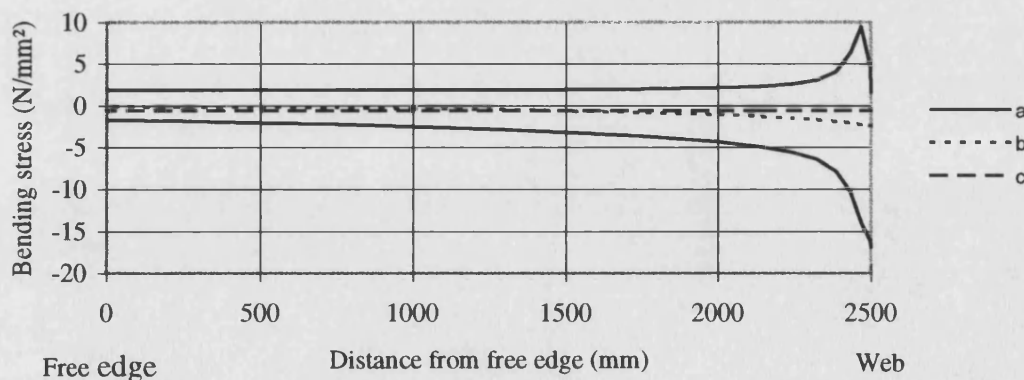


Figure 6.13 Finite element and algebraic analyses for bending stress distribution in the flange of a wide standard beam, spanning 5 m, 3 point bending, $P=12500 \text{ kN}$, $S_a=1250 \text{ N/mm}^2$. (a) Finite element solutions, top and bottom of flange, (b) Shear lag theory, (c) Ordinary composite theory.

load as a pressure has resolved the issue of the algebraic solution not lying midway between the finite element solutions. If the finite element stresses are averaged the error is generally two per cent. However, the peak stresses are still far higher in the finite element solution than the algebraic solution. This difference cannot be accounted for by the bending of the flange. It seems that the easiest way to determine which model is correct would be to strain gauge a real beam. If the finite element solution is correct we would expect to see an early failure of the beam.

If the algebraic solution is shown to be correct, and the work reported by Song and Scordelis would seem to suggest that it should be, then the method of finite element modelling needs to be examined. No further work into the finite element modelling has been conducted. However, it is suggested that the first approach might be to locally refine the finite element mesh in the region of the point load or localised pressure. If the algebraic solution is correct then it must be concluded that the application of point loads, or localised pressures, on a coarse finite element mesh will lead to excessively conservative stress predictions. This discussion is continued in section 9.

7 NUMERICAL IMPLEMENTATION OF BUCKLING EQUATIONS AND FINITE ELEMENT ANALYSIS

This section is concerned with assessing the buckling load of the laboratory test beam, Figure 7.1. The discussion addressing the reasons for this choice of beam may be found in Section 8. It has been determined by physical testing that over stressing of the web will occur before buckling of the flange, Section 9.4. Therefore only buckling of the web is considered. In the following discussions the results for the three algebraic models, see Section 5.4.1, three eigen value finite element models and two non-linear geometry finite element models are presented and discussed.

7.1 Algebraic models

In each case the buckling stress may be expressed as;

$$\sigma_{cr} = \frac{N_x}{h} = K \frac{\pi^2 D}{b^2 h}$$

For the section where the top edge of the web is assumed to be simply supported K may be determined from;

$$K = 0.456 + \frac{b^2}{a^2}$$

Therefore;

$$K = 0.456 + \frac{200^2}{2100^2} = 0.465$$

D is the plate constant and equals;

$$D = \frac{Eh^3}{12(1-\nu^2)} = \frac{70 \times 10^3 \times 10^3}{12(1-0.22^2)} = 6.130 \times 10^6 \text{ Nmm}$$

Therefore;

$$\sigma_{cr} = 0.465 \times \frac{\pi^2 \times 6.130 \times 10^6}{200^2 \times 10} = 70.3 \text{ N/mm}^2$$

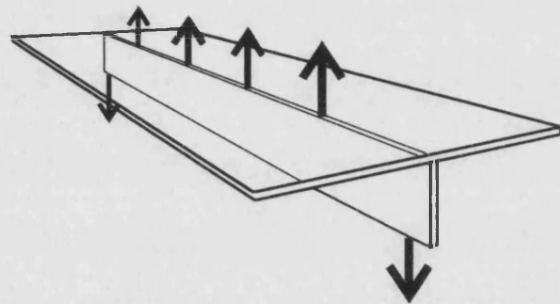


Figure 7.1 Beam and loading arrangement for buckling work. Flange 2250 mm x 800 mm x 6 mm toughened glass. Web 2250 mm x 200 mm x 10 mm toughened glass. Adhesive joint 1 mm x 10 mm with 3 mm leg length fillets. Simply supported 75 mm in from each end.

Dividing by E_G to obtain ε_b and substituting this value into Equation 4.2 it is possible to determine the critical load P_{cr} . This is found to be;

$$P_{cr} = 35.3 \text{ kN}$$

In this case the length of the web will buckle into one half wave.

For the case where the top edge of the web is considered fixed, K should be determined from **Figure 4.17**.

$$\frac{a}{b} = \frac{2100}{200} = 10.5 \therefore K = 1.404$$

Therefore;

$$\sigma_{cr} = 212 \text{ N/mm}^2$$

Calculating P_{cr} in the same way as last time we find that;

$$P_{cr} = 106 \text{ kN}$$

In this case the web will buckle into four half waves.

When considering the case of the elastic built-in edge it is necessary to determine the torsional rigidity of the flange and the quantity $r:b$, **Equation 4-41**.

$$r = 0.12 \text{ mm}$$

Using **Figure 4.16** K is then determined as;

$$K = 0.587$$

Therefore;

$$\sigma_{cr} = 88.8 \text{ N/mm}^2$$

Calculating P_{cr} in the same way as last time we find that;

$$P_{cr} = 44.6 \text{ kN}$$

In this case the web will buckle into three half waves.

7.2 Eigen value finite element problem

Three finite element models have been constructed to investigate the buckling of the laboratory T-beam. Model 1 is an all glass T-beam. It is constructed from 8 node isoparametric shell elements and uses half symmetry to reduce the size of the problem. At the support condition the base of the web is restricted against vertical movement. The web is also laterally restrained at its base and at its top. The loads are applied as forces at the nodes. The mesh and boundary conditions for model 1 are shown in Figure 7.2.

Model 2 incorporates the adhesive joint. It is constructed from 8 node isoparametric brick elements and half symmetry is again used to reduce the size of the problem. The beam is supported in an identical manner to model 1 although in this model the loads are applied as pressures. The area over which the pressure is distributed is the same as the area of the tension plates used in the laboratory tests, see Section 8.1.5. The beam section was modelled in two-dimensions and then extruded in the span direction. The adhesive joint is modelled as a single element. The web is modelled as seven elements and each half of the flange is modelled as five elements. The two-dimensional mesh was extruded 1125 mm in the span dimension with the maximum aspect ratio of the elements being 9:1. The mesh and boundary conditions for model 2 are shown in Figure 7.2.

Model three assumes no symmetry. It is constructed, supported and loaded in an identical manner to model 2. It was extruded 2250 mm in the span dimension with a maximum element aspect ratio of 15:1. The mesh and boundary conditions for model 3 are shown in Figure 7.2. This full length model was constructed and analysed to ensure that the half length models did not prohibit any of the buckling modes.

The buckling loads for the first three buckled modes of the three models are listed in Table 7.1. The first three buckled mode shapes for the three models are shown in Figure 7.3, Figure 7.4 and Figure 7.5.

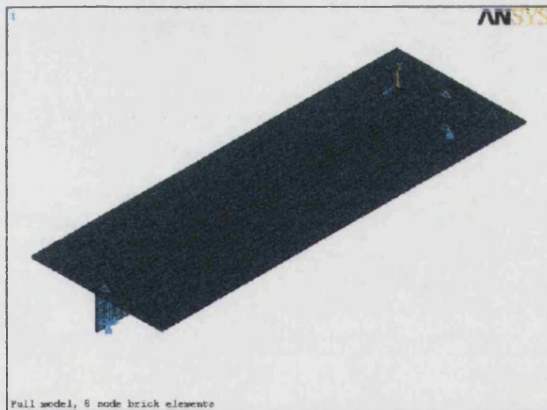
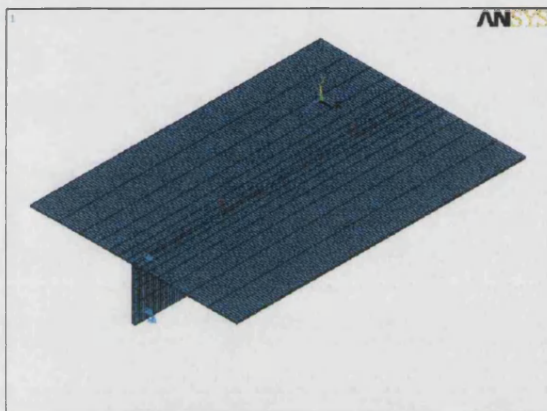
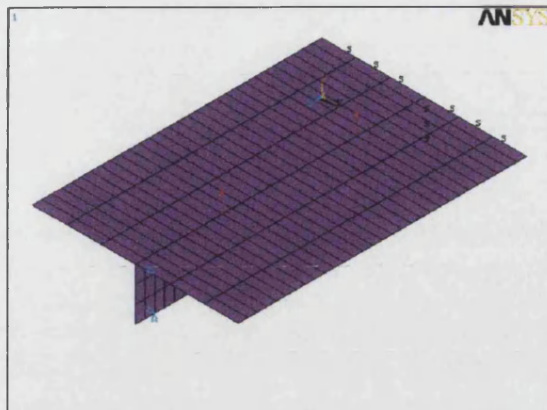
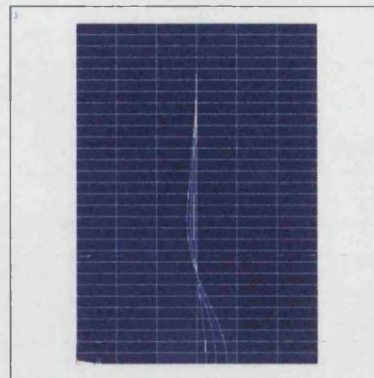
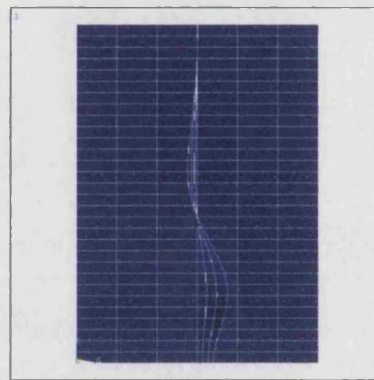


Figure 7.2 Finite elements models with boundary conditions for eigen value analyses. (Top) model 1, (Middle) model 2, (Bottom) model 3.



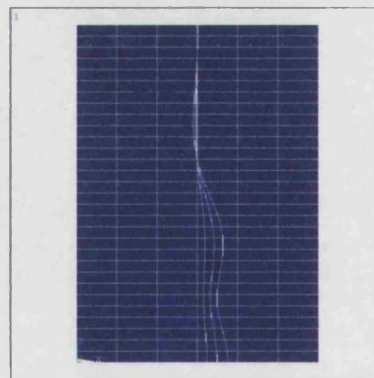
```
ANSYS 5.4
APR 1 1998
15:01:26
DISPLACEMENT
STEP=1
SUB =1
FACT=22185
PowerGraphics
EFACET=1
AVRES=Max
DMX =1

*DSCA=100
TV =-1
DIST=618.763
XF =399.911
YF =113.092
ZF =562.512
Z-BUFFER
```



```
ANSYS 5.4
APR 1 1998
15:02:09
DISPLACEMENT
STEP=1
SUB =2
FACT=28754
PowerGraphics
EFACET=1
AVRES=Max
DMX =1

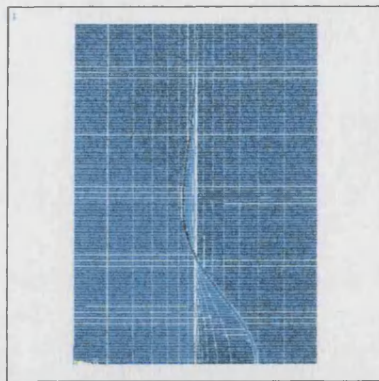
*DSCA=100
TV =-1
DIST=618.799
XF =399.35
YF =127.494
ZF =562.544
Z-BUFFER
```



```
ANSYS 5.4
APR 1 1998
15:02:51
DISPLACEMENT
STEP=1
SUB =3
FACT=36968
PowerGraphics
EFACET=1
AVRES=Max
DMX =1

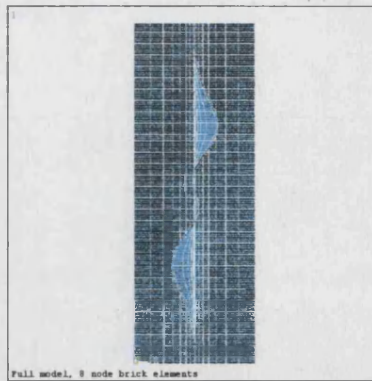
*DSCA=100
TV =-1
DIST=618.645
XF =398.78
YF =140.516
ZF =562.586
Z-BUFFER
```

Figure 7.3 Mode shapes for the first three buckled modes of model 1.



```

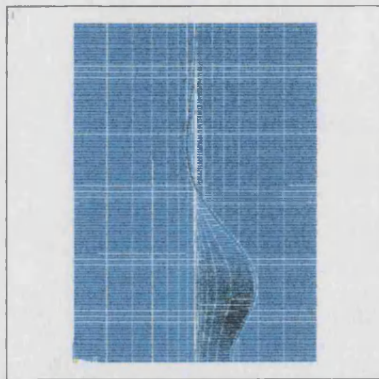
ANSYS 5.4
AUG 1 1998
14:01:19
DISPLACEMENT
STEP=1
SUB =1
TIME=14.047
PowerGraphics
EFACET=1
AVRES=Max
DMX =1
*MSCA=200
TY =-1
DIST=618.896
XF =399.881
YF =133.581
ZF =562.551
Z-BUFFER
    
```



```

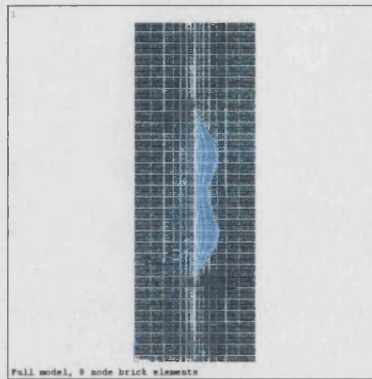
ANSYS 5.4
AUG 1 1998
14:08:19
DISPLACEMENT
STEP=1
SUB =1
FACT=170.433
PowerGraphics
EFACET=1
AVRES=Max
DMX =1
*MSCA=150
TY =-1
DIST=1238
XF =399.942
YF =121.212
ZF =1125
Z-BUFFER
    
```

Full model, 8 node brick elements



```

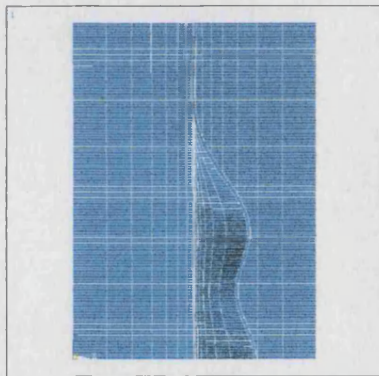
ANSYS 5.4
AUG 1 1998
14:02:21
DISPLACEMENT
STEP=1
SUB =2
TIME=285.174
PowerGraphics
EFACET=1
AVRES=Max
DMX =1
*MSCA=200
TY =-1
DIST=618.925
XF =399.532
YF =149.899
ZF =562.459
Z-BUFFER
    
```



```

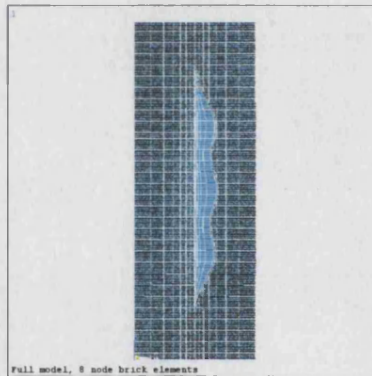
ANSYS 5.4
AUG 1 1998
14:10:19
DISPLACEMENT
STEP=1
SUB =2
FACT=173.569
PowerGraphics
EFACET=1
AVRES=Max
DMX =1
*MSCA=150
TY =-1
DIST=1238
XF =399.577
YF =154.154
ZF =1125
Z-BUFFER
    
```

Full model, 8 node brick elements



```

ANSYS 5.4
AUG 1 1998
14:03:11
DISPLACEMENT
STEP=1
SUB =3
TIME=37.082
PowerGraphics
EFACET=1
AVRES=Max
DMX =1
*MSCA=200
TY =-1
DIST=419.046
XF =399.250
YF =155.834
ZF =562.760
Z-BUFFER
    
```



```

ANSYS 5.4
AUG 1 1998
14:12:10
DISPLACEMENT
STEP=1
SUB =3
FACT=224.072
PowerGraphics
EFACET=1
AVRES=Max
DMX =1
*MSCA=150
TY =-1
DIST=1238
XF =399.356
YF =173.47
ZF =1125
Z-BUFFER
    
```

Full model, 8 node brick elements

Figure 7.4 Mode shapes for the first three buckled modes of model 2.

Figure 7.5 Mode shapes for the first three buckled modes of model 3.

Model/mode	Buckling load (kN)	Number of half waves
Model 1 (all-glass beam)		
Mode 1	88.7	3
Mode 2	115	5
Mode 3	148	5 or 7
Model 2 (glass-adhesive beam, half model)		
Mode 1	77.1	3
Mode 2	103	5
Mode 3	132	5 or 7
Model 3 (glass-adhesive beam, full model)		
Mode 1	102	2 or 4
Mode 2	104	5
Mode 3	134	5

Table 7.1 Summary of buckling loads and modes for models 1, 2 and 3.

Several models that incorporated the adhesive joint were built using shell elements. However, in these cases it was not possible to converge the solutions. One of the shell meshes is shown in Figure 7.6. The solution to this problem converged to a value of 1,972 kN. The first mode shape is shown in Figure 7.7. Clearly this solution is wrong.

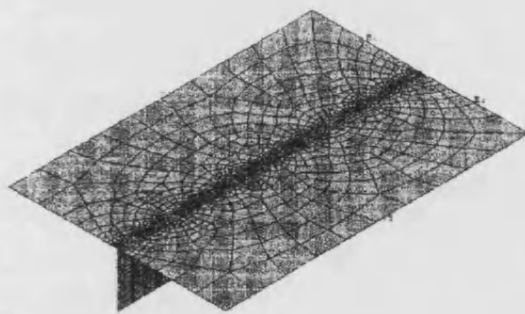


Figure 7.6 One of the shell meshes used in the solution of the eigen value buckling problems.

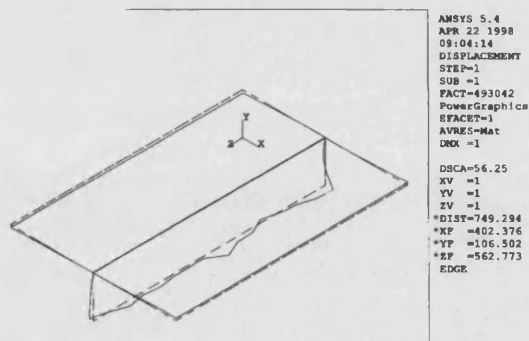


Figure 7.7 Eigen value buckling analyses based on shell models rarely converged. On the occasions that they did converge the eigen values and eigen modes made little sense.

7.2.1 The case of three half waves

Only models 1 and 2 gave buckled modes with three half waves. The eigen buckling load for model 1, the all-glass beam, is 15 per cent higher than for model 2. It therefore appears that the adhesive joint may have some effect in reducing buckling load. It is possible that the adhesive may allow relative rotation of the web and the flange at the adhesive joint. This would lead to a decrease in the buckling load and may partially account for the 15 per cent difference between models 1 and 2. The compressive stresses in the bottom of the composite beam are ten per cent higher than those in the monolithic beam because of the shearing action of the adhesive. This would also lead to a decrease in the buckling load and may partially account for the 15 per cent difference between models 1 and 2. The difference may also have been brought about because of the different ways the two models have been meshed. With hindsight it would have been sensible to re-run model 2 after attributing all of the elements with glass properties. Unfortunately this was not done.

7.2.2 The cases of four and five half waves

The buckled mode shapes with four and five half waves become complex. It is not always easy to determine the number of half waves and the reader may disagree with the values presented in Table 7.1. All three models indicate a second mode at about 110 kN. The buckling load for model 1, the all-glass beam, is 11 per cent higher than those for models 2 and 3. It appears that in these cases the web buckles into five half waves. All three models also indicate a third mode at approximately 140 kN. Again the buckling load for model 1, the all-glass beam, is 11 per cent higher than those for models 2 and 3. It appears that in these cases the web buckles into either five or seven half waves.

7.2.3 Non-linear geometry finite element problem

Model 3 was used for the non-linear analysis of the problem. A de-stabilising load is introduced. This was introduced as a point load, applied at the base of the web at the

midspan. Two versions of this model are considered. In the first the de-stabilising load is equal to two per cent of the total applied load. In the second this is reduced to 0.2 per cent of the total applied load. The total applied load was 50 kN in both cases. The minimum step size was equivalent to a load of 5 kN. A force criterion was used to control the convergence of the problem.

With a 2 per cent de-stabilising load the solution failed to converge beyond a total load of 30 kN. With a 0.2 per cent de-stabilising load the solution failed to converge beyond a total load of 40 kN. The time-history force-displacement plot for the 0.2 per cent solution is presented in Figure 7.9. Whilst the midspan deflection of 1.5 mm at 40 kN is not excessive it can be seen that the rate of increase of deflection with load is increasing. The lowering of the tolerance value used in the convergence criteria may have allowed the solution to converge to a higher level. However, at 40 kN it is apparent that the beam is already approaching its buckling load.

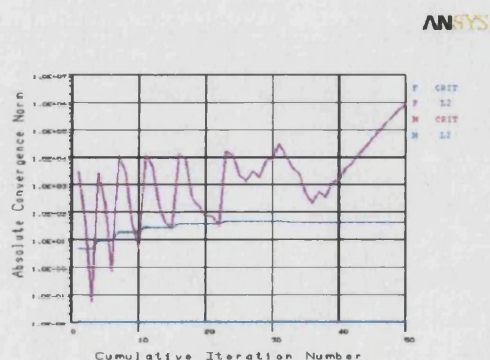


Figure 7.8 Convergence path for non-linear finite element solution with 0.2% destabilising load.

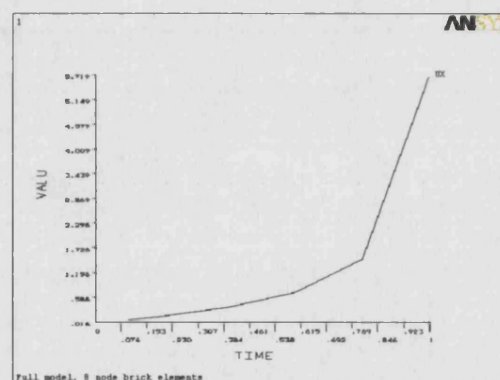


Figure 7.9 Time deflection plot for non-linear finite element solution with 0.2% destabilising load. Time 0 equivalent to zero load. Time 1 equivalent to full load.

In each case the buckled form was a single half wave along the length of the web, Figure 7.10. This is in clear contrast to the eigen value solutions that all predicted the occurrence of three or more half waves and is presumably due to the introduction of the

de-stabilising load. Figure 7.11 shows the rotation of the web and the flange. It would appear that the web remains perpendicular to the flange at the adhesive joint.

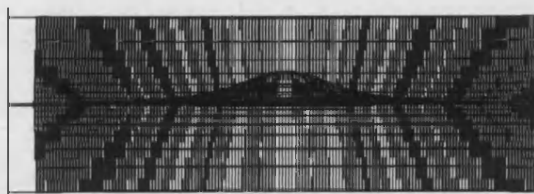


Figure 7.10 Plan view of buckled web from non-linear finite element analysis.

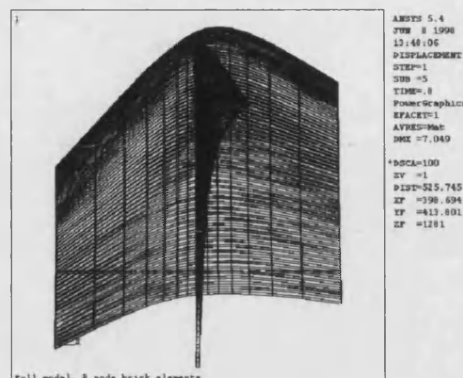


Figure 7.11 Elevation of buckled web from non-linear finite element analysis

7.2.4 Discussion of the various buckling models

The eight buckling models have given very different buckling loads that vary from 30 kN to 102 kN. In addition the predicted buckled modes differ. The range for the first buckled mode is from a single half wave to four half waves. The finite element models have all been restricted by the maximum mesh density which could be created.

The finite element plots have indicated that there is no relative rotation of the web and flange at the adhesive joint. However, they have also indicated that the buckling load for the composite is less than that for the monolithic section. It appears that the predominant reason for this may be the higher stresses at the base of the composite section.

Unfortunately, it is not possible to determine which method, if any, provides a suitable approach to determining the buckling load of the composite.

8 EXPERIMENTAL WORK

8.1 Introduction

Experimental work was undertaken to validate the theory developed in chapters 3 to 7. It was also necessary to establish the cyclic performance of the adhesive joint. However, the fabrication of the beams was as much a part of the experimental work as the tests that were performed on them. The fabrication method has been developed by learning from mistakes. The result is a process which leads to the production of a strong, consistent and neat joint.

In all, eleven beams have been constructed. They are nominally identical. Each is 2250 mm long and has a 6 mm thick, 800 mm wide flange and a 10 mm wide, 200 mm deep web. The beam size was chosen as one that could be handled by two people. The beams were loaded using a 50 kN hydraulic ram. The section properties of the tested beams are such that at 50 kN in a three point bending test the maximum glass stress would be 235 N/mm² and the maximum average adhesive stress would be 16 N/mm². These figures represent the maximum likely strengths of the glass and the adhesive. Whilst in practice design values may be less than half these values, this set up allows the beam to be tested to its limit. The length of the beam was dictated by the spacing of the channels in the laboratory strong floor. The width was dictated by the aperture in the H-frame in which the hydraulic ram was mounted.

Whilst it would have been possible to test beams of different cross-section and span, it was decided to rigorously test the one beam type. In this manner it has been possible to validate much of the theory and to show that the beams are not sensitive to minor variations in construction. The cost of materials for each beam is approximately £250. Each beam takes approximately two to three weeks to fabricate and prepare for testing. The number of beams was therefore limited by the quantity of glass that it was possible to obtain and the time necessary to fabricate and test each beam.

8.1.1 Basic beam types

Two variations of the basic beam were tested in four different load support conditions, Figure 8.1. Beam type 1 is shown in Figure 8.1a and b. These beams were simply supported along the two ends of the flange. It was envisaged that in practice these beams would be supported in channel sections and may find applications in tall glazed facades where the stiffness of the window plate needs to be increased, Figure 8.2. The web has been stopped short of the end of the beam in order that the support could be continuous. In the case of the tested beams the web was not tapered and to alleviate any stress concentrations in the adhesive two square glass plates were bonded in these locations. In practice a second alternative may be to taper the ends of the web to avoid this step in beam stiffness, Figure 8.2b.

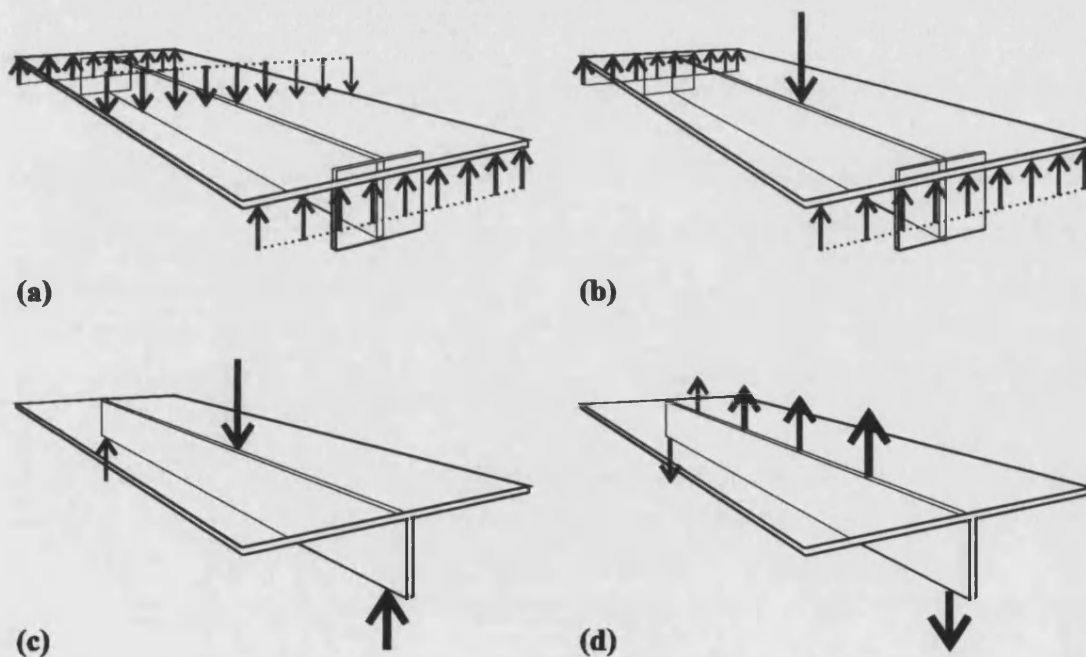
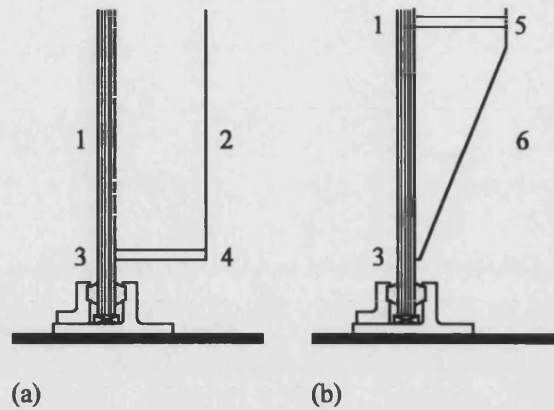


Figure 8.1 Different beam types and loading arrangements (a) & (b) beam type 1, (c) & (d) beam type 2

Figure 8.2 Potential application of type 1 beams. (a) Step change in stiffness, (b) Ramped change in stiffness. 1-Window glass, 2-Straight stiffening fin, 3-Standard clamp detail, 4-Stiffening plate to cope with large force transfer at end of stiffening fin and to restrict rotation of fin, 5-Stiffening plate to restrict rotation of fin, 6-Tapered fin to distribute force transfer.



Beam type two is shown in Figure 8.1c and d. In this scenario the web continues to the end of the beam and the whole beam is supported by clamping the web at each end.

8.1.2 Support arrangements

8.1.2.1 Beam type 1

The web was terminated 125 mm from each end of the flange using a 200 mm square 10 mm thick glass plate. Each end of the flange was supported on a 25 mm aluminium bar located 75 mm back from the end of the beam. The supports were articulated to account for any twist in the set up. Due to problems inherent in this support condition only three beams of this type were tested, see discussion in Section 9.1.1.

8.1.2.2 Beam type 2

Two patch plates were used to clamp each end of the web, Figure 8.3 and Figure 8.4. In the three point bending arrangement the roller simply rested upon a steel beam which was bolted to the strong floor. In the six point bending arrangement the patch plates were bolted to the same steel beam using four finger tight bolts. Oversized holes allowed lateral movement and rotation of the glass beam at the support conditions.

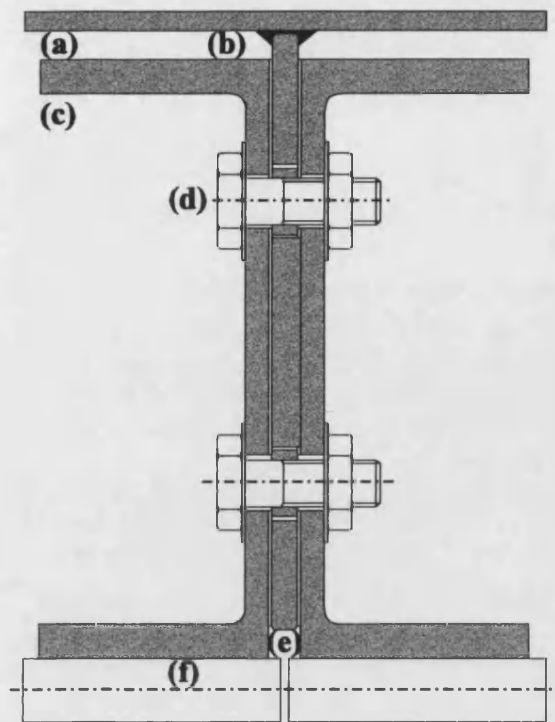


Figure 8.3 Cross section detail of web patch plates

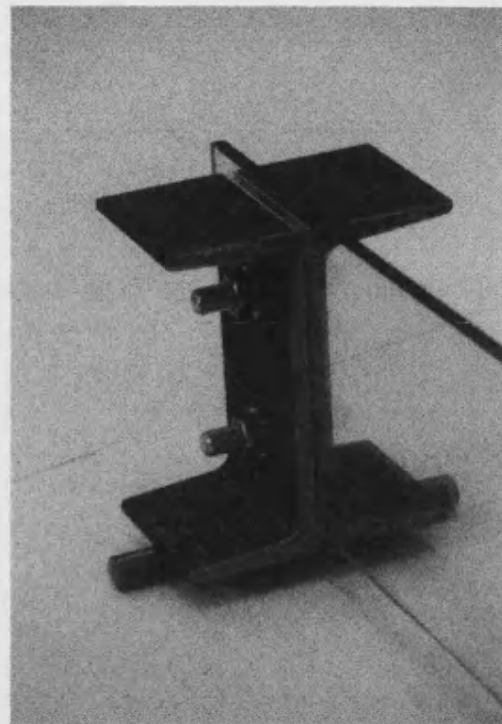


Figure 8.4 Web patch plates

8.1.3 Loading arrangements

All loading was restricted to the plane of the web as this is the manner in which the joint has been designed to work in practice. In practice any torsion would be restricted by the provision of suitable supports. Clearly the manner in which the loads are applied in practice will be highly dependent upon the manner in which the beam is used. A long wide flanged beam used in a vertical glazing application will be predominantly subject to a UDL perpendicular to the flange, Figure 8.5a. However, a long thin flanged beam used as a primary member in a large glass structure may be subject to point loads, Figure 8.5b. As no one loading pattern typifies the potential uses of this construction, it was decided that the applied loading should be that which could be most easily applied in the laboratory. Therefore the standard three point bending arrangement was used to test the beams, Figure 8.1a to c. However, when it was necessary to reverse the loading it was apparent that to transfer the whole tensile load through just one part of the adhesive

would be unrealistic. Instead a six point bending arrangement was utilised such that the tensile load was applied at four discrete points, Figure 8.1d.

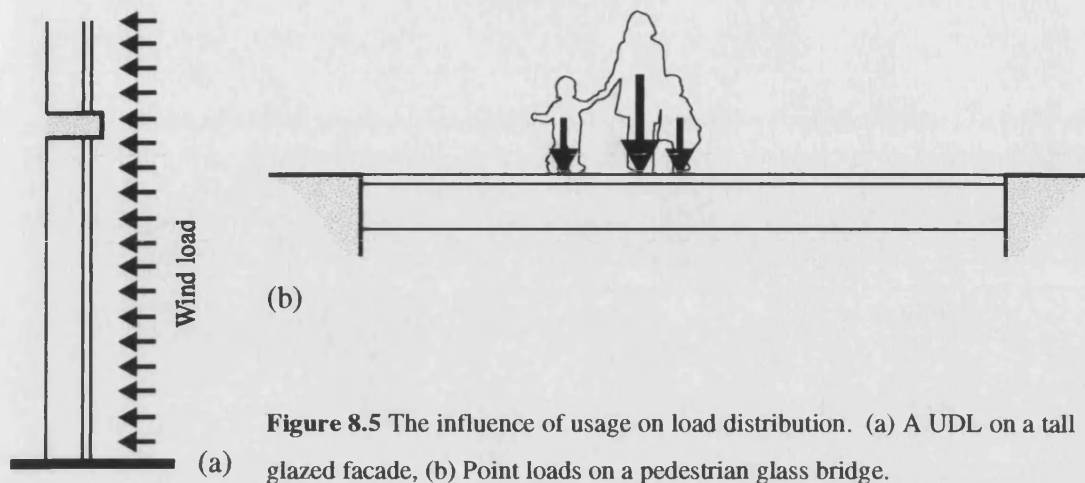


Figure 8.5 The influence of usage on load distribution. (a) A UDL on a tall glazed facade, (b) Point loads on a pedestrian glass bridge.

8.1.3.1 Load arrangement 1 (Figure 8.1a)

A long 25 mm diameter aluminium bar positioned at the centre span was used to apply load across the flange, Figure 8.6. In practice the flange was flexible and the only load transfer that occurred was immediately above the web.

8.1.3.2 Load arrangement 2 (Figure 8.1b and c)

Accepting that applying load across the width of the flange would be difficult it was decided to apply a single point load immediately above the web. This was done by a 70 mm diameter steel disc, Figure 8.7. The disc was articulated such that it made good contact with the flange and a gasket was used between the disc and the flange to minimise any stress concentrations.

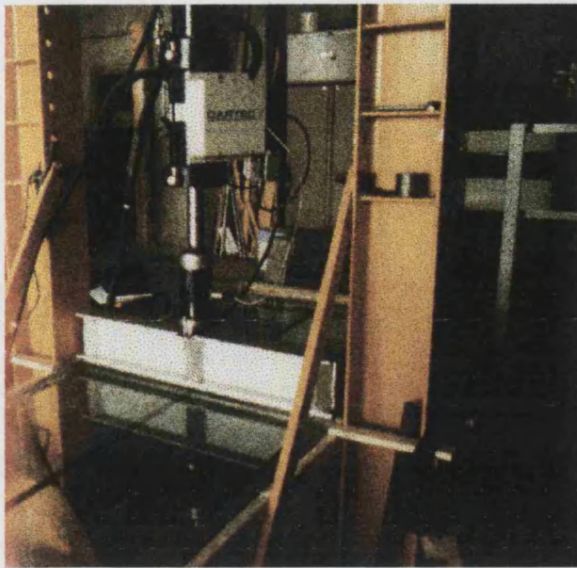


Figure 8.6 (Above) Load arrangement 1

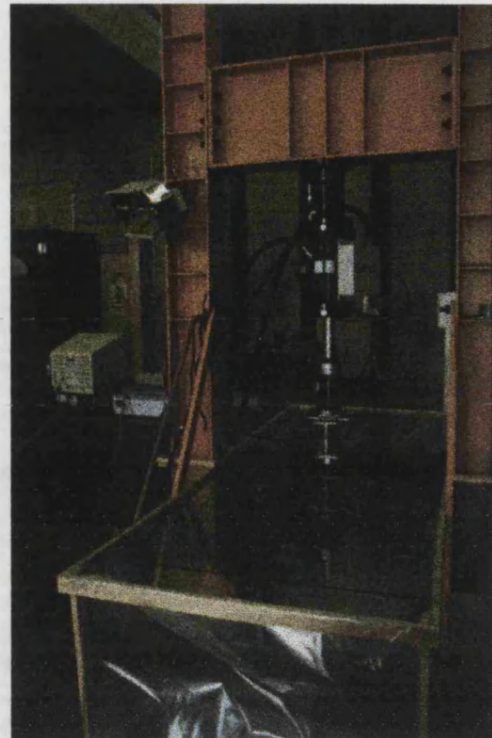


Figure 8.7 (Right) Load arrangement 2

8.1.3.3 Load arrangement 3 (Figure 8.1d)

Four 75 mm square steel plates were bonded to the surface of the flange. (See Section 8.1.5 for details of bonding procedure.) They were positioned immediately above the web at the $\frac{1}{8}$, $\frac{3}{8}$, $\frac{5}{8}$ and $\frac{7}{8}$ span positions. The plates were connected to a wiffel tree using an articulated connection and then back to the hydraulic ram, Figure 8.8 and Figure 8.9.



Figure 8.8 (Above) Bonded steel tension plates

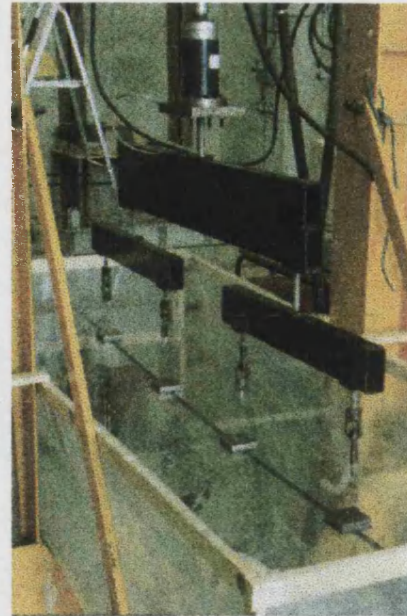


Figure 8.9 (Right) Load arrangement 3

8.1.4 Instrumentation

The manner in which the individual tests were instrumented was modified throughout the test programme. All tests were performed using a 50 kN Dartec hydraulic jack. The load-stroke data for tests 1 to 4 and test 8, Table 8.1, was recorded using the controller's data logger and were output graphically. Peak load and stroke readings were recorded manually. In all later tests this data was logged using an external Mowlem Microsystems 700 series ADU.

Test no.	Beam no.	Beam type	Load arrang.	Purpose of test	Instrumentation
1	1	1 (Short web)	1 (3PB)	CB	DD,VD
2	2	1 (Short web)	1 (3PB)	CB & SL	DD, SG
3	3	1 (Short web)	1 (3PB)	CB & SL	DD, SG,VD
4	4	2 (Long web)	2 (3PB)	CB & SL	DD, SG
5	4	2 (Long web)	3 (6PB)	CF	ED, SG, DT
6	4	2 (Long web)	3 (6PB)	CF	ED, SG, DT
7	4	2 (Long web)	2 (3PB)	CF	ED, SG, DT
8	5	2 (Long web)	2 (3PB)	CB & SL	DD, SG,DT
9	5	2 (Long web)	3 (6PB)	CB, SL & BU	ED, SG, DT
10	6	2 (Long web)	3 (6PB)	CF	ED, SG, DT
11	6	2 (Long web)	3 (6PB)	CB, SL & BU	ED, SG, DT,VD
12	7	2 (Long web)	3 (6PB)	CB, SL & BU	ED, SG, DT,VD
13	7	2 (Long web)	3 (6PB)	CF	ED, SG, DT
14	8	2 (LW & TAJ)	2 (3PB)	CB & SL	ED, SG, DT
15	8	2 (LW & TAJ)	2 (3PB)	CF	ED, SG, DT
16	8	2 (LW & TAJ)	2 (3PB)	CF	ED, SG, DT
17	8	2 (LW & TAJ)	3 (6PB)	CB & SL	ED, SG, DT
18	8	2 (LW & TAJ)	3 (6PB)	CF	ED, SG, DT
19	8	2 (LW & TAJ)	3 (6PB)	CF	ED, SG, DT

Table 8.1 Summary of test programme. LW-Long web, TAJ-Thin adhesive joint, CB-Composite bending, SL-Shear lag, CF-Cyclic fatigue, BU-Buckling, DD-Dartec data logger, ED-External data logger, SG-Strain gauges, DT-Displacement transducers, VD-Video

In tests 1 to 4 the only displacement data that was recorded was the ram stroke. Corrections were made for the displacement of the supports and in this manner the midspan displacement was calculated from the stroke. In all later tests a minimum of

three strain gauge displacement transducers were used to record the movement of the beam. One transducer was located at the midspan and positioned on the lower edge of the web. The two other transducers were located at each end of the web and were also positioned on the lower edge of the web. In the six point bending tests a fourth transducer was located at the midspan but was placed in contact with the lower face of the flange at the junction with the web. In all cases the reference for the transducers was the laboratory strong floor. The transducers were logged using the Mowlem Microsystems 700 series ADU.

With the exception of test 1 the beams were strain gauged using eight number 120 Ω gauges with a gauge factor of 2.05. These were wired back to the Mowlem Microsystems 700 series ADU in quarter bridge arrangements. All the gauges were positioned at the midspan. Three were located on one side of the web and five were located on the lower face of one half of the flange.

Tests 1, 3, 11 and 12 were recorded using a standard TV quality video camera recording at 25 frames a second. Despite this slow frame speed it was possible to use the videos to determine the origin of failure.

8.1.5 Sequence of events for beam fabrication process

8.1.5.1 Beam fabrication

1. Toughened glass plates with a minimum surface compression of 100 N/mm² were provided by Pilkington UK Ltd.. The glass was stored in laboratory for up to four months and no special measures were taken to protect glass.
2. During fabrication the plates were laid on a large, flat, felt covered table^a. The glass was washed using clean hot water and polished dry. The adhesive joints were marked using a continuous strip of masking tape. The joints were nominally 10 mm wide and 1.1 mm thick with a 3 mm leg length fillet.

3. The surfaces were primed using 3901 silane primer. The primer was applied using a paper towel in a wipe-on, wipe-off action. The primer was allowed to air dry for 12 to 24 hours during which time the glass surface was maintained at a minimum temperature of 25 °C.
4. 10 number 1.1 mm diameter glass beads were bonded to the flange along the centre line of the adhesive joint using a small quantity of DP 190^b. The adhesive was allowed to cure for up to six hours.
5. 150 g of 2216 was mixed by hand according to manufacturer's instructions ^c. The adhesive was poured from the mixing pot along joint line of flange. The adhesive was allowed to spread under its own viscous flow and any air bubbles were burst. The web was lowered onto the adhesive and kept vertical using timber props. The flange was protected by inserting a paper interlayer between the props and the glass ^d.
6. The adhesive was tooled using a plastic spatula which was profiled to give a 45° 3 mm fillet. The masking tape was removed and the adhesive was allowed to cure for a minimum of one day before moving the beam. The adhesive was allowed to cure for a further seven days before the beam was tested.
7. For type 1 beams steps 2 to 6 were repeated for the bonding of two end plates.

8.1.5.2 *Beam preparation*

If the beam was to be used in six point bending tests tension pads were bonded to the top surface of the flange. The glass was washed using hot water and was polished dry. The adhesive joints were marked with masking tape. The joints were nominally 81 mm square and 1.1 mm thick with a 3 mm leg length fillet. The base of steel tension plates were ground clean, washed in hot water and degreased using diclormethylethene. The glass and steel were primed using 3901 silane primer. The glass was covered with a 2 mm layer of DP 190 into which nine number 1.1 mm diameter glass beads were placed. The steel plate was pressed into the layer of adhesive which was then tooled as before. The masking tape was removed and the adhesive was cured for a minimum of seven days.

For the strain gauges the glass was cleaned using hot water and the strain gauge template was taped to the glass. The glass was cleaned and primed using proprietary Micro Measurement products. The gauges and contacts were bonded to the glass using a proprietary Micro Measurement adhesive. After having been soldered the gauges were painted with a coat of varnish to prevent the ingress of water °. The beams were stored in a vertical position for up to four months before testing. No special measures were taken to protect the glass.

8.1.5.3 Notes

- (a) It was found that the table needed to be at least as long as the beam. Figure 8.10 shows the original short table on which the beams were assembled. In this situation the glass flange will droop at the ends and the thickness of the adhesive joint will increase accordingly. A potentially more serious problem is that the increased air circulation around the adhesive joint and the consequent cooling of the glass may extend the cure period for that part of the joint.
- (b) Originally the beads were placed into the uncured adhesive that was to form the joint. However, when the web was lowered into place many of the beads would be pushed out of the joint. They were then not able to act as spacers. In addition if a bead became positioned at the surface of the joint there was a chance that it may act as a serious stress concentrator. To resolve this problem the beads were bonded directly to the flange glass using a fast curing translucent cyanoacrylate adhesive. However, this adhesive was visible against the grey 2216. For cosmetic reasons, the cyanoacrylate adhesive was therefore replaced with grey coloured DP190. 2216 was not used as it was difficult to apply in small quantities.
- (c) Initially the adhesive was mixed on a flat plastic palette. However, it appears that the adhesive in beam 2 may not have been mixed properly. All later batches of adhesive were mixed in a shallow pot to ensure better mixing of the components.

(d) After use the bases of the props became contaminated with small particles of grit.

This, in conjunction with the weights used to hold the props in place led to some severe scratching of the flange glass. Whilst this was not seen to have had any adverse effect on the test results later beams were protected from the base of the props by a paper interlayer.

(e) After storage some gauges were seen to de-bond from the glass surface. It is thought that this was due to the ingress of moisture which can creep along the surface of the glass by capillary action. Once between the glass and the adhesive this can quickly lead to the breakdown of the bond. However, the application of a coat of varnish appeared to alleviate this problem.

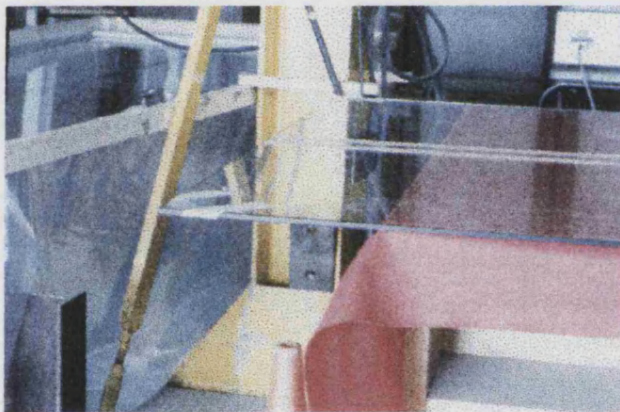


Figure 8.10 If the flange plate is not supported along its whole length it may deflect under its own weight and cause a significant variation in the thickness of the adhesive joint. In addition if the whole of the beam is not insulated the adhesive may take longer to cure

8.1.6 Safety issues

Toughened glass was used to reduce the risk of being cut by sharp shards of glass. During the tests the beams were contained within a plastic covered box to limit the damage caused by flying glass.. This did not greatly restrict the experimental observations as no visual distress could be seen before the beam failed. In addition all people handling or testing glass were required to wear safety goggles and to have their arms and legs fully covered. No injuries were sustained during the test programme.

8.2 Short term static testing

8.2.1 Basic three point and six point bending tests

Tests 1 to 4 and test 8 were conducted in stroke control although all subsequent tests were conducted in load control. The lack of plastic behaviour meant that there was no significant difference between the two test methods. The switch to load control came about only because of the need to perform cyclic testing in a fixed load range. In the non-cyclic tests the stroke rate, or load rate, was set such that the peak load was reached in 60 to 120 s. If the beams reached the peak load they were immediately unloaded at the same rate.

8.2.2 Shear lag tests

The differences between the finite element and algebraic solutions necessitated the need to determine the shear lag within the laboratory beams. The same beams were used for both the three-point bending and six point bending tests. It was therefore decided to strain gauge the beams in such a way that the same strain gauges could be used for both tests. The strain gauges allowed the investigation of the shear lag phenomena at the midspan. The spacing of the gauges allowed the shear lag to be determined across the full width of one half of the flange. As the curvature of the flange is generally small, only the lower face of the flange glass was strain gauged. This assumes that the difference between the upper and lower faces could be determined using conventional composite theory.

No special tests were conducted to investigate the shear lag effect. Instead all tests were strain gauged and data was recorded for the analysis of shear lag in each case.

8.3 Cyclic testing

Cyclic testing was undertaken to investigate the cyclic fatigue of the adhesive. It was hoped to demonstrate that the glass-adhesive composite could sustain repeated loading without damage or loss of performance. However, because of the small number of samples it was not possible to establish the fatigue performance. That is, it was not intended to produce data that could be used to determine the number of cycles to failure at particular load levels.

Glass does not suffer cyclic fatigue, Swedish Council for Building Research, (1993). The issue of static fatigue, see Section 2.1.1, should not be confused with cyclic fatigue. What is really being tested is the cyclic performance of the adhesive. It is generally known that most adhesives, including modified epoxies, suffer cyclic fatigue. It has been shown that one of the critical factors affecting the cyclic fatigue of adhesives is the peak stress, Harris and Fay (1992). It has also been suggested by Krieger (1986) that this is accelerated when the adhesive is stressed beyond its linear elastic stress-strain limit. The work in Sections 5.2.2 demonstrated that the predicted stress distribution within the adhesive joint was uniform. However, it is not possible to directly determine the stresses within the real adhesive joints. In the case of localised stress peaks within the adhesive it is possible that these could be sustained for a short period under static loading. However, cyclic loading damage could quickly accumulate in these areas and lead to the early failure of the beam. Therefore one reason for the cyclic testing is to determine the severity of any stress peaks. Adhesive stresses of 10 to 20 N/mm² in the 2216 might be expected to lead to the early failure of the adhesive (published ultimate shear strength is 17.2 N/mm²). However, adhesive stresses below this level might reasonably be expected to not cause cyclic fatigue.

It is not only the bulk adhesive that is tested in the cyclic test regime but also the strength of the bond to the glass surface. 2216 adhesive is not commonly used to bond glass and these tests were important to establish the performance of the adhesive and silane coupling agent at the glass-adhesive interface. Another reason for the cyclic testing was

to examine the dynamic response of the two different thickness adhesive joints. Harris and Fay (1992) report that thin adhesive joints are better able to resist cyclic fatigue than thicker joints. However, in the case of the thin joint tested here the thickness is known to vary and may cause severe stress concentrations within the adhesive. If this is the case it will be possible to demonstrate this during the cyclic testing.

It might have been suggested that cyclic tests should have been performed on smaller inexpensive samples in order that a cycles to failure versus load plot could have been constructed. If different adhesives were being evaluated this would have been a valuable exercise. Equally, had it been impossible to generate a stress distribution within a small test sample that was representative of the stress distribution within the beam then again this would have been a valuable exercise. However, as discussed in Section 2.2.6, all of the standard test methods setup severe stress concentrations. Certainly the standard lap joint test would have been unsuitable for this work as the stress concentrations at the two ends of the specimen are far more severe than those occurring in the beam joint.

One last reason for testing the whole beam is that it allows the investigation of potential post de-bond structural action. Liechti (1986) has shown that de-bonds must reach a critical length before they will cause failure of the joint. In the case of glass substrates this allows the potential to identify faults before they lead to the failure of the structural element.

It was stated in Section 9.1 that a 50 kN load in a three point bending arrangement would result in peak glass and adhesive stresses of 235 N/mm^2 and 16 N/mm^2 respectively. Whilst the beam may be able to sustain this load for a short period it is unlikely that it would ever be designed to carry such load. Currently toughened glass is rarely designed to carry an ultimate load of even 100 N/mm^2 , CEN (1996a), and factors of safety of 10 are often applied to the design of adhesives, Pye (1996a). **Table 2.1** summarises the peak glass and adhesive stresses for three and six point bending arrangements at different load levels.

Load (kN)	Peak stresses in three point bending		Peak stresses in six point bending	
	Glass (N/mm ²)	Adhesive (N/mm ²)	Glass (N/mm ²)	Adhesive (N/mm ²)
10	47	3.2	20	1.8 <i>4.9</i>
20	94	6.4	40	3.5 <i>9.8</i>
30	141	9.6	60	5. <i>14.6</i>
40	188	12.8	80	7.1 <i>19.5</i>
50	235	16	100	8.8 <i>24.4</i>

Table 8.2 Summary of peak stresses for different loading arrangements. Figures based upon composite theory, Section 4.2, except italicised figures which are based upon the results from the finite element model reported in section 7.2.

The italicised figures show the value of the first principal stress in the case of the six point bending arrangement. They are derived from the finite element model discussed in Section 7.2. Whilst the model has not been validated it gives some indication of the stress concentrations that will occur as a result of the point loads. The first principal stresses are not given in the case of the three point bending arrangement as they are the same as those derived from the composite theory.

The author believes that most engineers would limit the ultimate adhesive stress to either 5 or 6 N/mm². In the case of the three point bending arrangement this would limit the ultimate load to 20 kN. In the case of the six point bending arrangement this would limit the ultimate load to 10 kN. Therefore during cyclic testing the beams have generally been tested at either 10 kN or 20 kN loads. However one six point bending arrangement was loaded to 30 kN. In each case the minimum load was set to 10 per cent of the maximum load. Such large stress ranges are very severe. Far more severe for example than those experienced during a wind storm where a background load is likely to be periodically increased by gusts, BS 6399 pt II, BS (1997b). Therefore, if the beams can be shown to sustain such cyclic loading over a large number of cycles their performance should be seen as very good.

The cyclic tests were driven following a sine wave with a 3 second wave length. A sine wave was considered most representative of the type of loading that would occur in practice, BS (1997). Testing at a higher frequency would have shortened the total test time. However it was felt that the potential stiffening of the adhesive combined with its ability to carry higher loads when rapidly loaded may have reduced the validity of these tests for general design.

The minimum number of cycles was set at 10,000. This is considered as the norm within the construction industry, BRE (1989). In practice many samples were cycled more than 10,000 times because if they survived one load regime they were then used in a higher load regime. In most fatigue tests it is usual to use new untested specimens for each test. However, this was not practical in this case. Therefore some beams had already gone through extensive cyclic testing when tested at new higher load levels. Additionally they may have been previously loaded to extremely high loads in previous static tests. This should be borne in mind when examining the results presented in the next section.

8.4 Buckling

For the buckling of the web the six point bending arrangement was used to place the web into compression. In this case the limiting load was deemed to be the capacity of the hydraulic ram. Both T-beams 5 and 6 were tested in this manner. It was also decided to investigate the effect of introducing a web stiffener. To achieve this two 200 mm square glass plates were bonded either side of the web at the midspan. Each plate was 10 mm thick toughened glass, was bonded to the flange and used the usual 1 mm thick adhesive joint with a 3 mm leg length fillet. According to the algebraic theory with the simply supported edge this would increase the buckling load from 35 kN to 37.4 kN by forcing the web to buckle into two half waves. However, according to the algebraic theory with the elastically supported edge this would increase the buckling load from 44.6 kN to 48.6 kN.

Unfortunately no method of recording the mode shape was employed. With hindsight it is realised that the simple use of several displacement transducers positioned horizontally against the bottom edge of the beam may have been able to determine this. The video camera was used to determine the origin of failure.

9 RESULTS AND DISCUSSION

The results are presented and discussed under the headings of composite bending, shear lag, buckling and fatigue. Some tests are therefore discussed under several different headings, although in each case it is a different aspect of the beam's performance that will be addressed. A summary of the basic test results is presented in Table 9.1.

Test no.	Beam no.	Load arrang	Peak load (kN)	Peak midspan displacement / no. Cycles (mm / no.)	Comments
1	1	3PB	-7.6	-3.34	Failure of glass flange
2	2	3PB	-4.0	-4.35	Poorly mixed/ cured adhesive
3	3	3PB	-9.2	-2.75	Failure of glass flange
4	4	3PB	-36.3	-5.50	-
5	4	6PB	10.0	10,000	Slight shift in hysteresis loop
6	4	6PB	20.0	1,926	Tension plate de-bonded
7	4	3PB	-20.0	1,750	Extensive de-bond, test halted
8	5	3PB	-29.8	-4.40	-
9	5	6PB	38.3	3.00	Buckling failure of web
10	6	6PB	20.0	10,000	Slight shift in hysteresis loop
11	6	6PB	49.48	4.40	Buckling failure in web
12	7	6PB	49.44	4.75	-
13	7	6PB	30.0	6,882	Adhesive failure
14	8	3PB	-38.7	-5.1	-
15	8	3PB	-10.0	25,000	No shift in hysteresis loop
16	8	3PB	-20.0	25,000	No shift in hysteresis loop
17	8	6PB	29.05	2.10	-
18	8	6PB	10.0	10,000	No shift in hysteresis loop
19	8	6PB	20.0	5,892	Equipment malfunction, test halted

Table 9.1 Summary of the basic test results

9.1 Composite bending

9.1.1 Type 1 beams

All of the type one beams failed at low loads and the measured deflections and strains did not correlate with theory. However, the behaviour was linear and consistent, Figure 9.1. The slight anomaly in beam 2 was caused by poorly mixed/cured adhesive.

Video footage indicates that beam 1 failed at the midspan where the loading bar was in contact with the top of the flange. This can be seen in Figure 9.2. Beam two failed in a region of poorly mixed/cured adhesive at one end of the beam, Figure 9.3. However, as the fracture propagated into the region of properly cured adhesive the failure mode became one of glass plucking, Figure 9.5. Beam 3 failed in the flange near to the supports.

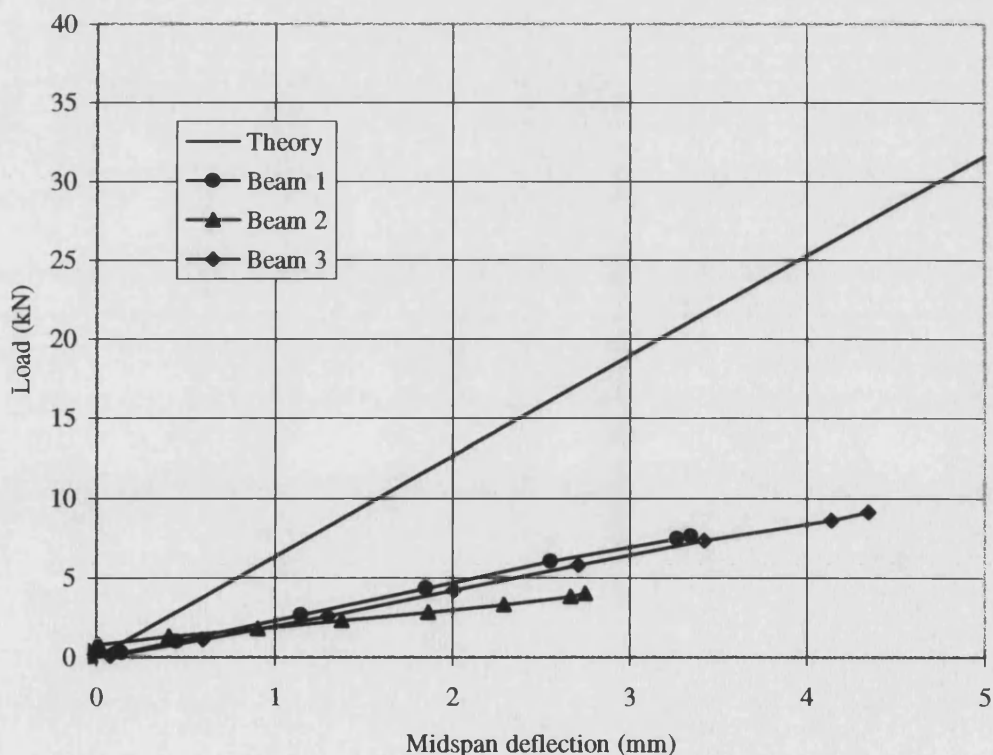


Figure 9.1 Load deflection plot for beams 1 to 3



Figure 9.2 Failure origin test 1. Fracture originates from point contact with loading bar

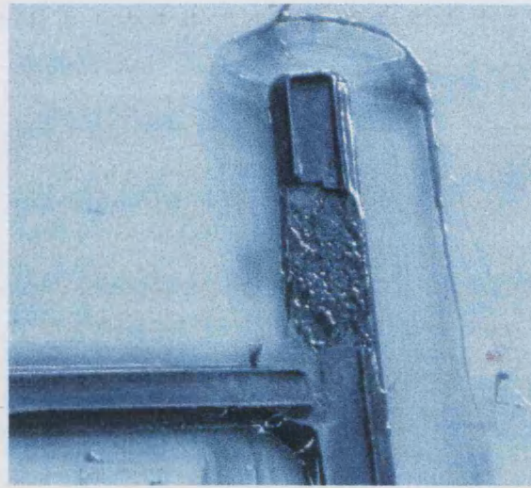


Figure 9.3 Region of poorly mixed/cured adhesive that initiated the failure of beam 2

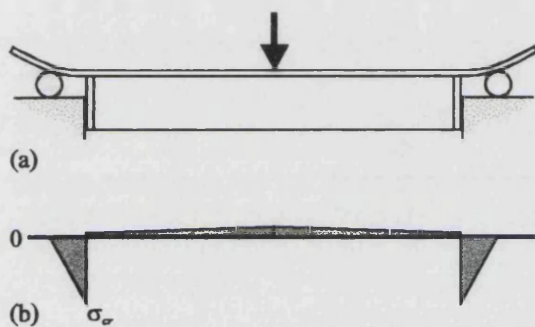


Figure 9.4 (Above) Diagrammatic illustration of the inherent flaws in the support arrangements for beams 1, 2 and 3



Figure 9.5 Beam 2, as the fracture front moved into the region of properly cured adhesive the failure mode became one of glass plucking.

The main problem with the type one beams was that the support condition was inherently flawed. As Figure 9.4 indicates, deflections were dramatically increased by the flexible nature of the flange. This also caused massive stress concentrations. If a condition of plane stress had existed in the flange a 10 kN load would have generated a maximum bending stress of approximately 50 N/mm^2 . As the flange glass probably had a bending strength of 150 N/mm^2 to 200 N/mm^2 it is apparent that a condition of plane stress did not exist. The bending stresses presumably peaked at the termination of the web. The provision of a thicker flange and a reduction in the distance from the support to the web

would have reduced this problem. However, this support arrangement was rejected in favour of the simpler web patch plate used in the type two beams

9.1.2 Type two beams

9.1.2.1 Three point bending tests

The behaviour of the beams tested in this arrangement was consistent and linear, and correlated well with the theory, Figure 9.6. The predicted stress concentrations in the thin joint beam did not materialise and this beam exhibited slightly stiffer behaviour than the two thick joint beams. Despite the maximum average shear stress being in the region of 10 N/mm^2 to 14 N/mm^2 (calculated) no failure of the adhesive joints occurred. It has not been possible to measure the peak stresses. However, it is suggested that the stress distribution must have been moderately uniform as the published shear strength of the adhesive is only 17 N/mm^2 .

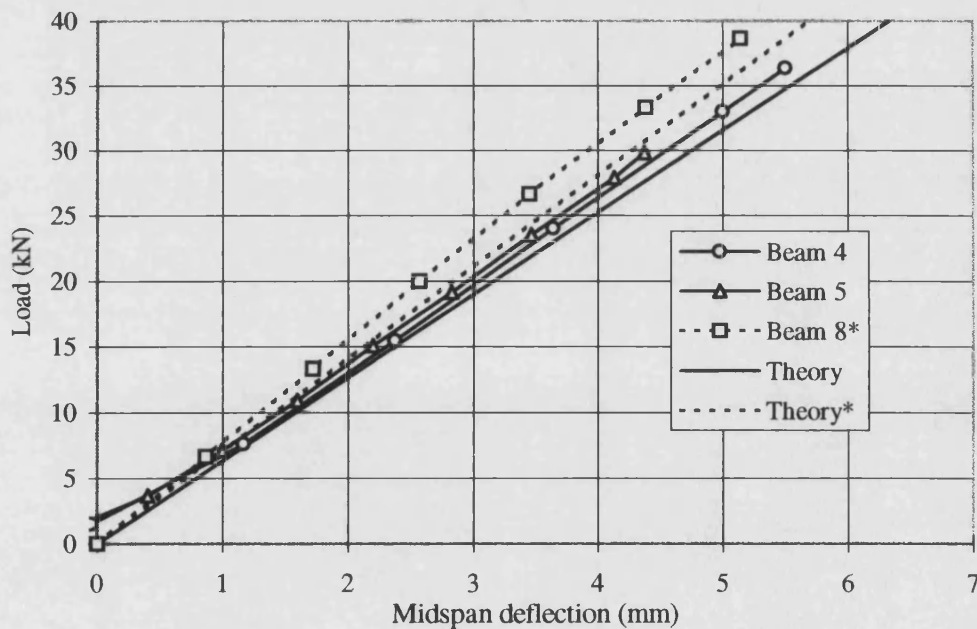


Figure 9.6 Load deflection plot for beams 4, 5 and 8. *indicates thin joint beams.

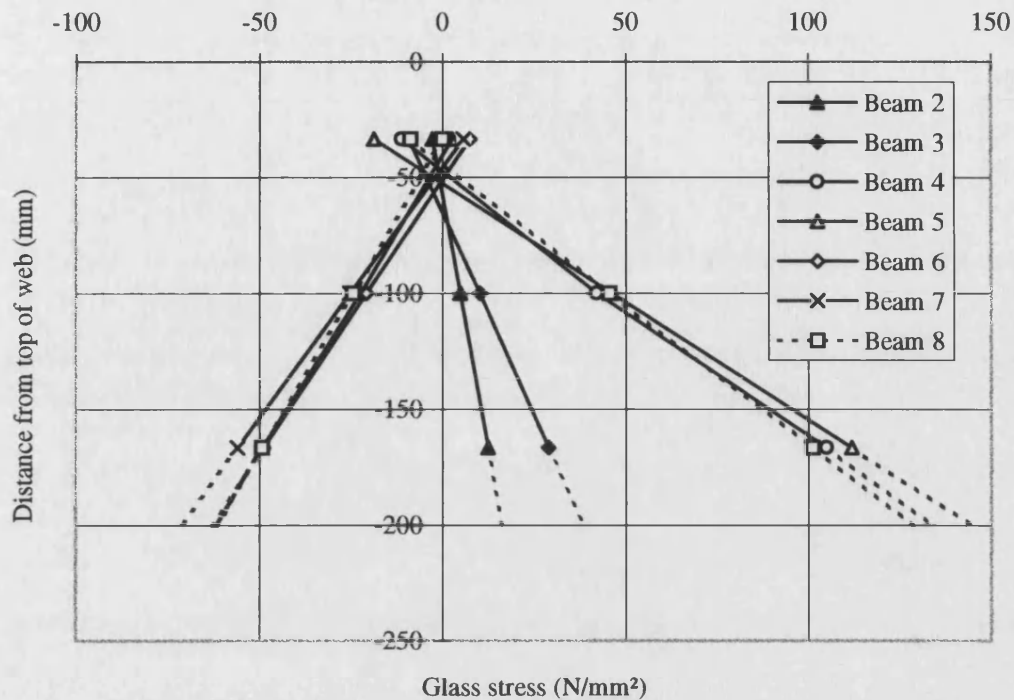


Figure 9.7 Midspan stress distribution in the webs of tested beams

Figure 9.7 shows the distribution of stresses within the web at a load of 30 kN. It indicates the maximum glass stress in the three point bending tests lies between 134 N/mm^2 and 145 N/mm^2 for the thick joint beams and is 129 N/mm^2 for the thin joint beams. This compares favourably with the theoretical values of 141 N/mm^2 and 125 N/mm^2 . Figure 9.8 shows that the neutral axis has been raised between 48 and 56 mm above the centroid of the web and indicates that a significant degree of composite action has been achieved. The percentage composite action varies from 91 per cent to 93 per cent for the thick joint beams. It reaches 97 per cent in the case of the thin joint beam.

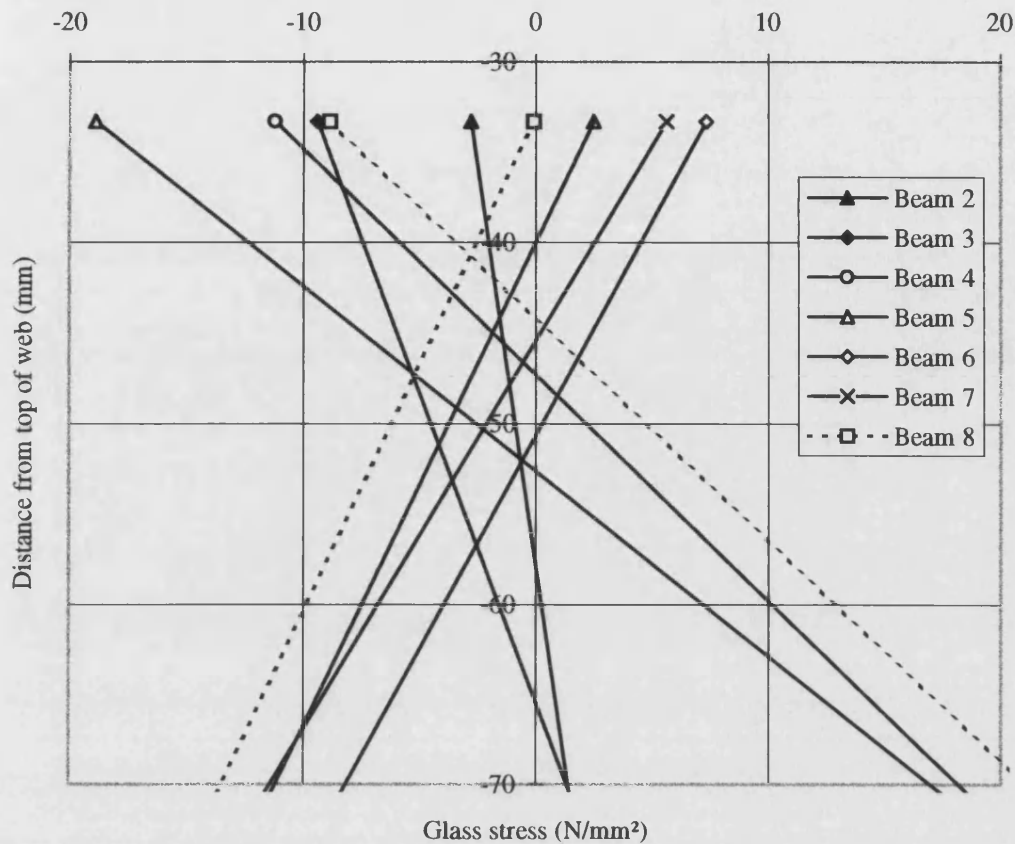


Figure 9.8 Position of neutral axis test 2 to 8

9.1.2.2 Six point bending tests

The beams tested in this arrangement performed well. The behaviour was again linear and consistent, and correlated well with the theory, Figure 9.9. Loads of up to 50 kN were applied and peak adhesive stresses were in the order of 14 N/mm^2 (calculated). In addition the adhesive maintained high tensile stresses across the joint at the location of the four tension plates. The ability to carry such high shear stress in addition to the high tensile stress again indicates that the adhesive shear stress distribution was reasonably uniform.

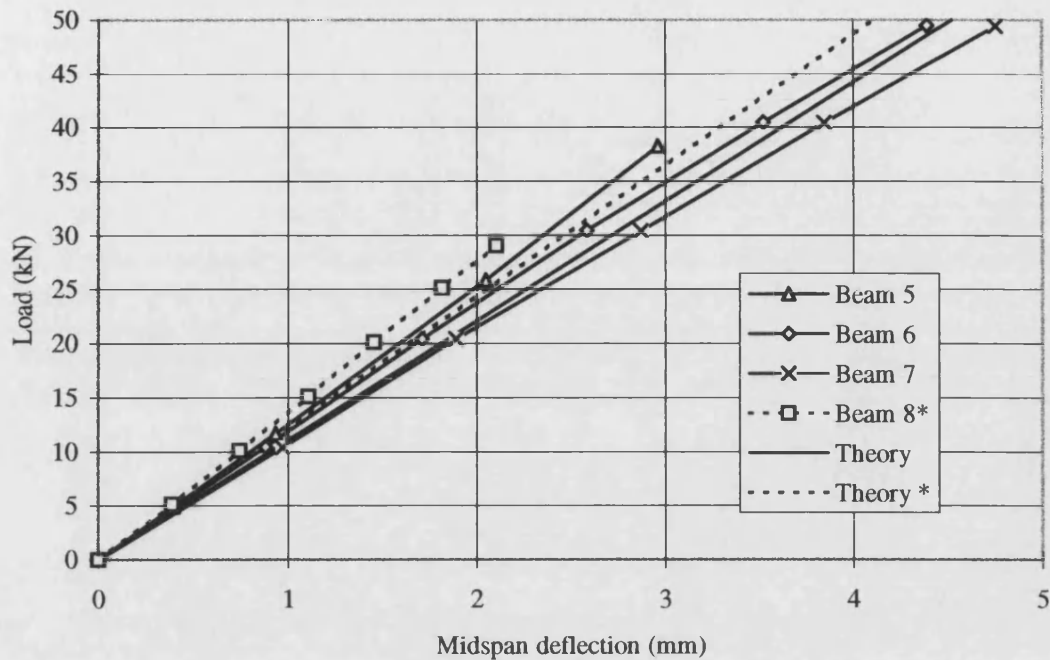


Figure 9.9 Load deflection plot for beams 5 to 8

9.2 Shear lag effects

The shear lag in the two laboratory beam set-ups was determined using the theory presented and discussed in chapters 5 and 7. All of the following discussions are based upon either three point or six point bending tests at a total load of 30 kN. This therefore excludes beams one to three which all failed well below this load. Surface stress plots calculated from the algebraic solutions are shown in Figure 9.10 and the variation of the stress ratio is shown in Figure 9.11. The finite element models that are reported here are constructed in the same manner as those discussed in Section 7. The loads are distributed over an area equivalent to the contact area used in the laboratory beam tests. Figure 9.12 shows the finite element mesh with boundary conditions for the six point bending arrangement.

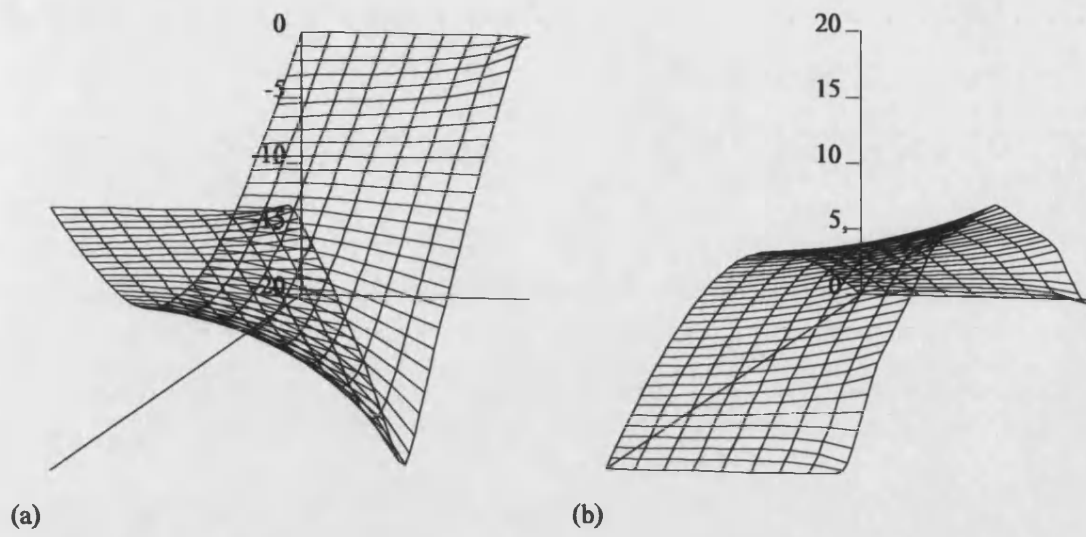


Figure 9.10 Shear lag in laboratory beam tests according to algebraic theory. (a) 3 point bending arrangement, (b) 6 point bending arrangement.

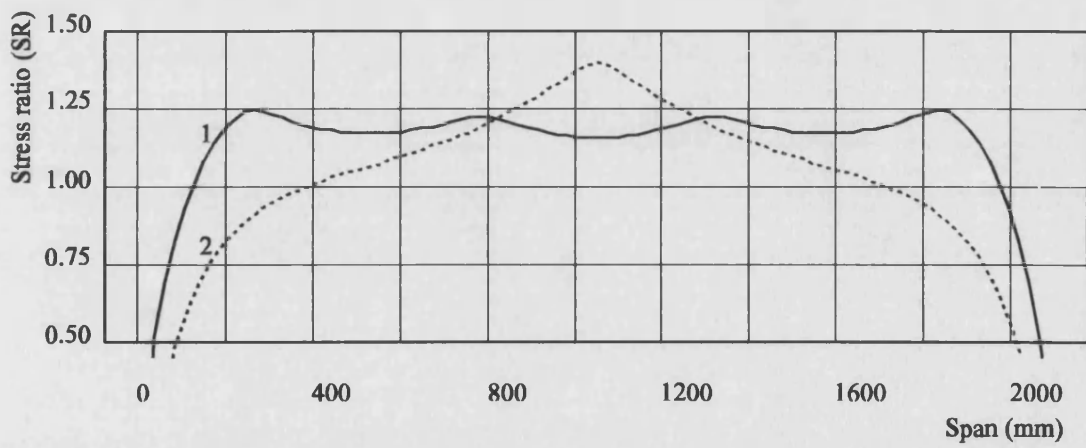


Figure 9.11 Stress ratio for laboratory beam tests according to algebraic theory. 1-6 point bending arrangement, 2-3 point bending arrangement.

Figure 9.13 shows the theoretical and recorded results for the three point bending arrangement. The recorded results correlated well with the algebraic solution and do not bear much relation to the finite element solution. The peak stress location according to the finite element analysis is at the edge of the loading pad, some 32 mm from the web flange interface. The finite element solution at this point is

-103.0 N/mm² on the top surface

and 55.0 N/mm² on the bottom face. In contrast the recorded stress 40 mm away from the web flange interface is between 28.0 N/mm² and 34.1 N/mm². It seems reasonable to conclude, as was suggested in Section 6, that this finite element model is inappropriate for determining the stress concentrations which result from the shear lag phenomenon. It is suggested that this may be due to the coarse density of the finite element mesh at this location. No work has been undertaken to confirm this.

The slight discrepancies between the recorded stresses on the bottom flange and the calculated stresses at the midplane are easily accounted for by the bending of the flange glass. However, the recorded values and algebraic values become coincident at the free edge. This either means that there is no bending of the plate at the free edge or else there is a small error in the algebraic solution. The finite element model does indicate that there should be some bending at the free edge. However, this anomaly is not a major cause for concern because the error, if there is one, is small. The critical issue as far as design is concerned is the stress concentration at the web-flange interface.

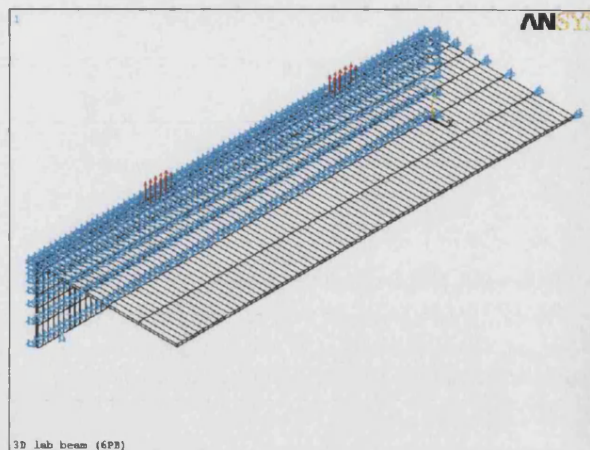


Figure 9.12 Finite element mesh for laboratory beam models. Shown with boundary conditions for six point bending tests.

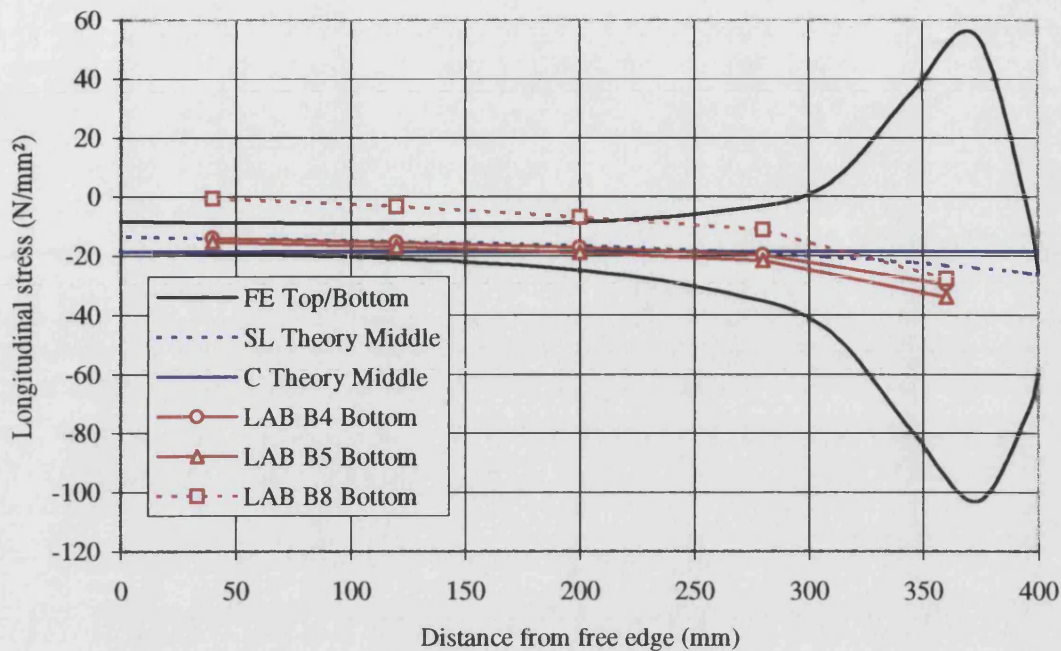


Figure 9.13 Summary of results for longitudinal stress distribution in flange of laboratory beams. Three point bending at 30 kN.

One last point worthy of note is the anomaly of beam 8. This beam included a thin adhesive joint and as such the flange stresses were expected to be slightly lower owing to the near monolithic action of this beam. However, they were not expected to fall to zero! It is thought that the beam may not have been properly supported as in the following test some rocking of this beam was noted. This is illustrated in Figure 9.14. In this scenario strain gauging of the whole width of the flange would have more adequately highlighted this problem. To the author's knowledge this test was the only one in which this problem occurred.

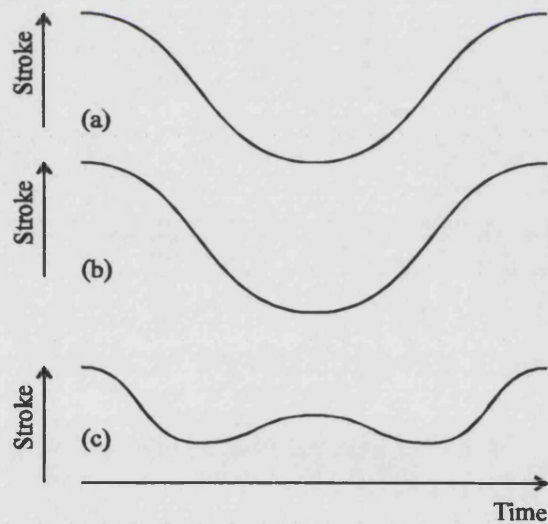


Figure 9.14 Explanation of the rocking behaviour of in test15. (a) Stroke-time plot for ram, (b) Displacement-time plot for RH free edge, (c) Displacement-time plot for LH free edge.

Figure 9.15 shows the theoretical and recorded value for the six point bending arrangements. Here the finite element model and the algebraic model agree. The only exceptions are the bottom face stresses in the region of the web flange interface. As already discussed, this may be due to an inappropriately coarse, or stiff, mesh. The reason for the better agreement between the two models is that the six point bending is closer to the UDL arrangement. The two models have already been shown to agree well in this case, Section 6. The difference between the upper and lower faces can again be explained by the bending of the flange and the algebraic solution can easily be adjusted using the conventional composite bending theory. The recorded values show a good correlation with the stresses predicted on the bottom face of a finite element model. However, these do deviate slightly at the approach to the free edge. As is the case with the three point bending arrangement this is not a cause for major concern as the area of primary interest is the stress concentration at the web-flange interface.

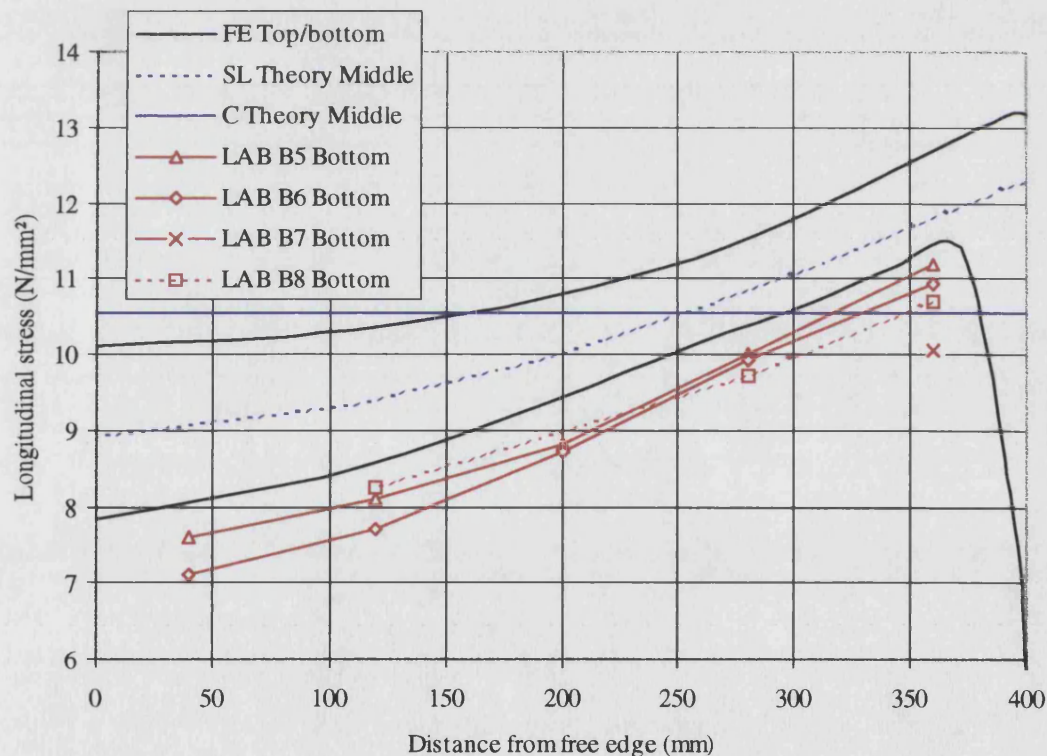


Figure 9.15 Summary of results for longitudinal stress distribution in flange of laboratory beams. Six point bending at 30 kN.

9.3 Cyclic testing

The numbers of cycles to failure are reported in Table 9.1. It can generally be concluded that all of the beams performed well under cyclic loading. The thick joint beams sustained 10,000 cycles at 10 kN and 20 kN in six point bending without major problem. At 30 kN failure occurred after 6,882 cycles. The thin joint beam sustained 25,000 cycles at 10 kN and 20 kN in three point bending and 10,000 cycles at 10 kN in six point bending. At 20 kN in six point bending the beam sustained only 5,892 cycles. Unfortunately it appears that instability of the hydraulic ram lead to this beam being over loaded. The p -gain and d -gain which control the behaviour of the ram were set for the thick adhesive beams. It appears that they may not have been appropriate for the stiffer thin joint beam. Load deflection and load stress plots are shown for tests 10, 15 and 19 in Figure 9.16 to Figure 9.21. Figure 9.18 to Figure 9.21 illustrate the instability of the hydraulic ram during the tests on the thin joint beams. It therefore remains a possibility that the cyclic capacity of the thin beam was actually far higher than can be reported here.

Figure 9.16 to Figure 9.21 are typical of all the cyclic tests. It can be seen that no softening of the adhesive has occurred by the fact that the gradients of the plots remain constant. However, hysteresis behaviour is seen in all plots and is more severe in the cases of thick adhesive joint, Figure 9.16 and Figure 9.17. More important is the tendency of the hysteresis loop to drift right which indicates that creeping of the adhesive is occurring. This is particularly apparent in the case of the thick adhesive joint. However, it is also apparent that while the rate of creep is initially high this decreases with the number of cycles. This is shown by the fact that the hysteresis loops become closer.

Table 9.2 summarises the peak stresses and displacements in each test. The values are quoted at the beginning and end of the test and theoretical values are based upon the composite bending theory presented in Section 4.2. Two important conclusions may be drawn. In the case of the beam with the thick adhesive joint, the measured deflections

and stresses are typically higher than the theoretical values. The converse is true for the beam with the thin adhesive joint. Secondly the differences in the deflections and stresses at the beginning and end of the tests for beams with the thick adhesive joints are far higher than for the beam with the thin adhesive joint. In the case of the thick adhesive joint the average increase in deflection is 33 per cent whilst in the case of the thin adhesive joint it is only four per cent. Similarly in the case of the thick adhesive joint the average increase in glass stress is eight per cent whilst in the case of thin adhesive joint it is only two per cent. This performance would seem to suggest that the thin adhesive joint is better in cyclic fatigue than the thick adhesive joint. It also dispels the idea that stress concentrations brought about by the variation in joint thickness would lead to the early failure of the adhesive.

Test	Midspan deflection (mm)				Peak glass stress (N/mm ²)			
	Start	End	Increase	Theory	Start	End	Increase	Theory
5	0.76	0.94	27%	0.84	-18.2	-19.5	7%	-16.0
7 ^a	-4.5	-7.4	64%	-2.8	75.9	94.9	25%	68.2
10	1.67	2.04	22%	1.77	-33.2	-36.1	9%	-32.1
13	1.6	2.4	50%	2.7	-50.6	-54.3	7%	-48.1
15 ^b	-1.12	-1.19	6%	-1.26	32.7	33.5	2%	32.0
18 ^b	0.75	0.78	4%	0.80	-17.7	-18.3	3%	-15.8
19 ^b	1.47	1.48	1%	1.59	-33.9	-34.2	1%	-31.6

Table 9.2 Summary of beam performance in cyclic testing. ^a This beam contained a de-bond in the adhesive joint. ^b Thin joint beam.

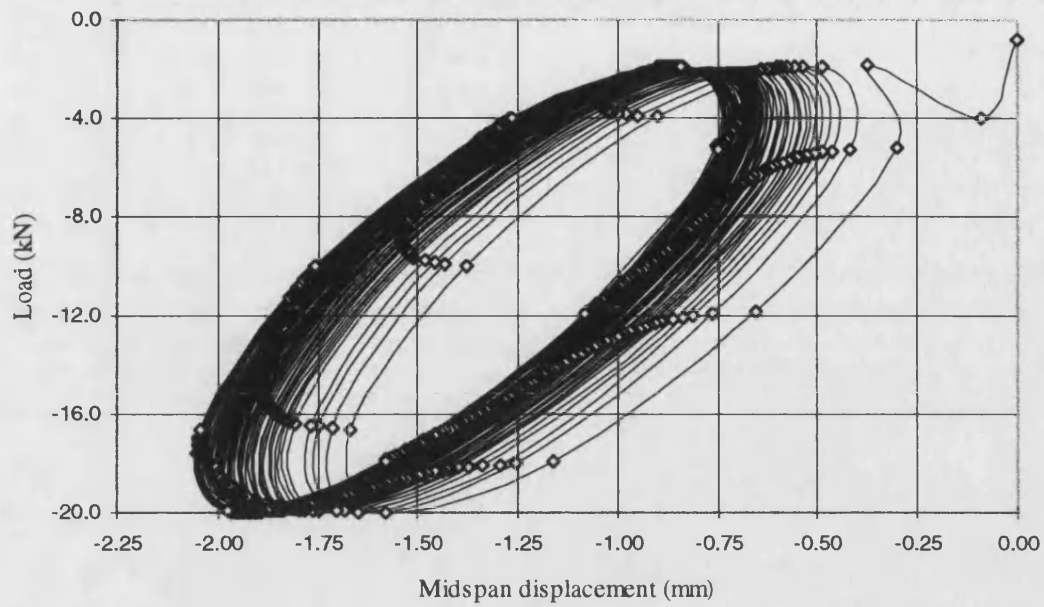


Figure 9.16 Load displacement plot for test 10. 10,000 six point bending cycles at 20 kN.

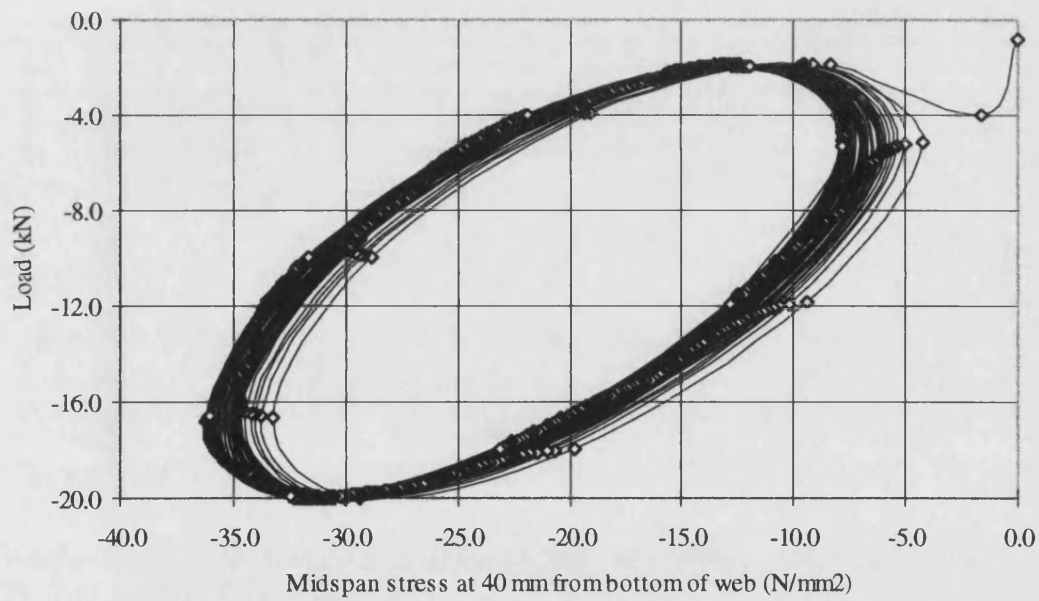


Figure 9.17 Load stress plot for test 10. 10,000 six point bending cycles at 20 kN.

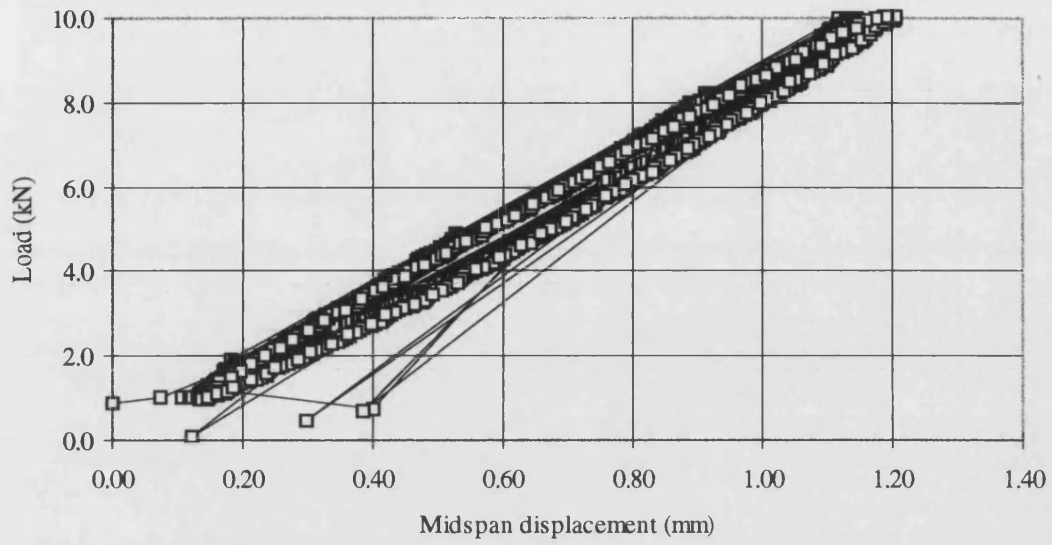


Figure 9.18 Load displacement plot for test 15. 25,000 three point bending cycles at 10 kN.

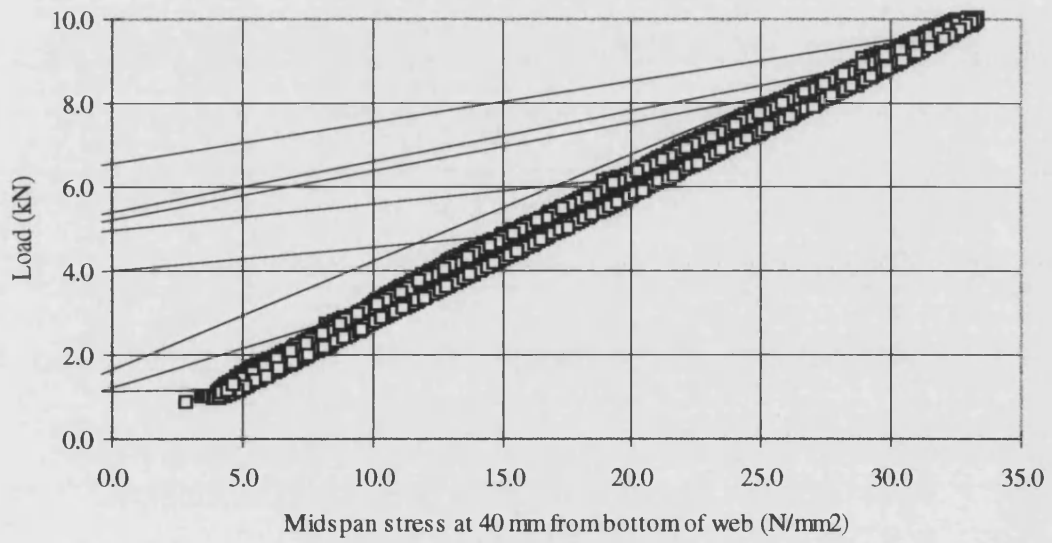


Figure 9.19 Load stress plot for test 15. 25,000 three point bending cycles at 10 kN.

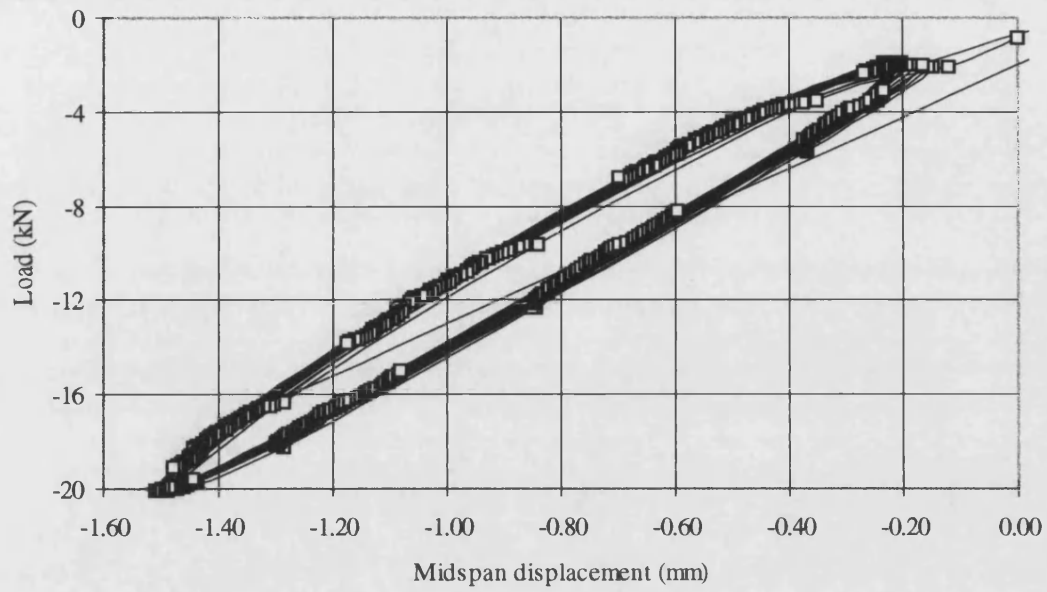


Figure 9.20 Load displacement plot for test 19. 5,892 six point bending cycles at 10 kN.

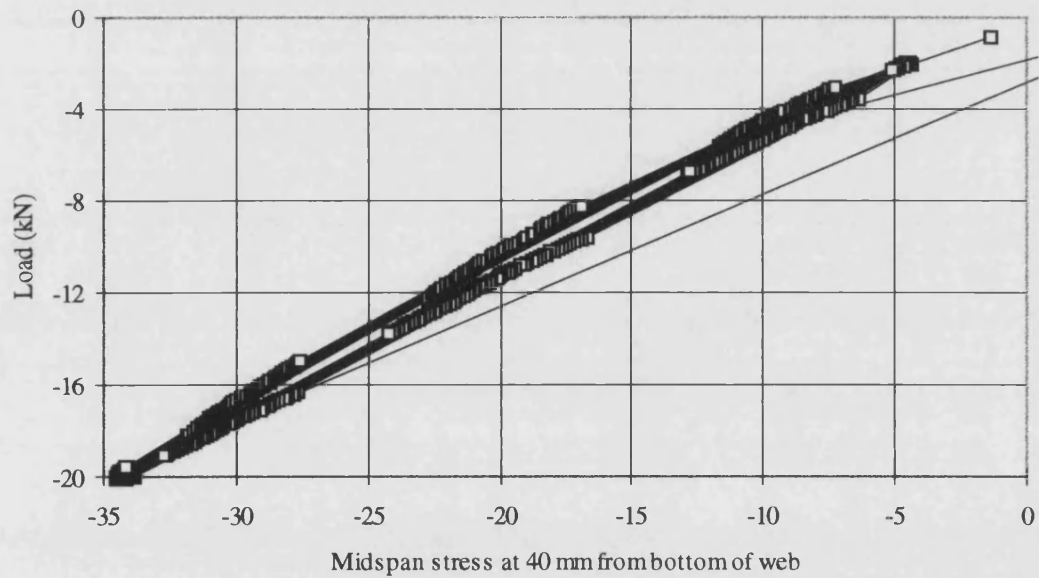


Figure 9.21 Load stress plot for test 19. 5,892 six point bending cycles at 20 kN.

During test 6 the de-bonding of the tension plate was coupled with a de-bond in the main structural adhesive joint, Figure 9.22 and Figure 9.23. It is not clear which de-bond occurred first or whether the stress concentration caused by one de-bond lead to the formation of the second. However, the opportunity was taken to investigate how the de-bond would grow under repeated loading. It was assumed that reapplying a tensile load would result in the rapid growth of the de-bond. Therefore it was decided to test the beam in three point bending. In this manner the de-bond would be placed in shear and compression rather than shear and tension.

Beam 6 sustained another 1750 cycles at 20 kN in three point bending before the test was halted because the de-bond had grown to half the length of the beam. Figure 9.24 and Figure 9.25 show the load-displacement and load-stress plots for this test. In this case a definite change in slope of the hysteresis loop can be seen. Whilst during the initial cycles the glass was stressed to 75.9 N/mm^2 , at the point the test was terminated this had increased to 94.9 N/mm^2 . The 75.9 N/mm^2 is only a little higher than the 68.2 N/mm^2 predicted by the composite theory. However, the 94.9 N/mm^2 correlates well with the 94.0 N/mm^2 value that would be expected if no composite action was developed.

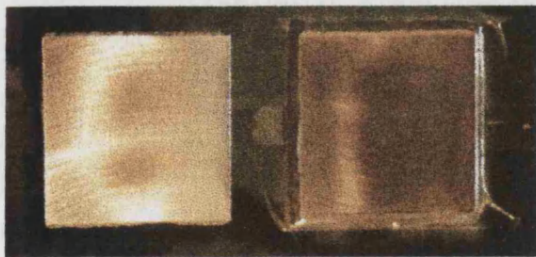


Figure 9.22 Top of flange after de-bond of tension plate.

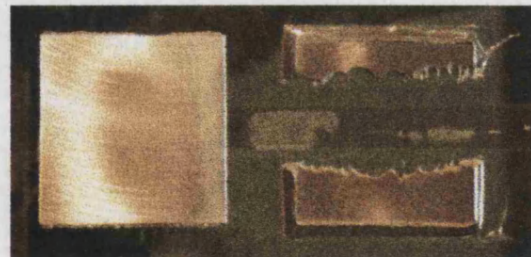


Figure 9.23 Top of flange after de-bond of tension plate (adhesive removed).

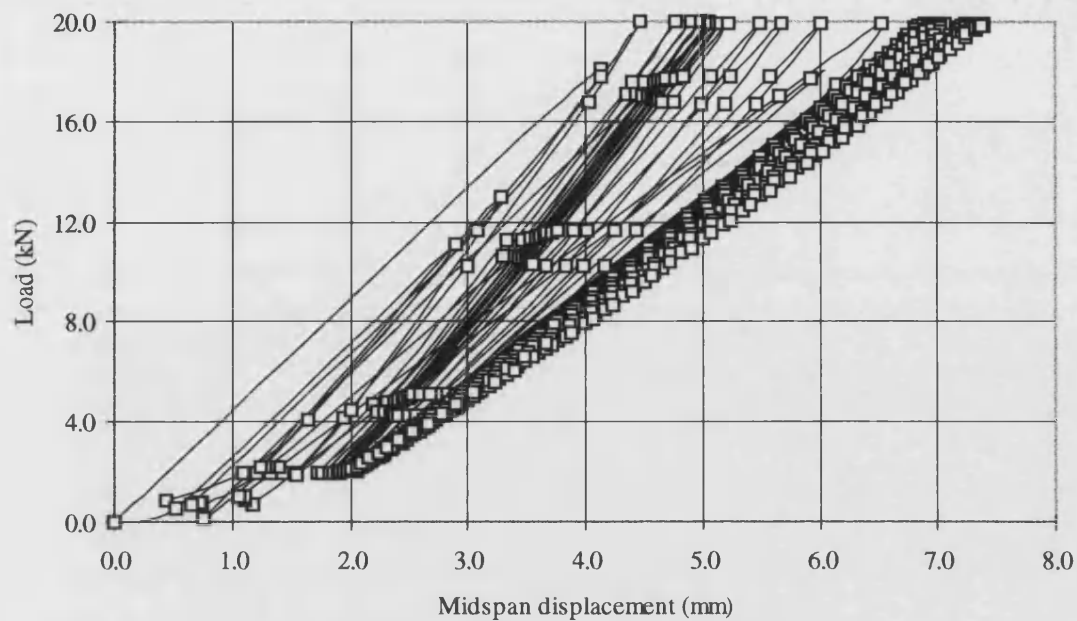


Figure 9.24 Load displacement plot for test 7. 1,750 three point bending cycles at 20 kN.

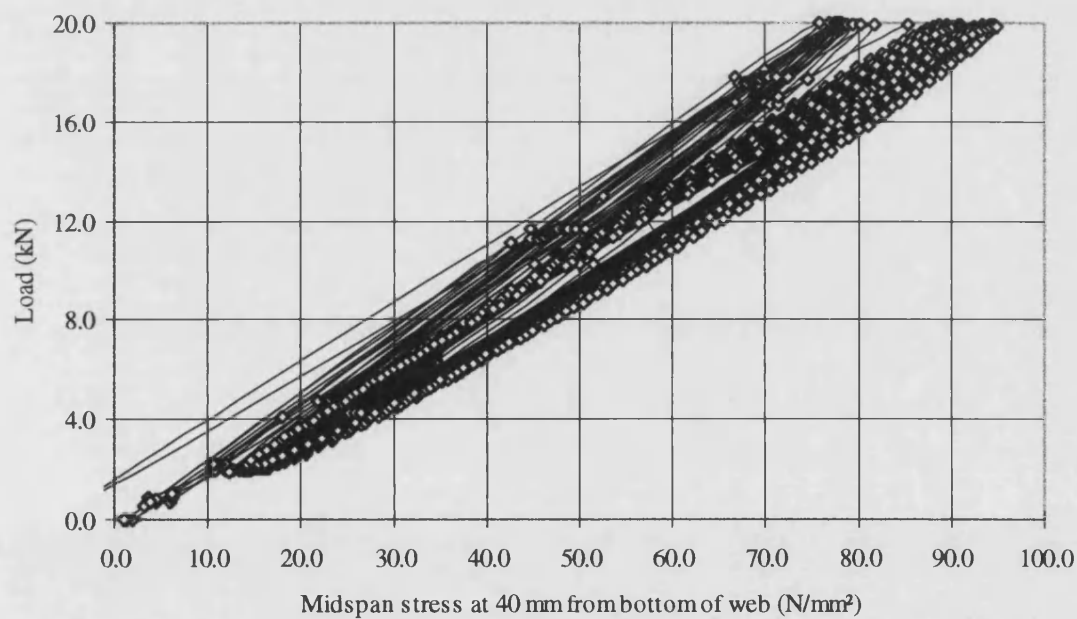


Figure 9.25 Load stress plot for test 7. 1,750 three point bending cycles at 20 kN.

Clearly, as the de-bond grows the beam's behaviour changes from near monolithic to layered. The important point is that the change was not instantaneous and that the growth in the de-bond was clearly visible. Therefore in practical design it may be

possible to inspect the adhesive joint to check for any de-bonding and thereby avert failure. The growth in the de-bond was accompanied by a great deal of noise as the adhesive fractured and free sliding of the flange and the web occurred. This may also act as a safety warning.

In the case of beam test 13 failure also originated because of a de-bond. Here the de-bond was seen just before the failure of the beam. However, after only two further cycles the de-bond had grown to a critical length and the beam failed. Presumably the tensile stress across the adhesive joint is a far better method of crack propagation than shear alone. In cases where high tensile stresses are repeatedly carried across the joint it should be assumed that there will be no warning of failure.

It may be concluded that the cyclic fatigue of the adhesive is governed by the magnitude of the peak stresses. In the case of the 20 kN six point bending tests the maximum adhesive stress was calculate as 9.8 N/mm^2 . In the case of the 30 kN six point bending tests the maximum stress was calculated as 14.6 N/mm^2 . It is suggested that cyclic fatigue will not occur whilst the adhesive is stressed below 10 N/mm^2 . However, as the design stresses used in practice are not likely to approach 5 N/mm^2 it is further suggested that cyclic fatigue is unlikely to be a major problem.

9.4 Buckling

The buckling loads for the two beams without web stiffeners were 38.3 kN and 49.5 kN. These were nominally identical beams loaded in a nominally identical manner. In both cases failure originated at the base of the web. The 25 per cent difference in buckling load illustrates the sensitivity of the beam to initial imperfections. These loads correlate well with the non-linear buckling analysis (40 kN with a 0.2% de-stabilising load). They also correlate well with the algebraic models which assume a simply supported edge (35.3 kN) and an elastic support (44.6 kN). It is not possible to comment on whether these models would suffice in the more general case. However, it must be concluded

that the finite element eigen value approach gave particularly optimistic loads (77.1 kN and 102 kN).

An important side point is that the high level of stress at the base of the web caused the glass in this location to fracture into long finger like fragments, Figure 9.26. This was only witnessed at the base of the web at the midspan. The longest of these were 400 mm long by 10 mm square. This would generally be considered an unacceptable particle size for fractured toughened glass. For example, BS 6206 states that when a plate of toughened glass is broken there must be a minimum of 40 particles in any 50 mm by 50 mm square.

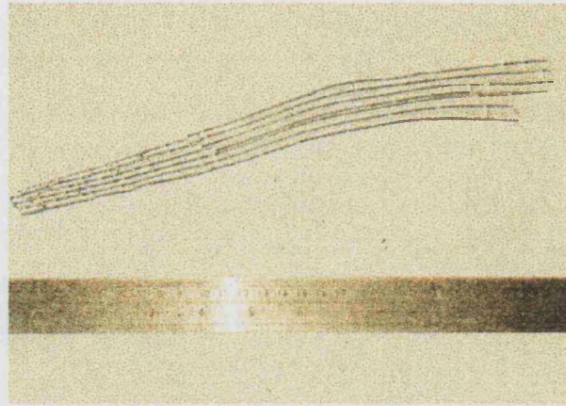


Figure 9.26 The high level of stress at the base of the web caused the glass in this location to fracture into long finger like fragments.

To understand why the fracture pattern originated requires an understanding of the fracture mechanics of toughened glass. New cracks are generally propagated in the direction normal to the largest tensile stress, Gardon (1980). In the case of the web under compression the largest stress will be in a direction perpendicular to the span. Therefore cracks will propagate parallel to the span. As the crack front is accelerated the fracture surface becomes progressively rougher. This will eventually lead to the bifurcation of the fracture. However, in this stress distribution the bifurcation of the fracture perpendicular to the original fracture is prevented by the high compressive stresses. Only as the stresses are reduced and the fracture surface reaches a critical roughness will fracture perpendicular to this original surface occur.

In the case of the stiffened web the beam was loaded to 50 kN without failure. Therefore the web stiffeners may have had some effect in increasing the buckling load. However, it was not possible to determine at what load this would have failed because of the 50 kN limit on the loading jack.

Given the variation in performance of the nominally identical beams it is apparent that any real understanding of this problem requires a statistical approach based upon a large number of test specimens. Unfortunately no more samples were available for testing. It must be concluded that the buckling of these beams is an area requiring more work.

10 CONCLUSIONS

Using flat architectural glass and a modified epoxy adhesive eight glass-adhesive T-beams have been constructed and tested. Each beam was manufactured from two plates of flat glass with an adhesive joint to carry shear at the web-flange interface.

The structural performance of the composite glass-adhesive T-beams approached that of the equivalent monolithic beam sections. The T-beams were able to carry higher loads than conventional glass beam structures whilst exhibiting minimal deflection. The failure load was governed by the glass strength and it was shown that the beams were able to sustain cyclic loading.

Twenty five glass samples have been tested in an attempt to determine its shear strength. However, the samples failed in bending rather than shear and it is concluded that it is not realistically possible to fail glass in shear.

Shear tests were performed on two epoxy adhesives in an attempt to evaluate their strength and their stress-strain behaviour. Difficulties in preparing the steel substrates meant that the full strength of the adhesives was not realised. Further difficulties in measuring the adhesive strains meant that it was not possible to determine accurate stress-strain relationships.

A differential equation based upon linear bending theory has been derived to describe the behaviour of the glass-adhesive T-beam. It may be used to calculate stresses and deflections and it has been validated against finite element models and laboratory test work. The equation contains a term called the composite constant which may be used to determine the degree of composite action. In cases where the degree of composite action approaches the monolithic limit it has been shown that the stresses and deflections may be calculated using conventional bending theory. In other cases a set of design charts may be used to simplify the calculation procedure.

The Song shear lag equation has been modified to describe the shear lag in a composite T-beam. A good correlation was shown between the equation and the laboratory test work. In cases where the degree of composite action approaches the monolithic limit it has been shown that the flange stresses may be calculated using the original Song equation. Attempts to use finite element modelling resulted in a significant overestimation of the flange stresses. This was attributed to an inadequate mesh density.

Buckling of the web was found to determine the failure load when the beam was bent with the web in compression. Modelling the web as an isolated plate which is simply supported along three edges and free along one long edge whilst applying a uniform compressive stress at the two ends resulted in a conservative assessment of the critical buckling stress. Treating the jointed edge as being elastically built-in may yield a more accurate solution in the case of the ideal beam although it was found necessary to consider a reduction factor to take into account practical eccentricities. Eigen value finite element analyses gave grossly optimistic buckling loads although non-linear finite element analyses were found to give realistic buckling loads. Three physical buckling tests were performed and a large variation in the buckling loads was observed.

A number of beams have been tested under cyclic loading. The beams exhibited no cyclic fatigue whilst the adhesive was stressed below 10 N/mm^2 . Above this level the beams failed before the 10,000 cycles were complete. It is suggested that the adhesive may be more resistant to cyclic fatigue when the adhesive is used in a thin joint although it has not been possible to perform sufficient tests to prove this. There is no evidence that the glass suffered any cyclic fatigue.

A simple method of constructing glass-adhesive T-beams has been outlined which ensures consistent structural performance and results in a neatly tooled joint. It has been shown that a plane metal edge may be used as a simple support condition for flat glass plates provided that good alignment is maintained between the glass and the metal edge.

It has also been shown that a thick metal plate bonded to the surface of a flat glass plate is a suitable method of applying tensile loads to glass beam structures during test work.

In summary it has been shown that it is possible to construct, analyse and test glass-adhesive beam structures that are both stiffer and stronger than conventional glass-beam structures.

11 FURTHER WORK

The potential uses of glass-adhesive T-beams and other glass-adhesive beam sections has not been directly addressed. This is left to engineers in practice. They will need to consider the merits of this form of construction on a project by project basis. Such work is currently being undertaken by David Burns of Whitby Bird and Partners in the construction of a large all-glass conservatory at Nordon Farm, Maidenhead.

Whilst the adhesive which was used in the construction of the glass-adhesive T-beams has a proven history in structural applications it is still necessary to address certain issues of environmental durability which are particular to this application. It will be necessary to determine the range of temperatures that the adhesive will be subjected to and to determine what effects this will have upon the adhesive shear modulus. It will also be necessary to determine the long term effect of high levels of ultraviolet radiation and it may be necessary to consider methods of shielding the adhesive from ultraviolet radiation.

The ability of the adhesive to carry high shear loads has been established in the absence of accurate stress-strain data. However, a better understanding of the stress-strain behaviour may lead to a better understanding of the cyclic fatigue of the adhesive, Krieger (1986).

Establishing the buckling load of the glass-adhesive T-beam has proved problematic because of the variation in the buckling loads observed during the physical testing and the variation in the buckling loads predicted by the algebraic and finite element models. Better methods of modelling this instability need to be developed and they must be backed up by more physical testing.

Laminated glass will undoubtedly be used if glass-adhesive beam structures are used in practice. It will therefore be necessary to establish the compatibility of the silane coupling agent, epoxy adhesive and the polyvinylbutyral interlayer. It will also be

necessary to establish the structural performance of the beam when the ply of glass which is in immediate contact with web is broken, Figure 11.2.

Dependent upon the application it may be necessary to consider the effects of eccentric loading across the width of the flange and the additional stresses that this may cause within the adhesive joint, Figure 11.2. It may be necessary to prescribe the use of web stiffeners in such cases.

Undoubtedly further work will be identified as and when this technology is considered for use in real projects.

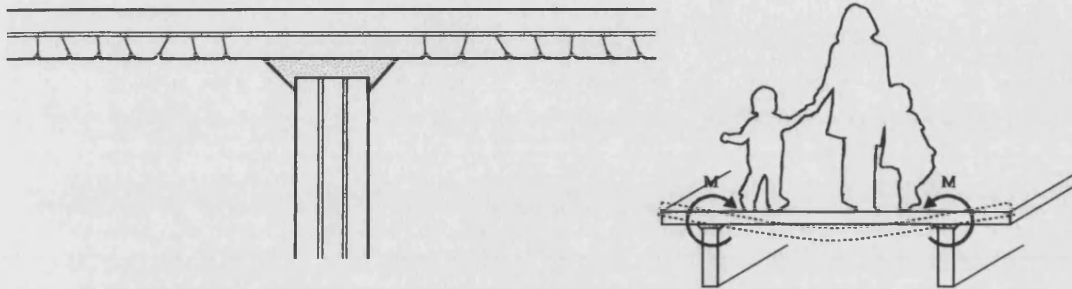


Figure 11.1 (Left) If the PVB interlayer used to laminate glass is able to transfer short term shear stresses then it may be possible to consider glass-adhesive T-beams which are manufactured from laminated plate glass as having a certain redundancy.

Figure 11.2 (Right) It may be that certain applications subject the adhesive joint to a significant moment. In this work it has been generally assumed that the adhesive joint had no rotational capacity. However, the adhesive joint clearly does possess some rotational capacity and this needs to be determined although in situations such as that shown above it may become necessary to consider the use of web stiffeners to prevent the relative rotation of the web and the flange.

12 REFERENCES

- Adams R., D., and Peppiatt, N., A., (1974), *Stress analysis of adhesively bonded lap joints*, J. Strain Analysis, vol. 9, p.p. 185-196.
- Adams, R., D., and Harris, J., A., (1987), *The influence of local geometry on the strength of adhesive joints*, Int. J. Adhesion and Adhesives, vol. 7, no. 2, p.p. 69-80.
- Allan, R., C., et al., (1986), *The use of adhesives in the repair of cracks in ship's structures*, Structural Adhesives in Engineering, Proc. Inst. of Mech. Engineers, p.p. 169-177.
- ANSYS, (1997), *ANSYS structural analysis guide*, SAS IP Inc.
- Armstrong, K., B., (1986), *British Airways experience with composite repairs*, Structural Adhesives in Engineering, Proc. Inst. of Mech. Engineers, p.p. 183-189.
- ASTM (1991), *ASTM C 1036 - 91, Standard specification for flat glass*, American Society of Civil Engineers, New York.
- ASTM, (1992), *ASTM C 1048-92, Standard specification for heat-treated flat glass - kind HS, kind FT coated and uncoated glass*, American Society of Civil Engineers, New York.
- ASTM (1993a), *ASTM D 638 M - 93, Standard test method for tensile properties of plastics (Metric)*, American Society of Civil Engineers, New York.
- ASTM, (1993b), *ASTM D 3983 M-93, Standard test method for measuring strength and shear modulus of non-rigid adhesives by the thick-adherend tensile-lap specimen*, American Society of Civil Engineers, New York.
- Baker, T., C., and Preston, F., W., (1946a), *The effect of water on the strength of glass*, Journal of Applied Physics, vol. 17, March 1946, p.p. 179-188.
- Baker, T., C., and Preston, F., W., (1946b), *Fatigue of glass under static loads*, Journal of Applied Physics, vol. 17, March 1946, p.p. 170-178.
- Baker, T., C., and Preston, F., W., (1946c), *Wide range static strength testing apparatus for glass rods*, Journal of Applied Physics, vol. 17, March 1946, p.p. 162-170.

- Bartholomew, R., and Garfinkel, H., (1980), *Glass science and technology, volume 5, chapter 6 - Chemical strengthening of glass*, Academic Press Inc., New York, p.p. 217-270.
- Behr, R. A., et al., (1985), *Laminated glass units under uniform lateral pressure*, Journal of Structural Engineering, vol. 111, no. 5, p.p. 1037-1050.
- Behr, R., A., et al., (1991), *Reliability analysis of window glass failure pressure data*, Structural Safety, vol. 11, p.p. 43-58.
- Behr, R., A., et al., (1993), *Structural behaviour of architectural laminated glass*, Journal of structural engineering, vol. 119, no. 1, p.p. 202-221.
- BRE, (1989), *BRE Digest 346, The assessment of wind loads, Part 7, Wind loads for serviceability and fatigue assessments*, ISBN 0851254217, BRE, Watford, England.
- Brockmann, W., G., (1986), *The importance of surface treatment prior to bonding*, Structural Adhesives in Engineering, Proc. Inst. of Mech. Engineers, p.p. 61-69.
- Broek, D., (1978), *Elementary engineering fracture mechanics*, Sijthoff and Noordhoff, Alphen aan den Rijn. Netherlands.
- Browne, J., (1993), *Aerospace adhesive's in the 90's*, Proc. 38th Int. SAMPE Symp., p.p. 771-784.
- BS, (1979), *Synthetic resin adhesives for wood*, BS, London.
- BS, (1982), *BS 6262, British standard code of practice for glazing buildings*, BS, London.
- BS, (1988), *BS 4169, Manufacture of glue-laminated timber structural members*, BS, London.
- BS, (1990a), *BS 5350 pt C5, Methods of test for adhesives - determination of bond strength in longitudinal shear*, BS, London.
- BS, (1990b), *BS 5350 pt C7, Methods of test for adhesives - determination of creep resistance to sustained application of force*, BS, London.
- BS, (1990c), *BS 5350 pt C15, Methods of test for adhesives - determination of bond strength in compressive shear*, BS, London.
- BS, (1991a), *British standard specification for impact performance of flat safety glass and safety plastics for use in buildings*, BS, London.

- BS, (1991b), *BS 5350 pt C1, Methods of test for adhesives - determination of cleavage strength of adhesive bonds*, BS, London.
- BS, (1991c), *BS 5350 pt C14, Methods of test for adhesives - 90° peel test for a rigid-to-rigid assembly*, BS, London.
- BS, (1994a), *BS EN 29653, Adhesives - test method for shear impact strength of adhesive bonds*, BS, London.
- BS, (1994b), *BS 5350 pt C12, Methods of test for adhesives - 180° peel test for flexible-to-flexible bonded assemblies*, BS, London.
- BS, (1997a), *BS 6262 pt 6, Draft for public comment, Code of practice for glazing for building - special applications*, BS, London.
- BS, (1997b), *BS 6399 pt II, Code of practice for wind loads*, BS, London.
- BS, (1993a), *BS EN 26922, Adhesives - determination of tensile strength of butt joints*, BS, London.
- BS, (1993b), *BS EN 28610, Adhesives - peel test for a flexible-bonded-to rigid test assembly*, BS, London.
- Button, D., and Pye, B., (1993), *Glass in building*, ISBN 0-7506-0590-1, Butterworth Architectural, Oxford.
- Case, J., et al, (1993), *Strength of Materials and Structures*, ISBN 0-340-56829-1, Edward Arnold, London.
- CEN, (1996a), *CEN/TC/129/WG8/TG1, Draft for the design of glass panes, Part 1: General basis of design*, CEN, Brussels.
- CEN, (1996b), *CEN prEN 1863 Glass in building - heat strengthened glass*, CEN, Brussels.
- CEN, (1996c), *CEN prEN 12543-3 Glass in building - laminated glass*, CEN, Brussels.
- CEN, (1996d), *Draft European standard prEN 1288-5, Determination of bending strength of glass. Part 5. Coaxial double ring on flat specimens with small test surface areas*, CEN, Brussels.
- Chalkley, P., D., and Chiu, W., K., (1993), *An improved method for testing the shear stress/strain behaviour of adhesives*, Int. J. Adhesion and Adhesives, vol. 13, no. 4, p.p. 237-242.

- Chang, Y., F., et al., (1985), *Induction curing adhesives for automotive hoods to eliminate spot welds*, conf. paper, Adhesives 85, Society of Manufacturing Engineers, p.p. 787.1-787.9.
- Charles, R., J., (1958a), *Static fatigue of glass I*, Journal of Applied Physics, vol. 29, no. 11, p.p. 1549-1553.
- Charles, R., J., (1958b), *Static fatigue of glass II*, Journal of Applied Physics, vol. 29, no. 11, 1554-1560.
- Cooper, P., A., and Sawyer J., W., (1979), *A critical examination of stresses in an elastic single lap joint*, NASA, TP 1507.
- Cope, B., C., (1995), *Adhesive classification*, Handbook of Adhesion, D. E. Packham, Ed., Longman Scientific and Technical, Essex, p.p. 27-31.
- Cressy, K., D., (1990), *Adhesives meet aerospace challenges*, Assembly Engineering, vol. 33, no. 4, p.p. 26-28.
- Crocombe, A., D., and Adams, R., D., (1981), *Influence of the spew fillet and other parameters on the stress distribution in a single lap joint*, J. Adhesion, vol.13, no. 2, p.p. 141-155.
- Dawson, S., (1996), *At the cutting edge*, The Architect's Journal, 24 October 1996, p.p. 36-37.
- Dawson, S., (1997), *Glass breaks a new barrier*, The Architect's Journal, 9 January 1997, p.p. 37.
- Demarkles, L., R., (1955), *Investigation of the use of a rubber analogue in the study of the stress distribution in riveted and cemented joints*, NASA, TN 3413.
- Dutton H., and Rice, P., (1995), *Structural glass*, ISBN 0419199403, Spon, London.
- Eekhout, M., (1990), *Glass space structures*, Int. J. of Space Structures, vol. 5, no. 2, p.p. 68-89.
- Fay, P., A., (1994), *Structural adhesives in automotive applications*, Materials World, August 1994, p.p. 418-420.
- Feakes, M., N., (1997), *Shear and shear failure mechanisms in structural glass*, Undergraduate Thesis, School of Architecture and Civil Engineering, University of Bath.

- Flat Glass Marketing Association, (1990), *Glazing Manual*, Flat Glass Marketing Association, Kansas.
- Friedland, L., (1992), *Glass structure; a private house*, The Architect's Journal, 22 July 1992, p.p. 40-43.
- Gardon, R., (1980), *Glass science and technology, volume 5, chapter 5 - Thermal tempering of glass*, Academic Press Inc., New York, p.p. 145-216.
- Gillespie, et al., (1997), *Steel girder rehabilitation through adhesive bonding of composite materials*, Proc. Annual ANTEC Technical Conf., ANTEC, p.p. 1171-1175.
- Goland M., and Reisner, E., (1944), *Stresses in cemented joints*, J. Applied Mechanics, Trans. ASME 66, p.p. A17-A27.
- Gordon, J., E., (1976), *The new science of strong materials*, Penguin Books, London.
- Griffith, A., A., (1921), Transactions of the Royal Society, London, Series A, vol. 221, no. 163, 1921.
- Harris, J., A., and Adams., R., D., (1984), *Strength prediction of bonded single lap joints by non-linear finite element methods*, Int. J. Adhesion and Adhesives, vol. 4, no. 2, p.p. 69-78.
- Harris, J., A., and Fay, P., A., (1992), *Fatigue life evaluation of structural adhesives for automotive applications*, Int. J. Adhesion and Adhesives, vol. 12, no. 1, p.p. 9-18.
- Harrison, K., W., (1986), *Application of epoxy and acrylic adhesives*, Structural Adhesives in Engineering, Proc. Inst. of Mech. Engineers, p.p. 179-182.
- Hart-Smith, L., J., (1973), *Adhesive-bonded scarf and stepped-lap joints*, NASA, CR 112237.
- Hart-Smith, L., J., (1981), *Stress analysis - a continuum mechanics approach*, Developments in adhesives - 2, Applied Science Publishers, p.p. 1-44.
- Haugby, M., H., (1988), *Methods for calculating structural silicone sealant joint dimensions*, Science and Technology of Glazing Systems, ASTM STP 1054, C. J. Praise, Ed., American Society for Testing of Materials, Philadelphia, p.p. 46-57.
- Hooper, J., (1972), *On the bending of architectural laminated glass*, International Journal of Mechanical Science, vol. 15, p.p. 309-323.

- Hutchinson, A., R., (1976) *Bridge management 3 - Strengthening of the Quinton bridges with externally bonded steel plate reinforcement*, ISBN 0-419-21210-8, E & FN Spon, London, p.p. 745-750.
- ISO (1997), *Adhesives - durability of structural adhesive joints - exposure to humidity and temperature under load*, ISO, Geneva.
- Kemp, P., W., P., (1986), *Some practical applications*, Structural Adhesives in Engineering, Proc. Inst. of Mech. Engineers, p.p. 235-240.
- Kreigh, J., D., and Richard, R., M., (1966) *Final report on epoxy bonded composite T-beams for highway bridges*, Arizona Transportation and Traffic Institute Report Series, Report no. 12, University of Arizona, Tucson, Arizona.
- Krieger R., B., (1985), *Analyzing joint stresses using an extensometer*, Adhesives Age, October 1985, p.p. 26-28.
- Krieger, R., B., (1986), *Stress analysis concepts for adhesive bonding of aircraft primary structure*, Structural Adhesives in Engineering, Proc. Inst. of Mech. Engineers, p.p. 1-10.
- Kuno, J., K., (1979), *Structural adhesives continue to gain foothold in aerospace and industrial use*, Int. Conf. Structural Adhesives and Bonding, p.p. 396-423.
- Laufs, W., (1998), *Private correspondence to Chris Jofeh, Ove Arup and Partners, Cardiff from Wilfried Laufs, RWTH, Aachen - Ref. 52252/CJ/KH Distribution of thermal stresses*.
- Lees, W., A., (1986), *Adhesive selection*, Structural Adhesives in Engineering, Proc. Inst. of Mech. Engineers, p.p. 207-214.
- Leone-Bay, A., (1994), *Structural aerospace adhesives*, Flight-Vehicle Materials, Structures and Dynamics - Assessment and Future Directions, p.p. 416-421.
- Liechti, K., M., (1986), *An examination of fracture parameters governing mixed mode cyclic debonding in structural adhesively bonded joints*, Structural Adhesives in Engineering, Proc. Inst. of Mech. Engineers, p.p. 83-91.
- Loctite, (1996), *Loctite world design handbook*, Loctite Corporation.
- Mays, G., C., and Vardy, A., E., (1982), *Adhesive-bonded steel/concrete composite construction*, Int. J. Adhesion and Adhesives, vol. 12, no. 2, p.p. 103-107.

- McCann, J., D., (1984), *The structural properties of glass and its application in the construction industry*, The Structural Engineer, vol. 60a, no. 3, p.p. 73-78.
- Meier, U., (1997), *Repair using advanced composites*, Int. Conf. Composite Construction, IABSE, p.p. 113-124.
- Meier, U., and Meier, H., (1997), *Evolution of stay cables through the use of CFRP*, Int. Conf. Composite Construction, IABSE, p.p. 747-752.
- Minor, J., and Reznik, P., (1990), *Failure strength of laminated glass*, Journal of Structural Engineering, vol. 116, no. 4, p.p. 1030-1039.
- Murray, N., W., (1984), *Thin walled structures*, ISBN 0198561512, Clarendon Press, Oxford.
- NAFEMS, (1987), *NAFEMS a finite element primer*, NAFEMS, Glasgow.
- Natterer, J., and Hamm, J., (1997), *Timber-glass composite in structural glazing*, Int. Conf. Composite Construction, IABSE, p.p. 932-933.
- O'Connor, X., (1988), *Design considerations in structural sealant glazing*, Science and Technology of Glazing Systems, ASTM STP 1054, C. J. Praise, Ed., American Society for Testing of Materials, Philadelphia, p.p. 5-21.
- Packham, D., E., (1995), *Adhesion*, Handbook of Adhesion, D. E. Packham, Ed., Longman Scientific and Technical, Essex, p.p. 18-20.
- Pantelides, C., et al., (1992), *Post-breakage behaviour of architectural glazing in windstorms*, Journal of Wind Engineering and Industrial Aerodynamics, vol. 141, no. 44, p.p. 2425-2435.
- Pilkington (1995), *Standard specification for Pilkington Planar system*, Pilkington UK Ltd., St. Helens.
- Plueddemann, E., P., (1982), *Silane coupling agents*, ISBN 0306409577, Plenum Press, New York.
- Pye, A., J., (1996a), *Meeting: Dr Stephen Ledbetter and Andrew Pye with John Colvin, Dr Howard McKenzie at Pilkington Research and Development, Lathom, March 1996*.
- Pye, A., J., (1996b), *Meeting: Dr Stephen Ledbetter and Andrew Pye with Dr Bernard Sikkell and Dr Keith Fisher at 3M Technology Centre, Bracknell, August 1996*.

- Pye, A., J., (1996c), *Meeting: Dr Stephen Ledbetter and Andrew Pye with David Bamber and John Evason at Pilkington Research and Development, Lathom, October 1996.*
- Pye, A., J., (1996d), *Telephone conversation: Andrew Pye with Dr Alan Hutchinson of the Joining Technology Research Centre at Oxford Brookes University, September 1996.*
- Pye, A., J., (1997a), *Meeting: Andrew Pye with Professor Bob Adams and Dr Felicity Guild at Bristol University, April 1997.*
- Pye, A., J., (1998), *Meeting: Andrew Pye with Hugh Lovegrove, Saint-Gobain Solaglass, at Bath University, March 1998.*
- Pye, A., J., and Ledbetter. S., (1998), *The selection of an adhesive for the construction of a glass-adhesive T-beam*, Int. J. Adhesion and Adhesives, vol. 18, p.p. 159-165.
- Reed, D., A., and Simiu, E., (1983) *NBS building science series 154 - Wind loading and strength of cladding glass*, National Bureau of Standards, Washington, DC.
- Reid, S., (1985), *Risk assessments and safety standards: lessons from architectural safety glazing*, Civil Engineering Transactions, The Institution of Engineers, Australia, p.p. 98-104.
- Roberts, J., E., (1997), *Composite construction in California bridge seismic retrofitting*, Int. Conf. Composite Construction, IABSE, p.p. 943-952.
- Ryan, P., et al. (1997), *Steel supported glazing systems*, ISBN 1-85942-070-2, The Steel Construction Institute, Ascot.
- Saint-Venant, B., (1855), *Memoirs des Savants Etrangers*, vol. 14.
- Sandberg, L., B., (1988), *Specimen length effects on mechanical properties of a silicone elastomeric sealant*, Science and Technology of Glazing Systems, ASTM STP 1054, C. J. Praise, Ed., American Society for Testing of Materials, Philadelphia, p.p. 105-111..
- Satoh, T., et al., (1996), *On the development of structural adhesive technology for the automotive body in Japan*, JSAE Review, Soc. Automotive Engineers of Japan, vol. 17, p.p. 165-178.

- Schmidt, C., M., et al. (1988), *Performance properties of silicone structural adhesives*, Science and Technology of Glazing Systems, ASTM STP 1054, C. J. Praise, Ed., American Society for Testing of Materials, Philadelphia, p.p. 22-45.
- Schwegler, G., (1997), *Earthquake resistance of masonry structures strengthened with CFRP-sheets*, Int. Conf. Composite Construction, IABSE, p.p. 735-740.
- Sedlacek, G., (1995), *Glass in structural engineering - discussion*, The Structural Engineer, vol. 73, no. 14, p.p. 229-232.
- Sedlacek, G., et al., (1995), *Glass in structural engineering*, The Structural Engineer, vol. 73, no. 2, p.p. 17-22.
- Seible, F., (1997), *Advanced composites for bridge infrastructure rehabilitation and renewal*, Int. Conf. Composite Construction, IABSE, p.p. 741-746.
- Shand, E., B., (1958), *Glass engineering handbook, chapter 4 - Stress release and annealing*, The Maple Press Company, York, PA, p.p. 103 to 118.
- Song, Q., (1984), *Shear lag analysis of simple and continuous T, I and box beams*, Report no. UCB/SESM-84/10, Division of Structural Engineering and Structural Mechanics, Department of Civil Engineering, University of California, Berkeley, California.
- Song, Q., and Scordelis, A., C., (1990a), *Shear-lag analysis of T-, I- and box beams*, Journal of Structural Engineering, vol. 116, no. 5, p.p. 1290-1305.
- Song, Q., and Scordelis, A., C., (1990b), *Formulas for shear-lag effect of T-, I- and box beams*, Journal of Structural Engineering, vol. 116, no. 5, p.p. 1306-1318.
- Swedish Council for Building Research, (1993), *Stochastic characterization of glass strength properties*, ISBN 91-540-5523-7, Modin Tryck, Stockholm.
- Tanno, S., (1997) *Structural silicone glazing; design, application and maintenance*, International Conference on Building Envelope Systems and Technology (ICBEST), CWCT, Bath, p.p. 185-189.
- Tham, F., (1976), *Stress distribution in lap joints with partially thinned adherends*, J. Adhesion, vol. 7, p.p. 301-309.
- Timoshenko, S., (1934), *Theory of elasticity*, McGraw Hill Book Company, London.
- Timoshenko, S., and Winowsky-Kreiger, S., (1959), *Theory of plates and shells*, McGraw Hill Book Company, London.

- Timoshenko, S., P., and Gere, J., M., (1961), *Theory of elastic stability*, McGraw Hill Book Company, London.
- Todd, D., A., (1995), *Test of adhesion*, Handbook of Adhesion, D. E. Packham, Ed., Longman Scientific and Technical, Essex, p.p. 470-472.
- Vardy, A., E., and Hutchinson, A., R., (1996), *Some uses of adhesives in civil engineering*, Structural Adhesives in Engineering, Proc. Inst. of Mech. Engineers, p.p. 199-205.
- Vinceti, W., G., (1990), *What engineers know and how they know it - analytical studies from aeronautical history*, ISBN 0801845882, Johns Hopkins University Press, Baltimore.
- Volkersen, O., (1938), *Die Nietkraftverteilung in Zugbeanspruchten mit Konstanten Laschenquerschnitten*, Luftfahrtforschung, vol. 15, p.p. 41-47.
- Wah, T., (1976), *The adhesive scarf joint in pure bending*, Int. J. Mechanical Science, vol. 18, p.p. 223-228.
- Wake, W., C., (1986), *Structural applications of adhesives*, Structural Adhesives in Engineering, Proc. Inst. of Mech. Engineers, p.p. 161-167.
- Webber, J., P., (1981), Scarf repair joints in carbon fibre reinforced plastic strips, J. Adhesion, vol. 12, no. 4, p.p. 257-281.
- Weibull, W. (1939), *A statistical theory of the strength of materials*, The Royal Swedish Institute for Engineering Research, Proc. no. 151, p.p. 1-45.
- Wiederhorn, S., M., (1967), *Influence of water vapour on crack propagation in soda-lime glass*, Journal of the American Ceramic Society, vol. 50, no. 8, p.p. 407-414.
- Wilson, M., (1986), *Robots for adhesive application in the automotive industry*, Structural Adhesives in Engineering, Proc. Inst. of Mech. Engineers, p.p. 57-60.
- Wooley G., R., and Carver D., R., (1971), *Stress concentration factors for bonded lap joint*, J. Aircraft, vol. 8, no. 8, p.p. 817-820.
- Xiao, Y., (1997), *Seismic retrofit of concrete columns using advanced composite materials*, Int. Conf. Composite Construction, IABSE, p.p. 928-929.

13 APPENDIX A

13.1 Testing of aluminium-polyamide composite cladding sections

Before constructing the first glass-adhesive T-beam it was considered necessary to validate the composite bending equation. This was done by performing four point bending tests on two aluminium-polyamide composite cladding sections. The two sections are shown in Figure 13.1 and Figure 13.2. Both beams were deformed to a deflection of span over 180. This was chosen as the most severe deflection that the section would be likely to experience in practice. This also ensured that the aluminium and the polyamide would only be stressed within their elastic range.

The calculated section properties are summarised in Table 13.1. It was assumed that the elastic modulus of the aluminium was $70 \times 10^3 \text{ N/mm}^2$ and that the shear modulus of the polyamide was 586 N/mm^2 .

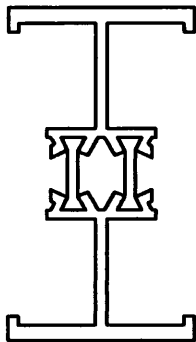


Figure 13.1 Briggs Amasco aluminium-polyamide composite cladding section

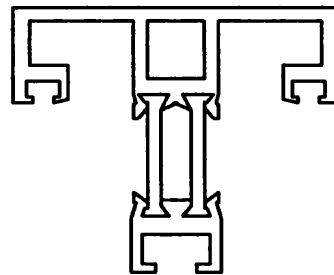


Figure 13.2 Heuck aluminium-polyamide composite cladding section

	Layered stiffness	Monolithic stiffness	Composite constant
Briggs Amasco section	$3.92 \times 10^9 \text{ Nmm}^2$	$18.67 \times 10^9 \text{ Nmm}^2$	$2.42 \times 10^{-5} \text{ mm}^{-2}$
Heuck section	$1.04 \times 10^9 \text{ Nmm}^2$	$7.99 \times 10^9 \text{ Nmm}^2$	$2.03 \times 10^{-5} \text{ mm}^{-2}$

Table 13.1 Section properties of composite cladding sections

13.1.1 Results

	Span	Overhang	Load	Observed deflection	Calculated deflection
Briggs Amasco section	900 mm	2 x 47.5 mm	5.4 kN	5.0 mm	4.9 mm
Heuck section	1400 mm	2 x 50 mm	1.4 kN	8.4 mm	9.9 mm

13.1.2 Conclusion

The case of the Briggs Amasco section validates the composite bending equation. The case of the Heuck section caused some concern. However, the shear modulus of the polyamide was taken from data provided by Briggs Amasco. It was therefore concluded that the polyamide dog-bone used in the Heuck section may have had different properties to that used in the Briggs Amasco section. The composite bending equation was assumed valid and was used to determine suitable section properties for the laboratory T-beams.

14 APPENDIX B

14.1 Derivation of Equation 4-14

From Equation 4-5 and Equation 4-11;

$$F'_t = -F'_b = G_a \gamma_a w \quad \text{Equation B-1}$$

From Equation 4-3 and Equations 4-6 and 4-7;

$$M - E_g (I_t + I_b) z' = F_b z_b - F_t z_t \quad \text{Equation B-2}$$

Substituting Equation B-1 into Equation B-2 and differentiating wrt x ;

$$\frac{d}{dx} [M - E_g (I_t + I_b) z'] = -G_a \gamma_a w (z_b - z_t) \quad \text{Equation B-3}$$

Defining $\gamma_a = \frac{s}{t}$ and $I_t = I_t + I_b$;

$$\frac{d}{dx} [M - E_g I_t z''] = -\frac{G_a w}{t} (z_b - z_t) s \quad \text{Equation B-4}$$

Differentiating Equation B-4 and substituting Equation 4-10;

$$\frac{d^2}{dx^2} [M - E_g I_t z''] = -\frac{G_a w}{t} (z_b - z_t) (\epsilon_{tb} - \epsilon_{bt} + z'' t) \quad \text{Equation B-5}$$

Noting that $y_b + t + y_{bt} = y_t + y_b$ and substituting Equations 4-8 and 4-9;

$$\frac{d^2}{dx^2} [M - E_g I_t z''] = -\frac{G_a w}{t} (z_b - z_t) (\epsilon_t - \epsilon_b + z'' (z_t + z_n)) \quad \text{Equation B-6}$$

Taking $E_g A_t y_t$ out of the right hand bracket of Equation B-6 and substituting equations 4-12 and 4-13;

$$\begin{aligned} \frac{d^2}{dx^2} [M - E_g I_t z''] = & \quad \text{Equation B-7} \\ & -\frac{G_a w}{E_g A_g z_t t} (z_b - z_t) (F_t z_t - F_b z_b + z'' E_g A_t z_t (z_t + z_n)) \end{aligned}$$

Substituting Equation 4-3 into Equation B-7;

$$\frac{d^2}{dx^2} [M - E_g I_t z''] = C (M - M_t - M_b + z'' E_g A_t z_t (z_t + z_n)) \quad \text{Equation B-8}$$

Substituting Equations 4-6 and 4-7 into Equation B-8 and noting that $A_t y_t = A_b y_b$;

$$\frac{d^2}{dx} [M - E_s I_t z''] = C (M - z'' (E_s I_t + E_s I_b + E_s A_t z_t'^2 + E_s A_b z_b'^2)) \quad \text{Equation B-9}$$

Therefore noting that $S_m = E_s I_t + E_s I_b + E_s A_t y_t'^2 + E_s A_b y_b'^2$ and re-arranging;

$$E_s I_t \frac{d^4 z}{dx^4} - C E_s I_m \frac{d^2 z}{dx^2} = \frac{d^2 M}{dx^2} - C M$$